# OPTIMIZING ENERGY MANAGEMENT OF A DUAL-SOURCE RENEWABLE ENERGY SYSTEM WITH THERMAL STORAGE FOR HOT WATER PRODUCTION

By

**TSHOLOFELO PRISCILLA GAONWE**

Thesis submitted in fulfilment of the requirements for the degree:

**Doctor of Engineering in Mechanical Engineering**

In the department of Mechanical and Mechatronic Engineering

Faculty of Engineering, Built Environment and Information Technology

Central University of Technology, Free State

Supervisor: Prof. K. Kusakana

Co-Supervisor: Dr. P.A. Hohne

Co-Supervisor: Dr. T.C.K. Dzogbewu

November 2025

# DECLARATION

I, TSHOLOFELO PRISCILLA GAONWE, _____, do hereby declare that this research project, which has been submitted to the Central University of Technology Free State, for the degree: Doctor of Engineering in Mechanical Engineering, is my own independent work and complies with the Code of Academic Integrity, as well as other relevant policies, procedures, rules and regulations of the Central University of Technology, Free State. This project has not been submitted before by any person in fulfilment (or partial fulfilment) of the requirements for the attainment of any qualification.

**T.P. Gaonwe** Date: **November 2025**

# DEDICATION

I hereby dedicate this thesis to my whole family, who have continuously believed in me and supported me throughout my journey. I am forever grateful to them in all the support, encouragement and all the sacrifices.

Above all, I thank my Heavenly Father for the strength, wisdom and knowledge throughout this journey, which has not been easy to carry alone.

# ACKNOWLEDGMENTS

I would like to express my most sincere gratitude to my supervisors, Prof. K. Kusakana and Dr P.A Hohne, for their continued support, valuable guidance, encouragement and above all, their patience throughout this challenging journey.

I acknowledge the Central University of Technology (CUT), Free State, for their financial support and assistance.

# LIST OF ABBREVIATIONS

| | |
|---|---|
| AC | Air Conditioning |
| ANFIS | Adaptive Neuro-Fuzzy Inference System |
| ANN | Artificial Neural Networks |
| ARE | Average Relative Error |
| ASHP | Air-Source Heat Pump |
| AWHP | Air-to-water Heat Pump |
| BEP | Break-Even Point |
| BHE | Borehole Heat Exchangers |
| BNMF | Bayesian Non-Negative Matrix Factorization |
| BPNN | Backpropagation Neural Networks |
| BRNN | Bayesian regularized Neural Networks |
| CCHP | Combined Cooling, Heating and Power |
| CHP | Combined Heating and Power |
| CNN | Convolutional Neural Networks |
| $CO_2$ | Carbon Dioxide Emissions |
| COP | Coefficient of Performance |
| CoV | Coefficient of Variance |
| CVRMSE | Coefficient of Variation Root Mean Square Error |
| DBN | Deep Belief Network |
| DH | District Heating |
| DR | Demand Response |
| DSM | Demand-Side Management |
| DWH | Domestic water heating |
| ESC | Extremum Seeking Control |
| ESTWH | Electric Storage Tank-Water Heater |
| ETC | Evacuated Tubes Collectors |

| | |
|---|---|
| FFNN | Feed-Forward Neural Networks |
| FL | Fuzzy Logic Controller |
| GA | Genetic Algorithm |
| GD | Gradient Decent |
| GRNN | Generalized Regression Neural Networks |
| GSHP | Ground-Source Heat Pump |
| HP | Heat Pump |
| HPHX | Heat Pipe Heat Exchangers |
| HSRG | Heat Recovery Steam Generator |
| HTS | High-Throughput Screening |
| HVAC | Heating, Ventilation, and Air Conditioning |
| HX | Heat Exchangers |
| KNN | K-Nearest Neighbour |
| LCC | Life Cycle Costs |
| LM | Levenberg-Marquardt |
| LPG | Liquefied Petroleum Gas |
| LSTM | Long Short-Time Memory |
| MAD | Mean Absolute Deviation |
| MAE | Mean Absolute Error |
| MAPE | Mean Absolute Percentage Error |
| MBE | Mean Bias Error |
| MINLP | Mixed Integer Nonlinear Programming |
| MLP | Multilayer Perceptron |
| MLR | Multiple Linear Regression |
| MPC | Model Predictive Control |
| MSE | Mean Squared Error |
| NLP | Nonlinear Programming |
| NMBE | Normalized Mean Bias Error |

| | |
|---|---|
| ORC | Organic Rankine Cycle |
| PCM | Phase Change Material |
| PID | Proportional Integral Derivative |
| PSO | Particle Swarm Optimization |
| PV/T | Photovoltaic-Thermal |
| R | Correlation Coefficient |
| $R^2$ | Coefficient of Determination |
| RBFN | Radial Basis Function Network |
| RF | Random Forest |
| RMSE | Root Mean Square Error |
| RNN | Recurrent Neural Networks |
| SAHP | Solar-Assisted Heat Pump |
| SAURAN | Southern African Universities Radiometric Network |
| SCADA | Supervisory Control and Data Acquisition |
| SCG | Scaled Conjugate Gradient |
| SCIP | Solving Constraint Integer Programs |
| SH | Solar Heating |
| STC | Solar Thermal Collector |
| SVM | Support Vector Machine |
| SWH | Solar water heating |
| TES | Thermal Energy Storage |
| TWS | Thermal Water Storage |
| ToU | Time-of-Use Tariff |
| UTES | Underground TES |
| WGET-SWH | Water-in-Glass Evacuated Tube Solar Water Heater |
| WHO | World Health Organization |
| WHR | Waste Heat Recovery |
| WSHP | Water Source Heat Pump |

| | |
|---|---|
| WWHP | Water-to-Water Heat Pumps |
| WWHR | Wastewater Heat Recovery |

# ABSTRACT

Healthcare facilities are one of the most energy-intensive buildings in the commercial sector due to the high energy consumption of space cooling and ventilation, as well as the high-water heating loads, continuous 24-hour operation for the majority of the facilities, and the high number of medical equipment. With South Africa relying almost exclusively on electricity for energy, a considerable increase in electricity prices has been noted in recent years which has placed a major strain on the country's electricity supplier. Therefore, healthcare facilities tend to experience simultaneously high electricity demand, which exerts significant peak load pressure on the grid. This has, therefore, had a negative effect on both electricity suppliers and customers, resulting in financial and capacity challenges.

Water heating is essential in high-capacity healthcare facilities for hygiene, medical operations, and space heating and is one of the high energy consuming processes in these buildings. Most water heating systems used are conventional, relying on fossil fuels or electricity as primary heat sources such as the electric storage tank water heating (ESTWH) systems. These systems are one of the highest contributors to the energy consumption during the high morning and evening peak periods, which may consume approximately 40-50% of the electricity bill, as well as the increase in the carbon dioxide ($CO_2$) emissions.

An effective energy conservation measure in the commercial sector is the implementation of demand-side management (DSM) strategies to reduce energy consumption and operating costs. One method explored involves using waste heat recovery (WHR) with thermal energy storage (TES) as a supplementary heat source to preheat water. As this practice is used for the purpose of load shifting under time-of-use (ToU) tariff price signals and optimal control, it guarantees to fulfil the above-mentioned purposes. Additionally, in high-capacity buildings, the high energy consumption may still be a challenge due to the continuous high demands of hot water supply.

Incorporating energy-efficient and renewable energy systems such as solar thermal heating (STH) and heat pumps (HP) offers viable energy-saving solutions. These systems may be retrofitted as stand-alone supplementary thermal heat sources or be integrated as the solar-assisted heat pump (SAHP) system enabling energy efficient, stable, reliable and cost-effective heating system, working independently and simultaneously as heat sources.

This study contributes to the field by developing an energy management and optimal control of the water heating processes, of WHR-TES tanks integrated with SAHP system, as a hybrid supplementary heat supply. The hybrid source-TES tanks are used to feed water to the 57 ESTWH systems in a high-capacity healthcare building. The system is developed through mathematical model using the analytical formulation approach, developing the system and formulating the optimal control problem for optimal control under the demand-side management (DSM) strategy. The baseline system and the proposed optimally controlled system was then simulated using MATLAB software to obtain the operation profiles of the system performance. Using the same formulation approach, the energy consumption and operational costs were determined for the economic analysis to evaluate energy and cost savings compared with the baseline system.

In addition, the artificial neural networks (ANN) modelling was conducted for the performance validation of the proposed system, using some of the acquired data and the simulation results for variable selection, determining the input and output and training the model. The ANN model was developed and generated to train, validate and test the system under the summer and winter conditions using the Levenberg Marquardt (LM) backpropagation function. The ANN was modelled at the proportions of 70%, 15% and 15% of the training, validation and testing models, with each variable having 288 data points. Due to the tanks' different parameters of the TWS tanks and the 57 ESTWH systems, with different sizes of 100L, 150L, 200L and 250L, the tanks were grouped by their parameters and different models were developed for summer and winter cases. The TWS tanks had 5 input variables and one output variable, which is the pre-heated water temperature inside the TWS tank and the ESTWH systems 4 input variables and one output variable, which is the hot water temperature inside the each ESTWH system. The data used for the ANN modelling was prepared, cleaned and processed using the MATLAB and Microsoft Excel worksheet.

From the simulation results of the analytical models obtained, the optimally controlled system was able to shift the heating loads of the multifarious ESTWH systems to the off-peak periods of the ToU pricing structure. Additionally, the SAHP system, heating the preheated water in the TWS tanks and supplying the makeup hot water to the multifarious ESTWH systems has resulted in reducing, and even eliminating, the use of the

electric resistive elements for most of the multifarious ESTWH systems. Consequently, the hot water temperatures inside the multifarious ESTWH systems were maintained within the range of 50 ℃ to 60 ℃, which is safe considering the health of the patients. The system was able to reduce the use of electrical power, during the operation, and shift the heating loads to the cheapest ToU pricing signals while maintaining the required heating loads, as well as the delivering the water at the safe temperature to the end users.

For the economic analysis, the initial costs of the baseline case were lower as compared to the optimally controlled proposed case, which have however accumulated to be very high at the end of the project lifespan. This is due to the high cumulative costs incurred because of the continuous energy consumption throughout the day, even during the peak periods, where the energy costs are very high. Conversely, the optimally controlled proposed system accumulated lower costs at the end of the project lifespan due to the retrofitted renewable energy source water heating system, the optimal control and shifting the water heating loads to the ToU pricing signals.

The analysis indicated the accumulated energy costs of 261.57 USD and 133.57 USD for the summer case and 625.34 USD and 145.09 USD for the winter case for the baseline system and optimally controlled proposed system, respectively, from the simulated results for a period of 24 hours. From the economic analysis calculations, in a typical day, the cumulative energy costs obtained for the baseline system and proposed optimally controlled system are 32.05 USD and 15.61 USD for the summer case and 83.96 USD and 18.55 USD for the winter case, respectively.

For the energy and cost-saving analysis, the estimated potential annual energy savings were 15,001.93 kWh, equivalent to approximately 49.6% per annum. This amount of energy may equate to 15.93 metric tons of $CO_2$ per year. At the beginning of the project, the costs of implementation of the baseline and the proposed systems are approximated to 40,464,82 USD and 93,335.37 USD, respectively. Over the estimated project duration of 20 years, based on the calculated results, the baseline system and the proposed optimally controlled system may achieve 943,559.91 USD and 341,860.80 USD of the cumulative energy costs, 74,817.81 USD and 94,755.08 USD of the cumulative replacement costs, 13,996.05 USD and 32,283.01 USD of the cumulative operation and maintenance costs and 8,092.96 USD and 18,667.07 USD of the salvage costs, respectively.

Finally, at the end of the project span, comparing the proposed optimally controlled system with the baseline system, the total life-cycle costs may therefore be approximated to 1,064,745.62 USD and 543,567.18 USD, respectively. These estimates equate to the cost savings of 521,178.43 USD, which is about 48.95% of the costs of the baseline system saved. These results show significant economic and energy-saving potential, demonstrating a viable solution for reducing the energy consumption and operational costs in healthcare facilities.

The ANN models indicated high prediction accuracy, with correlation coefficients (R-values) above 0.95 across training, validation, and test phases. TWS tank obtained higher R-values for the summer case of 0.99414, 0.99518, and 0.98063 and 0.99219 for training, validation and test, respectively. For the ESTWHS, the 100L and 150L size parameters obtaining higher R-values for the summer case and 200L and 250L size parameter models for the winter case. The 250L size parameter obtained the highest R-values of 0.99988, 0.99984 and 0.99988 for the summer case and 0.99986, 0.99984 and 99981 for the winter case, respectively, for training, validation, test results.

For performance validation of the models, TWS tanks obtained the lowest MSE errors for the winter case, training for 16 epochs and indicating training phase MSE, cross-validation phase MSE and the testing phase MSE errors of 2.22e-05, 2.14e-05 and 1.97e-05, respectively, at 10th epoch. For the ESTWH systems, comparing the MSE errors between summer and winter cases for each season, 100L and 150L size parameters achieved lower MSE errors indicating more effective training for the winter case, whereas for the 200L and 250L size parameters it was for the summer case. When comparing between the size parameters, the 250L size parameters obtained the lowest errors for both cases, training for 21 epochs, obtaining 2.91e-08, 4.08e-08 and 3.08e-08 at 21st epoch for the summer case and training for 13 epochs, obtaining 3.26e-08, 4.54e-08 and 6.00e-08 at 13th epoch of training phase MSE, cross-validation phase MSE and the testing phase MSE results, respectively.

For error distribution, TWS tanks indicate good concentration ranging between 70 – 80% around the zero for both summer and winter cases, indicating lowest maximum error range of ±0.015 for the winter case. For the ESTWH systems, the 200L and 250L size parameters show strong concentration of data points over 90% around the zero-error

region, for both the summer and winter cases, with the lowest maximum error range obtained in the summer case for both size parameters, within ±0.05 and ±0.0007, respectively. For the 100L size parameter, good concentration ranges between 70 – 80% around the zero and the maximum error range obtained in the winter case within ±0.04. Whereas the 150L size parameter shows strong concentration over 90% of data plots around the zero-error region for the summer case and good concentration ranging between 70 – 80% around zero, where the lowest maximum error range is obtained in the winter case within ±0.04.

These results confirm the robustness and adaptability of the developed ANN model across diverse operating conditions, making it a valuable tool for predicting the thermal performance of advanced hybrid water heating systems. Overall, this study contributes a practical, rapid, and reliable AI-based modelling approach for thermal heating systems, offering opportunities for improved energy efficiency, system responsiveness, and informed decision-making in building and industrial energy management contexts.

For future research, the proposed water heating process of incorporating WHR-TES, SAHP system and energy management and optimal control may further be customized for various commercial buildings, from small clinics to large hospitals, hotels, etc., depending on their energy needs and available infrastructure. Additionally, other types of solar heating systems or heat pump setup may be explored in different climate conditions considering the geographical locations, for the system to work efficiently and assist in energy and costs savings. Furthermore, the integration of optimisation algorithms (e.g. GA, PSO) to the ANN model of the particular or similar system and also incorporating hybrid AI models (e.g. ANFIS or ANN-LSTM), may be explored.

**Keyword**: Waste Heat Recovery, Thermal Energy Storage, Solar-Assisted Heat Pump, Large-Capacity Water Heating, Energy and Cost Savings, Artificial Neural Network, Levenberg Marquardt Backpropagation

# TABLE OF CONTENTS

# LIST OF FIGURES

# LIST OF TABLES

# CHAPTER 1: INTRODUCTION

## 1.1 BACKGROUND

The building sector represents one-third of the global total energy consumption [1], with healthcare facilities being among the most energy-intensive due to significant cooling, ventilation, and water heating demands. This problem is exacerbated by continuous 24-hour operation in the majority of the facilities and the high number of medical equipment [2]. South Africa's near-exclusive reliance on electricity for energy [3] has led to a considerable increase in electricity prices in recent years, due to financial stress and capacity constraints placing a major strain on the country's electricity supplier [4]. This strain is intensified by healthcare facilities, whose high, simultaneous electricity demands cause significant peak demand on the grid. The resulting financial and capacity challenges negatively impact both the electricity suppliers and their customers [5].

Water heating is essential in high-capacity healthcare facilities for hygiene, medical operations, and space heating and is one of the high energy consuming processes in these buildings [6], [7]. Water heating systems are the fourth largest energy consumers in the commercial buildings sector, after heating, air-conditioning, and lighting [8]. Most of the water heating systems used are conventional systems that rely on fossil fuels or electricity as primary heat sources such as the electric storage tank water heating (ESTWH) systems. These systems are one of the highest contributors to the energy consumption during the high morning and evening peak periods, which may consume approximately 40-50% of the electricity bill [9], as well as the increase in the carbon dioxide ($CO_2$) emissions [10], [11].

A key energy conservation measure for minimizing water heating energy consumption in commercial sectors is implementing demand-side management through waste heat recovery [12]. This strategy uses thermal storage systems as a supplementary heat source to preheat water for the ESTWH systems [13,14].

This practice is commonly used for the purpose of load shifting under time-of-use (ToU) tariff price signals and optimal control, which aims to reduce the energy consumption by shifting the heating load to the off-peak and standard periods, where the operation costs may be further reduced [15]. However, in high-capacity buildings, waste heat recovery alone

may not be an efficient method to minimise the energy consumption of the hot water production as there may still be a challenge of high energy consumption during peak demand periods.

Furthermore, retrofitting the renewable energy and energy efficient sources, such as solar heating (SH) systems and heat pumps (HP), are among the energy saving solutions [16]. These systems may further be integrated as the solar-assisted heat pump (SAHP) system enabling energy efficient, stable, reliable and cost-effective heating system, working independently as heat sources and simultaneously [17].

In the field of research, the possibility to predict, through the use of a proper model, the system performance under specific conditions of use and the expected user benefits, is important. The main approaches of model development that these types of systems can follow are the analytical approach models and machine learning (i.e., black-box-type) models [18]–[20]. The analytical model development approach relies on derived theories, such as the first-principles equations or laws of physics, interpretable system knowledge and the simplified realities to make the system solvable. However, the two main drawbacks for these models are the complexity to derive the some of the equations, which may require assumptions and simplifications, and that the processes are time-consuming [21], [22].

The machine learning approach, on the other hand, such as artificial neural networks (ANN), aims to correlate input parameters influencing system behavior (inputs), with one or more operational parameters characterising its performance (outputs). The mathematical relations used for this correlation do not often refer to some physical explanation; rather, they are selected with regard to the effective description of the experimental output values by the respective experimental input values [20], [23], [24]. The basic advantage of the black-box models is the pass-over of problems related to the lack of information regarding the structure and the exact characteristics of the complete system, as well as its subsystems, or even the weakness to theoretically and mathematically express the involved processes [19], [25].

## 1.2 PROBLEM STATEMENT

Water heating processes account for approximately 50% of the total energy consumed in commercial buildings [26]. Healthcare facilities have a substantial demand for hot water

for various purposes within their facilities. While waste heat recovery from multifunctional chiller systems has been employed to preheat water inside thermal water storage tanks, which is then used to preheat electric storage tank water heaters with the aim of reducing the energy and cost consumptions, the continuous high demand for hot water from multiple heaters pose a challenge. The need for continuous hot water generation can lead to increased electricity usage for water heating, particularly during peak hours when grid electricity is more expensive.

To create a more efficient system without compromising patient comfort and health, it is essential to implement demand-side management (DSM) strategies and optimal control. Integrating renewable energy systems further enhances energy optimisation. These practices may assist in energy optimisation, which may reduce energy consumption and operating costs while ensuring a reliable supply of hot water for healthcare facilities. It has further been noted that there is minimal research in addressing this problem, particularly for the unique type of water heating setup in healthcare facilities. One of these water heating setups is a multifarious water heating systems consisting of 57 ESTWH system, which is supplied preheated water by the thermal water storage (TWS) tanks, recovering waste heat from the multifunctional chiller systems.

## 1.3 AIM AND OBJECTIVES

The aim of this study is to develop an optimal control and energy management method for high-capacity water heating processes that integrate solar-assisted heat pump (SAHP) and waste heat recovery (WHR) systems under DSM strategies. The proposed method presents TWS tanks utilising thermal waste heat from the multifunctional chiller systems to preheat the water from the main water supply. In the current study, the TWS tanks are also main source of makeup water supplied to the multifarious water heating systems, consisting of 57 ESTWH systems, already existing at the Mediclinic healthcare building, located in Bloemfontein in South Africa, and used as a case study. The proposed method consist of solar thermal collectors (STC) and a HP unit retrofitted to the TWS tanks, supplementing simultaneous heating, to increase the pre-warmed water temperature before being transferred to the multifarious water heating loads.

Based on the problem outlined in sections 1.1 and 1.2, the purpose of the method is to assist in the load shifting of the energy demand from the peak periods to the off-peak periods, which will consequently reduce peak load demand, while maintaining the load requirement. Additionally, the implementation of a control algorithm to showcase the real-world behaviour and effectiveness of the controller for large-capacity buildings, such as healthcare facilities. The study further aims to assist in improving energy efficiency of the system, decrease energy consumption in buildings and may, therefore, decrease the costs of operation, as well as indirectly, the $CO_2$ emissions.

Furthermore, this study presents the application of ANN modelling for the validation of the thermal performance of complex water heating systems. Training an ANN model on simulated data allows this study to determine accurate predictions of the system's thermal temperatures across various operating conditions. This provides a practical, rapid, and reliable tool for the system analysis of thermal heating applications by achieving a significant reduction in the required modelling and simulation time.

**Objectives:**

The objectives of the study are as follows:

- To develop a mathematical model of the proposed system by including the components of the retrofitted system to the baseline mathematical model and formulate an optimal control and energy management algorithm for the proposed systems under the ToU time-based pricing.
- To conduct the simulations of the baseline and the proposed system and size the SAHP system and the TWS tanks based on water heating loads in the case study analyse and compare the results of the two systems.
- To conduct the economic analysis of the two systems, evaluate the feasibility of the proposed method.
- To conduct performance evaluation of the proposed method using ANN modelling, for validation, and analyse the results.

## 1.4 CONTRIBUTIONS AND NOVELTY OF THE STUDY:

With the aim and objectives of the study as stated in section 1.3, this study contributes to the analytical approach and machine learning application:

- **Analytical approach**: The original contribution of the study is integrating SAHP system to WHR-TWS system to provide supplementary thermal heating and incorporating control optimization and DSM strategy for the water heating process of the high-capacity buildings. This approach is novel as it incorporates the both the STCs, HP unit and WHR to the integration of TWS system and the application of open-loop optimal control algorithm with ToU pricing structure, all in the same operation. Additionally, this research contributes to the existing literature on the economic feasibility of implementing the proposed system and the benefits peak shaving, load shifting, energy efficiency, cost savings, improved grid stability and reducing $CO_2$ emissions as compared to conventional water heating approaches in large-capacity buildings.
- **Machine learning**: This study makes significant contributions to the field of advanced water heating technologies in the commercial sector by applying ANN modelling to complex technologies by developing ANN model to predict thermal temperature outputs of the complex water heating systems. The study also contributes to conducting modelling and simulations of complex water heating systems at a significantly reduced time to overcome the challenges of traditional analytical approaches, which enable practical and rapid performance evaluation. Finally, demonstrating the ability of the ANN model to efficiently learn and represent highly nonlinear and dynamic relationships between input parameters and thermal output temperatures of complex water heating systems.
- **Novelty of the study**: This study presents a unique approach of the application of the optimal control with ToU pricing structure to a multifarious water heating system consisting of hybrid thermal energy sources (STCs, HP and WHR) integrated to TWS system, preheating the makeup water of the multifarious ESTWH systems. The application of SAHP system, WHR, TES and optimal control with ToU pricing structure in one approach, where limited research has been observed to be conducted

in this area. Also, applying the ANN model to complex technological combination like this has not been investigated or presented in the reviewed literature.

## 1.5 RESEARCH METHODOLOGY & RESEARCH DESIGN

### 1.5.1 The literature review:

A thorough review of literature related to:

- Energy management with the applications of thermal storage (energy/water) systems and their integrations to waste heat recovery, solar systems, heat pump systems, and a combination of these systems integrated to thermal storage systems, where possible. Studies of techno-economic analysis of these systems in the case of water heating processes was conducted.
- The application of ANN modelling of these systems and studies of performance validation and accuracy of the TES systems and the technological approaches as mentioned in the previous point.

### 1.5.2 Data collection and Case study:

- Real input data collected from the supervisory control and data acquisition (SCADA) systems connected to the already existing baseline system at Mediclinic Hospital, Bloemfontein was used; which includes hot water demand flow rates, temperature of the water preheated by the thermal heat from the multifunctional chiller systems, temperature of the water from the main supply, outlet water temperature of the multi-chiller systems, temperature of the water inside multiple ESTWHs.
- Real input data of the ambient air temperatures and solar irradiances collected from the Southern African Universities Radiometric Network (SAURAN) devices placed at the top of the building at the Central University of Technology (CUT) (Latitude: −29.121337; Longitude: 26.215909; Elevation: 1397 m).
- Rated specification of the main components from the current South African market.

### 1.5.3 System formulation and modelling processes

- **Analytical formulation and modelling processes**

The process of formulating the baseline system is straightforward and involves few processing steps. The system does not incorporate the TWS tank and treats the water supplied from this tank as if it were supplied directly from the main. When formulating the model of the baseline system, only the components of the system that already exist at the case study location are incorporated. The input data used for the system simulations include datasets collected from the previous operating period of the system and the ambient temperature, as well as the standard parameters of the components for system sizing. The only limits set during system operation are the switching bounds of the electric resistive elements and the temperature limits of the water inside each ESTWH system. Lastly, no energy management strategy or optimal control optimisation is applied in the simulations conducted.

In contrast, the proposed system includes additional steps, incorporating the SAHP system retrofitted to the TWS tank, which feeds into the main system. Additionally, the energy management and optimisation control algorithm is formulated prior to simulating the operation of the model. The process of formulation and modelling of the proposed system is depicted in a form of a flowchart shown in Figure 1.1.

- **ANN modelling process**

For the ANN modelling, the process adopted for the development, training, and evaluation of the artificial neural network is presented. The selection of variables and data processing procedures are first described, where the parameters used for ANN model training are determined from the energy balance equations employed to model the thermal performance of the TWS tanks and ESTWH systems. Based on these equations, the input and output variables are selected according to the parameters that contribute to thermal energy gains and losses within the system. The datasets are then processed by grouping the data according to size and parameter type, followed by data cleaning to remove inconsistencies and missing values. Data normalization is subsequently applied to ensure numerical stability and to improve the efficiency and convergence of the ANN training process.

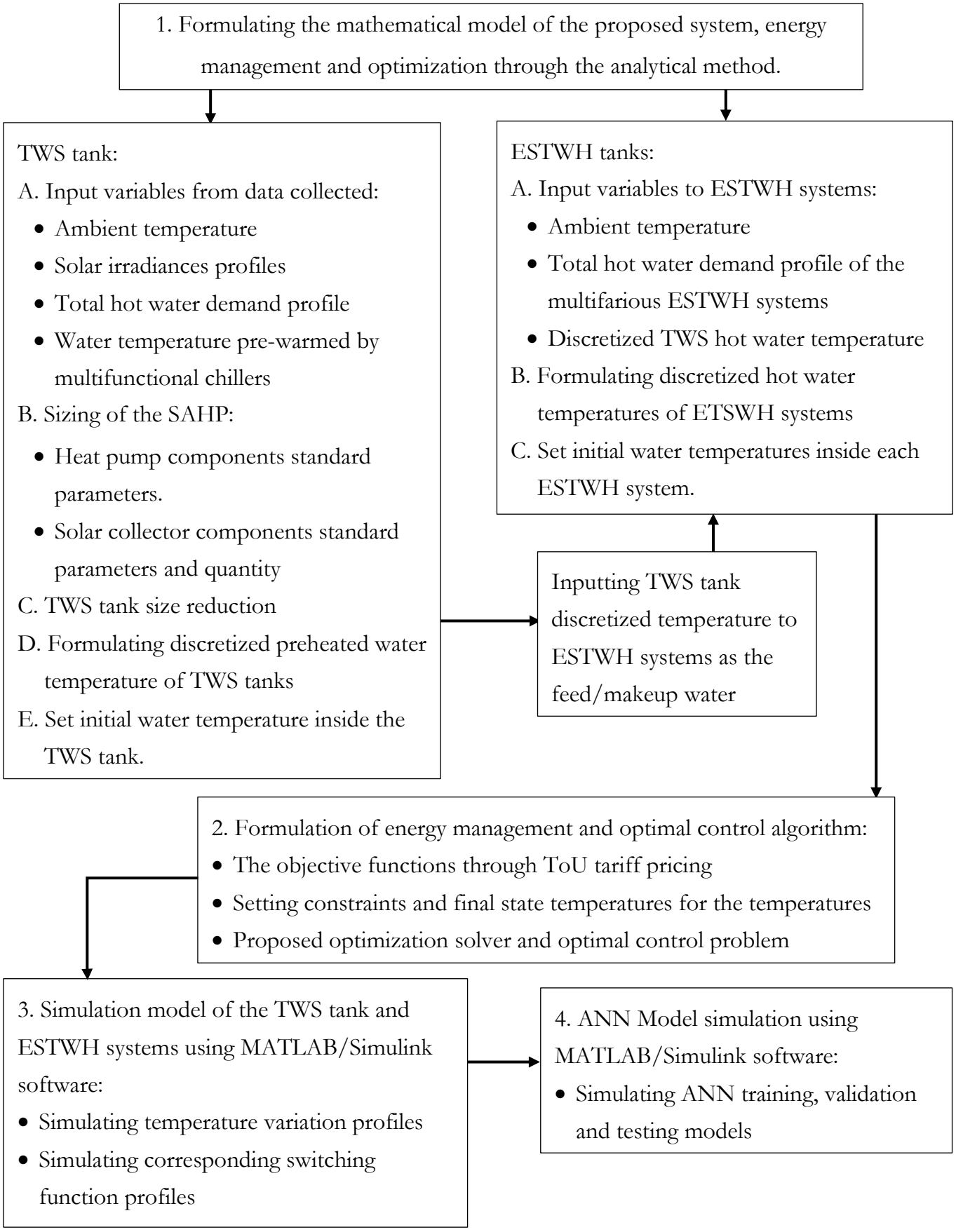


Figure 1.1. System formulation and modelling process of the proposed system.

The ANN model is then formulated to capture the nonlinear relationships between the selected input and output variables, and the modelling process involves training, validation, and testing using MATLAB software. The neural network tools within the MATLAB environment are employed to import the processed input and output variables and specify the required training settings.

Finally, the simulation results obtained from the evaluation of the ANN model are presented and discussed, with emphasis on the model's performance in reproducing system behaviour and its suitability for further analysis within the study.

## 1.6 DELIMITATIONS

- The study will only focus on commercial buildings, particularly large capacity healthcare facilities.
- Optimization in terms of operation control will only be conducted on the thermal preheated storage tank to maintain the hot water temperature at the desired thermal level. Additionally, in terms of optimal control of the system, optimization will be conducted on the heat pump and the ESTWHs based on the ToU tariff applicable for the region.
- The study will only focus on model development and real-time simulation data.
- The simulations and analysis of the system are limited to the storage tanks and do not include the circulation within the pipe systems. This limitation may affect the results of future studies when fluid flow through the pipe systems is incorporated.

## 1.7 PUBLICATIONS DURING THE STUDY

Journals:

- T. P. Gaonwe, K. Kusakana, and P. A. Hohne. "Energy Management and Optimal Control of a Multifarious Water Heating Systems with Waste Heat Recovery and a Solar-Assisted Heat Pump: A Case of Large-Capacity Healthcare Building." *Preprint*, January 2025.

- T. P. Gaonwe, K. Kusakana, and P. A. Hohne, "The Application of an Artificial Neural Network Prediction Model for Output Temperatures of Multifarious Water Heating Systems" *submitted*.

Conferences:

- T.P Gaonwe, K. Kusakana, and P. A. Hohne. "Optimal Energy Management for Healthcare Water Heating: Integrating Waste Heat Recovery and Solar-Assisted Heat Pumps." *Applied Energy Symposium and Forum: Resilient Energy Systems*, Västerås, Sweden, September 23–25, 2025.

## 1.8 THESIS LAYTOUT

This thesis has been divided into six Chapters, with the main research results being presented in Chapters **4** and **5**.

**Chapter 1** comprises the research background, the problem statement, objectives and methodology of the current study.

**Chapter 2** presents a literature review of waste heat recovery and the application of thermal energy storage integrations with the renewable and energy efficient systems. The previous studies of the water heating processes with these systems, incorporating demand-side management strategies and optimal control approach have also been conducted and the key findings are discussed.

In **Chapter 3**, data acquisition and descriptions, with simulation figures of the ambient conditions and the water profiles, are presented and a mathematical model of the proposed WHR-TWS integrated with SAHP system and the ESTWH system (only one tank was modelled at this stage) has been developed and presented.

In **Chapter 4** the optimal control problem formulation, applied to the system, has been developed and presented. The proposed model in Chapter **3**, has been simulated, using MATLAB and the results are presented and the baseline model, without the retrofit of the SAHP was also modelled and the results presented. Additionally, the techno-economic analysis of the proposed and baseline systems was conducted and compared. The energy cost profiles of the summer and winter seasons, for both systems, were further presented.

Finally, the life cycle costs of the SAHP and baseline systems, where calculated and compared, to discover the possible savings at the end of the project lifetime.

**Chapter 5** describes the ANN modelling approach for validation of the proposed system and presents the results obtained from the simulated models.

**Chapter 6** presents a summary of the findings of the whole thesis and the conclusions made. Finally, suggestions for the future research were given in this Chapter.

# CHAPTER 2: LITERATURE REVIEW

## 2.1 INTRODUCTION

This Chapter presents the review of existing literature of energy management and optimal control of the water heating processes through the process of WHR and also through the application of TES, as well as the application of ANN modelling for system validation and accuracy analysis.

This chapter comprises four sections following the introduction. Section 2.2 presents literature of the energy management of water heating processes through the waste heat recovery and thermal energy storage approaches. Furthermore, it presents a background of studies conducted to evaluate the techno-economic analysis of these systems. In section 2.3, a background literature of the application of ANN modelling for system validation and evaluation of the system accuracy in the same context. Section 2.4 discusses the key findings, and section 2.5 summarizes the chapter.

## 2.2 ENERGY MANAGEMENT OF THE WATER HEATING PROCESSES WITH WASTE HEAT RECOVERY AND THERMAL STORAGE SYSTEMS

### The roles of waste heat recovery and thermal energy storage systems in energy management strategies

Demand-side management (DSM) strategies aim to reduce energy consumption and alleviate high energy demands during peak periods without compromising user comfort [27]. Since there are different demand time periods, electricity tariffs vary by demand level, with lower rates during off-peak periods and higher costs during peak hours [28]. This is part of a DSM approach known as the Demand Response (DR) programme, which utilizes Time-of-Use (ToU) pricing to encourage consumers to shift demand to off-peak periods [29].

Waste heat is the energy generated in the form of steam or gas and is often released into the environment without recovery [30]. WHR is the process of capturing waste heat and utilizing it for heating or generating electrical or mechanical power. For this process to be economical, there must be a waste heat source and a simultaneous need for heating, and that heat requirement must match the quality and temperature level of the available waste heat source [31], [32]. WHR emerges as a promising DSM strategy for enhancing energy efficiency

in commercial buildings [33]. The benefits of WHR include reduction of energy, capital and operating cost consumptions and the mitigation of environmental degradation through the reduction of the emission of air pollutants and greenhouse gases [34], [35]. However, WHR may experience the imbalance of the fluctuating hot-water production and unstable supply temperatures, reducing comfort and reliability compared to a conventional boiler system [36]–[38].

Thermal energy storage (TES) is another DSM strategy that conserves energy by retaining it for later use. This practice is being applied more widely due to the mismatch of the energy demand periods and the supply. Energy can be stored chemically, mechanically, or thermally, with TES referring specifically to heat storage. When energy is stored in the form of heat, this is known as TES [39], [40]. In a DSM program, a TES can be used for electric load management in buildings by shifting electrical heating and cooling demands from peak periods to off-peak periods. This is achieved by storing thermal energy during off-peak periods for use during peak demand periods. In this way, heating equipment can be turned off when electricity prices or emissions are high [41]. The application of TES offers several benefits, including improved system efficiency, cost savings through load shifting, and reduced peak demand for utilities [42], [43].

In water heating applications, integrating TES with WHR systems is a promising DSM approach that mitigates temperature fluctuations and improves system reliability. Integrating TES systems to WHR may minimise the fluctuation of the imbalance between hot water production and supply demand [44]–[46]. TES systems, therefore, provide a continuous heat source, which significantly expands the potential applications of recovered heat [47] and may improve waste heat utilisation and increase the system efficiency [48].

Additionally, integrating renewable and energy-efficient systems such as solar collectors and heat pumps can further reduce energy consumption and emissions in commercial buildings.[49]. This is due to the fact that solar systems owing to their simple structure, low cost, stable operation, and effective solar energy collection. The effect of using solar energy on the environment for a variety of applications is minimal, as it produces no harmful pollutants and is a completely free energy source [50]. systems maximize the benefits of solar energy integration, offering reliable alternatives to conventional energy sources [51]. Whereas heat pump systems use only a small amount of electricity (approximately 30%) of the traditional systems to produce the same amount of heat energy [52].

Furthermore, incorporating optimal control with DSM strategies for the optimal operation of the system in shifting the heating load to off-peak periods, where the operation costs may be further reduced and the systems to operate optimally during the off-peak periods in the future [53]–[55].

**Review of the water heating processes through WHR in healthcare institutions.**

In the context of healthcare facilities, the following studies presents research on WHR primarily used for hot water production. Vahidifar et al. [56] designed a heat exchanger to provide hot water for laundry in a hospital by recovering heat from an air-cooled chiller system to reduce the gas consumption during the hot water production. The results indicated that approximately 8170 kcal/m³ of thermal energy were recovered, saving 7.5 m³ of gas per hour, and improving the chiller's coefficient of performance (COP) by 0.03. Dudkiewicz et al. [57] assessed the energy saving of utilising waste heat recovered from the greywater system, draining sewage from wash basins and showers. Two hospitals in Poland were used as case studies and comparing four different types of heat exchangers (HX). The shell-and-tube heat exchanger achieved the best results, reducing energy demand by 30%. The energy recovery of 2.49 and 2.80 GJ/year per bed with a constant cold-water temperature were obtained and decreased slightly to 2.35 and 2.65 GJ/year/bed, when the cold-water temperature was variable, in Hospital A and Hospital B, respectively.

Putra et al. [58] investigated the thermal performance of a Heat Pipe HX (HPHX) in recovering heat from exhaust air in a hospital HVAC system. The system recovered between 204.72 and 1,404.29 kJ/h of waste heat at air velocities of 1.5–2 m/s, reducing annual energy consumption by approximately 4.1 GJ. Sohail et al. [59] evaluated the potential of wastewater heat recovery (WWHR) in a large hospital in Canada. The system achieved savings of $404,853 in annual operating cost and $171,659 of global adjustment, with a capital cost of $6,499,000. Additionally, the system would achieve annual savings of $576,512, with simple payback period of 11.27 years and an IRR of 11.05% over a 20-year project and the potential to offset 5355 tons of $CO_2$ emissions annually, primarily by displacing natural gas use.

Advanced energy system designs due to the integration of one or more systems have also been evaluated whereby some of which in addition to heating and cooling, includes generating power or electricity. These systems configurations therefore focus on hybrid

approaches to meet multiple energy demands, including water heating production, space heating and cooling, and generation of power/electricity. Ahn et al. [60] investigated a new strategy for a hybrid chiller-based Combined Cooling, Heating and Power (CCHP) for the office and hospital buildings. The proposed system saved up to 13.6 GWh/year compared to the conventional system and the reduced emissions by 3.5 kton/year compared to absorption-only systems. Bujak [61] evaluated a medical waste incineration installation designed for both electrical and heat recovery with the system including the three components, a Heat Recovery Steam Generator (HSRG), a Microturbine and a Heat/Steam Exchanger. The system was operated at 78%, 79% and 99% thermal efficiencies of the mentioned components, respectively. An average of 31.6 kWe were produced as electricity and 729 kW (95.8%) was recovered as hot-water enthalpy. From the economic analysis, the system showed a simple payback period of 3.1 years, and after 15 years of the duration of the project, the project is expected to yield profits of approximately $4.93 million, with an Internal Rate of Return of 23.6%, significantly higher that the discounted rate of 8.1%.

Alam et al. [62] designed and evaluated the performance of a retrofitted HVAC system with a heat recovery wheel for a hospital building. From the results obtained, the heat recovery wheel reduced the cooling load, leading to a 30% reduction in electrical energy consumption. Analytical findings revealed a 28.31% reduction in the total work done by the system. The integration of the heat recovery wheel also conserved approximately 29.87% of the electrical energy spent on cooling the hospital building. Ghoreishinejad et al. [63] proposes a combined system utilizing an absorption chiller, organic Rankine cycle (ORC), heat exchangers, and air handlers to supply heating, cooling, electricity, and hot water in hospital buildings, recovering waste heat from the oxygen generation units. The system achieved a Net Present Value (NPV) break-even point in 13 years for one unit and less than one year for 20 units. In this configuration, operating two hours per day, the system achieved an annual heating output of 59,448 kWh.

Gulseven and Zeki Yilmazoglu [64] conducted a study of energy optimisation by replacing the oil-air compressors with oil-free compressors and integrating the air-to-water heat pumps as heat recovery systems to provide hot tap water during summer mode and heating water for radiators placed in an emergency waiting room during winter mode at a University Hospital in Turkey. Overall energy use decreased, with electricity consumption

reduced by 974,811 kWh, resulting in a payback period of 2–4 years depending on heating load. Kalina and Pohl [65] conducted a study of waste heat recovery integrating district heating (DH) system with a large hospital's energy infrastructure. The system achieved annual $CO_2$ reductions between 1,243 and 2,812 tons, with an IRR of 19.2% and a payback period of 5.2 years.

Incorporating solar and heat pump systems to the waste heat recovery system, particularly in the hospital/healthcare buildings, Bekele et al. [66] investigating the feasibility of utilizing solar energy for large-scale water heating systems in Ethiopia using single-glass-cover flat plate collector solar water heating system. Among t the case studies, maximum solar contributions reached 97.5% in winter and 66.9% in summer, with an annual solar coverage of 81.8%. Ooshaksaraei [67] conducted a study to evaluate the potential of solar energy in reducing energy consumption, specifically in the hot water systems of hospitals and hotels in Malaysia. The results indicated that the system could save more than 20% savings in liquefied petroleum gas (LPG) usage and that, with the average solar radiation of 16.92 MJ/m²/day at the location of the case study, the solar energy output from the evacuated tube collectors could offset some of the LPG consumption. which could lead to both cost savings on fuel and a reduction in $CO_2$ emissions.

Matera et al. [68] evaluated the performance, energy savings, and carbon emission reductions of a heat pump system replacing a natural gas boiler for supplying hot water in a medium-sized hospital in central Taiwan. The system reduced energy costs by USD 90,000 and $CO_2$ emissions by 256 tons over seven months. The second refilling strategy saved 30% of energy costs by utilizing off-peak electricity for heating. Chiang et al. [69] investigated energy-saving and efficiency improvement potential of Heating, Ventilation, and Air Conditioning (HVAC) system integrated with a water source heat pump (WSHP) in a large-scale hospital, in Taiwan, to meet the hospital's simultaneous cooling and hot water demands with enhanced energy efficiency and operational safety. The WSHP achieved a COP of 3.62 in heating mode and 2.62 in cooling mode. The proposed system achieved annual cost reduction of $102,564 with a payback period of 1.2 years.

Furthermore, integrating solar systems and heat pumps as dual-source systems which may enable energy efficient, stable, reliable and cost-effective heating system and the two working independently as heat sources (or even one for generating power and the other for

heating) to the system [70]–[72]. The use of the dual-source system may assist in significantly reducing the use of electricity or fossil fuel, by producing thermal heat or power and free or low costs as compared to the traditional energy consuming systems [73], [74]. This may result in further energy and cost savings as well as a shorter payback period [71], [72], [75]. However, few studies have also been conducted incorporating the two systems.

Todorović et al. [76] developed and evaluated the proposed system of the integration of the PV electricity generation, heat recovery, and heat pumps, utilizing cold wastewater for air conditioning for air conditioning and sanitary water heating in the Special Hospital of Spa. The proposed system achieved the shortest simple payback period of 5.4 years and had the lowest Lifecycle cost (LCC) achieving the investment returned within one year. Zhang et al. [77] developed and validated a dual-objective optimization model to enhance the thermal performance and economic efficiency of concentrated solar district heating systems integrated with water-to-water heat pumps (WWHPs). The system case study was in Nagarze County, China. For thermal performance, the heat collection efficiency and solar fraction increased from 41.51% to 45.30% and 53.26% to 74.17%, respectively. Economic performance improvements indicated reduction of levelized cost of heat from 0.2750 CNY/kWh (0.038 USD/kWh) to 0.2297 CNY/kWh (0.032 USD/kWh).

## Literature review of the energy management and optimal control of heating processes incorporating TES systems.

Studies that investigate the economic analysis of the TES systems with different integrations have been widely explored under DSM strategies. For large-capacity water heating systems integrated with TES technologies, Ju et al. [78] investigated the peak shaving potential of a stratified TES tank with district heating (DH) water supply integrated into a substation of a Finnish office building. The system was simulated with varying temperature control curves and mass flow rates, achieving up to 31.5% peak power reduction on colder days. Additionally, reducing the mass flow by up to 30% provided an additional peak power reduction without sacrificing thermal comfort. Mostafavi et al. [79] investigated the system performance and energy saving potential of a incorporating TES system to a DH network integrated with a combined heating and power (CHP) station. Optimal TES size is investigated from energetic, environmental and economical viewpoints. Results depict that

by coupling five 1100 $m^3$ TES tanks with CHP/DH plant, the annual CHP efficiency increases by 1.12%, and annual fuel consumption rate and $CO_2$ emissions decrease by 2.6%.

Investigating the application of WHR-TES systems, Li et al. [80] analysed the techno-economic potential of implementing TES for peak load shaving for a DH system with WHR from the campus data centre in Norway. The results showed significant peak load shaving and WHR with up to 112 000 EUR saved for heating bills annually, and the heating bill paid for the peak load could be reduced by 15%. Additionally, with the optimal sizing and operation, the payback period of the water tank could be decreased to 13 years. Ren et al. [81] conducted a parametric study of WHR system integrated with TES tanks recovering and storing wasted heat in air conditioning (AC) systems to explore the effectiveness of WHR, the effect of phase change material (PCM) and influence of TES volume to the system. The results showed that increasing WHR effectiveness from 0.55 to 0.85 extended constant thermal power recovery duration and raised outlet water temperature while reducing pump energy consumption. Furthermore, latent heat storage (PCM tank) extends the duration of stable thermal power recovery by over 61 %.

Integrating energy efficient systems such as heat pump (HP)systems, Sultan et al. [82] conducted a techno-economic study of a novel heat pump integrated TES system using an idealized approach modelled for space heating and cooling loads in residential buildings in three different climates in the US for a duration of 1 year. The maximum reduction in electric consumption, utility cost and peak electric demand was achieved between 20 – 30 ℃. The peak energy consumption was reduced by 47 – 70% by shifting peak load to off-peak using a time-of-use utility schedule. Ryan et al. [83] investigated the potential cost and emissions impacts of TES, in the form of stratified water storage, integrated with Ground source HP (GSHP) systems. An established method of TRNSYS modelling is used for the heat pumps and borehole heat exchangers (BHEs), along with the TES. The results show that the integration of TES to the GSHP system could reduce operating costs by 4.5% and could incur a potential reduction of 7-22% in annual peak demand kW, dependent on the rate structure. Shi et al. [84] assessed the potential of the proposed novel GSHP system integrated with underground TES (UTES) to level the electric demand of buildings while still satisfying their thermal demands. The impacts on the electricity demand in various electricity markets were quantified. The results show that, within the capacity of the existing electric grids, the

maximum penetration rate of the proposed system in different wholesale markets could range from 51% to 100%. By implementing the proposed system at its maximum penetration rate, the grid-level summer peak demand can be reduced by 9.1% to 18.2%. In addition, the annual electricity consumption would change by −12 % to 2%. The nationwide total electricity consumption would be reduced by 9%.

Additionally, for the integration the solar systems, Wang et al. [85] investigated the optimal design of STC and TES systems integrated in the existing 12 MWth CHP plant. The optimal STC–TES configuration outperformed single integrations, reducing annual costs by 3% and carbon emissions by 10%. The use of TES increased efficiency from 88 – 92% and the optimal share of STC is then increased from 7 – 10%. Mellouli et al. [86] perform a parametric analysis of the solar water heater (SWH) integrated with a PCM-based TES on the basis of the thermophysical properties of the PCM. Various numerical simulations were performed, and the results indicating 20.2% of thermal energy peak periods load shifted to the off-peak period. Additionally, increasing the density and enthalpy increased load shifting and the lower melting power of the PCM may help the SWH retain water temperature for a longer period of time.

Yildiz et al. [87] analysed the potential of storing and using excess photovoltaics (PV) generation using ESTWH systems as a thermal storage. The authors also investigated the impact of different daily hot water draw profiles, PV and TS size on the potential for excess PV utilization. The results show that on average, excess PV generation from a 4.5 kW PV system can provide 48% of daily TS energy for a household with a typical working family profile, which corresponds to a 28% increase in PV self-consumption. Sánchez-Barroso [55] conducted a study of analysis of the potential savings from implementing solar thermal energy systems for producing domestic hot water (DHW) in 25 hospitals across Extremadura, Spain. Approximated €145,933 (150,220.29 USD) and 637.99 tons of annual cost savings and $CO_2$ emissions reduction were obtained, respectively. The average payback period was approximated to 4.74 years, and the system exhibited an energy efficiency of 4.29 kWh per euro invested (SD = 0.20).

Few studies have explored the integration of the TES systems and the SAHP system, such as the study conducted by Li et al. [88] investigated the energy performance of integrations of HPs with TES systems and combined with onsite PV systems for various

buildings, thermal characteristics, orientations, occupancy profiles, and solar panel directions. The findings of this study reveal significant grid electricity savings achieved by these integrated systems, ranging from approximately 50% to 80% in both heating- and cooling-dominated regions with diverse climates, even under reasonable extreme conditions. By utilising thermal energy storage to store surplus solar energy, the system enhances the PV self-consumption ratio and solar fraction by approximately 30% irrespective of moderate deviations in PV direction.

## 2.3 MODEL DEVELOPMENT OF THERMAL ENERGY SYSTEMS THROUGH THE ARTIFICIAL NEURAL NETWORK MODELLING

### Machine learning modelling explored in building energy management.

Artificial Neural Networks (ANNs) embody a category of machine learning algorithms inspired by biological neural networks (NNs). These models, noted for their robust ability to represent and model nonlinear relationships between inputs and outputs, are aimed to mimic neuronal behaviours in the human brain [89], [90]. A wide range of ANN modelling have been explored in building energy management (BEM) to enhance energy efficiency of the in buildings, amongst other reasons, for the purpose of heating, which may also be employed for energy (electricity/power) generation. Different types of ANN models may be classified based on their architecture and functionality, categorised in three main types, namely, Feed-Forward NNs (FFNNs), Recurrent NNs (RNNs) and Convolutional NNs (RNNs). The FFNNs and RNNs are commonly used types mainly for forecasting heating demand, thermal efficiency of the systems and demand profiles in heating and energy systems [91], [92].

FFNNs are ANN types used for prediction and modelling tasks and their different models include Multilayer Perceptron (MLP), Radial Basis Function Networks (RBFN), Bayesian Regularized Neural Network (BRNN) and Generalized Regression Neural Network (GRNN). MLP models are the most widely used of all the ANN models. RNN types are used for time-series predictions with Long Short-Time Memory (LSTM) being the commonly used models [93]. Additionally, various approaches have been explored using the ANN models by incorporating other artificial intelligence (AI) methods such as learning algorithms, machine learning models and optimization techniques to enhance the accuracy

and robustness of the models. Learning algorithms include Backpropagation NN (BPNN), Levenberg-Marquardt (LM) learning algorithm and Gradient Decent (GD) [94]. Learning algorithms, which are also train ANN models. Machine learning models include K-Nearest Neighbour (KNN), Random Forest (RF), Support Vector Machine (SVM), Deep Belief Network (DBN), Bayesian Non-negative Matrix Factorization (BNMF) algorithm and Multiple Linear Regression (MLR). Optimisation techniques include Particle Swarm Optimization (PSO), Genetic Algorithm (GA) and Bayesian optimisation. The studies have further explored the use of the hybrid AI models such as the adaptive Neuro-Fuzzy Inference System (ANFIS) [95]–[98].

In evaluating the quality of prediction to assess model accuracy of the ANN models, there are different evaluation metrics commonly used to interpret the outcomes of the systems investigated or the outcomes of the studies. The evaluation metrics include the Correlation Coefficient (R), Coefficient of Determination ($R^2$), Coefficient of Variance (CoV), Mean Absolute Deviation (MAD), Mean Squared Error (MSE), Root Mean Square Error (RMSE), Mean Absolute Error (MAE), Mean Absolute Percentage Error (MAPE), Coefficient of Variation Root Mean Square Error (CVRMSE), Mean Bias Error (MBE), Normalized Mean Bias Error (NMBE), Average Relative Error (ARE) and Maximum error [94], [99]–[101].

## Literature review on the application of the ANN modelling to the heating and energy systems in buildings

From the given background, the background literature of the application of ANN modelling is presented in Table 2.1. the review focus on the heating and energy generation systems in buildings (residential/domestic, commercial and industrial). The review was focussed on systems that incorporating renewable energy and energy efficient technologies such as SH systems (e.g., solar thermal collectors, solar water heating (SWH) and photovoltaic-thermal (PV/T) systems) and HPs (e.g., air-source/air-to-water HP (ASHP/AWHP) and ground-source HP (GSHP)). Additionally, the systems integrating these systems with TES tanks, as well as the hybrid-source systems such as the SAHP systems, have also been reviewed. The ANN models, incorporated with the learning,

optimisation and training AI models, as mentioned above, have been indicated, as well as the findings of the studies conducted, particularly focussing on the evaluation metrics.

Table 2.1 Literature review of Machine learning application in heating systems

| Authors | ANN model | Study purpose | System/Technology - Application | Evaluation Metrics and ANN findings |
|---|---|---|---|---|
| Alnaqi et al. [106] | PSO and MLPNN | Evaluation and comparison of ANN models for performance prediction | Building-Integrated BIPV/T system - Thermal energy and power generation | • Best $R^2$ = 0.9997 (train and test)<br>• Lowest RMSE = 0.0175 (train), 0.0178 (test) |
| Al-Waeli et al. [107] | MLPNN | Prediction and evaluation of system performance | Several PV/T technologies - Thermal heating and electricity generation | • MSE = 0.0229 (train), 0.0282 (cross-val)<br>• Optimal MSE = Electrical (4.87%), Thermal (35.92%)<br>• MAE = Electrical (1.72%), Thermal (4.85%)<br>• R = Electrical (0.59), Thermal (0.58) |
| Lu et al. [100] | RF and BPNN | Evaluation and comparison of ANN model for system performance prediction | GSHP system - Thermal energy and cooling | • MRE: COP within 10% and EER within 15%<br>• RF over BPNN: CVRMSE (+3.3%), RMSE (+0.7%), MAD (+1.2%), MAPE (+1.2%) and $R^2$ (+1.3%) |
| Ghritlahre and Prasad [108] | MLPNN, GRNN and RBF | Comparing prediction performance of ANN models | Solar Air Heater (SAH) with absorber plates - Thermal heating | • $R^2$ (0.99999), MSE ($2.73 \times 10^{-6}$), RMSE (0.001652), MAE ($2.86 \times 10^{-4}$), ME (0.99998) and 98% errors within ±0.0024<br>• Average relative errors: MLP (0.8338%), GRNN (0.2317%) and RBF: (0.0914%) |
| Gunasekar et al. [109] | MLFFNN | Prediction of system energy performance | PV/T-Evaporator (PV/T-E) integrated with SAHP - Thermal heating and power generation | • Best: $R^2$ (0.9999)<br>• Lowest: RMS (0. 0139), CoV (0.0477) |
| Jovanović et al. [110] | MLPNN, RBFN and ANFIS | Performance prediction and comparison analysis of the ANN models. | Thermal energy systems - Thermal heating | • Best $R^2$: 0.9845 (ensemble AV, M1)<br>• Low MAPE: training - 3.44% (FFNN, M1), testing - 5.25% (FFNN, M3) |
| Park et al. [111] | ANN, DBN and MLR | Performance prediction, monitoring and | GSHP system - Thermal heating | • $R^2$: MLR model (0.9253) and Adjusted (0.9251) |

| | | | | |
|---|---|---|---|---|
| | | system optimisation | | • Prediction Accuracy (CVRMSE): MLR (3.56%) and ANN (1.75%) |
| Maltais and Gosselin [102] | RNN and RF | Performance and accuracy prediction of the system | SAHP system, with flat plate collectors - Thermal heating | • Overall demand prediction: RMSE (142.02 L/h) and $R^2$ (0.71)<br>• Filtered demand prediction: RMSE (29.22 L/h) and $R^2$ (0.99)<br>• Noise prediction: RMSE (145.20 L/h) and $R^2$ (0.78) |
| Kalani et al. [112] | RBFNN, MLPNN, ANFIS and PSO | Performance prediction of the system | Domestic hot water (DHW) system - Water heating | • All three models (MLPANN, RBFANN, ANFIS) were capable of accurate predictions |
| Jer y et al. [113] | ANN models | Performance prediction of the system to replace computational simulations | Vapor-injection ASHP system - Thermal heating and electricity generation | • Heat transfer prediction: MAE (1.67%) and $R^2$ (0.97)<br>• Entropy generation prediction: MAE (1.06%) and $R^2$ (0.99) |
| Yılmaz et al. [114] | MLFFNN | Performance evaluation of the system | Four PV/T system configurations - Thermal heating and electricity generation | • Performance: $5.13 \times 10^{-9}$ (training) and $9.4 \times 10^{-4}$ (testing) |
| Deka et al. [115] | MLPNN and LM algorithm | Performance prediction comparison of different system configurations | SAHP system - Water heating | • Best R-values (0.99843), Training phase MSE (0.3134) |
| Heidari and Khovalyg [116] | (ALSTM), (ALSTM-D) and FFNN (baseline model) | Prediction of energy use and advance prediction for improved prediction accuracy. | Grid-connected PV/T system - Water heating, thermal heating and electricity generation | • ALSTM-D: MSE (65% lower), MAE (41% lower). |
| Motahar and Bagheri-Esfeh [117] | MLPNN, FFNN and LM algorithm | Performance prediction of the system | Solar water heating system - Water heating | • R: training (0.9877), testing (0.9901), validation (0.9687) |
| Kulkarni et al. [118] | BPNN and LM algorithm | Performance prediction of the system | Geothermal heat exchanger - Thermal heating | • R-values: training (0.99998), validation (0.99998), testing (0.99974), overall (0.99991) |
| Wang et al. [119] | BRNN, BPNN and LM algorithm | Performance and accuracy prediction of the system | Solar-assisted heating system - Thermal heating and electricity generation | • CVRMSE, MAPE and NME are all below 10% in most cases.<br>• $R^2$ above 90%, |

| | | | | |
|---|---|---|---|---|
| Pang et al. [120] | ANN AND RNN | Prediction for enhancement of advanced controls and comparison of the ANN models | Solar trigeneration system of PV/T, auxiliary heater and absorption chiller - Thermal heating, cooling and electricity generation | • RNN: RMSE (26% improvement), CVRMSE (reduced from 9.83% to 7.64%), NMBE (improved from 0.9% to 0.2%). |
| Borhani et al. [121] | MLPNN | Forecasting of the daily power production | GSHP system with underground heat exchangers - Thermal heating | • EPP: $R^2$ (0.999), MAE (0.72) and MSE (0.872)<br>• Overall efficiency: $R^2$ (0.983), MAE (0.62) and MSE (1.896) and best RMSE (1.38) |
| Cho et al. [122] | ML models (ANN, Tree Ensemble, SVM) and Bayesian optimisation | Performance prediction and optimisation of the system | Vertical closed-loop GSHP system - Thermal heating | • Best: $R^2$ (0.9966), CVRMSE (0.0226%), average error (0.0041), max error (0.106) and 97.5% of errors within ±0.025. |
| Tangwe and Kusakana [104] | ANN and BPNN | Prediction performance assessment and optimisation of the system | AWHP system - Water heating | • MSE: training (0.0393), validation (0.0389), testing (0.078).<br>• R=0.9995<br>• Evaluated outputs (E and COP): R=0.9999 |
| Ma et al. [123] | MLPNN, SVM and RF | Performance prediction, system monitoring and comparison of the ANN models | SAHP system - Thermal heating | • Training set: MAE (2.42%), RMSE (4.01%), Max Error (0.73).<br>• Testing set: MAE (2.35%), RMSE (3.84%), Max Error (0.54). |

The studies highlight the shift towards the holistic, intelligent and energy-efficient system modelling, however, few studies conducted on the water heating technologies have been explored. Maltais and Gosselin [102], developed a predictive tool to control of domestic hot water systems to forecast demand use and reduce energy consumption. combining RNN for predicting the filtered domestic water heating (DHW) demand and a RF for noise component. The prediction achieved accuracy of 142.02 L/h and 0.71 for RMSE and $R^2$, respectively. Afram et al. [103] developed and applied ANN-based MPC for residential HVAC system with buffer tank water. A new BNMI algorithm was introduced to improve training performance, predicting thermal behaviour and optimizing temperature set-points for HVAC using MPC. From the results obtained, the MPC reduced operational costs by 6–

73% compared with fixed set-points, BNMI improved model accuracy by 6–59% over standard ANN and energy savings achieved varied seasonally.

Tangwe and Kanzumba [104] developed and train an ANN to predict electrical energy consumption and COP of a 1.2 kW split type AWHP using LM-BPNN. Relief F test ranking to identify primary and secondary input factors influencing outputs. The system obtained high correlation coefficients of 0.967, 0.962, 0.945 and 0.996 for training, validation, testing and evaluation, respectively. The MSE coefficients were 0.0393, 0.0389, 0.078 for training validation and testing, respectively. Additionally, low mean square errors indicating accurate prediction and deviation of ±0.019 between modelled and actual outputs. For overall findings, the system showed high prediction accuracy for both E and COP. Mathioulakis et al. [21] investigated the suitability of ANN to model and predict the performance of AWHPs using the three-layer FFNN with linear and log-sigmoid functions. The model was trained on experimental data from 900+ points to conduct the thermal modelling, performance prediction, and behaviour analysis of HPs. The overall findings indicated that the ANN model accurately predicts the AWHP performance, effective ANN structure was defined, and the model was suitable for simulation and behaviour analysis under varied conditions.

Liu et al. [105] used a machine learning-based high-throughput screening (HTS) method to design and screen water-in-glass evacuated tube SWH (WGET-SWH) with high heat collection rates. The study was aimed for design optimization of solar water heaters for improved heat collection efficiency. The ANN model to predict heat collection rates from possible design combinations comparing two new designs with 915 previous samples. The new designs showed experimentally higher heat collection rates of 11.32 and 11.44 MJ/m².

Kalogirou et al. [124] use ANN for predicting daily energy output and storage tank temperature of a large solar STES under typical operating conditions, supporting users in system evaluation and performance monitoring. ANN was trained on 226 days of experimental data to predict performance indicators. ANN was also compared with input-output model and multiple linear regression. From the results, $R^2 > 0.95$ for both predicted outputs and ANN outperformed multiple linear regression.

Eldokaishi et al. [125] investigate the potential of ANN modelling for predicting performance and optimizing design of a hybrid STES system, for water heating, integrated with PCMs. The ANN model was trained from a data validated numerical model with 39 ANN models tested using different sampling methods hyperparameter tuning performed.

ANN predicted 84,480 samples in 5 seconds vs 120 hours for numerical model and the optimized ANN achieved $R^2$ of 0.9999. Yaïci and Entchev [126] developed and validated an ANN model to predict the performance of a STES used for domestic hot water and space heating under various seasonal and weather conditions in Ottawa, Canada. The experimental data from STES operations over 22 months were used to train, validate, and test ANN models. Back-propagation algorithm with LM and scaled conjugate gradient (SCG) was applied and the optimal network had 10 inputs, 20 hidden neurons, and 8 outputs. The ANN results predicted stratified tank temperatures and solar fraction predictions within ±3% and ±10% errors and the mean relative errors ~1.09–1.18% and for solar fraction ~8.26%, respectively. LM outperformed SCG in network performance.

Heidari and Khovalyg [116] conducted a study of advance prediction model of the SAHP water heating systems in residential setup to predict the energy use of the system. The attention mechanism and decomposition of input time series data were integrated to improve the prediction accuracy. The FFNN model was used as baseline and compared with attention-base LSTM (ALSTM) without the decomposed data and with the decomposed data (ALSTM-D). The results obtained indicated the MSE of the FFNN to be 0.028 kW of ALSTM and the ALSTM-D obtaining significantly lower MSE that is 65% lower than the FFNN. Additionally, the MAE of the FFNN was 0.122 kW and 0.100 kW for the ALSTM, which was 25% lower than the FFNN, and the ALSTM-D was much lower at 41% lower than the FFNN.

## 2.4 DISCUSSION OF THE KEY-FINDINGS

The above studies from sections 2.2 and 2.3 highlight significant potential of waste heat recovery, solar energy and heat pump technologies to enhance the energy performance of healthcare buildings. These technologies bring solution to the issue of intensive energy use continuous operation throughout the day, and simultaneous operation of the energy demand systems or processes, which include the water heating production. These technologies are suitable for integrated energy solution that can capture utilised the waste heat, incorporate renewable and energy efficient resources and optimise system efficiency. From the studies reviewed, implementing WHR technologies consistently demonstrated the reductions in energy consumption, operational costs and $CO_2$ emissions. Additionally, these

solutions were shown to maintain or improve end user comfort which are critical in the healthcare environment. In general, the findings demonstrate that hospitals can achieve substantial improvements in energy efficiency, cost savings, and environmental performance by strategically adopting and integrating waste heat recovery, solar, and heat pump technologies.

In the context of energy management, integrating thermal energy storage (TES) with heating and cooling systems significantly enhances system flexibility, efficiency, and cost-effectiveness. The reviewed studies show that implementing TES systems as energy solutions enables peak shaving, load shifting, and improved matching of energy supply and demand. When integrated with optimal control strategies, TES systems reduce operational costs, flatten energy consumption, and maximize the benefits of intermittent renewable sources. Also, incorporating WHR, solar thermal systems and heat pumps further lowers fuel use and $CO_2$ emissions while improving system efficiency. Overall, the research consistently supports implementing TES alongside smart energy management and hybrid renewable technologies.

Studies where the WHR, TES systems, SAHP system (particularly the solar thermal systems such as evacuated tube collectors) and the optimal control and ToU pricing structure, in one collective approach are very limited, particularly in the commercial sector. Additionally, this approach has not been explored to the complex water heating system with TES tank feeding such a huge number of ESTWH systems.

Furthermore, the above reviewed studies show that ANN modelling is a powerful tool for prediction, optimising and designing thermal energy systems and also that the HPs, SWH, TES and SAHP technologies have been broadly explored. The ANN models have demonstrated superior performance over conventional correlations or regression models, capturing complex nonlinear relationships with high prediction accuracy. With key findings showing most studies reporting R and $R^2$ -values above 0.95 and low errors, particularly for the hybrid systems, which also highlighted the reduction of simulation times, enhancing the design, optimisation and real-time control feasibility. Additionally, the reviewed evaluation metrics highlight that ANNs proved ease of integration with hybrid ML/AI approaches providing reliable, fast, and scalable solutions for improving energy system performance and supporting sustainable energy design and operation strategies.

Although studies focusing solely on or incorporating the application of water heating systems were comparatively fewer, results of these studies have demonstrated the capabilities of modelling complex nonlinear relationships and optimising system configurations efficiently due to their consistency in achieving high prediction accuracies with minimal errors.

While the reviewed studies consistently demonstrate the potential of WHR, TES, SAHP systems, and ANN modelling to improve energy efficiency, reduce operational costs, and lower emissions, several limitations are evident. Most studies focus on individual technologies or simplified systems, with few exploring integrated approaches combining WHR, TES, SAHP, and optimal control in large-scale, complex water heating systems. Additionally, although ANN models achieve high predictive accuracy, their interpretability and generalisability across different building types and climates remain limited. These gaps highlight the need for studies, such as the present work, that consider fully integrated systems with real-world operational data and robust predictive modelling to address complex energy management challenges in commercial buildings.

## 2.5 SUMMARY

This chapter presented a review of background literature on energy management and optimal control of water heating processes, focusing on waste heat recovery (WHR), the application of thermal energy storage (TES), and the use of artificial neural network (ANN) modelling for system validation and accuracy analysis. The findings were discussed, and the following were highlighted:

From section 2.2, the reviewed studies on WHR technologies consistently highlight reductions in energy consumption, operational costs, and $CO_2$ emissions. These approaches are also shown to maintain or enhance end-user comfort, which is particularly important in healthcare facilities. Overall, the findings demonstrate that hospitals can achieve significant improvements in energy efficiency, cost savings, and environmental performance through the strategic adoption and integration of WHR, solar, and heat pump technologies. The studies further indicate that TES systems support peak shaving, load shifting, and improved alignment of energy supply and demand. When coupled with optimal control strategies, TES solutions reduce operational costs, smooth demand profiles, and maximize the use of

intermittent renewable sources. Integrating TES with WHR, solar thermal systems, and heat pumps further reduces fuel consumption and emissions while improving system efficiency. Collectively, the literature strongly supports the implementation of TES in combination with advanced energy management and hybrid renewable technologies.

In section 2.3, ANN models have also demonstrated strong potential, outperforming conventional correlations or regression-based methods by capturing complex nonlinear relationships with high prediction accuracy. Reported results consistently show R and $R^2$ values above 0.95 and low error margins, particularly in hybrid system applications.

Although these results have demonstrated the best solutions, it has therefore been indicated in this chapter of the limitations of implementation of the WHR, TES systems and SAHP systems incorporating the optimal control with ToU pricing signal, particularly for complex water heating systems such as the multifarious water heating system with TES system feeding makeup water to the 57 ESTWH network. This approach has been explored in this study the methodology is presented in the chapters that follow.

Despite the demonstrated potential of WHR, TES, SAHP systems, and ANN modelling to improve energy efficiency, operational costs, and emissions, several limitations remain. Most studies focus on individual technologies or simplified systems, with limited exploration of fully integrated approaches combining WHR, TES, SAHP, and optimal control in complex water heating systems. Furthermore, while ANN models provide high predictive accuracy, their interpretability and generalisability across different building types, climates, and operational conditions are sometimes constrained. These limitations suggest opportunities for future research to focus on integrated systems, real-world operational validation, and the development of models that balance predictive accuracy with interpretability.

# CHAPTER 3: DESCRIPTION OF DATA PARAMETERS AND MATHEMATICAL MODELLING OF THE PROPOSED SYSTEM

## 3.1 INTRODUCTION

In this chapter, the system model, data, and formulation of the proposed hybrid-source water heating system are presented. The proposed multifarious water heating systems incorporates hybrid-source WHR-TWS tanks integrated with an indirect (parallel mode) SAHP system that supplies preheated water to the multifarious ESTWH loads. WHR serves as the primary heat source for the TWS tanks, while the SAHP system provides supplementary heating to further raise the water temperature before it is supplied to the 57 ESTWH units.

This section describes the proposed model and data and presents the mathematical formulation.

## 3.2 DESCRIPTION OF THE DYNAMIC MODEL, DATA ACQUISITION, SIZING AND SIMULATION PARAMETERS

This section presents and describes the dynamic model of the proposed system and the underlying assumptions. The section is followed by a case study and datasets describing environmental conditions, water demands, and standard component sizes.

In this section, the dynamic model of the system and the associated assumptions are presented, followed by a description of the case study and the acquired datasets, and subsequently the component sizing and simulation parameters.

### Dynamic model description of the proposed system

This study focuses on the water heating process using thermal waste heat recovered from multifunctional chiller systems to preheat cold water supplied from the main building source to the TWS tanks. The TWS tanks serve as primary makeup water source to the multifarious electric water heating loads, consisting of 57 ESTWH systems.

The proposed process includes an ASHP unit and solar thermal collectors (STCs) operating as an indirect (parallel mode) SAHP system retrofitted to the TWS tanks that utilize waste heat recovered from the multifunctional chillers. The retrofitted system also provides supplementary heating to further increase the water temperature to the desired range (50–60 °C), thereby improving efficiency. Preheated water is supplied to the multifarious ESTWH loads, reducing or eliminating the need for electric resistive elements. As the hot water is drawn by the consumers, the cold water is then fed from the source into the TWS tanks, and the water heating process continues.

To simplify model development and reduce computational requirements, a single-tank model representing one ESTWH system and one TWS tank was developed (Figure 3.1).

The system modelling is limited to the ESTWH systems and TWS tanks, excluding the piping network. For modelling simplicity of the system, the following assumptions have been made:

- TWS and ESTWH tanks
  - The temperature distribution of the "hot water" inside each tank is assumed well-stratified during charging (when water is heated) and discharging (during the hot water withdrawals) [39], and the flow of the fluids is assumed to be steady as the changes in flow rate are assumed to be negligible.
  - The whole system, including the TWS tanks, is assumed to be well-insulated to minimize the standby losses, particularly during the idle periods for the ESTWH systems and only the standby and demand-related energy losses are modelled.
- For the heat pump unit:
  - The power demand rating and COP of the heat pump unit are assumed to vary from zero during idle operation to full rated power when activated.
  - Energy losses in the heat pump unit and circulating water are assumed negligible to minimize the number of loss parameters requiring estimation.
- For the solar thermal collectors and the evacuated tube collectors:
  - The thermal performance was integrated over the absorber area, assuming a uniform aperture area and consistent transmittance–absorptance product.

Only the heat losses from the collector manifold to the environment were considered.

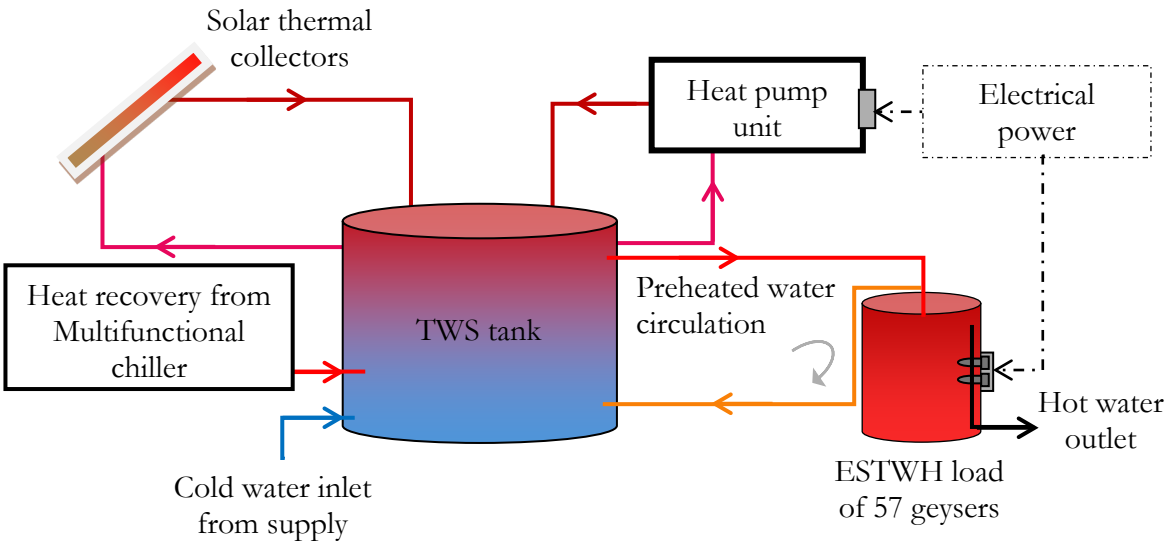


Figure 3.1. The schematic of the proposed water heating technology.

These assumptions balance modelling accuracy and computational efficiency, ensuring practicality for energy management and control development. Further refinements, such as heat loss calculations, may be added later for improved precision after validation.

**Case study and data acquisition**

The baseline system is based on an existing integration of the multifunctional chiller system and TWS tanks that recover waste heat in a high-capacity healthcare building. The current study focuses on the hot water production (pre-warmed water) by the multifunctional chiller, whereby the TWS tank is used to pre-warm the water supplemented to the multifarious ESTWH load.

The case study facility is a large healthcare institution in Bloemfontein, Free State Province. The facility includes 12 theatres, 383 beds (75 ICU), and an additional 22 beds pending medical admission. The main building covers approximately 10,500 m². The hospital's main water heating network comprises 57 ESTWH systems supplied with pre-warmed water from the WHR system. The layout of the multifarious ESTWH systems showing all the 57 ESTWH tanks is shown in Figure 3.2.

Figure 3.3 shows the components of the existing system installed at the Mediclinic Hospital building. The system shows one of the multifunctional chillers of the building which are linked to the two storage tanks by the water circulation pipes. These tanks are used

as TWS tanks to recover thermal heat from the multifunctional chillers and pumping the water through the circulation pumps shown. The three pumps are for the makeup water from the building water supply and the two circulation pumps for the preheated/hot water that supplies makeup water to the multifarious ESTWH loads. Lastly, the system controller box is also shown, that controls the operation of the system.

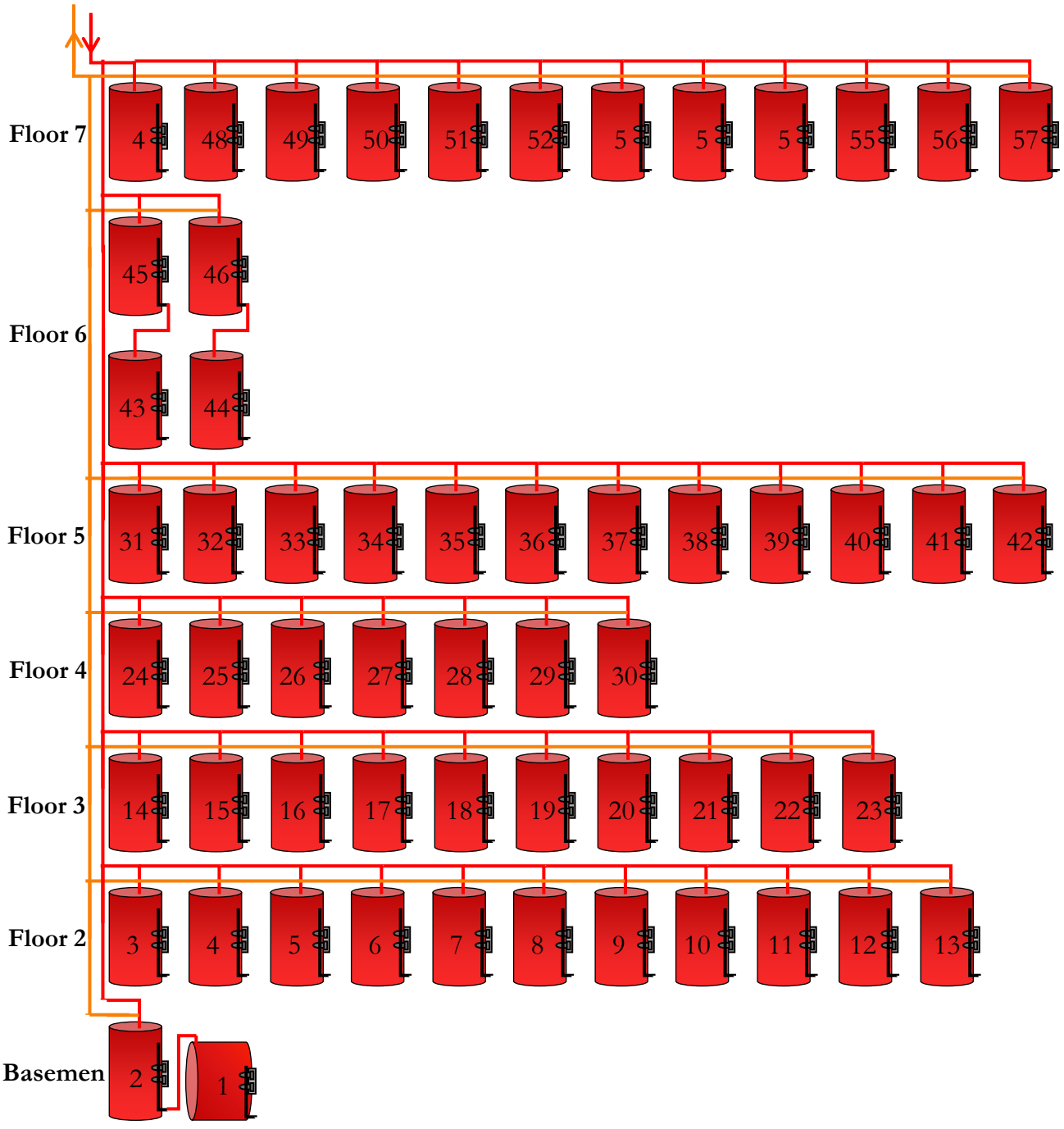


Figure 3.2. The layout of the ESTWH systems setup

The input data for the baseline and proposed models include pre-warmed water and ambient air temperatures, solar irradiance, and hot water demand profiles for summer and winter. Ambient temperature and solar irradiance data were obtained from SAURAN devices installed at the Central University of Technology (CUT) in Bloemfontein (Latitude – 29.121337, Longitude 26.215909, Elevation 1397 m), shown in Figure 3.4. The seasonal extremes of a typical day for each season were used, which occurred in the months of January 2024 and July 2024, respectively.


Figure 3.3. Heat recovery system installed at the Mediclinc Hospital, Bloemfontein.


Figure 3.4. SAURAN located at the Central University of Technology [17].

Different datasets were acquired, including weather conditions, water supply temperatures, and hot water demand data. Two sets of data were collected for each dataset which were of one typical extreme day of the summer season (hot) and one typical extreme day of the winter season (cold) weather conditions. The datasets were divided into 5-minute time intervals for the period of 24 hours in each day.

The first datasets acquired were ambient temperatures and total solar radiation, calculated from global, diffuse, and normal radiation readings. The profiles of the ambient temperatures and the average solar irradiances are presented in Figures 3.5 and 3.6 for the summer and winter seasons, respectively.

Additional datasets included profiles of pre-warmed water temperatures and water demand measured by the SCADA system within the building. These datasets were collected from the baseline system comprising the TWS tank and 57 ESTWH systems at the case study facility. The profiles of the pre-warmed water temperatures (inside the TWS tanks) and water demands (from the multifarious ESTWH systems) for the summer and winter seasons are presented in Figure 3.7 and 3.8.

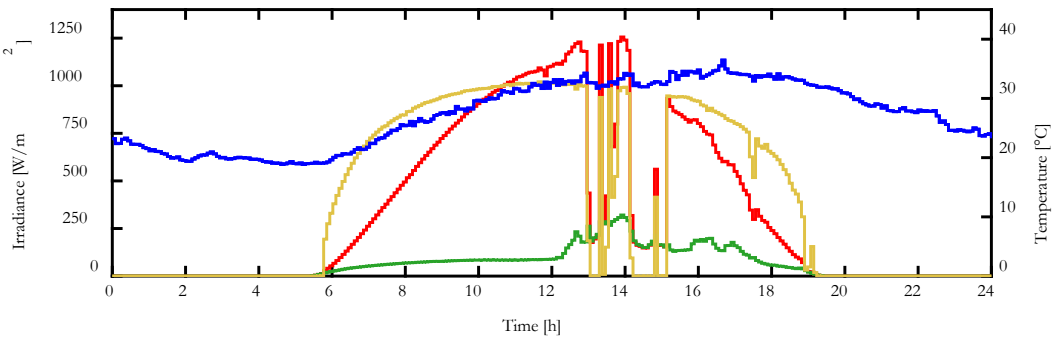


Figure 3.5. Ambient temperature and Solar irradiances for the summer season (January 2024).

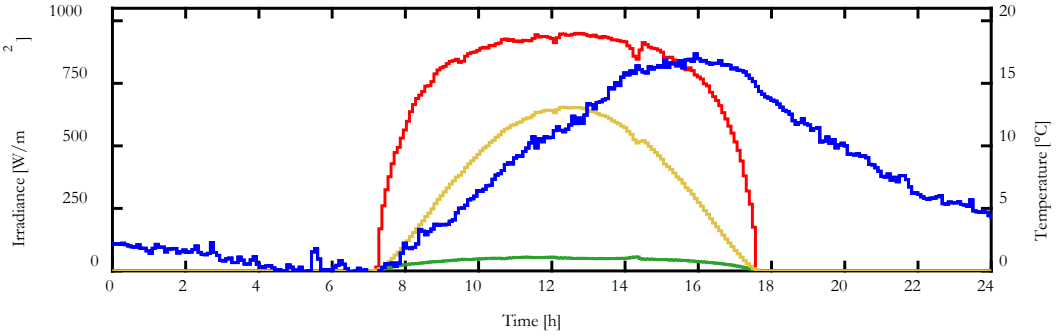


Figure 3.6. Ambient temperature and Solar irradiances for the winter season (July 2024).

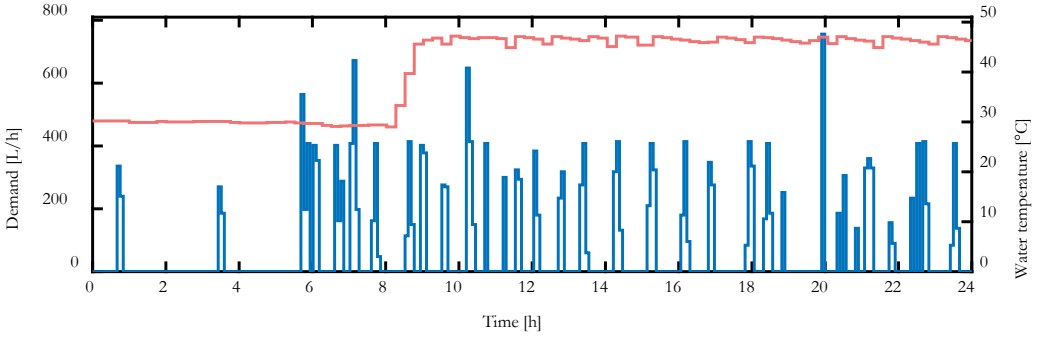


Figure 3.7. Pre-warmed water temperature and Hot water demand from multifarious ESTWH systems for the summer season.

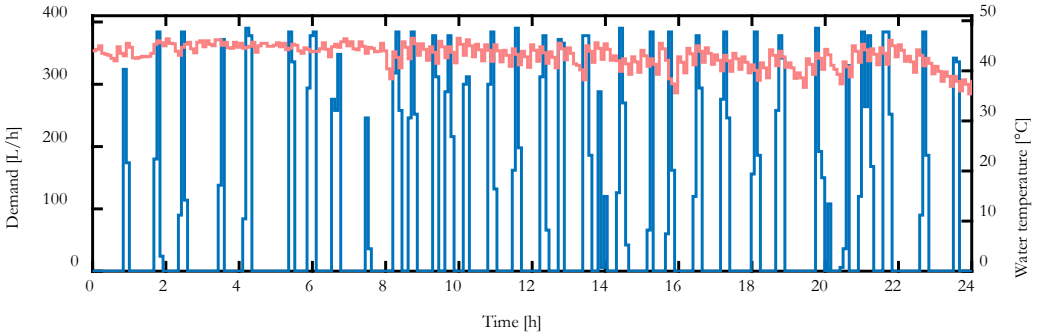


Figure 3.8. Pre-warmed water temperature and Hot water demand from multifarious ESTWH systems for the winter season.

**Component sizes and simulation parameters**

The rated specifications of the TWS tanks, ESTWH systems, ASHP unit, and STCs used for system sizing are presented in Tables 3.1 and 3.2. These are the main components of the baseline and proposed systems, and the specifications were obtained from the products, available online in South Africa.

The simulation parameters for sampling, time-of-use (ToU) structure, and tariff pricing are summarized in Tables 3.3 and 3.4, respectively

Table 3.1. Component parameters and sizes of storage tanks.

| Description | 100 L | 150 L | 200 L | 250 L | 2000 L |
|---|---|---|---|---|---|
| Diameter - D [m] | 0.543 | 0.543 | 0.596 | 0.596 | 1.44 |
| Height - H [m] | 0.93 | 1.32 | 1.33 | 1.64 | 2.12m |
| Area of the storage tank - $A_s$ [m²] | 2.05 | 2.72 | 3.05 | 3.62 | 12.88 |
| Specific capacity of water - $c_{p.w}$ [J/kg °C] | 4184 | 4184 | 4184 | 4184 | 4184 |
| Overall heat loss capacity - $U_s$ [W/ m² °C] | 0.20 | 0.19 | 0.16 | 0.12 | 0.04 |
| Electric resistive element - $P_{EL}$ [kW] | 2 | 3 | 4 | 4 | - |
| Number of storage tanks used | 18 | 19 | 18 | 2 | 2 |
| ESTWH desired temperature - $T_s$ [°C] | 55 | 55 | 55 | 55 | 55 |
| ESTWH minimum temperature - $T_{min}$ [°C] | 50 | 50 | 50 | 50 | 50 |
| ESTWH maximum temperature - $T_{max}$ [°C] | 60 | 60 | 60 | 60 | 90 |

Table 3.2. Component parameters and sizes of the ASHP unit and the STC.

| Description | Parameter | Value |
|---|---|---|
| **Heat Pump Unit** | | |
| Input power (kW) | $P_{hp}$ | 4.8 |
| Coefficient of performance (-) | COP | 4 |
| **Solar Thermal Collectors** | | |
| Specific heat capacity of the transfer fluid (J/kg°C) | $C_{p.c}$ | 3550 |
| Collector tube efficiency factor (-) | $\eta$ | 0.79 |
| Manifold area (m²) – [diameter = 60mm] | $A_{man}$ | 0.0007069 |
| Aperture area (m²) – [diameter = 60mm] | $A_{ap}$ | 1.808 |
| Absorber area (m²) – [diameter = 60mm] | $A_{abs}$ | 1.62 |
| Heat loss coefficient (W/m²°C) | $U_{coll\_Loss}$ | ≤ 0.60 |
| Absorptive Coefficient (-) | $\tau$ | 0.94 |
| Transmittance (-) | $\alpha$ | 0.92 |
| Foreground's albedo (-) | $\rho$ | 0.2 |
| Number of collectors used | - | 8 |

Table 3.3. Simulation parameters.

| Parameter | Description | Value |
|---|---|---|
| ts | Sampling time (min) | 5 |
| N | Control horizon (–) | 288 |
| Hours | Total hours in control horizon (hour) | 24 |

Table 3.4. Mega-flex single phase ToU tariff structure and pricing.

| Season | Months | Period | Time-of-use Periods | Rate (USD) |
|---|---|---|---|---|
| Low Demand (Summer) | September - May | Off-peak | 00:00–06:00, 22:00–24:00 | 8.76 |
| | | Standard | 06:00–07:00, 10:00–18:00, 20:00–22:00 | 9.39 |
| | | Peak | 07:00–10:00, 18:00–20:00 | 16.82 |
| High Demand (Winter) | June-August | Off-peak | 00:00–06:00, 22:00–24:00 | 10.41 |
| | | Standard | 09:00–17:00, 19:00–22:00 | 14.18 |
| | | Peak | 06:00–09:00, 17:00–19:00 | 23.20 |

## 3.3 MATHEMATICAL MODEL FORMULATION

This section presents the analytical formulation of the mathematical model used to determine temperature states in the TWS tank and ESTWH systems. Two separate models were developed, one for the TWS tank and the other for the ESTWH system, which represents each ESTWH of the multifarious ESTWH systems.

This section presents the mathematical models of the individual components of the TWS tank and the ESTWH system and then provides the mathematical discrete formulation of the hot water temperature in the TWS tank and the ESTWH system.

**Mathematical model of the proposed system: Heat energy formulation**

- Heat energy in the TWS tank.

The hot water demands from each storage tank of the multifarious ESTWHs systems causes hot water flow from the TWS tank. The hot water is then subsequently replaced by the hot water which is preheated through the thermal waste heat recovered from the multifunctional chillers. The pre-warmed water temperature from the waste heat recovered thermal heat is taken as the makeup water to the water inside the TWS tank. Whereby the pre-warmed water is further heated by the SAHP system simultaneously. The dynamic model of the TWS tank is, therefore, based on open energy balance, that leads to a differential equation which describes the average thermal response and is expressed as in Eq. (3.1) and is also demonstrated by the diagram in Figure 3.9 [127]:

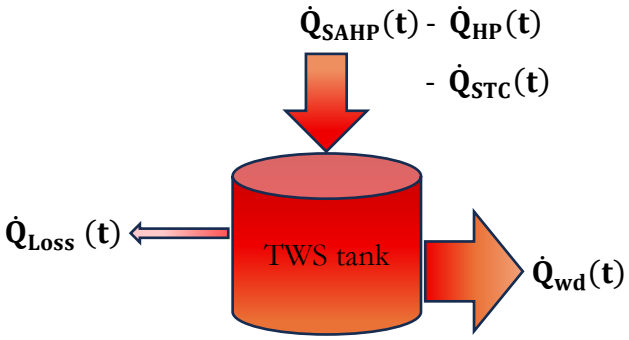


Figure 3.9. Parameters of the energy gains and energy losses in the TWS.

$$\dot{Q}_{TWS}(t) = \dot{Q}_{SAHP}(t) - \dot{Q}_{wd}(t) - \dot{Q}_{L-TWS}(t) \quad (3.1)$$

Where: $\dot{Q}_{TWS}(t)$ is the total thermal heating energy in the TWS tank; $\dot{Q}_{SAHP}(t)$ is the energy gain due to the thermal heat transfer from the retrofitted SAHP system; $\dot{Q}_{wd}(t)$ is the energy losses by the water drawn from the TWS tank to the ESTWHs and $\dot{Q}_{L}(t)$ is the standby heat losses of the TWS tank.

A. Solar-assisted heat pump (SAHP)

*A.1 Heat pump unit*

The thermal heat from the SAHP which incorporates the thermal heat gain from the heat pump ($\dot{W}_{hp}(t)$) unit and the solar thermal collectors ($\dot{Q}_{coll}(t)$) and is expressed as [127]:

$$\dot{Q}_{SAHP}(t) = \dot{W}_{hp}(t) + \dot{Q}_{coll}(t) \tag{3.2}$$

To calculate the heat supply of the heat pump to the TWS tank, considering the power input of the heat pump controlled by the switch ($S_{hp}(t)$) and is given as [127] [128]:

$$\dot{W}_{hp}(t) = COP \times P_{hp}t_{(h)}S_{hp}(t) \tag{3.3}$$

Where: $P_{hp}(t)$ is the input power to the heat pump (kW); $t_{(h)}$ is time of operation (hour) and $S_{hp}(t)$ is the control switch of the heat pump.

*A.2 Solar thermal collectors*

Evacuated tube solar thermal collectors are used for the study. The model of the collector that will be adopted from the model developed in [17], and is summarised based on the key components that are used in the study. For the calculations, the following was considered:

- ✓ The solar radiation is determined in terms of the isotropic diffuse model and is integrated over the whole absorber area of the collector.
- ✓ The aperture area is assumed to be the same throughout the thermal collector.
- ✓ Only the manifold heat losses to the environment were considered.

The energy balance of the collector may be calculated by the heat gain from the total radiation absorbed by the solar collector tubes ($G_{\beta}(t)$), integrated over the whole absorber area of the collector ($A_{abs}$), and the heat losses though the collector manifold, as shown in Eq. (3.4)

$$\dot{Q}_{coll}(t) = G_{\beta}(t)A_{abs}t_{(h)} - \dot{Q}_{man}(t)t_{(h)} \quad (3.4)$$

The total radiation absorbed by the solar collector tubes ($G_{\beta}(t)$) is analysed by Eq. (5):

$$G_{\beta}(t) = \tau\alpha\left[G_b \cos\theta_{\beta} + G_d(t)\left(\frac{1+\cos\beta}{2}\right) + \rho G_g(t)\left(\frac{1-\cos\beta}{2}\right)\right] \quad (3.5)$$

Where: ($\tau\alpha$) is the transmittance absorptance product, $G_b$ is the horizontal direct radiation ($W/m^2$); $G_d$ is the horizontal diffuse radiation ($W/m^2$); $G_g$ is the horizontal reflected radiation ($W/m^2$); $\theta_{\beta}$ incidence angle of beam radiation (°); $\beta$ is the tilt angle (°); $\rho$ is the foreground's albedo; and $A_{ap}$ is the collector aperture area ($m^2$).

The heat losses through the collector manifold ($\dot{Q}_{man}(t)$) is determined by Eq. (3.6):

$$\dot{Q}_{man}(t) = U_{Lm}A_m t_{(h)}\left[\frac{T_{f,o}(t) + T_{f,i}(t)}{2} - T_a(t)\right] \quad (3.6)$$

Where: ($U_{Lm}$) is the manifold heat loss coefficient from the manufacturer data ($W/m^2\,°C$); $A_m$ is the internal area of the manifold ($m^2$); ($T_{f.o}(t)$) and ($T_{f.i}(t)$) are the outlet and inlet temperatures of the heat transfer fluid (°C), respectively.

The ($T_{f.i}(t)$) is assumed to be in relation to the ambient temperature and ($T_{f.o}(t)$) is calculated by the following equation:

$$T_{f,o}(t) = 2\left[\frac{G_{\beta}(t)A_{abs}t_{(h)} + \eta I_{\beta}(t)A_{abs}t_{(h)}}{U_{Lm}A_m t_{(h)}} + T_a(t)\right] - T_{f,i}(t) \quad (3.7)$$

Where: $\eta$ is the tube efficiency of the collector.

($I_{\beta}(t)A_{abs}$) is the total incidence radiation of the solar collector tubes is given in as:

$$I_{\beta}(t)A_{abs} = A_{ap}\left[G_b \cos\theta_{\beta} + G_d(t)\left(\frac{1+\cos\beta}{2}\right) + \rho G_g(t)\left(\frac{1-\cos\beta}{2}\right)\right] \quad (3.8)$$

Where: $A_{ap}$ is the aperture area of a collector.

The energy balance of the collector may therefore be expressed by substituting Eqs. (3.5) and (3.6) into Eq. (3.4):

$$\dot{Q}_{coll}(t) = A_{abs}t_{(h)}\tau\alpha\left[G_b\cos\theta_\beta + G_d(t)\left(\frac{1+\cos\beta}{2}\right) + \rho G_g(t)\left(\frac{1-\cos\beta}{2}\right)\right] - U_{Lm}A_m t_{(h)}\left[\frac{T_{f,o}(t)+T_{f,i}(t)}{2} - T_a(t)\right] \quad (3.9)$$

For the SAHP system, by substituting Eqs. (3.3) and (3.9) into by Eq. (3.2) and for simplification, keeping the energy balance of the collector as $\dot{Q}_{coll}(t)$, energy balance is given as:

$$\dot{Q}_{SAHP}(t) = \dot{Q}_{coll}(t) + COP \times P_{hp}t_{(h)}S_{hp}(t) \quad (3.10)$$

B. Make-up water losses

The hot water drawn from the TWS tank to the ESTWHs ($\dot{Q}_{wd}(t)$) occur as a makeup water when water is drawn from the ESTWHs by the end users and the energy losses due to the makeup water fill up is given as follows [127]:

$$\dot{Q}_{wd}(t) = \dot{m}_{TWS}(t)C_{p,w}[T_{TWS}(t) - T_{pre}(t)] \quad (3.11)$$

Where: $\dot{m}_{TWS}(t)$ is the flow rate of the water drawn from the TWS tank (kg/s), $\dot{T}_{TWS}(t)$ is the variable temperature of the water inside the TWS tank (°C) and $T_{pre}(t)$ is the temperature of the pre-warmed water by the heat recovered from the Multifunctional chillers.

C. Standby losses for the TWS tank

The standby losses, $\dot{Q}_L(t)$, denote power losses resulting from the surface conduction of the casing material and is given as in Eq. (3.12)[128]:

$$\dot{Q}_{L-TWS}(t) = U_{TWS}t_{(h)}A_{TWS}[T_{TWS}(t) - T_a(t)] \quad (3.12)$$

Where: $U_{TWS}$ is the coefficient of the heat loss of the TWS tank in (W/m² °C) and $A_{TWS}$ is the surface area of the TWS tank (m²).

D. TWS tank

The energy balance of the TWS tank ($Q_{TWS}(t)$), may also be expressed as a first derivative differential function, representing the heat energy in the TWS tank equates to the following [128]:

$$\dot{Q}_{TWS}(t) = M_{TWS}C_{p,w}\dot{T}_{TWS}(t) \tag{3.13}$$

Where: $\dot{M}_{TWS}(t)$ is the mass of the water inside the TWS tank (kg/s and $C_{p,w}$ is the specific heat capacity of water (J/kg °C).

By substituting Eqs. (3.10)- (3.13)into (3.1), the energy balance of the TWS tank becomes:

$$\begin{aligned} M_{TWS}C_{p,w}\dot{T}_{TWS}(t) &= \dot{Q}_{coll}(t) + COP \times P_{hp}t_{(h)}S_{hp}(t) - \dot{m}_{TWS}(t)C_{p,w}[T_{TWS}(t) - T_{pre}(t)] \\ &\quad - U_{TWS}t_{(h)}A_{TWS}[T_{TWS}(t) - T_a(t)] \end{aligned} \tag{3.14}$$

To determine the variable temperature profile of the of the water inside the TWS tank, the variables of the state space equation are derived from the Eq. (3.15). This method is adopted from the study [128] and has been modified to the relevance of the current study.

The temperature of the water inside the storage tank $\dot{T}_{TWS}$ is isolated as the state variable and made the subject of the formula:

$$\dot{T}_{TWS}(t) = \frac{\dot{Q}_{coll}(t)}{M_{TWS}C_{p,w}} + COP \times \frac{P_{hp}t_{(h)}S_{hp}(t)}{M_{TWS}C_{p,w}} - \frac{\dot{m}_{TWS}(t)C_{p,w}[T_{TWS}(t) - T_{pre}(t)]}{M_{TWS}C_{p,w}} - \frac{U_{TWS}t_{(h)}A_{TWS}[T_{TWS}(t) - T_a(t)]}{M_{TWS}C_{p,w}} \tag{3.15}$$

To simplify:

$$\dot{T}_{TWS}(t) = \frac{\dot{Q}_{coll}(t)}{M_{TWS}C_{p,w}} + COP \times \frac{P_{hp}t_{(h)}S_{hp}(t)}{M_{TWS}C_{p,w}} - \frac{T_{TWS}(t)\left[\dot{m}_{TWS}(t)C_{p,w} + U_{TWS}t_{(h)}A_{TWS}\right]}{M_{TWS}C_{p,w}} + \frac{\dot{m}_{TWS}(t)C_{p,w}T_{pre}(t) + U_{TWS}t_{(h)}A_{TWS}T_a(t)}{M_{TWS}C_{p,w}} \quad (3.16)$$

Eq.(3.16), is separated into the following components, as shown in Eqs. (3.17) – (3.19)so that a state space equation is formulated:

$$A_{TWS}(t) = \frac{\left[\dot{m}_{TWS}(t)C_{p,w} + U_{TWS}t_{(h)}A_{TWS}\right]}{M_{TWS}C_{p,w}} \quad (3.17)$$

$$B_{TWS} = COP \times \frac{P_{hp}t_{(h)}}{M_{TWS}C_{p,w}} \quad (3.18)$$

$$\gamma_{TWS}(t) = \frac{\dot{Q}_{coll}(t)}{M_{TWS}C_{p,w}} + \frac{\dot{m}_{TWS}(t)C_{p,w}T_{pre}(t) + U_{TWS}t_{(h)}A_{TWS}T_a(t)}{M_{TWS}C_{p,w}} \quad (3.19)$$

The state space equation has three variables which are the state variable ($\dot{T}_{TWS}$), the control or decision variables ($S_{hp}(t)$) and the disturbance variable in the system ($\gamma_{TWS}$) and the expression is given in Eq. (3.20):

$$\dot{T}_{TWS}(t) = -A_{TWS}(t)T_{TWS}(t) + B_{TWS}S_{hp}(t) + \gamma_{TWS}(t) \quad (3.20)$$

- Heat energy balance in the ESTWH system.

The process of developing the model of the ESTWH tank is the same as of the TWS tank in this Section, however, the method slightly differs as some of the components employed on the previous model differ or may not be used for this model.

A single ESTWH system is modelled, which assumes that the same operation is the same for the whole multifarious setup. The makeup water from the TWS tank enters the multifarious ESTWH systems at a high temperature supplemented by the thermal energy gains in the TWS tank, which may be higher than the desired maximum or slightly higher. The open energy balance for the ESTWH system is expressed as the thermal energy gain from the electric resistive element ($\dot{Q}_{EL}(t)$) and the energy losses due to hot water demand ($\dot{Q}_{D}(t)$) and standby losses ($\dot{Q}_{L}(t)$), as demonstrated in Figure 3.10.

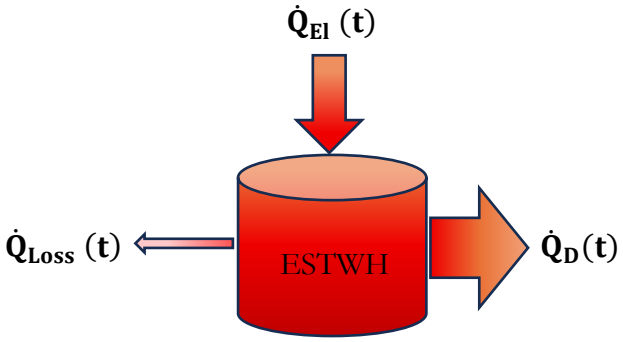


Figure 3.10. Parameters of the energy gains and energy losses in each ESTWH system.

The resulting energy balance ($\dot{Q}_S(t)$) equation, with the heat gains and losses in the system, is given in Eq. (3.21):

$$\dot{Q}_S(t) = \dot{Q}_{EL}(t) - \dot{Q}_D(t) - \dot{Q}_L(t) \tag{3.21}$$

A. Electric resistive element

The electric resistive element serves as a backup energy source to enhance hot water availability in the event of low thermal energy from the solar-assisted heat pump system. Therefore, electrical energy ($\dot{Q}_{EL}(t)$) will be supplied to the electric resistive element, which is controlled by the switch $S_{EL}(t)$, to sustain the desired temperature, as presented:

$$\dot{Q}_{EL}(t) = P_{EL}t_{(h)}S_{EL}(t) \tag{3.22}$$

Where: $P_{EL}$ is the input power to the electric resistive element of the storage tank (kW); $S_e(t)$ is the control switch of the electric resistive element of the storage tank.

B. Demand losses

For the baseline case, the heat losses in the ESTWH are caused by the makeup water which enters at a low temperature whenever there is hot water demand draw-offs occurring. As a result, there is temperature decrease inside the ESTWH system when cold water flows into the tank to maintain a consistent volume. However, in this case the makeup water mostly, if not always, enters at a temperature equal or slightly higher than the maximum

desired (set) temperature. The thermal energy losses of the hot water demand $Q_D(t)$ is, therefore, given in Eq. (3.23):

$$\dot{Q}_D(t) = \dot{W}_D(t)C_{p,w}[T_{TWS}(t) - T_S(t)] \quad (3.23)$$

Where: $\dot{W}_D$ is the variable hot water demand mass flow rate (kg/h).

C. Standby losses for each ESTWH system

The other losses in the ESTWH are standby losses, $\dot{Q}_L(t)$, for the ESTWH given as in Eq. (3.24):

$$\dot{Q}_L(t) = U_S t_{(h)} A_S[T_S(t) - T_a(t)] \quad (3.24)$$

C. ESTWH system

The energy balance ($Q_S(t)$), expressed as a first derivative differential function, representing the heat energy in the ESTWH equates to the following:

$$\dot{Q}_S(t) = M_w C_{p,w} \dot{T}_S(t) \quad (3.25)$$

Where: $M_w$ is the mass of water inside the storage tank (kg) and $\dot{T}_S(t)$ is the variable temperature of the water inside the ESTWH system (°C).

Substituting all variables and coefficients (parameters) from Eqs. (3.22) – (3.25), into the energy balance, Eq. (3.21), result in Eq. (3.26):

$$M_w C_{p,w} \dot{T}_S(t) = P_{EL} t_{(h)} S_{EL}(t) - \dot{W}_D(t) C_{p,w}[T_{TWS}(t) - T_S(t)] - U_S t_{(h)} A_S[T_S(t) - T_a(t)] \quad (3.26)$$

For simplification:

$$M_w C_{p,w} \dot{T}_S(t) = P_{EL} t_{(h)} S_{EL}(t) - [U_S t_{(h)} A_S - \dot{W}_D(t) C_{p,w}] T_S(t) - \dot{W}_D(t) C_{p,w} T_{TWS}(t) + U_S t_{(h)} A_S T_a(t) \quad (3.27)$$

The temperature of the water inside the storage tank $\dot{T}_S$ is isolated as the state variable and made the subject of the formula:

$$\dot{T}_S(t) = \frac{P_{EL}t_{(h)}}{M_w C_{p,w}} S_{EL}(t) - \frac{\left[U_S t_{(h)} A_S - \dot{W}_D(t) C_{p,w}\right]}{M_w C_{p,w}} T_S(t) - \frac{\dot{W}_D(t) C_{p,w} T_{TWS}(t)}{M_w C_{p,w}} + \frac{U_S t_{(h)} A_S T_a(t)}{M_w C_{p,w}} \quad (3.28)$$

Separating Eq. (3.28) into the following system variables, as shown in Eqs. (3.29) – (3.31) so that a state space equation is formulated:

$$A_s(t) = \frac{\left[U_s t_{(h)} A_s - \dot{W}_D(t) C_{p,w}\right]}{M_w C_{p,w}} \quad (3.29)$$

$$B_s = \frac{P_{EL}t_{(h)}}{M_w C_{p,w}} \quad (3.30)$$

$$\gamma_s(t) = \frac{U_s t_{(h)} A_s T_a(t)}{M_w C_{p,w}} - \frac{\dot{W}_D(t) C_{p,w} T_{TWS}(t)}{M_w C_{p,w}} \quad (3.31)$$

In the state space equation, given by Eq. (3.32), the variables are the state variable ($\dot{T}_S$), the control or decision variable is ($S_{el}(t)$) and the disturbance variable in the ESTWH system ($\gamma_S$):

$$\dot{T}_S(t) = -A_S(t) T_S(t) + B_S S_{el}(t) + \gamma_S(t) \quad (3.32)$$

**Discretized hot water temperature**

Eq. (3.33) is a function that is continuous, with an infinite number of degrees of freedom and is to be conveyed into its general discrete formulation, in terms of the $k^{th}$ hot water equation. This, of course, brings limitations to the degrees of freedom. Due to the limited nature of the subsequent calculating procedures, the restriction is essential. Function spaces have an unlimited dimension since they are required to supply all potential solutions for the boundary and initial conditions. As a result, discretization is necessary to generate a

function space in which a realistic finite number of base functions providing appropriate approximations to the analytical solution may be determined [128].

$$T_{k-1} = T_k(1 - t_s A_k) + t_s B S_k + t_s \gamma_k \tag{3.33}$$

Where $k$ denotes the variation of temperature inside the hot water storage tank.

The state variable, $T_{k+1}$ may be conveyed in terms of its initial value, $T_0$ and the control variable, $S_e(t)$, of the initial, $T_{k+1}$ at every interval, is first obtained as [128]:

When substituting $k = 0$, the expression of Eq. (3.33) is simplified to $T_1$ in Eq.(3.34):

$$T_{0-1} = T_1 = T_0(1 - t_s A_0) + t_s B S_0 + t_s \gamma_0 \tag{3.34}$$

Correspondingly, when $k = 1$, $T_2$ is given by:

$$T_2 = T_1(1 - t_s A_1) + t_s B S_1 + t_s \gamma_1 \tag{3.35}$$

Substitute $T_1$ of Eq. (3.34)into $T_2$ Eq. (3.35), to achieve Eq. (3.36):

$$T_2 = [T_0(1 - t_s A_0) + t_s B S_0 + t_s \gamma_0](1 - t_s A_1) + t_s B S_1 + t_s \gamma_1 \tag{3.36}$$

Simplifying Eq. (3.36), to get the following expression:

$$T_2 = T_0(1 - t_s A_0)(1 - t_s A_1) + [(1 - t_s A_1)S_0 + S_1]Bt_s + [(1 - t_s A_1)\gamma_0 + \gamma_1]t_s \tag{3.37}$$

Furthermore, when $k = 2$, $T_3$ will be denoted in by:

$$\begin{aligned} T_3 = {} & T_0(1 - t_s A_0)(1 - t_s A_1)(1 - t_s A_2) \\ & + [(1 - t_s A_1)(1 - t_s A_2)S_0 + (1 - t_s A_2)S_1 + S_2]Bt_s \\ & + [(1 - t_s A_1)(1 - t_s A_2)\gamma_0 + (1 - t_s A_2)\gamma_1 + \gamma_2]t_s \end{aligned} \tag{3.38}$$

The state space equation may be created, using the energy balance equation. To show how the temperature of the water inside the storage tank changes, the continuous

temperature function ($\dot{T}_k$) is converted into a generic discrete formulation, yielding Eq. (3.39):

$$T_{(z),k+1} = T_{(z),0}\prod_{j=0}^{k}\left(1 - t_s A_{(z),j}\right) + t_s B_{(z)}\sum_{j=0}^{k} S_{(y),j}\prod_{i=j+1}^{k}\left(1 - t_s A_{(z),j}\right) + t_s\sum_{j=0}^{k}\gamma_{(z)}\prod_{i=j+1}^{k}\left(1 - t_s A_{(z),j}\right) \quad (3.39)$$

Where: z indicates either the TWS tank or ESTWH system and y indicates the switching of either the heat pump unit or the electric resistive element, respectively.

## 3.4 SUMMARY

The first part of this chapter describes the proposed hybrid-source WHR-TWS system integrated with the indirect (parallel mode) SAHP system that supplies preheated water to the multifarious ESTWH loads. The case study presented the datasets of hot water temperatures, demand profiles, and environmental conditions, along with component sizing and simulation parameters.

The second part presents the mathematical formulations of the energy balance of the TWS tanks and the ESTWH systems of the proposed system. The energy balance formulations are rearranged to develop the discretised hot water temperature of the water inside the TWS tanks and the ESTWH systems.

All data and parameters developed in this chapter, including the discretized temperature formulations, will be applied in chapters 4 and 5.

The following chapter will present the formulation of the energy management and optimal control algorithm and the simulation parameters.

# CHAPTER 4: RESULTS OF THE SYSTEM PERFOMANCE AND THE ECONOMIC ANALYSIS OF THE PROPOSED SYSTEM AND THE BASELINE SYSTEM

## 4.1 INTRODUCTION

This chapter formulates the control problem of the proposed system using the mathematical models of the TWS tanks and ESTWH systems under the ToU tariff structure to optimize the hybrid-source water-heating system. The baseline and optimally controlled systems were simulated and compared, and an economic analysis was performed to evaluate potential energy-cost savings.

Section 4.2 presents the mathematical model formulation for the optimisation control of the proposed system. The simulation results of operation for the baseline and the proposed systems are presented and analysed in Section 4.3. This is followed by a cost analysis of the two systems in Section 4.4. Finally, the summary of the Chapter is presented in Section 4.5.

## 4.2 FORMULATION OF THE OPTIMIZATION CONTROL PROBLEM

This section outlines the mathematical formulation of the optimization control problem, including the objective functions, constraints, and solver conditions.

This section defines the objective functions, presents the temperature constraints of the TWS tanks and ESTWH systems and explains the solver and control problem.

### Objective functions

Figure 4.1 presents the time-based tariff chart illustrating the Time-of-Use (ToU) tariff periods structure. The low-demand chart is used for the summer season, during the months of September to May, whereas the high-demand chart is used for the winter season during the months of June to August [129]. The ToU tariff periods were the primary basis for developing the objective function, aimed at minimizing energy costs for the compressor and electric resistive elements by activating them during low-cost periods.

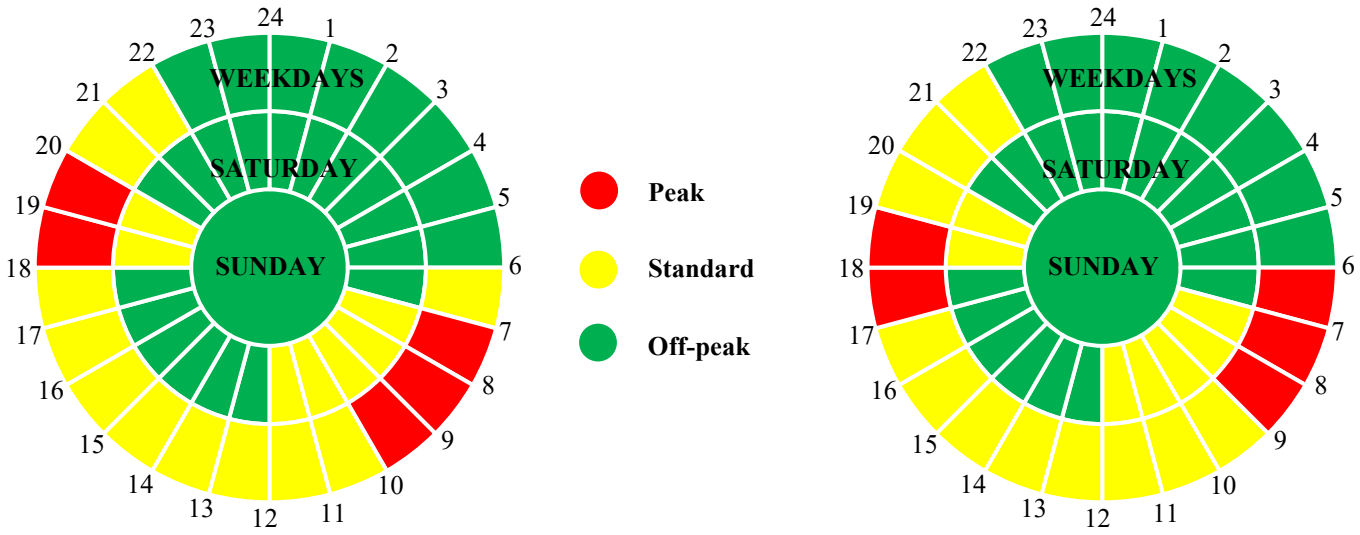


(a) Summer season (b) Winter season

Figure 4.1. Time-of-Use tariff Periods [129]

The purpose of optimisation control is to minimize the cost of the energy supplied to the multifarious ESTWH loads within the building and the integrated heat pump unit. This method may be divided into two objective functions: a primary and secondary objective. The primary objective may be achieved by minimizing the cost of energy subjected to the ToU tariff. The secondary objective is to mitigate simultaneous switching of the ESTWHs and reduce the maximum demand to within acceptable limits [130].

- Primary objective functions

Fundamentally, the control algorithm is designed to determine the switching solution that shifts the energy usage of the system to the low-cost regions while avoiding the peak periods. By incorporating the power rating, the value of the objective function after optimisation will be equal to the total energy cost incurred [130]. Therefore, the primary objective function minimizes the energy costs associated with the electric resistive elements of the multifarious ESTWH systems as given in Eq. (4.1).

$$\min J_{EL,t} = t_s\left(\sum_{k=1}^{N} P_{EL(1),k}S_{EL(2),k} \times p_k + \sum_{k=1}^{N} P_{EL(1),k}S_{EL(2),k} \times p_k + \cdots + \sum_{k=1}^{N} P_{EL(N),k}S_{EL(N),k} \times p_k\right) + t_s \times p_{k,MAX}\sum_{k=1}^{N}\left(P_{EL(1),k}S_{EL(2),k} + P_{EL(1),k}S_{EL(2),k} + \cdots + P_{EL(N),k}S_{EL(N),k}\right) \quad (4.1)$$

Where $t_s$ is the sample time (hours); $N$ is the 24-hour period; $P_{EL(N),k}$ are the input powers of the electric resistive elements (kW); $S_{EL(N),k}$ are the switching function statuses of the electric resistive elements; $p_k$ is the ToU price function (USD/kWh); $p_{k,MAX}$ is the maximum demand costs.

- Secondary objective functions

The introduction of the heat pump serves to reduce the costs of the electric resistive elements. Furthermore, the heat pump's power rating is incorporated to determine the total energy cost incurred after optimisation. The secondary objective function, which governs the cost minimisation of the heat pump, is defined by Eq. (4.2).

$$\min J_{hp,t} = t_s\sum_{k=1}^{N}\left(COP \times P_{hp,k}S_{hp,k}\right) \times p_k + t_s \times p_{k,MAX}\sum_{k=1}^{N}\left(COP \times P_{hp,k}S_{hp,k}\right) \quad (4.2)$$

Where $t_s$ is the sample time (hours); $P_{hp,k}$ is the input power to the heat pump unit (kW); $S_{hp,k}$ is the switching function status of the heat pump.

- Aggregate objective functions

The aggregate objective function combines Eqs. (4.1) and (4.2) to represent the total energy cost costs incurred (Eq. 4.3).

$$\min J = t_s\left(\sum_{k=1}^{N} P_{EL(1),k}S_{EL(2),k} \times p_k + \sum_{k=1}^{N} P_{EL(1),k}S_{EL(2),k} \times p_k + \cdots + \sum_{k=1}^{N} P_{EL(N),k}S_{EL(N),k} \times p_k\right) + t_s \times p_{k,MAX}\sum_{k=1}^{N}\left(P_{EL(1),k}S_{EL(2),k} + P_{EL(1),k}S_{EL(2),k} + \cdots + P_{EL(N),k}S_{EL(N),k}\right) + t_s\sum_{k=1}^{N}(COP \times P_{hp,k}S_{hp,k}) \times p_k + t_s \times p_{k,MAX}\sum_{k=1}^{N}(COP \times P_{hp,k}S_{hp,k}) \quad (4.3)$$

The aggregate objective function (Eq. 4.3) is a non-linear mixed-integer function with binary control variables requiring solution for the optimal switching status of the heat-pump and resistive elements[130].

**Constraints on the state of temperatures inside the TWS tank and the ESTWH system**

The switching status variable is binary (1 = ON, 0 = OFF), delivering either full-rated power or none to the heating units as required [128]. The switching functions of the heat pump unit and the multifarious ESTWH systems are defined by Eq. (4.4).

$$S_{hp,k}\epsilon\{0,1\}$$
$$S_{el,k}\epsilon\{0,1\} \quad (4.4)$$

Therefore, the objective functions are subject to the following temperature constraints (Eqs. 4.5 and 4.6).

$$T_k^{min} \leq T_{(z),0}\prod_{j=0}^{k}(1 - t_sA_{(z),j}) + t_sB_{(z)}\sum_{j=0}^{k}S_{(z),j}\prod_{i=j+1}^{k}(1 - t_sA_{(z),j}) + t_s\sum_{j=0}^{k}\gamma_{(z)}\prod_{i=j+1}^{k}(1 - t_sA_{(z),j}) \quad (4.5)$$

$$T_{(z),0}\prod_{j=0}^{k}(1 - t_sA_{(z),j}) + t_sB_{(z)}\sum_{j=0}^{k}S_{(z),j}\prod_{i=j+1}^{k}(1 - t_sA_{(z),j}) + t_s\sum_{j=0}^{k}\gamma_{(z)}\prod_{i=j+1}^{k}(1 - t_sA_{(z),j}) \leq T_k^{max} \quad (4.6)$$

Where z represents either the TWS tank or ESTWH system; $T_k^{min}$ is the minimum permissible temperature for the hot water inside the TWS tank and ESTWH system; and $T_k^{max}$ is the maximum threshold that the temperature must not exceed, for any given interval.

The general expression attained in Eqs. (3.20) and (3.32), represent the actual temperatures of the water in the TWS tank and ESTWH system, respectively. These constraints maintain the water temperatures of the TWS tank and ESTWH system within desired operational limits [130].

**Proposed optimization solver and optimal control problem**

The objective function is nonlinear with integrated binary control variables and is solved to determine the optimal switching scheme for the heat pump and ESTWH systems. The universal Solving Constraint Integer Programs (SCIP) solver in the MATLAB optimization toolbox may then be used to solve this type of problem, as shown in Eq. (4.7) [17]:

$$\begin{gathered} \min_x f(x) \\ \text{Subject to: } Ax \leq b \\ A_{eq}x = b_{eq} \\ lb \leq x \leq ub \\ c(x) \leq d \\ c_{eq}x = d_{eq} \\ x_i \in \mathbb{Z} \\ x_j \in \{0,1\} \end{gathered} \tag{4.7}$$

Where $f(x)$ is the objective function; $Ax \leq b$ is the linear inequality constraint; $A_{eq}x = b_{eq}$ is the linear equality constraint; $lb \leq x \leq ub$ is the decision variable bounds; $c(x) \leq d$ is the nonlinear inequality constraint; $c_{eq}(x) = d_{eq}$ is the nonlinear equality constraints; $x_i$ is an integer number decision variable; $x_j$ is a binary number decision variable.

The objective function is expressed as f(x). No linear inequality or equality constraints present; the decision variables are binary (1 or 0), as shown in Eqs. (4.8) and (4.9) [128].

$$lb^T = [0 \ldots 0_N] \tag{4.8}$$

$$ub^T = [1 \ldots 1_N] \tag{4.9}$$

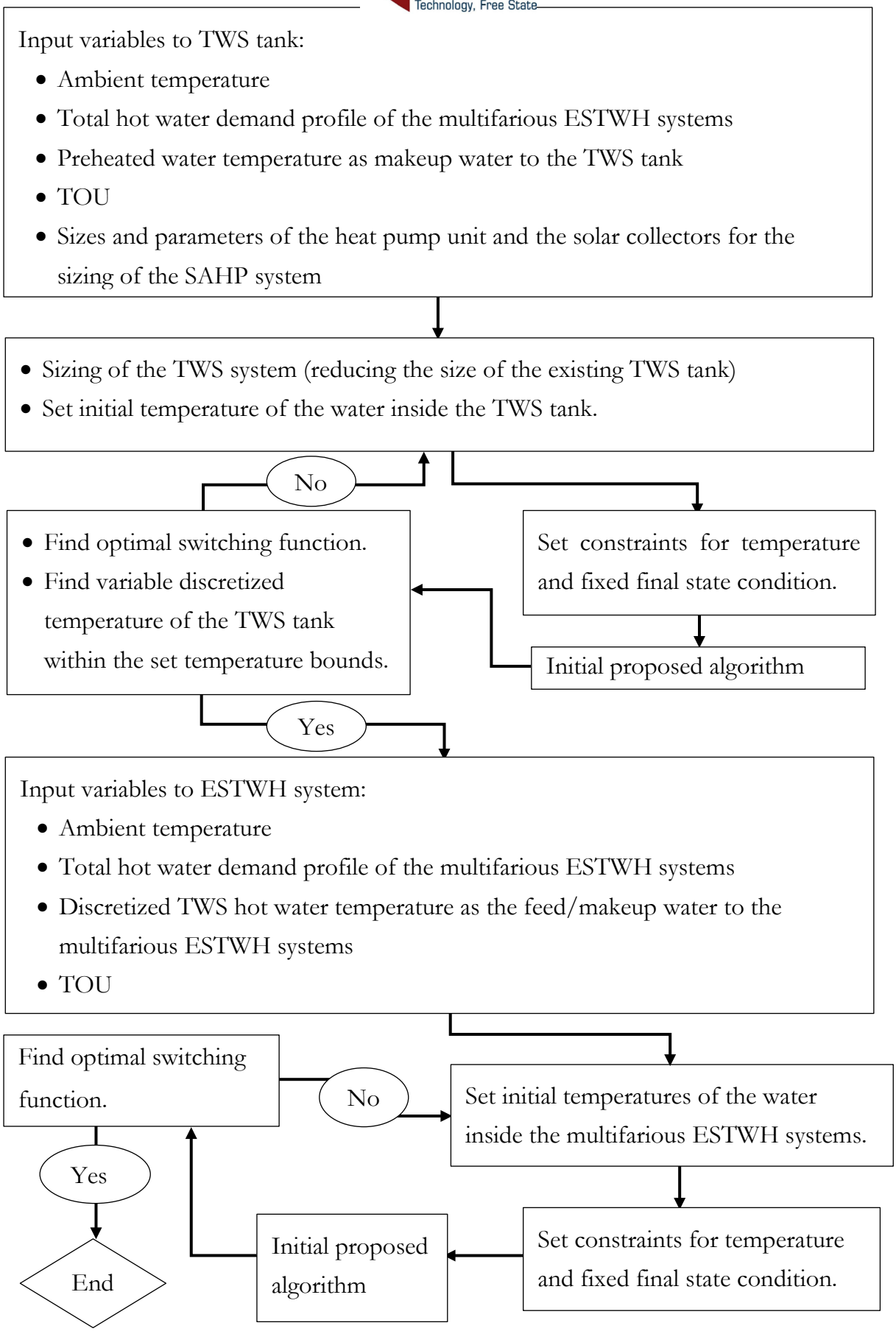


Figure 4.2. Flowchart demonstrating the optimisation process.

The control variable to be optimized is constrained as shown in Eq. (4.10) [17]:

$$lb \leq x \leq ub \tag{4.10}$$

The solver determines the optimal binary decision variable x for each switching function. The objective function includes the "max ()" function. For large-scale nonlinear optimisation, the IPOPT (Interior Point Optimizer) solver in the OPTI toolbox was used, employing a primal–dual interior-point method with filter-based line searches [16]. A flowchart illustrates the process for solving the optimization problem in Figure 4.2.

- **Scope of optimisation and decision variables**

The optimisation undertaken is limited to the operational control of the geyser system rather than the optimisation of component sizes or physical design parameters. All system components sizes were pre-defined on design requirements, literature, and system constraints, and were therefore treated as fixed parameters throughout the analysis. Therefore, the optimisation focus was on the scheduling, water temperature limits and switching behaviour of the geyser heating elements under the ToU structure and tariff pricing, enabling load shifting from peak to off-peak periods. The associated operational control variables are explicitly defined and summarised in Table 4.1.

Table 4.1 Operational Control Variables Used in the Optimisation

| **Control variable** | **Description** | **Allowable state(s)** | **Time resolution / constraint** | **Role in objective function** |
|---|---|---|---|---|
| Switching functions | Binary control of geyser heating element operation | ON (1), OFF (0) | Hourly intervals aligned with ToU tariff periods | Minimisation of electricity cost |
| Water temperature limit | Control of thermal heating temperature | 50 – 60°C | Thermal limits for lower and higher temperature levels | Thermal comfort |
| Load shifting schedule | Shifting of heating demand | Discrete time slots | Off-peak and standard periods prioritised | Peak load reduction and cost minimisation |
| Heating operation window | Permitted operating time for heating | Defined daily intervals | Constrained by user demand and comfort requirements | Energy cost optimisation |

- **Model validation**

The validation of the developed modelling framework was undertaken through a combination of literature benchmarking and the use of real-world operational data. The mathematical and control formulations adopted in this study are grounded in well-established thermodynamic principles and demand-side management approaches that have been widely reported in the literature for water heating, thermal energy storage, heat pump, and waste heat recovery systems. Key modelling assumptions, system configurations, and control strategies were aligned with those reported in prior peer-reviewed studies to ensure methodological consistency and credibility.

Furthermore, the simulation inputs were informed by measured operational and demand data representative of real-world conditions for the selected application context. These data were used to parameterise the system and to evaluate the operational behaviour of both the baseline and optimally controlled scenarios. The simulated performance trends, including energy consumption patterns, load shifting behaviour, and cost responses under Time-of-Use tariffs, were found to be consistent with outcomes reported in comparable studies, thereby providing confidence in the model's validity.

## 4.3 SIMULATIONS RESULTS OF THE BASELINE AND PROPOSED SYSTEMS

This section presents simulation results for baseline and optimally controlled systems from the formulations developed in Section 4.2. The results include the electric switching patterns and water temperature profiles during the operation. For the baseline system, the make-up water temperature supplied to the ESTWH units was assumed equal to the pre-warmed temperature from the multifunctional chillers as presented in Figures 3.7 and 3.8, for summer and winter seasons, respectively. The system is operated without the ToU tariff pricing structure of optimal control strategies.

In the optimally controlled system, the SAHP system has been retrofitted to the TWS tank which further preheats the pre-warmed water to a higher temperature. Therefore, the makeup water entering the multifarious ESTWH systems may be higher than the desired temperatures which may results in reduced operation of the electric resistive elements. The system is also operated optimally in accordance with the ToU tariffs in Table 3.4. The

simulations for the switching functions and water temperatures of the TWS tank and the multifarious ESTWH systems were conducted separately. Additionally, the proposed system utilises the solar thermal energy through the STCs, as shown in Figures 3.5 and 3.6 for the summer and winter seasons, respectively.

In this section, the simulated results of the switching functions of the electric resistive elements and the corresponding ESTWH systems temperatures of the baseline multifarious ESTWH systems are presented and the analysed, for the summer and winter cases, respectively. The results of the optimally controlled systems, where the SAHP system is incorporated as the supplementary heating hybrid-source system to the TWS tank. The power consumption profiles of the baseline and optimally controlled systems are presented and analysed, indicating the power consumed by the electric resistive elements and the heat pump unit throughout the day. Finally, the comparison of the baseline system and the optimally controlled systems based on the simulation results obtained is conducted.

**System performance: baseline cases (without optimal control)**

A. Baseline switching profiles and water temperatures: summer season.

- Off-peak period (00h00 – 06h00)

There is little switching occurring during this period to maintain the water temperature within the set range and to raise the temperature of ESTWH systems below the set temperature of 50 ℃ (Figure 4.11). There is a steady decrease in temperature of the water for most of the ESTWH systems and a few temperatures drops (Figure 4.12).

- Standard period (06h00 - 07h00)

There are several switching occurrences (Figures 4.9, 4.11 and 4.13) during this period and most of the ESTWH system experience temperature drops, even below the 50 ℃ (Figures 4.10, 4.12 and 4.14).

- Peak period (07h00 - 10h00)

The majority of the ESTWH systems experience a temperature drop (Figures 4.11, 4.13 and 4.15). Therefore there is a high volume of switching occurring to maintain the temperature above 50 ℃ (Figures 4.12, 4.14 and 4.16).

- Standard period (10h00 – 18h00)

Switching occurs (Figures 4.3, 4.5, 4.7, 4.9, 4.11, 4.13 and 4.15) throughout this period, mainly to maintain the temperature of the hot water. Only a few temperatures rise from below 50 ℃ (Figures 4.4, 4.6, 4.8, 4.10, 4.12, 4.14 and 4.16).

- Peak period (18h00 – 20h00)

Switching (Figures 4.3, 4.7, 4.11 and 4.13) occurs throughout the period and many ESTWH systems experience a temperature drop (Figures 4.4, 4.8, 4.12 and 4.14) to below 50 ℃.

- Standard period (20h00 – 22h00)

The majority of the water temperatures decrease to below 55 ℃. Switching (Figures 4.11 and 4.15) occurs throughout the period to increase the hot water temperature that has dropped below 50 ℃ (Figures 4.12 and 4.16).

- Off-peak period (22h00 – 24h00)

The hot water temperatures are between 50 ℃ and 55 ℃ while some of the temperatures dropping below 50 ℃. Switching (Figures 4.5, 4.7, 4.9, 4.11, 4.13 and 4.15) occurs throughout the period to increase the hot water temperature that has dropped below 50 ℃ (Figure 4.6, 4.8, 4.10, 4.12, 4.14 and 4.16).

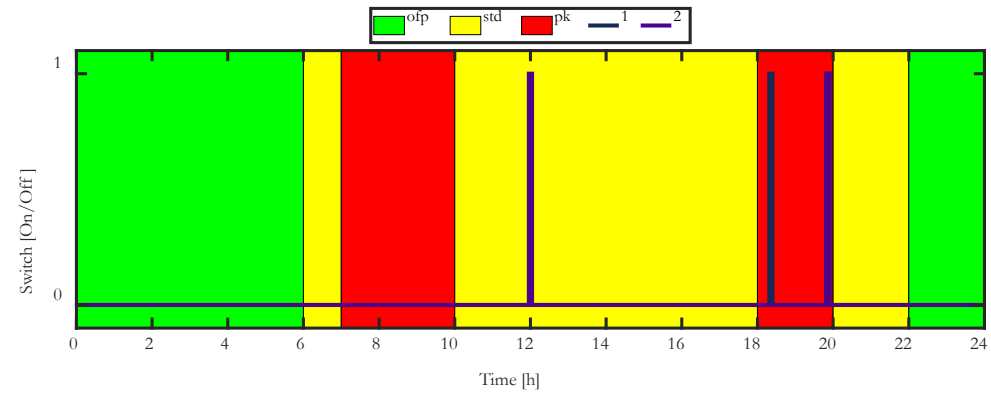


Figure 4.3. Switching functions of the basement ESTWH systems for the baseline summer season.

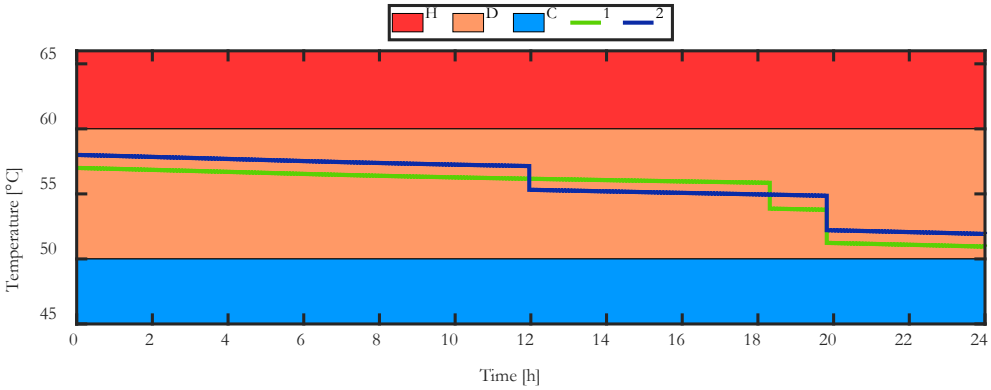


Figure 4.4. Storage tank temperatures of the basement ESTWH systems for the baseline summer season.

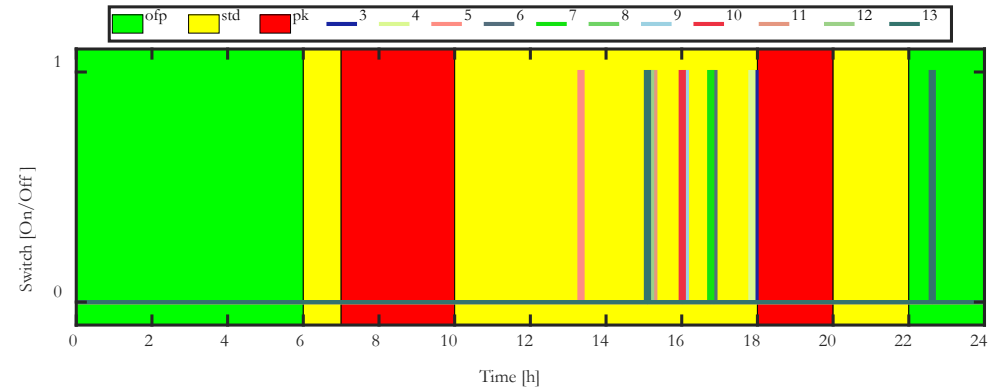


Figure 4.5. Switching functions of the floor 2 ESTWH systems for the baseline summer season.

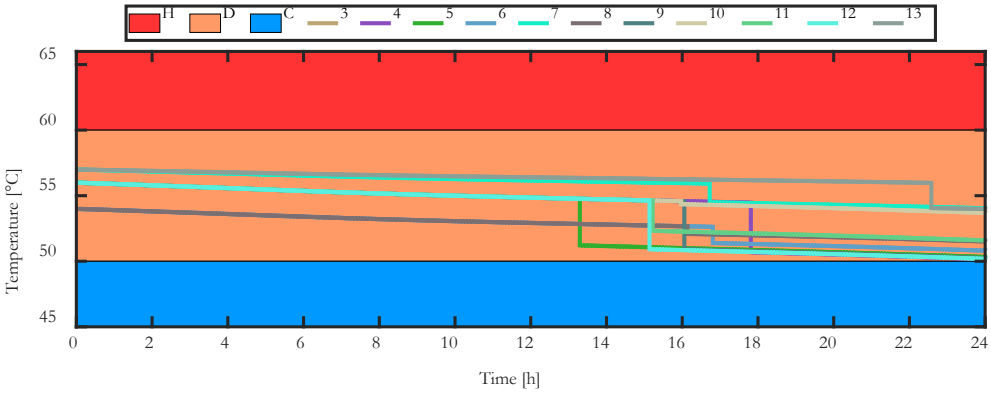


Figure 4.6. Storage tank temperatures of the floor 2 ESTWH systems for the baseline summer season.

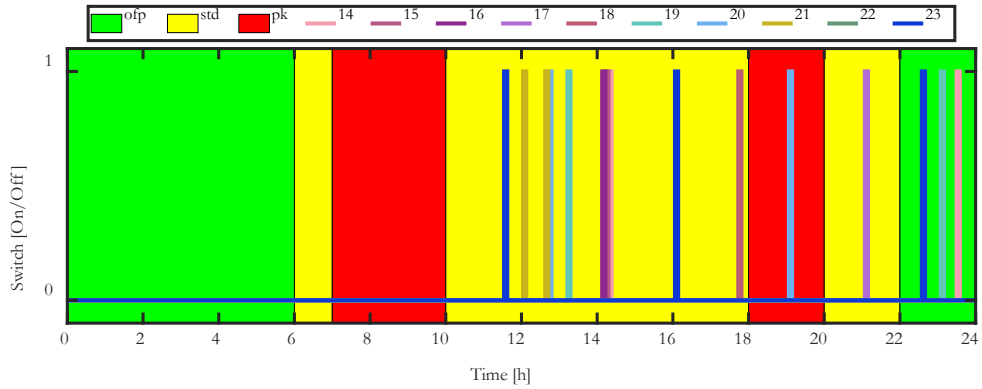


Figure 4.7. Switching functions of the floor 3 ESTWH systems for the baseline summer season.

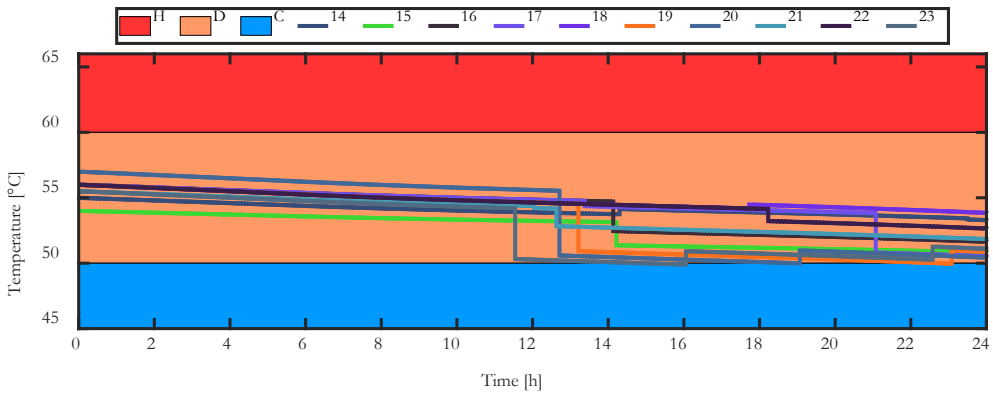


Figure 4.8. Storage tank temperatures of the floor 3 ESTWH systems for the baseline summer season.

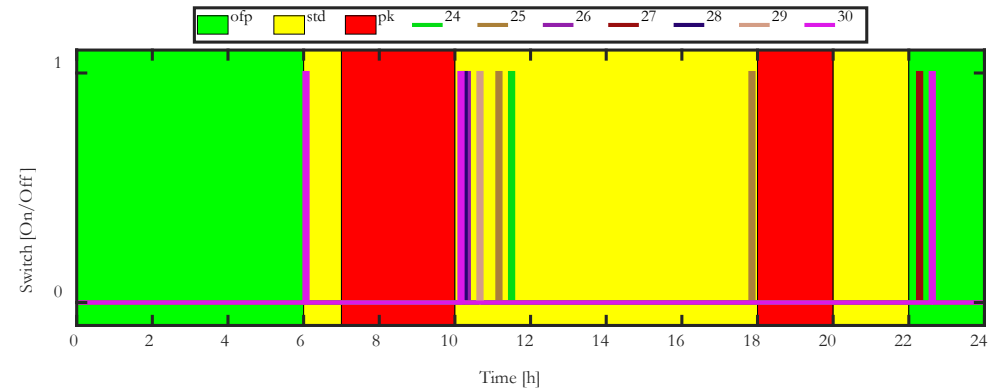


Figure 4.9. Switching functions of the floor 4 ESTWH systems for the baseline summer season.

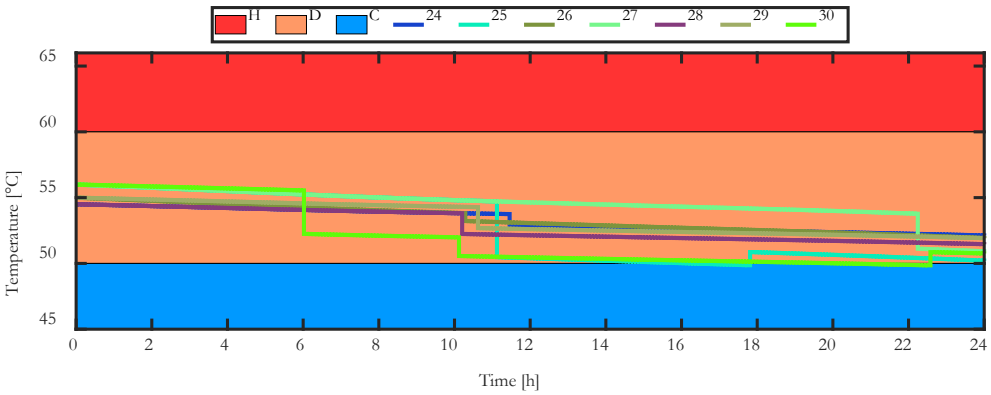


Figure 4.10. Storage tank temperatures of the floor 4 ESTWH systems for the baseline summer season.

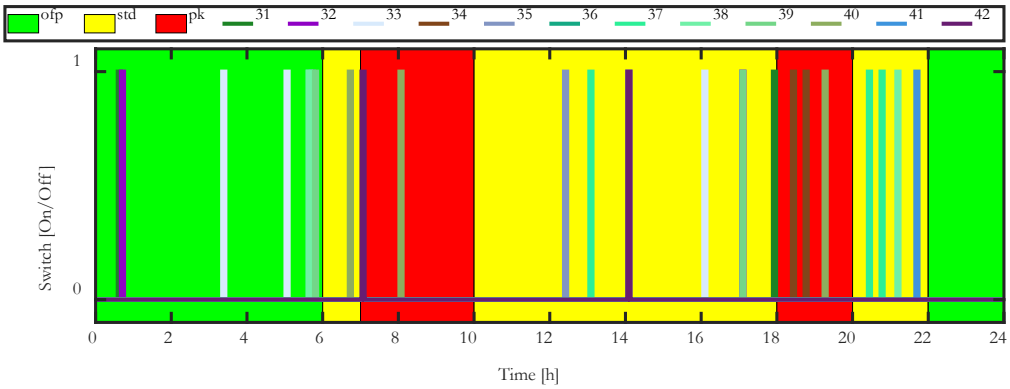


Figure 4.11. Switching functions of the floor 5 ESTWH systems for the baseline summer season.

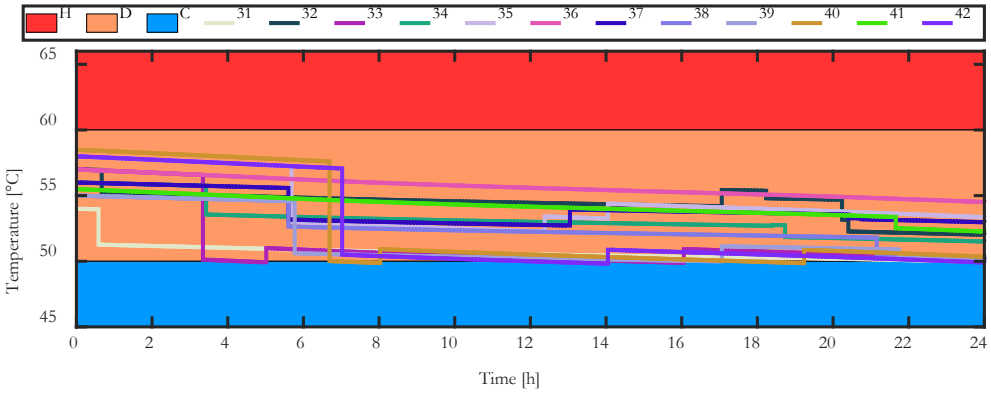


Figure 4.12. Storage tank temperatures of the floor 5 ESTWH systems for the baseline summer season.

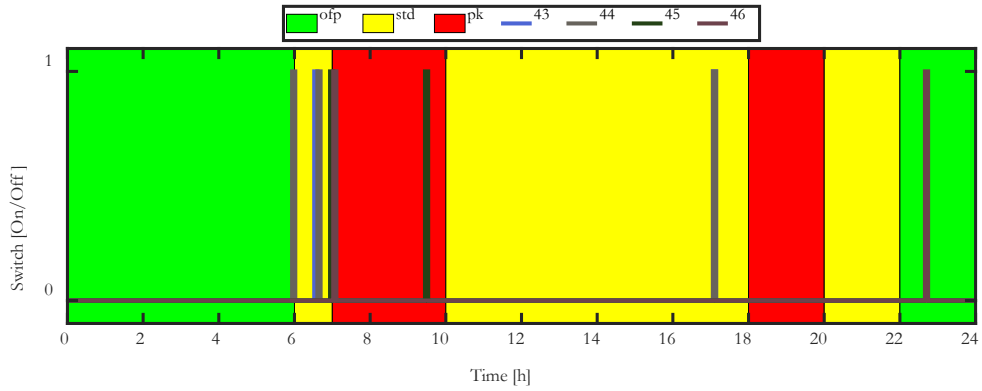


Figure 4.13. Switching functions of the floor 6 ESTWH systems for the baseline summer season.

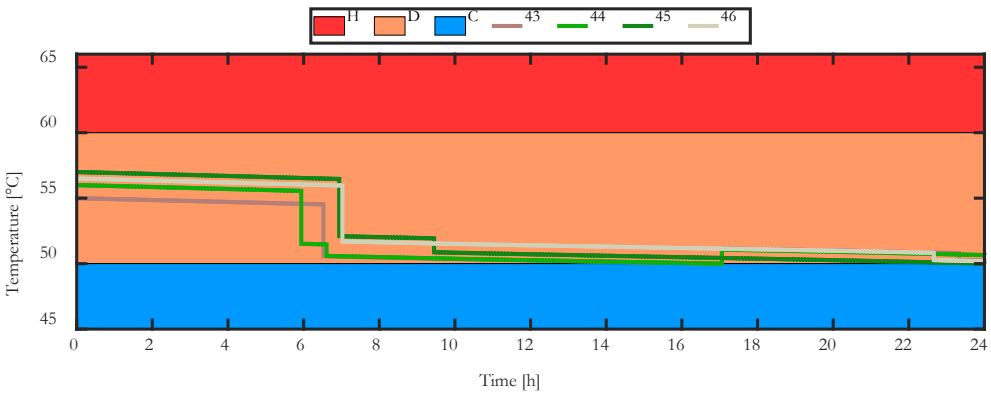


Figure 4.14. Storage tank temperatures of the floor 6 ESTWH systems for the baseline summer season.

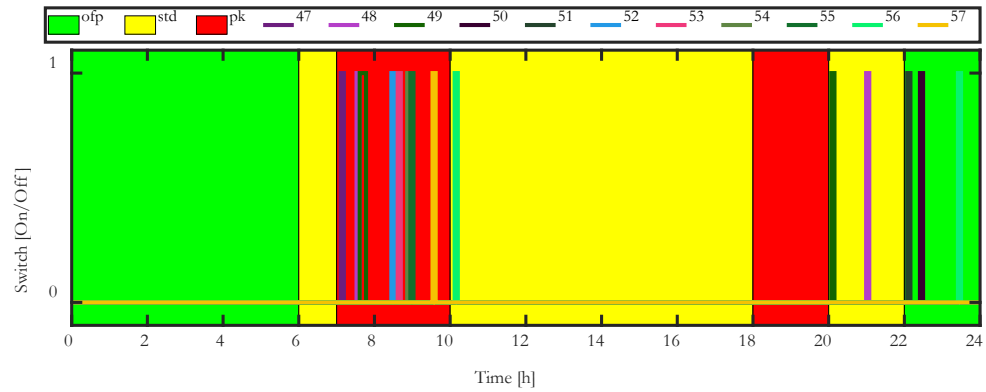


Figure 4.15. Switching functions of the floor 7 ESTWH systems for the baseline summer season.

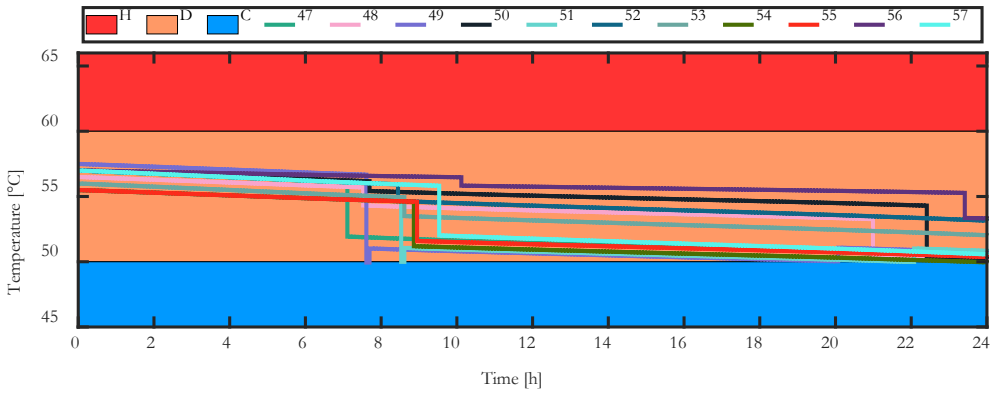


Figure 4.16. Floor 7 Storage tank temperatures of the floor 7 ESTWH systems for the baseline summer season.

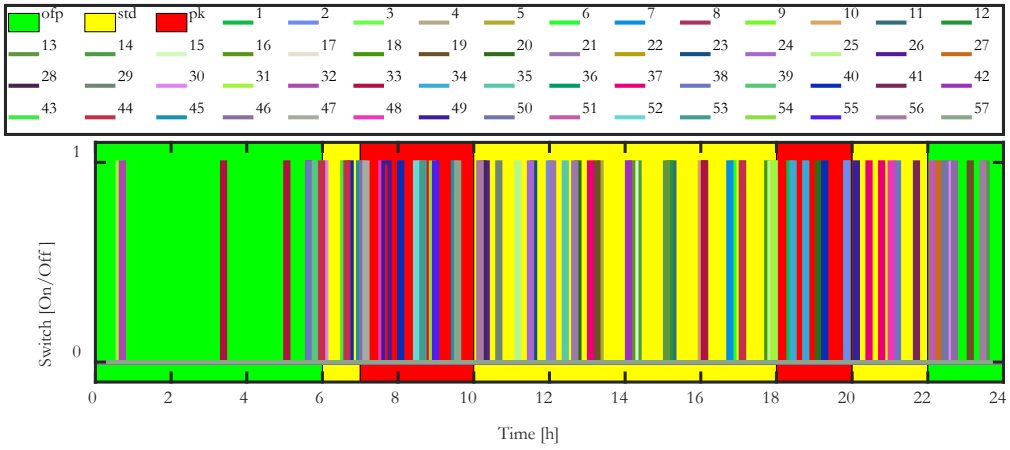


Figure 4.17. Switching functions of the multifarious ESTWH systems for the baseline summer season.

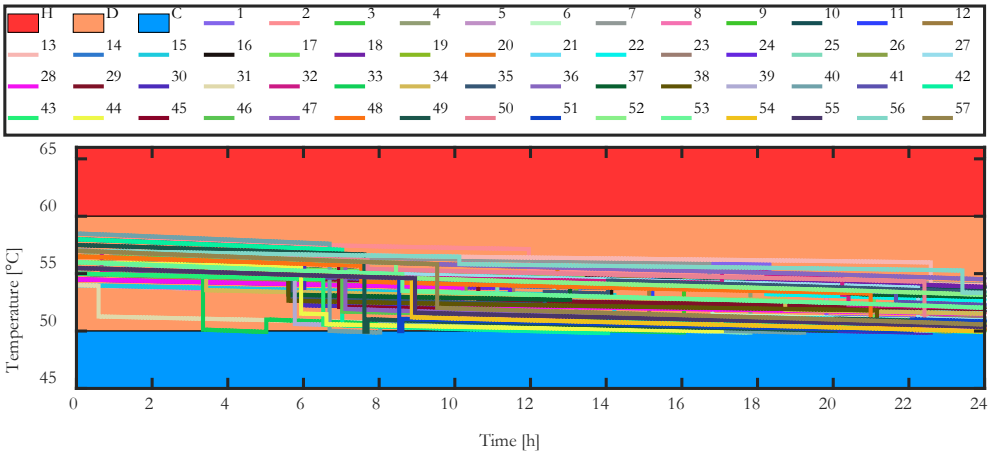


Figure 4.18. Storage tank temperatures of the multifarious ESTWH systems for the baseline summer season.

Overall, the entire system operates continuously throughout the day, where the electric resistive elements of different ESTWH systems switch on randomly at any time of the day as there is a hot water demand within the building. Figures 4.17 and 4.18 demonstrate the operation of the whole system throughout the day for the switching functions and the hot water temperatures of the ESTWH systems, respectively.

B. Baseline switching profiles and water temperatures: winter season.

- Off-peak period (00h00 – 06h00)

Switching (Figures 4.19, 4.21, 4.23, 4.25, 4.27, 4.29, 4.31 and 4.33) occurs throughout this period from the early morning hours to raise the temperatures (Figures 4.20, 4.22, 4.24, 4.26, 4.28, 4.30, 4.32 and 4.34) of the water above 55 ℃ on all the floor.

- Peak period (06h00 - 09h00)

Switching (Figures 4.23, 4.29 and 4.31) occurs throughout this period to maintain the hot water temperatures (Figures 4.24,4.30 and 4.32). There is a steady water temperature decrease, and a few temperatures drop below 50 ℃.

- Standard period (09h00 – 17h00)

Switching ((Figures 4.19, 4.21, 4.23, 4.25, 4.27, 4.29, 4.31 and 4.33) occurs throughout the period. The hot water temperatures of the ESTWH systems (Figures 4.20, 4.22, 4.24, 4.26, 4.28, 4.30, 4.32 and 4.34) continue to decrease steadily, with some dropping below 50 ℃. The switching raises the temperatures to above 50 ℃.

- Peak period (17h00 – 19h00)

Switching (Figures 4.21 and 4.23) occurs throughout the period. The hot water temperatures of the ESTWH systems (Figures 4.22 and 4.24) continue to decrease steadily, with several systems dropping below 50 ℃. The switching raises these temperatures to above 50 ℃.

- Standard period (19h00 – 22h00)

Switching (Figures 4.23, 4.25, 4.27, 4.29 and 4.31) occurs throughout the period. The hot water temperatures of the ESTWH systems (Figures 4.24, 4.26, 4.28, 4.30 and 4.32) continue to decrease steadily, with several systems dropping below 50 ℃. The switching raises the temperatures back to above 50 ℃.

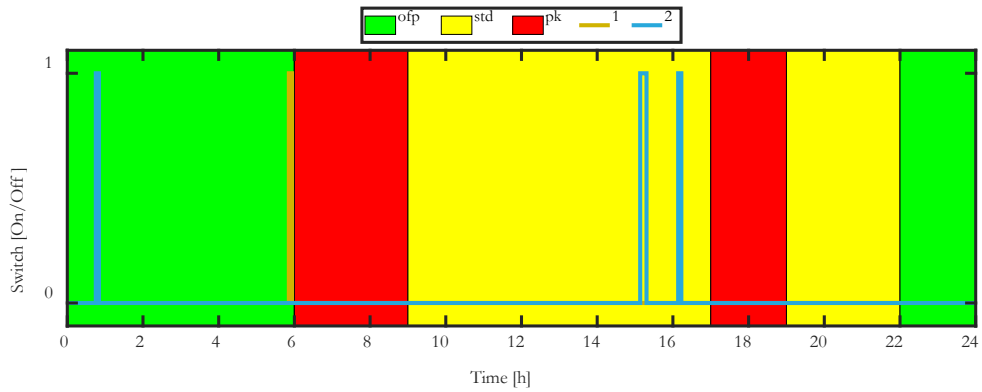


Figure 4.19. Switching functions of the basement ESTWH systems for the baseline winter season.

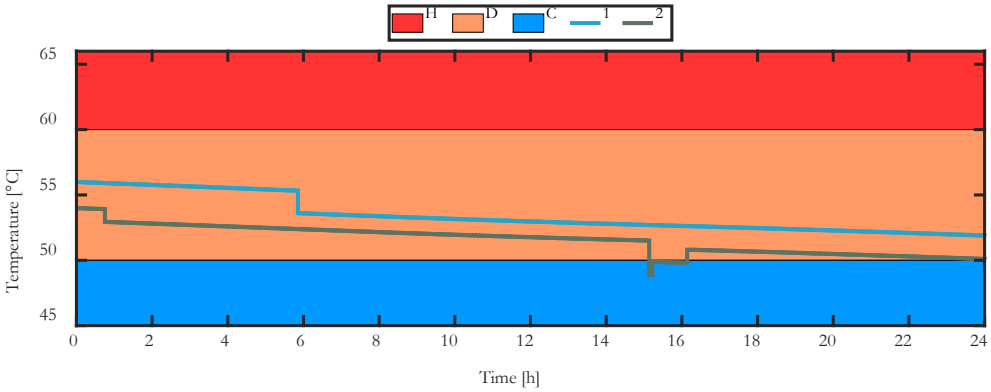


Figure 4.20. Storage tank temperatures of the floor baseline ESTWH systems for the baseline winter season.

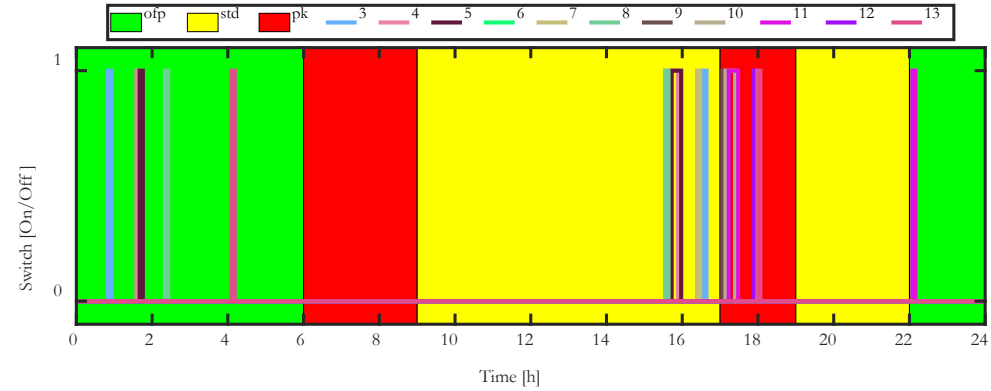


Figure 4.21. Switching functions of the floor 2 ESTWH systems for the baseline winter season.

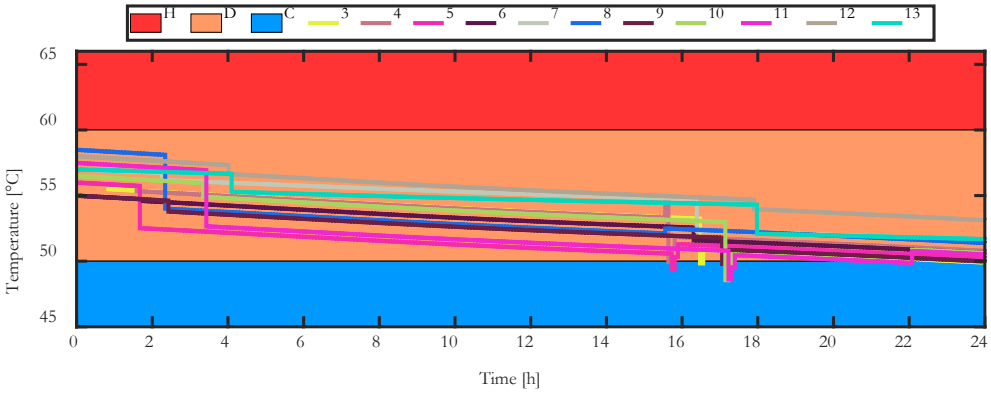


Figure 4.22. Storage tank temperatures of the floor 2 ESTWH systems for the baseline winter season.

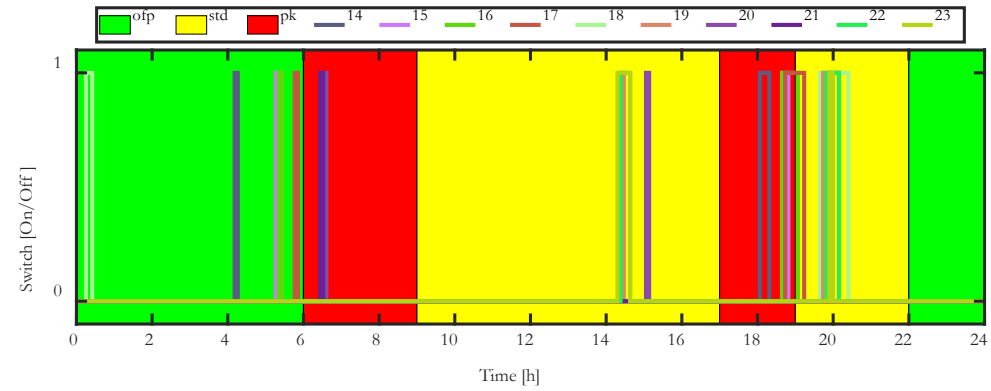


Figure 4.23. Switching functions of the floor 3 ESTWH systems for the baseline winter season.

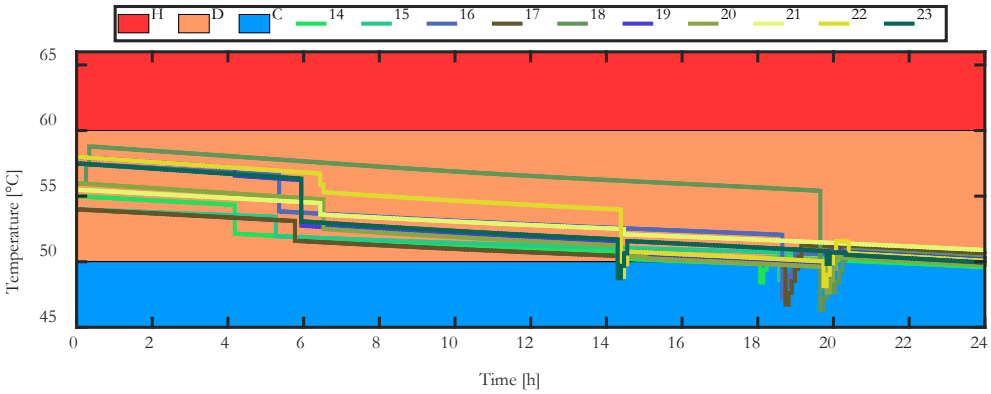


Figure 4.24. Storage tank temperatures of the floor 3 ESTWH systems for the baseline winter season.

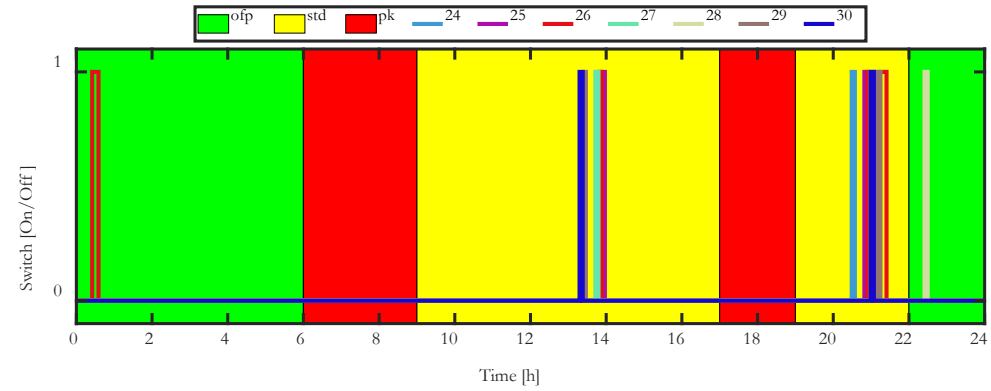


Figure 4.25. Switching functions of the floor 4 ESTWH systems for the baseline winter season.

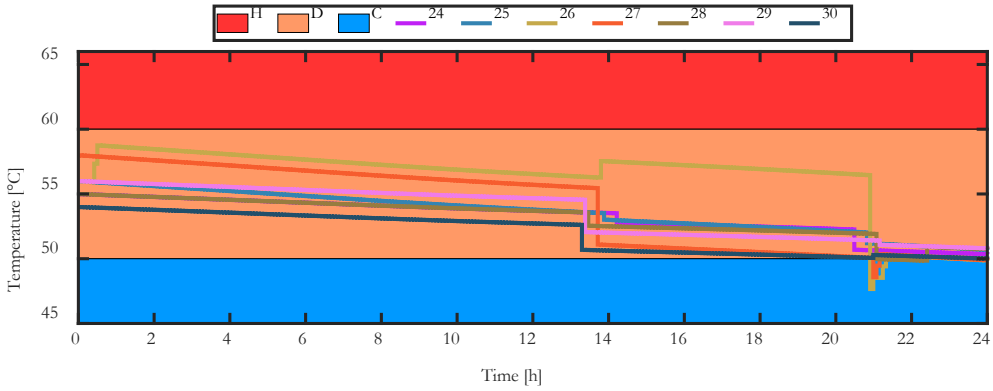


Figure 4.26. Storage tank temperatures of the floor 4 ESTWH systems for the baseline winter season.

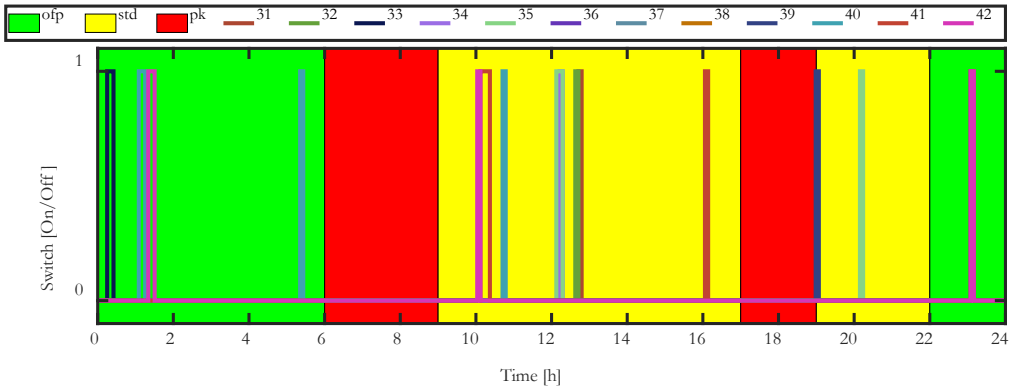


Figure 4.27. Switching functions of the floor 5 ESTWH systems for the baseline winter season.

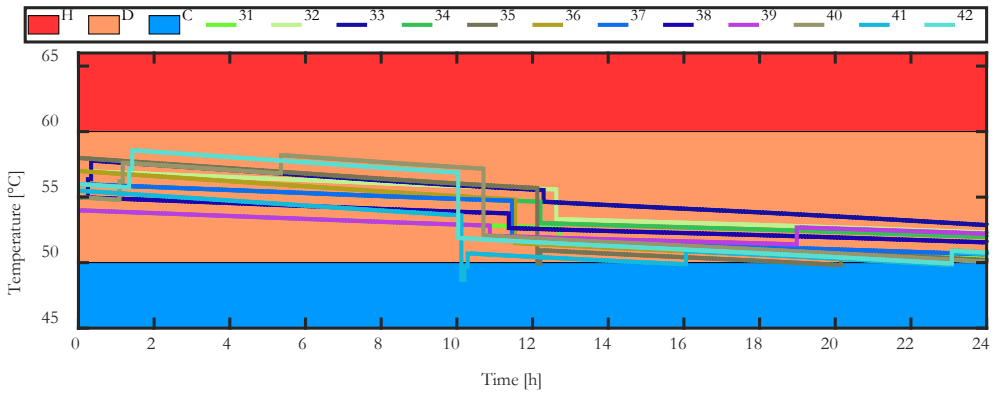


Figure 4.28. Storage tank temperatures of the floor 5 ESTWH systems for the baseline winter season.

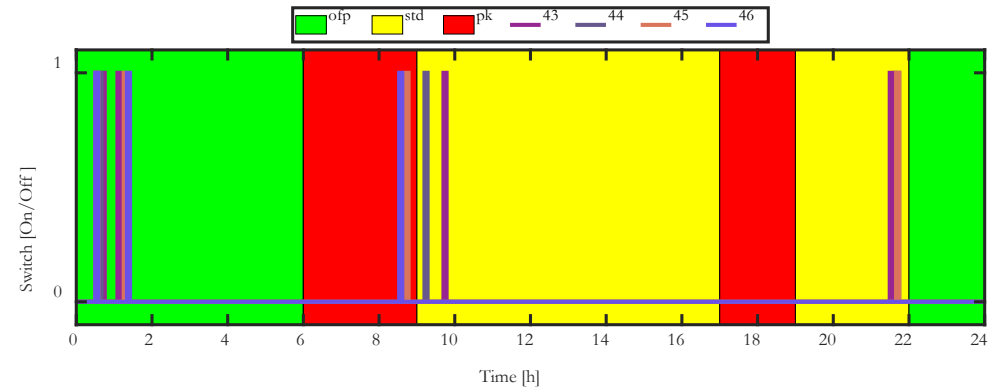


Figure 4.29. Switching functions of the floor 6 ESTWH systems for the baseline winter season.

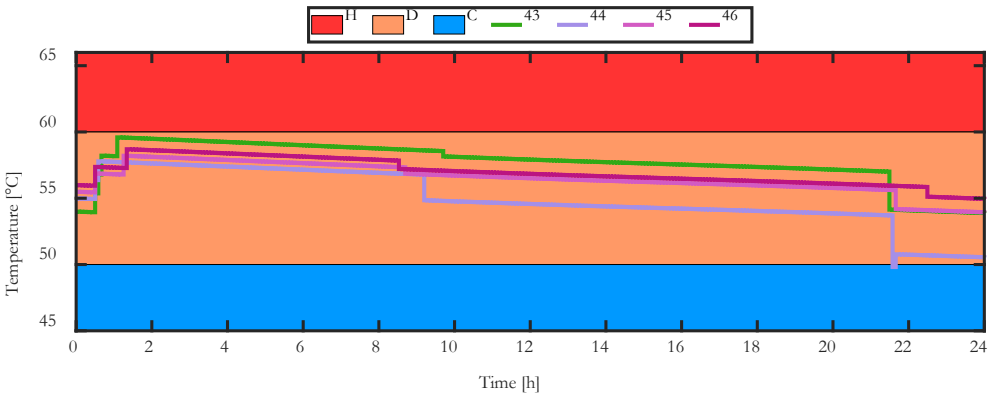


Figure 4.30. Storage tank temperatures of the floor 6 ESTWH systems for the baseline winter season.

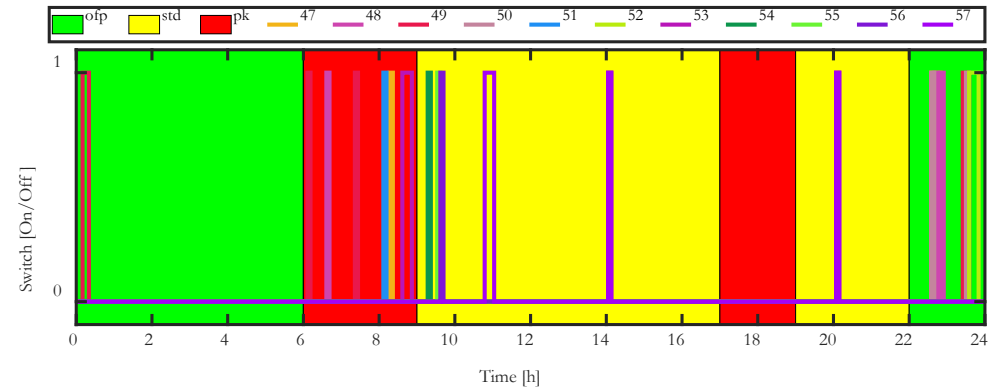


Figure 4.31. Switching functions of the floor 7 ESTWH systems for the baseline winter season.

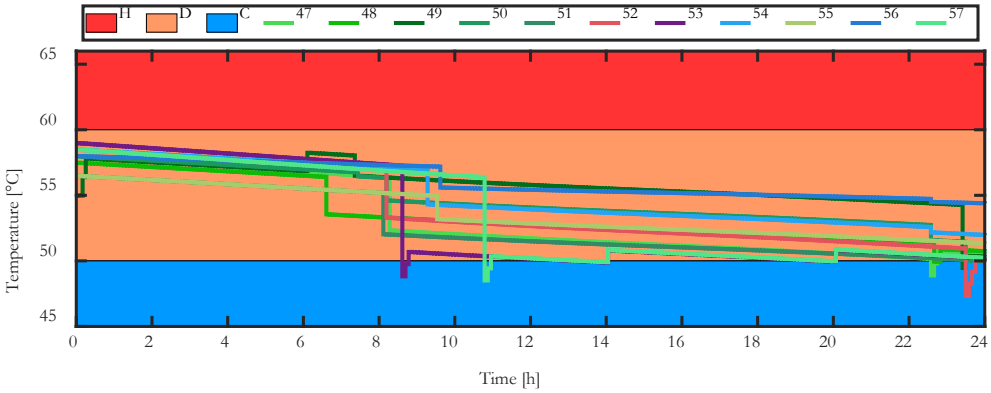


Figure 4.32. Storage tank temperatures of the floor 7 ESTWH systems for the baseline winter season.

- Off-peak period (22h00 – 24h00)

Switching (Figures 4.21, 4.25, 4.27 and 4.29)) occurs throughout the period. The hot water temperatures of the ESTWH systems (Figures 4.22, 4.26, 4.28 and 4.30) continue to decrease steadily, with few droppings below 50 ℃. The switching raises the temperatures back to above 50 ℃.

Similarly, for the winter baseline case, the whole system operates continuously throughout the day, where the switching of the electric resistive elements of different ESTWH systems occurs randomly at any time of the day. The hot water demand within the building also occurs throughout the day, as shown in Figures 4.33 and 4.34 for the switching functions and the hot water temperatures of the ESTWH systems, respectively.

**System performance: optimally controlled cases**

A. Optimally controlled switching profiles and water temperatures: summer season

- Off-peak period (00h00 – 06h00)

There is no switching in the heat pump unit (Figure 4.35) during this period and the temperature of the pre-heated water inside the TWS tank (Figure 4.36) decreases slowly from 56 ℃ to 55 ℃ at the end of this period. For the multifarious ESTWH systems, majority of the switching (Figures 4.37, 4.39, 4.41, 4.43, 4.45, 4.47 and 4.49) has shifted to this period. The hot water temperatures (Figures 4.38, 4.40, 4.42, 4.44, 4.46, 4.48 and 4.50) begin to

increase from the early hours of the morning; however, there are also a few temperature decreases experienced by some of the ESTWH systems (Figures 4.46 and 4.48).

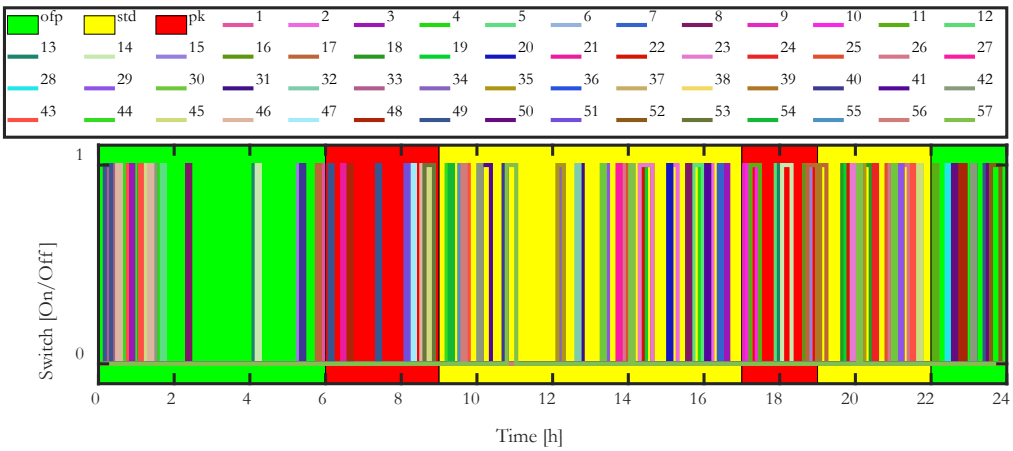


Figure 4.33. Switching functions of the multifarious ESTWH systems for the baseline winter season.

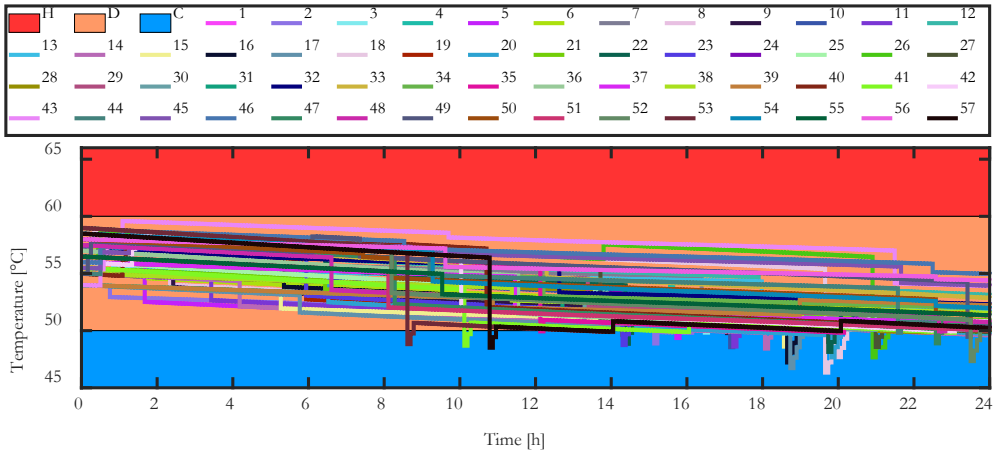


Figure 4.34. Storage tank temperatures of the multifarious ESTWH systems for the baseline winter season.

- Standard period (06h00 - 07h00)

No switching occurs for the heat pump (Figure 4.35) and the temperature of the pre-heated water inside the TWS tank (Figure 4.36) continues to decrease. No switching (Figures 4.37, 4.39, 4.41, 4.43, 4.45, 4.47 and 4.49) occurs for the ESTWH systems either, and the hot water temperatures decrease gradually in most of the ESTWH systems (Figures 4.38, 4.40

and 4.42). A temperature drop also occurs for other ESTWH systems (Figures 4.44, 4.46, 4.48 and 4.50), but it remains above 50 ℃.

- Peak period (07h00 - 10h00)

No switching occurs for the heat pump (Figure 4.35) and the temperature of the pre-heated water inside the TWS tank (Figure 4.36) continues to decrease steadily and starts to increase again, steadily, from 08h00. No switching (Figures 4.37, 4.39, 4.41, 4.43, 4.45, 4.47 and 4.49) occurs during this period. Temperatures continue to decrease gradually for most of the ESTWH systems (Figures 4.38, 4.40, 4.42 and 4.44), and several temperature drops occur (Figures 4.46, 4.48 and 4.50).

- Standard period (10h00 – 18h00)

No switching occurs for the heat pump (Figure 4.35). The temperature of the pre-heated water inside the TWS tank (Figure 4.36) continues increasing until it reaches above 60 ℃ at 18h00 in the evening. No switching (Figures 4.37, 4.39, 4.41, 4.43, 4.45, 4.47 and 4.49) of the ESTWH systems occurs during this period and there are very few continuous steady temperatures decrease in some ESTWH systems (Figure 4.48) whilst other ESTWH systems (Figures 4.38, 4.40, 4.42, 4.44, 4.46 and 4.50) experience temperature drops.

- Standard period (18h00 – 20h00)

No switching occurs for the heat pump (Figure 4.35). The temperature of the pre-heated water inside the TWS tank (Figure 4.36) starts to gradually decrease at the beginning of this period and continues until the end. No switching (Figures 4.37, 4.39, 4.41, 4.43, 4.45, 4.47 and 4.49) taking place in the multifarious ESTWH systems. There are temperature drops for several ESTWH systems (Figures 4.38 and 4.46) and a continual steady decrease in water temperature for the rest of ESTWH systems (Figures 4.40, 4.42, 4.44, 4.48 and 4.50).

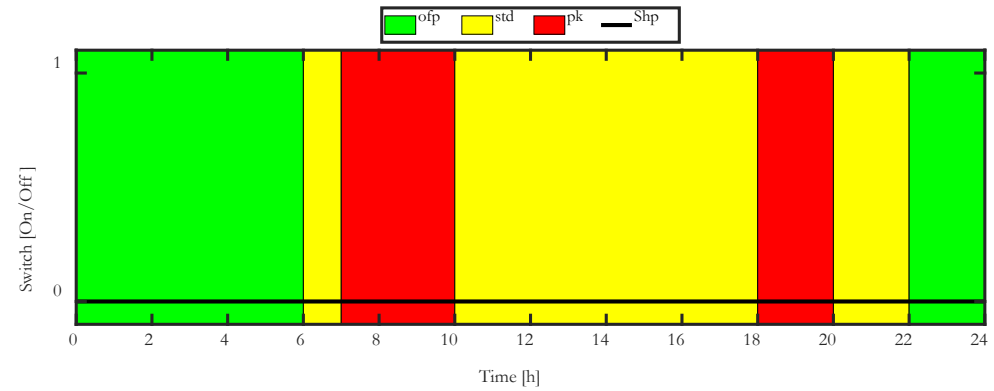


Figure 4.35. Switching function of the heat pump unit for the optimal summer season.

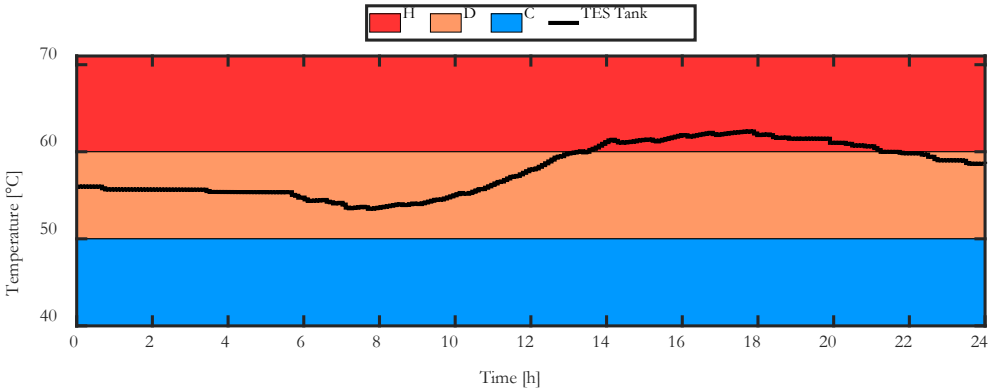


Figure 4.36. Storage tank temperature of the TWS tank for the summer season.

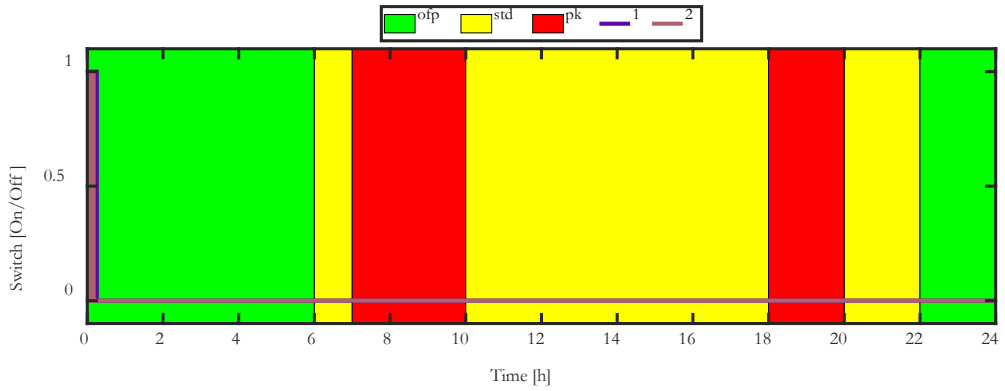


Figure 4.37. Switching functions of the basement ESTWH systems for the optimal summer season.

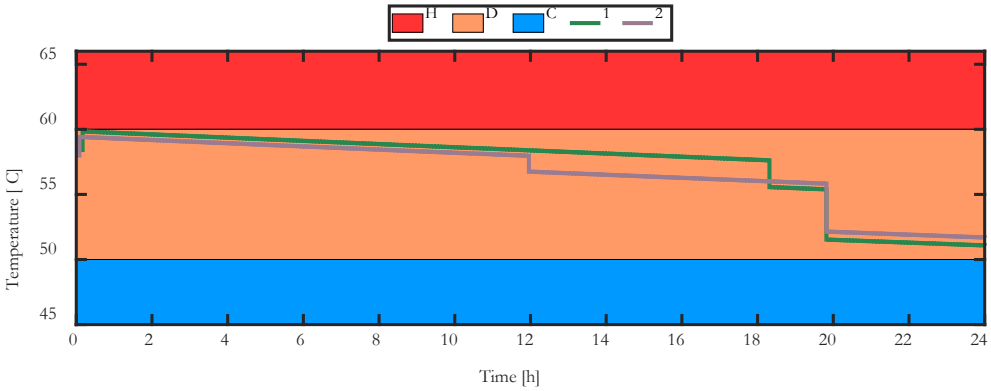


Figure 4.38. Storage tank temperatures of the basement ESTWH systems for the summer season.

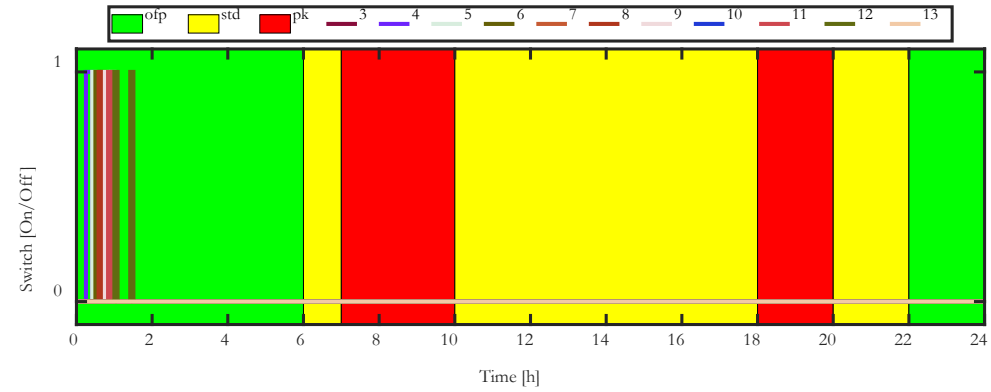


Figure 4.39. Switching functions of the floor 2 ESTWH systems for the optimal summer season.

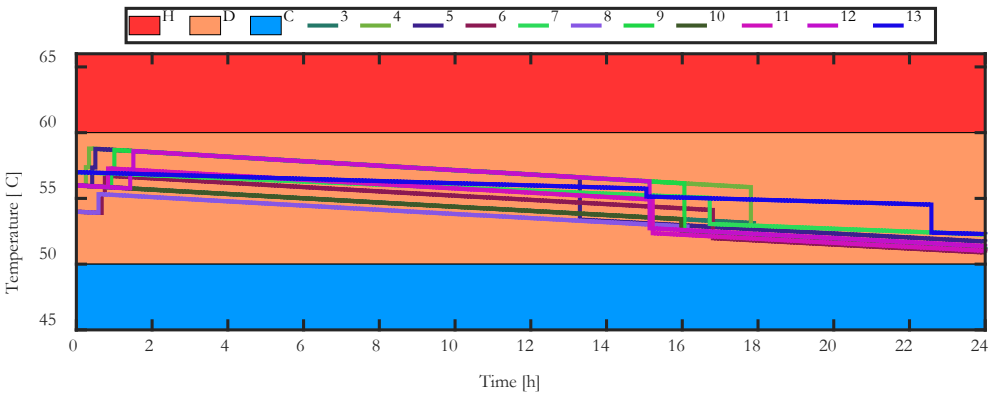


Figure 4.40. Storage tank temperatures of the floor 2 ESTWH systems for the summer season.

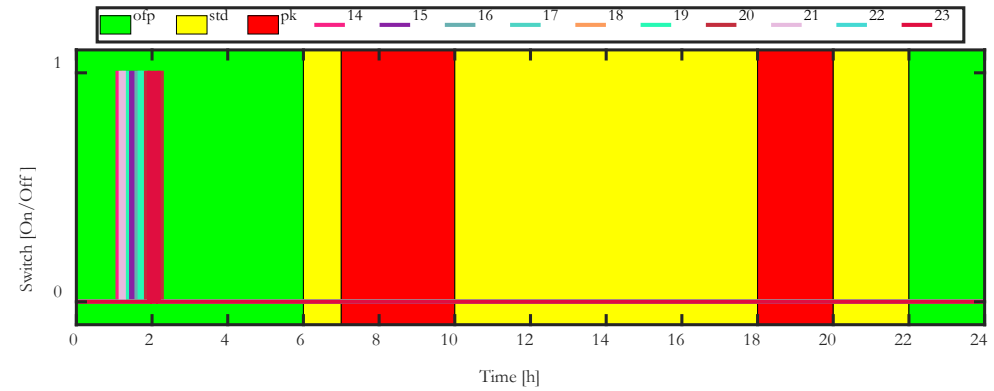


Figure 4.41. Switching functions of the floor 3 ESTWH systems for the optimal summer season.

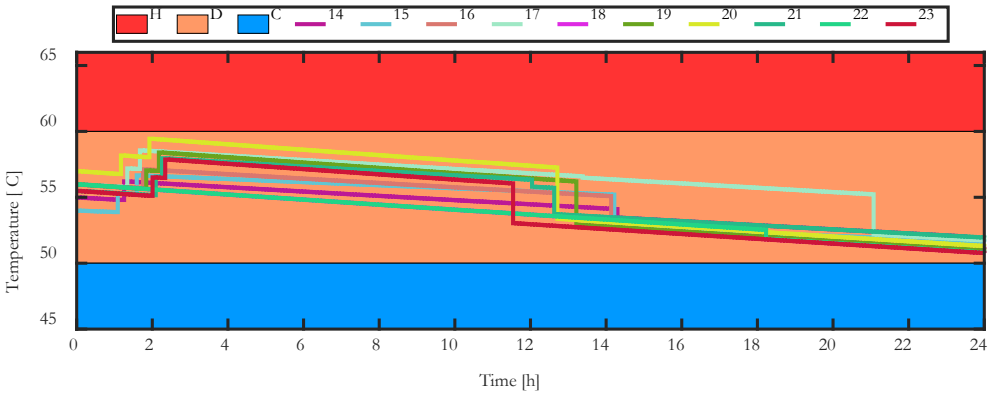


Figure 4.42. Storage tank temperatures of the floor 3 ESTWH systems for the summer season.

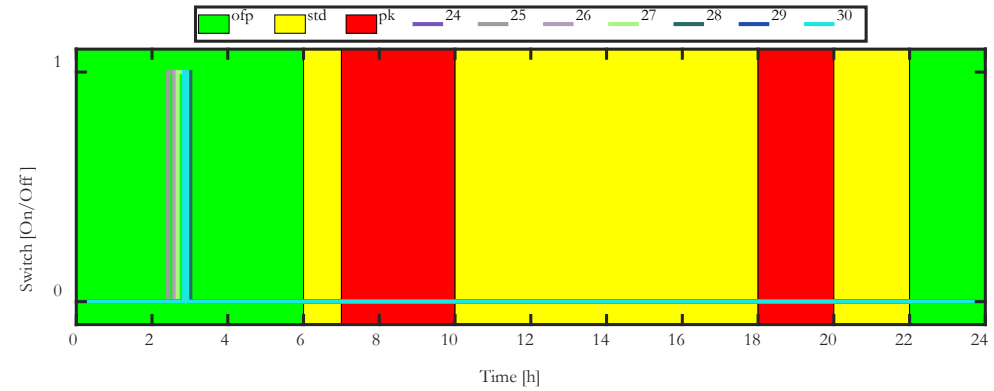


Figure 4.43. Switching functions of the floor 4 ESTWH systems for the optimal summer season.

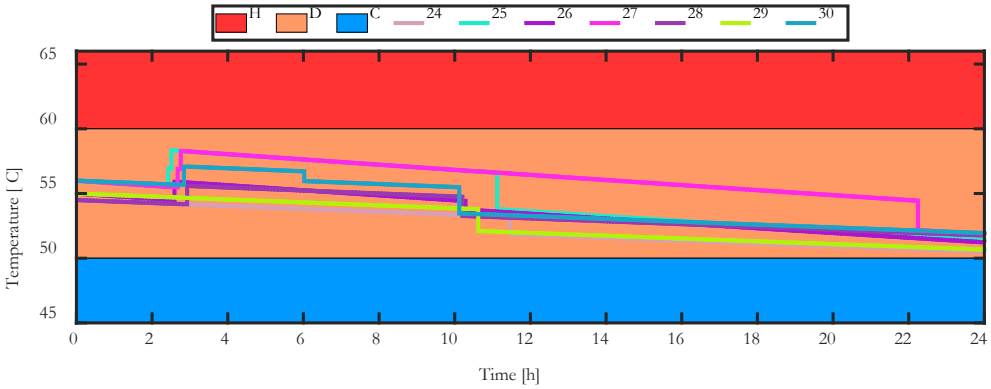


Figure 4.44. Storage tank temperatures of the floor 4 ESTWH systems for the summer season.

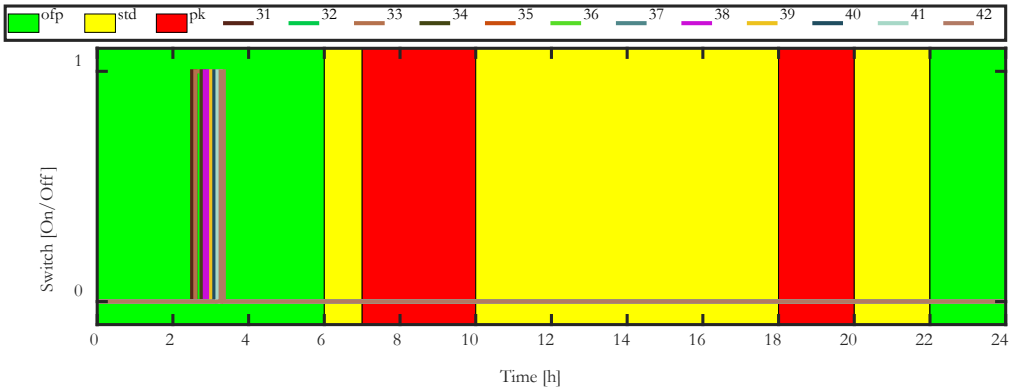


Figure 4.45. Switching functions of the floor 5 ESTWH systems for the optimal summer season.

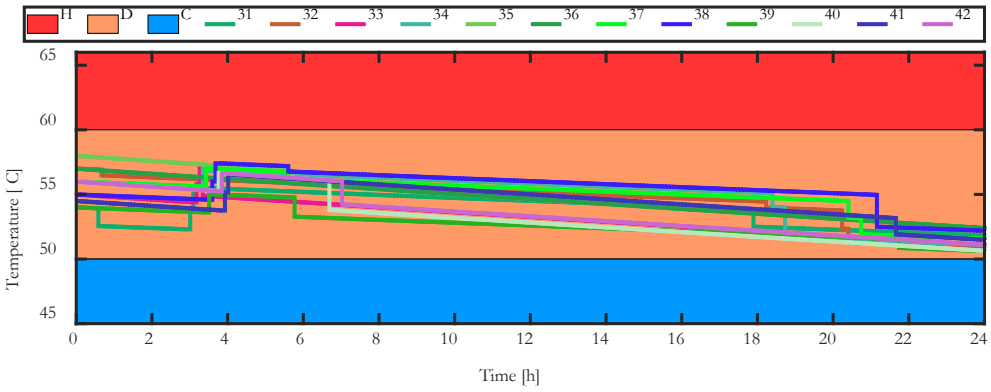


Figure 4.46. Storage tank temperatures of the floor 5 ESTWH systems for the summer season.

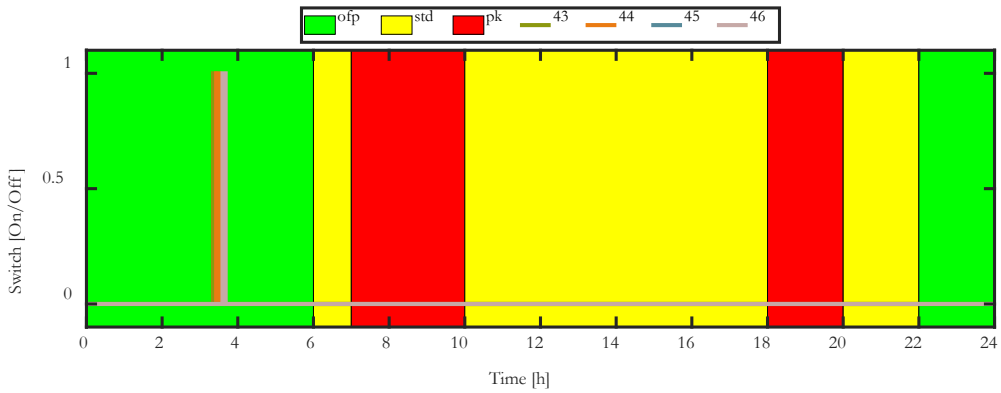


Figure 4.47. Switching functions of the floor 6 ESTWH systems for the optimal summer season.

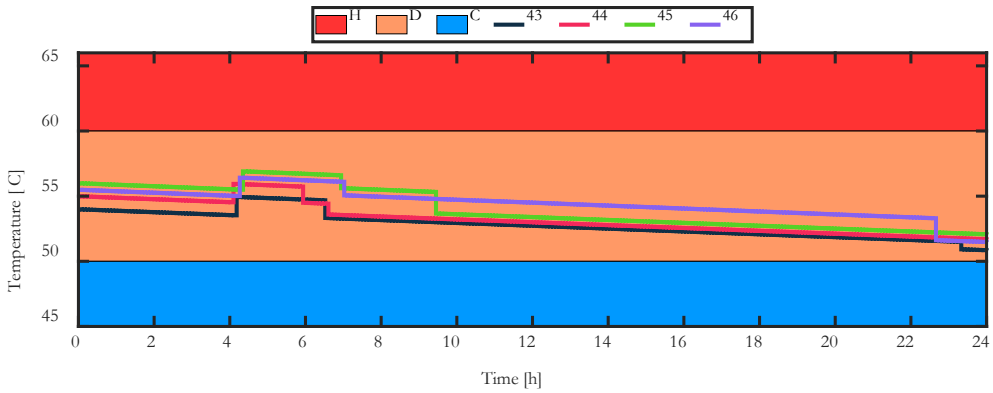


Figure 4.48. Storage tank temperatures of the floor 6 ESTWH systems for the summer season.

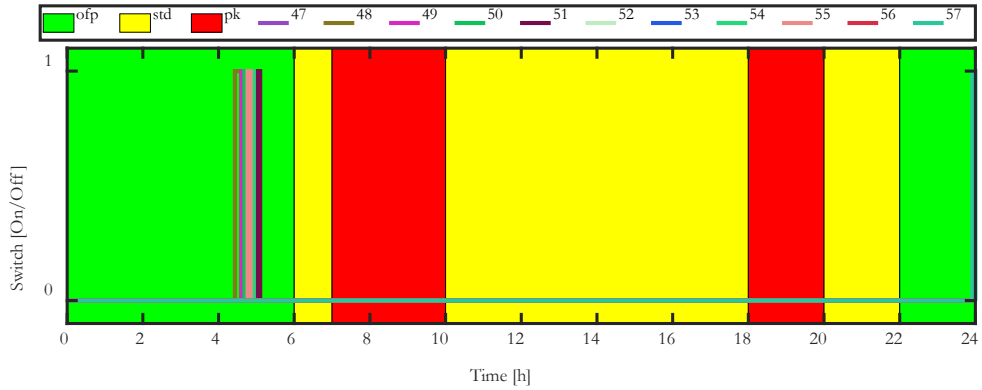


Figure 4.49. Switching functions of the floor 7 ESTWH systems for the optimal summer season.

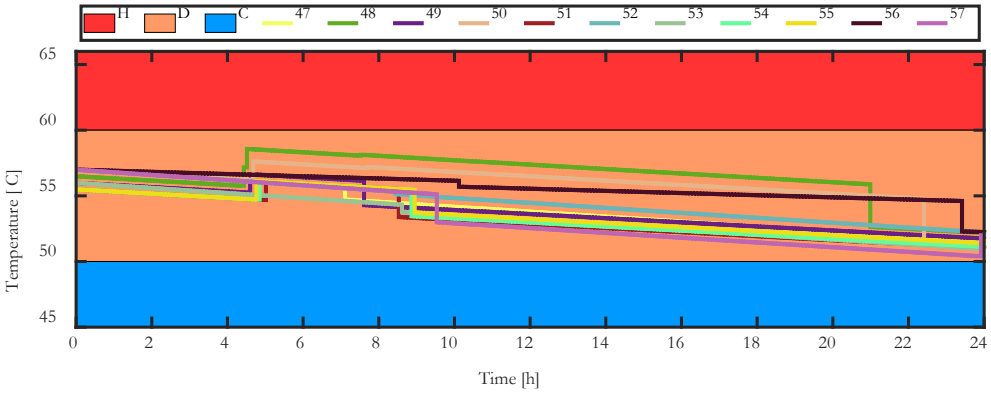


Figure 4.50. Storage tank temperatures of the floor 7 ESTWH systems for the summer season.

- Standard period (20h00 – 22h00)

No switching occurs for the heat pump (Figure 4.35 ). The temperature of the pre-heated water inside the TWS tank (Figure 4.36) continues to gradually decrease during this period and persists until the end of the period. No switching (Figures 4.37, 4.39, 4.41, 4.43, 4.45, 4.47 and 4.49) takes place during this period. The ESTWH systems experience temperatures decreasing (Figures 4.38, 4.40, 4.44 and 4.46) and dropping (Figures 4.42, 4.48 and 4.50).

- Off-peak period (22h00 – 24h00)

No switching occurs for the heat pump (Figure 4.35). The temperature of the pre-heated water inside the TWS tank (Figure 4.36) starts to gradually decrease during this period and persists until the end. A last hour switching event (Figure 4.49) takes place in the multifarious ESTWH systems. There are temperatures drops for several ESTWH systems (Figures 4.40, 4.44, 4.48 and 4.50), and a continual steady decrease in water temperatures of the water for the rest of ESTWH systems (Figures 4.38, 4.42, and 4.46). A temperature increase also occurs towards the end of the last hour (Figure 4.48).

For the optimally controlled system in the summer case, the whole system now operates optimally, and the loads have been shifted to the off-peak regions of the Time-of-Use (ToU) pricing. The use of electric resistive elements have been eliminated during the

standard and peak periods. The use of the elements have also been reduced, as the solar thermal energy may be sufficient to sustain the system throughout the day. The hot water temperatures is maintained between 50 ℃ and 60 ℃ throughout the day, while the system is able to meet the hot water demand within the building, as shown in Figures 4.51 and 4.52 for the switching functions and the hot water temperatures of the optimally controlled ESTWH systems, respectively.

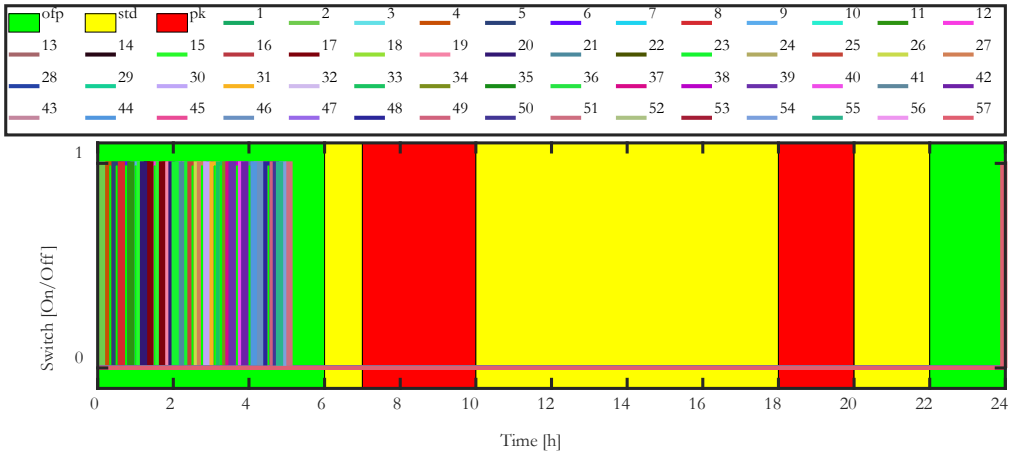


Figure 4.51. Switching functions of the multifarious ESTWH systems for the optimal summer season.

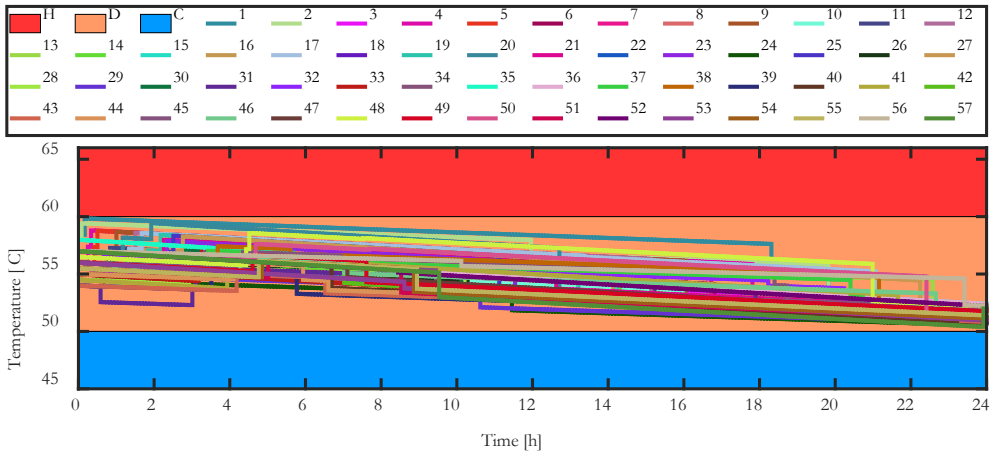


Figure 4.52. Storage tank temperatures of the multifarious ESTWH systems for the summer season.

B. Optimally controlled switching profiles and water temperatures: winter season

- Off-peak period (00h00 – 06h00)

Early morning switching (Figure 4.53) occurs for the heat pump at the beginning of the day. The pre-heated water inside the TWS tank (Figure 4.54) shows a slight increase in temperature, which then begins to decrease very slowly and fluctuates continuously within a small range. For the majority of the floors, switching occurs (Figures 4.55, 4.57, 4.59, 4.61, 4.63 and 4.65) during the early hours, except on the last floor of the building (Figure 4.67). Correspondingly, there are increasing temperatures of the hot water inside the ESTWH tanks (Figures 4.56, 4.58, 4.60, 4.62, 4.64 and 4.66). Additionally, some of the ESTWH systems experience temperature drops (Figures 4.56, 4.58 and 4.60), while temperatures in other ESTWH systems (Figures 4.62, 4.64, 4.66 and 4.68) decrease gradually.

- Peak period (06h00 - 09h00)

No switching occurs for the heat pump (Figure 4.53) during this period. The TWS tank pre-heated water temperature (Figure 4.54) shows a slight temperature decrease not exceeding 5 ℃ from beginning to end of this period. No switching occurs (Figures 4.55, 4.57, 4.59, 4.61, 4.63, 4.66 and 4.67) for the ESTWH systems either. There are several temperatures drops (Figures 4.56, 4.66 and 4.68) and a steady decrease in temperature for most of the ESTWH systems (Figures 4.58, 4.60, 4.62 and 4.64).

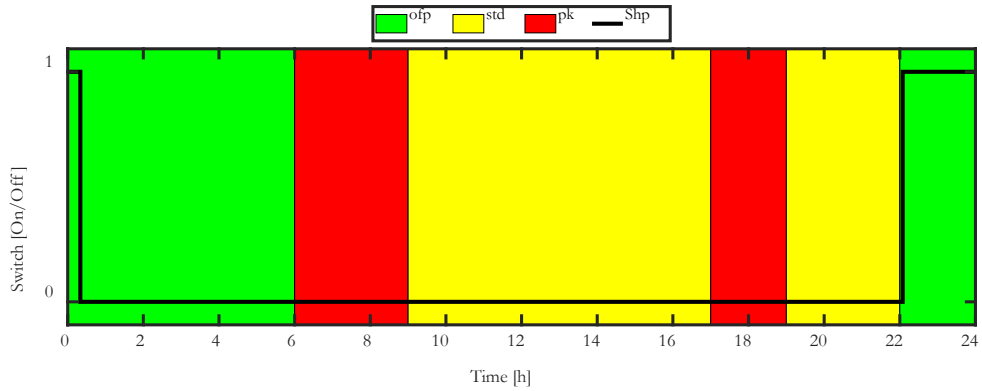


Figure 4.53. Switching function of the heat pump for the optimal winter season.

- Standard period (09h00 – 17h00)

No switching of the heat pump (Figure 4.53) occurs. The temperature of the pre-heated water inside the TWS tank (Figure 4.54) shows very little fluctuation and remains almost constant during this period. No switching (Figures 4.55, 4.57, 4.59, 4.61, 4.63, 4.65 and 4.67) takes place, and temperatures continue to drop in all the ESTWH systems (Figures 4.56, 4.58, 4.60, 4.62, 4.64, 4.66 and 4.68).

- Peak period (17h00 – 19h00)

No switching of the heat pump (Figure 4.53) occurs. The temperature of the pre-heated water inside the TWS tank (Figure 4.54) starts to decrease steadily until the end of the period. No switching occurs during this period (Figures 4.55, 4.57, 4.59, 4.61, 4.63, 4.65 and 4.67). The water temperature continues to decrease steadily for most of the ESTWH system (Figures 4.56, 4.62, 4.64, 4.66 and 4.68), whereas some of the ESTWH systems experiences a temperature drop (Figures 4.58 and 4.60).

- Standard period (19h00 – 22h00)

No switching of the heat pump (Figure 4.53) occurs. The temperature of the pre-heated water inside the TWS tank (Figure 4.54) continues to decrease steadily until the end of the period. No switching occurs during this period (Figures 4.55, 4.57, 4.59, 4.61, 4.63, 4.65 and 4.67). The storage tanks' temperature profiles of the ESTWH systems show several temperatures drops for some systems (Figures 4.60, 4.62, 4.66 and 4.68) and a steady decrease in temperature for most of the systems (Figures 4.56, 4.58, 4.64 and 4.68).

- Off-peak period (22h00 – 24h00)

The heat pump switching (Figure 4.53) starts at the beginning of this period and continues until the end of the day, as it raises the pre-heated water temperature inside the TWS tank to 55 ℃ (Figure 4.54). No switching (Figures 4.55, 4.57, 4.59, 4.61, 4.63, 4.65 and 4.67), occurs until the end of the day. However, there is continuous steady temperature decrease for the majority of the ESTWH systems (Figures 4.56, 4.58, 4.60, 4.62, and 4.64) and a few temperatures drops (Figures 4.66 and 4.68).

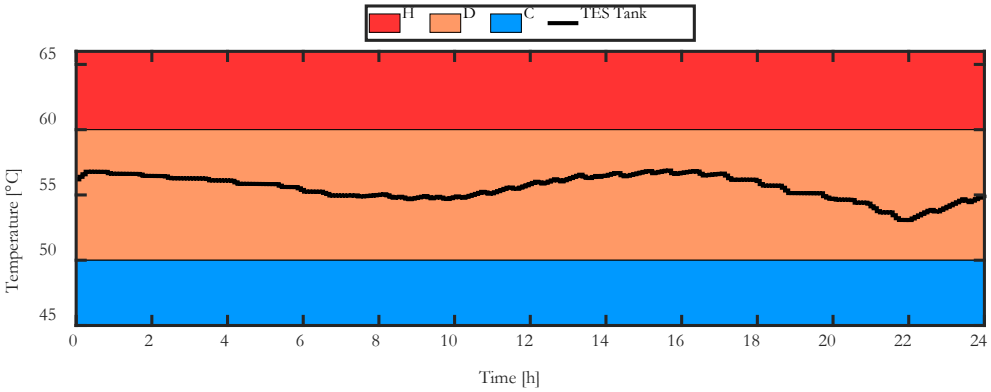


Figure 4.54. Storage tank temperature of the TWS tank for the optimal winter season.

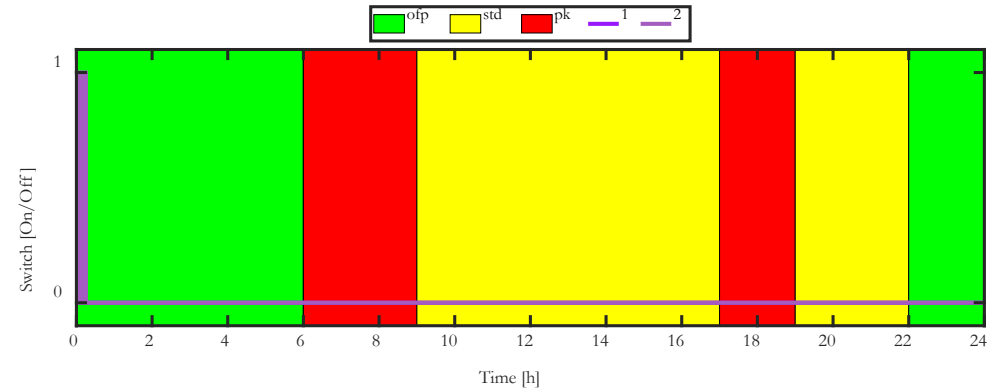


Figure 4.55. Switching functions of the basement ESTWH systems for the optimal winter season.

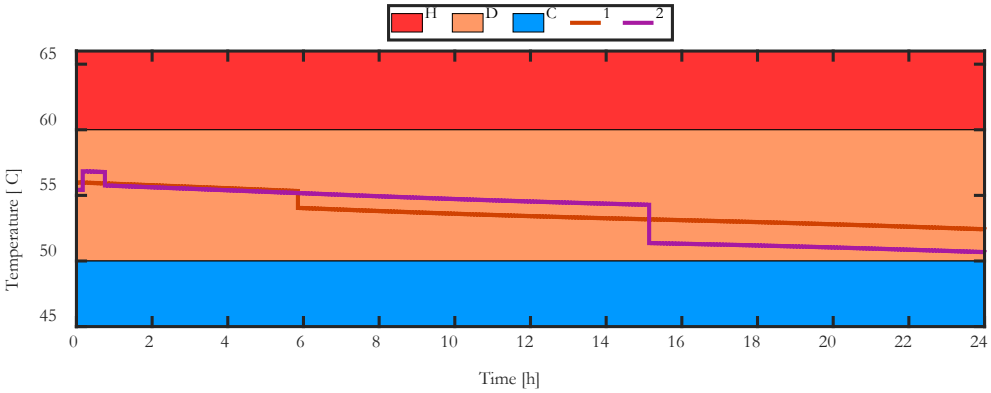


Figure 4.56. Storage tank temperatures of the basement ESTWH systems for the optimal winter season.

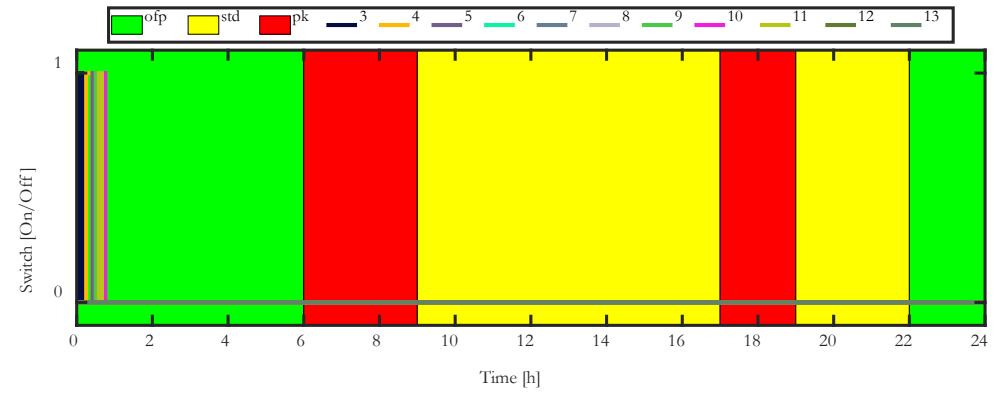


Figure 4.57. Switching functions of the floor 2 ESTWH systems for the optimal winter season.

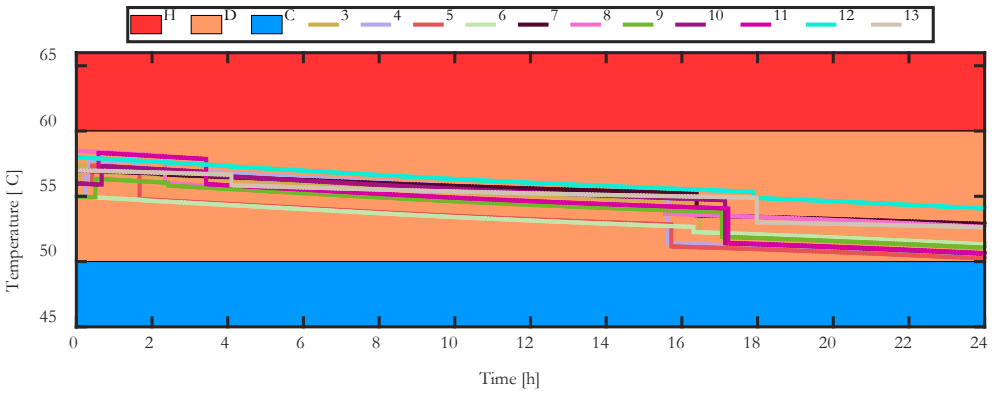


Figure 4.58. Storage tank temperatures of the floor 2 ESTWH systems for the optimal winter season.

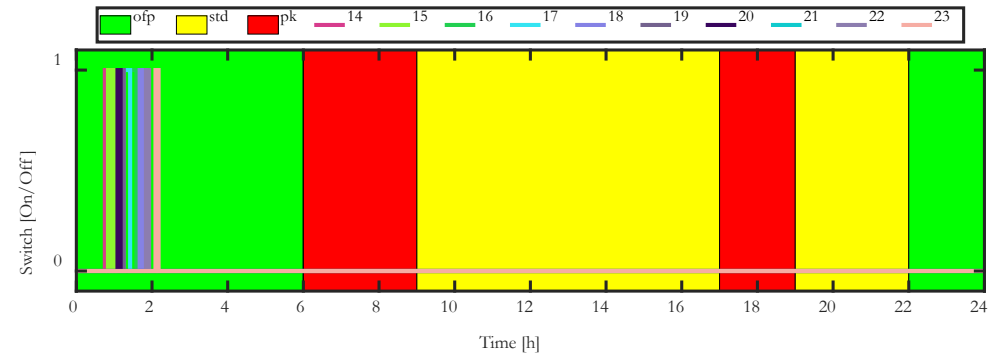


Figure 4.59. Switching functions of the floor 3 ESTWH systems for the optimal winter season.

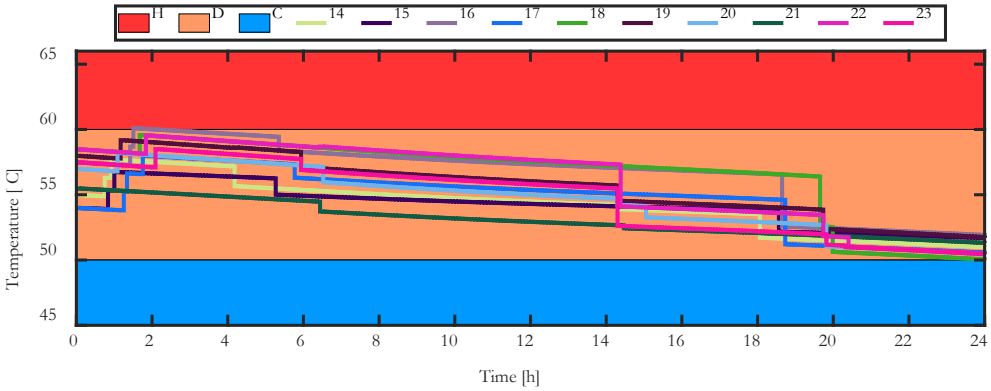


Figure 4.60. Storage tank temperatures of the floor 3 ESTWH systems for the optimal winter season.

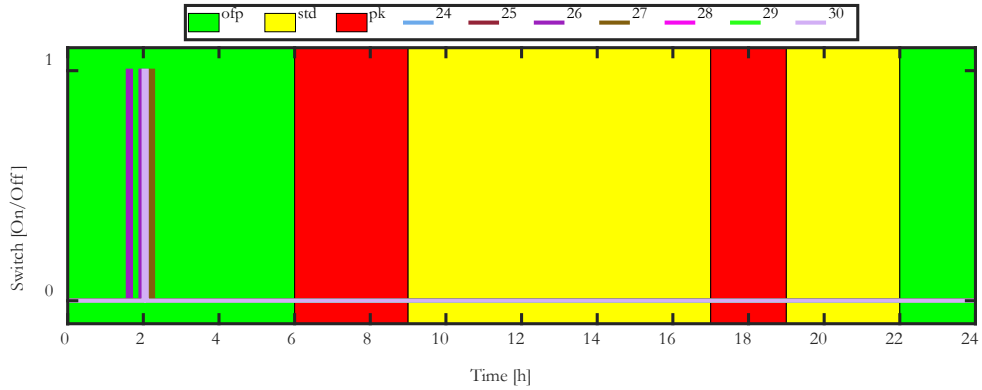


Figure 4.61. Switching functions of the floor 4 ESTWH systems for the optimal winter season.

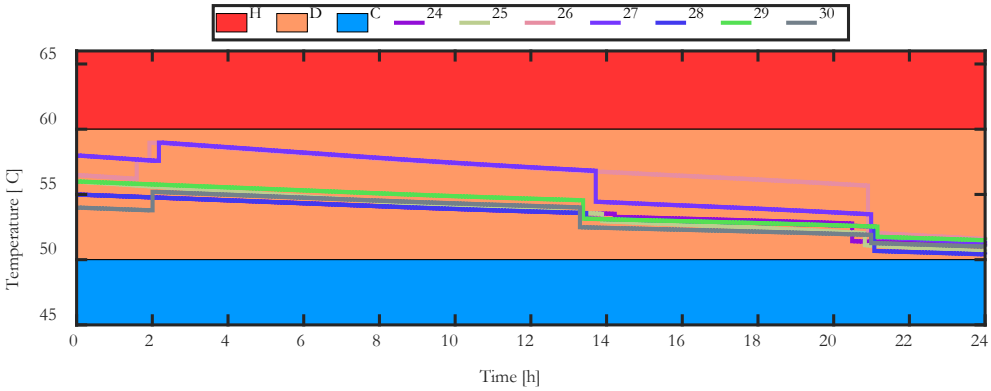


Figure 4.62. Storage tank temperatures of the floor 4 ESTWH systems for the optimal winter season.

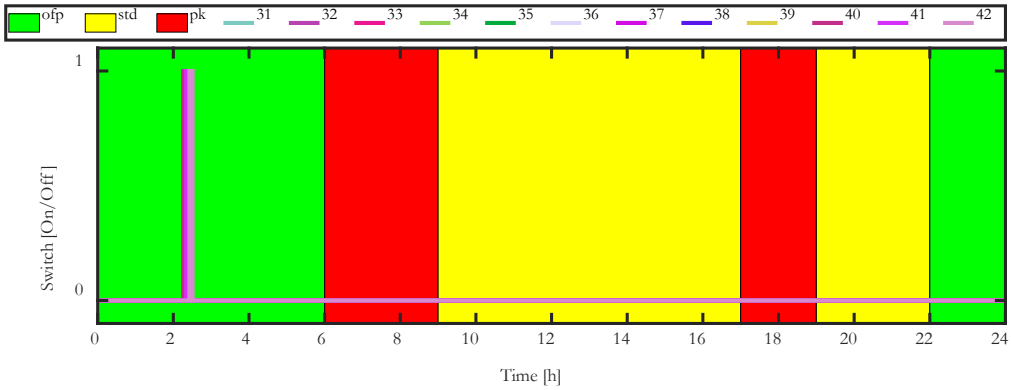


Figure 4.63. Switching functions of the floor 5 ESTWH systems for the optimal winter season.

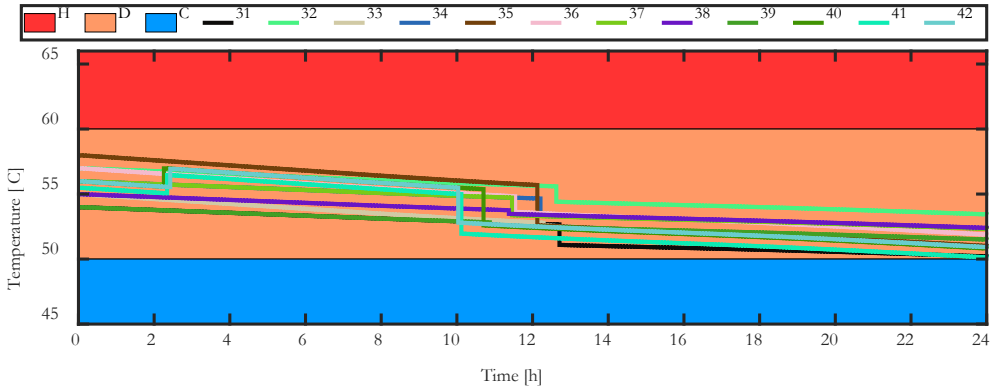


Figure 4.64. Storage tank temperatures of the floor 5 ESTWH systems for the optimal winter season.

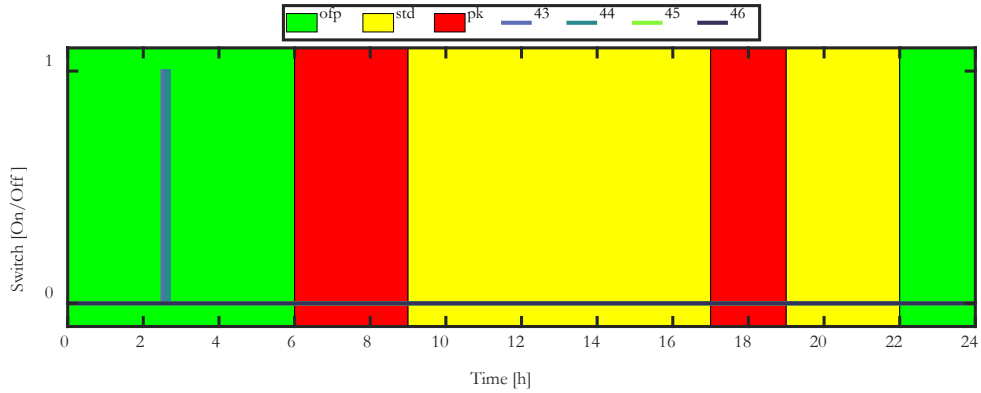


Figure 4.65. Switching functions of the floor 6 ESTWH systems for the optimal winter season.

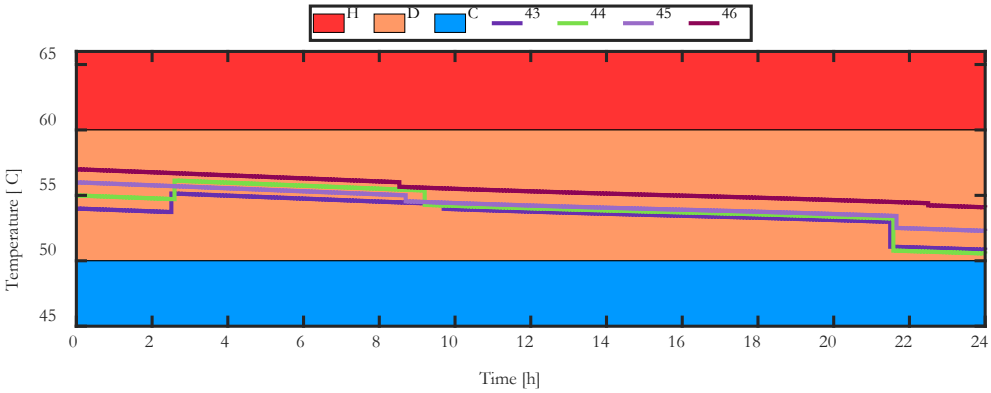


Figure 4.66. Storage tank temperatures of the floor 6 ESTWH systems for the optimal winter season.

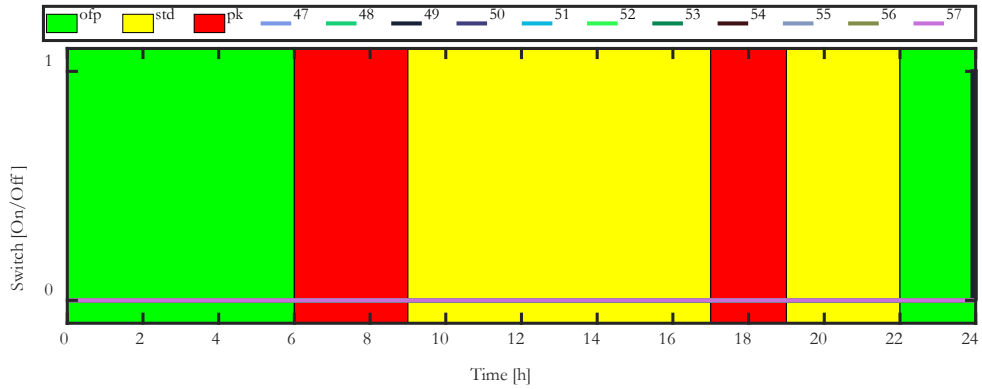


Figure 4.67. Switching functions of the floor 7 ESTWH systems for the optimal winter season.

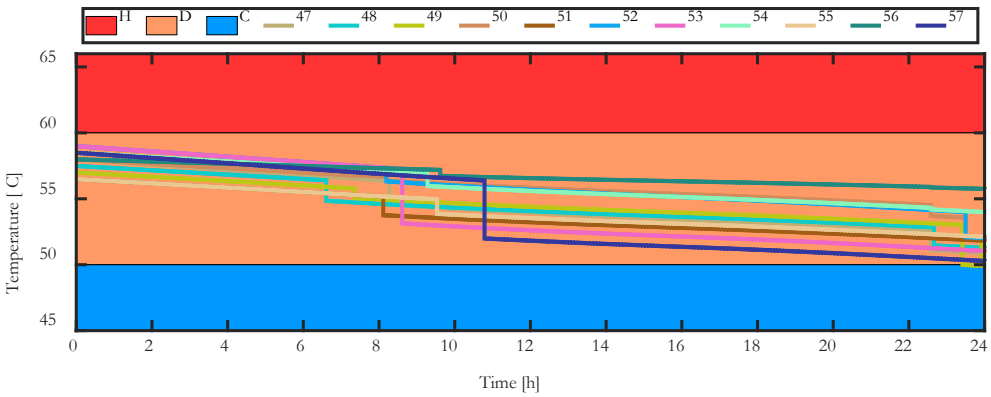


Figure 4.68. Storage tank temperatures of the floor 7 ESTWH systems for the optimal winter season.

For the winter case, the optimally controlled system has also shifted the loads to the off-peak regions of the ToU pricing. Fewer electric resistive elements are operating compared to the summer case, due to the operation of the heat pump unit during the morning and evening off-peak periods. The temperature profile of the multifarious ESTWH systems also show that the solar thermal energy may be sufficient to sustain the system throughout the day, maintaining the hot water temperatures between 50 ℃ and 60 ℃ throughout the day, even during periods of hot water demand within the building. Figures 4.69 and 4.70 present the switching functions and the hot water temperatures of the optimally controlled ESTWH systems for the winter case, respectively.

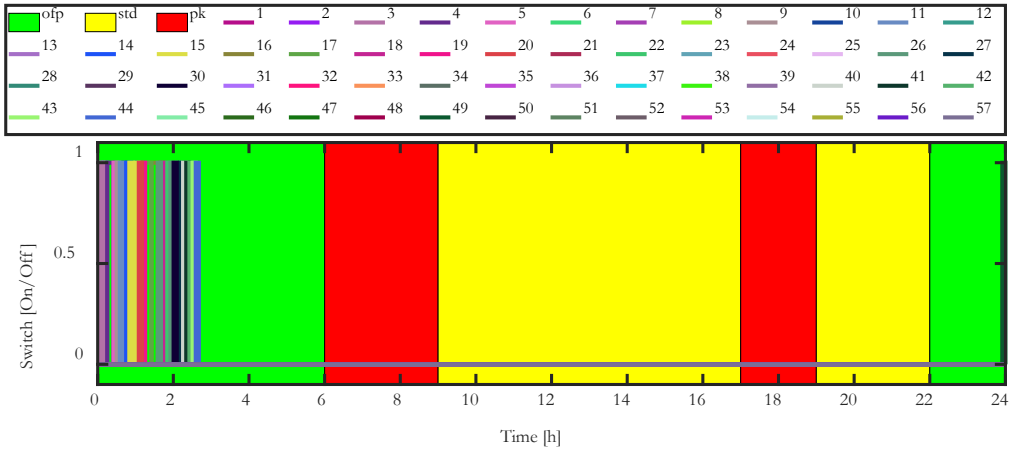


Figure 4.69. Switching functions of the floor 7 ESTWH systems for the optimal winter season.

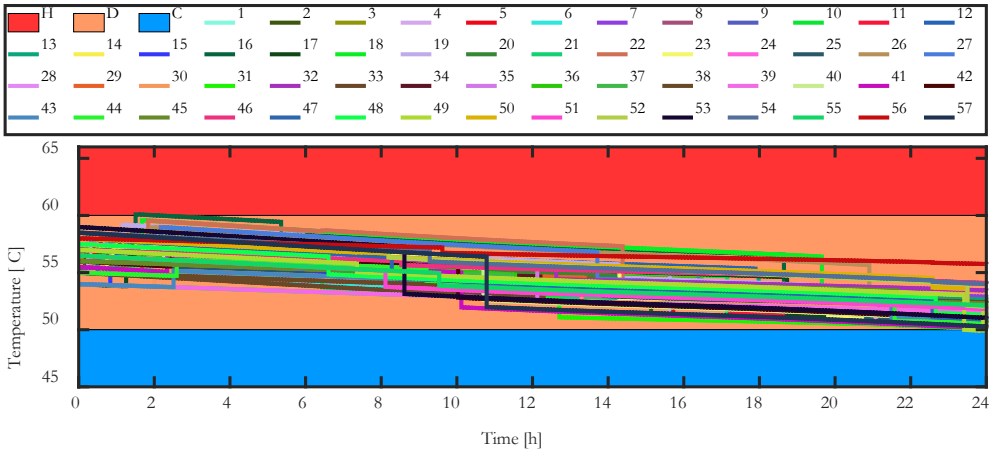


Figure 4.70. Storage tank temperatures of the multifarious ESTWH systems for the optimal winter season.

**Power consumption**

- Power consumption comparison for the summer cases.

Figure 4.71 shows the comparison of the power consumptions for the baseline multifarious ESTWH systems, the optimal multifarious ESTWH systems, and the optimal heat pump unit during the summer season. The individual power consumptions of the multifarious ESTWH systems have been aggregated and presented as a single profile to show the simultaneous operation of the ESTWH systems. For the baseline case, power is consumed continuously throughout the day, which results in a high-power demand during the evening peak period.

For the optimal case, the multifarious ESTWH systems show power consumption during the early morning hours, the peak period and the evening off-peak period at the end of the last hour of the day. Additionally, the system shows that there was no power consumption for the heat pump unit in the summer.

- Power consumption comparison for the winter cases.

For the winter season, the comparison of the power consumptions for the baseline multifarious ESTWH systems, optimal multifarious ESTWH systems, and the optimal heat pump unit is presented in Figure 4.72. Similar to the summer season, the baseline case indicates continuous power consumption throughout the day. However, the peak power demand occurs in the early hours of the morning during the off-peak period.

For the optimal case, the multifarious ESTWH systems also show power consumption during the early morning hours of the off-peak period and during the evening off-peak period, roughly few minutes before the end of the day. However, the heat pump unit consumed power within the first hour of the day during the off-peak period, as well as during the entire evening off-peak period, until the end of the day.

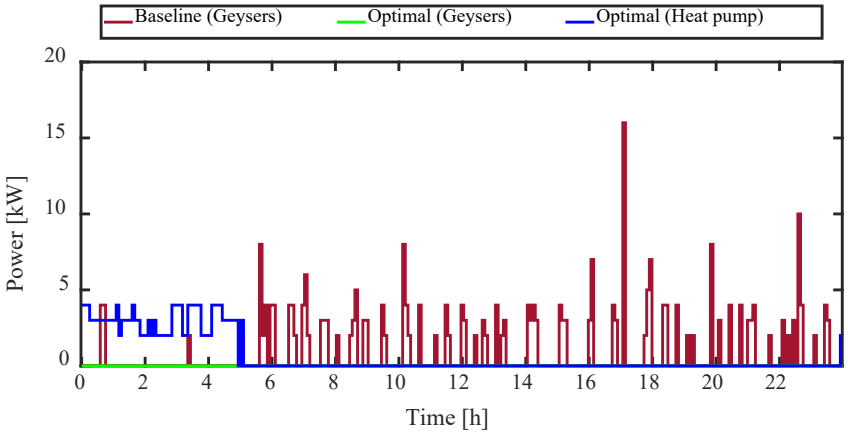


Figure 4.71. Seasonal power consumption for summer season.

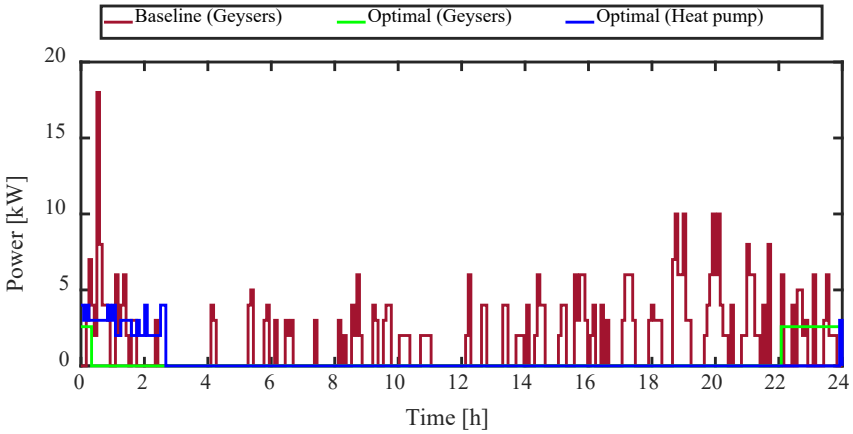


Figure 4.72. Seasonal power consumption for winter season.

**Comparison between the baseline and optimally controlled systems**

For the baseline case, continuous switching operation of the elements occurs throughout the day, which even take place during the morning and evening peak periods of the ToU price signals. The system operates anytime of the day to maintain the desired hot water temperature for the end user.

In the optimal case, the supplementary hybrid-source SAHP system has contributed to the reduction of the power consumption. The benefits are due to the use of:

- Thermal heating from the solar system, which is provided free and without electricity consumption; and
- The heat pump, which is at a very low consuming power but producing very high output power for the system.

Additionally, for the optimal operation, the system has been programmed to control power consumption with the aid of loads shifting using the Time-of-Use (ToU) tariff pricing signals. This shifts the loads from the high and costly peak periods to the low-cost periods, such as off-peak periods.

As a result, all switching has shifted to the off-peak periods. With the retrofitted system in the TWS tank, the supplementary energy source system can supply enough thermal heating which raises the temperature of the makeup water entering the multifarious ESTWH systems to a high enough level to maintain the desired temperature in the multifarious ESTWH systems. This has, therefore, resulted in the elimination of operation of some of the electric resistive elements. Additionally, no switching of the heat pump occurs for the summer season due to the high solar thermal energy gained by the solar collector. The TWS tank was able to utilize the thermal energy from the solar thermal collectors only to further heat the water that was pre-warmed by the building's multifunctional chillers.

The power consumptions of the baseline system occur even during the peak periods: in the summer case, a high-power demand is incurred during the evening peak period, whereas for the winter case, the high power demand is incurred during the early hours of the morning during the off-peak period. Furthermore, no operation of the heat pump occurs for the summer case. In the winter case, the heat pump operates during the morning and evening off-peak periods. Finally, for the optimally controlled cases in the summer and winter seasons, the power consumed by the multifarious ESTWH systems is incurred during the off-peak periods only.

## 4.4 COSTS CALCULATIONS AND ECONOMIC ANALYSIS

This section presents and analyses the techno-economic performance of the baseline and optimally controlled systems. The two systems are then compared to determine the costs savings and the reduction in energy and $CO_2$ emission for the project lifespan of 20 years.

This section presents the initial implementation costs, estimated using current prices from South African manufacturers and suppliers to determine the total initial cost of the project. This is followed by the presentation and comparison of the possible cumulative energy consumption and the associated costs that the two systems may incur during hot water production. The possible cumulative replacement costs, based on the manufacturers'

recorded lifespan of each component within the project duration, are then presented. Additionally, the calculations of the operation and maintenance costs are indicated. Moreover, the salvage costs of the system are presented, and finally, the total life-cycle costs of the baseline and the proposed system are calculated and compared.

**Initial implementation cost of the proposed system**

The initial implementation costs of the baseline and proposed systems are determined by the costs of the Bills of Quantities (BoQ) for the components used. These bills focus on the main components of the systems only, and the breakdown of the components with their respective costs is presented in Table 4.2 and Table 4.3 for the baseline and proposed systems, respectively. These costs are then summed up to determine the total initial implementation costs for each system. The average prices of these components were obtained from the manufacturers and companies in the South African market. The specification of these products conforms to Eskom (South Africa's main electricity supplier) and the South African Bureau of Standards (SABS) [17].

The total initial implementation costs ($C_{ini-imp}$) for the baseline and the proposed systems are approximated to 40,464,82 USD and 93,335.37 USD, respectively.

Table 4.2. Bill of quantity for the Baseline system.

| Description | Quantity | Unit price (USD) | Net price (USD) |
|---|---|---|---|
| AL-2000L Hot Water Storage Tank | 2 | 7,056.00 | 14,112.00 |
| Kwikot Superline 400 Dual Electric Geyser 100 L | 18 | 344.34 | 6,198.19 |
| Kwikot Superline 600 Dual Electric Geyser 150 L | 19 | 345.46 | 6,563.82 |
| Kwikot Superline 400 Dual Electric Geyser 200 L | 18 | 542.58 | 9,766.51 |
| Kwikot Superline 400 Dual Electric Geyser 250 L | 2 | 1,098.66 | 2,197.33 |
| 2kW Spiral Element (KwiKot) | 18 | 17.86 | 321.55 |
| 3kW Spiral Element (KwiKot) | 19 | 18.48 | 351.12 |
| 4kW Spiral Element (KwiKot) | 20 | 19.10 | 381.92 |
| Acm60 0.60kw centrifugal booster pump | 3 | 190.79 | 572.38 |
| | | Total initial investment costs of a Baseline system: | **40,464.82** |

Table 4.3. Bill of quantity for the Proposed system.

| Description | Quantity | Unit price (USD) | Net price (USD) |
|---|---|---|---|
| AL-2000L Hot Water Storage Tank | 2 | 7,056.00 | 14,112.00 |
| Kwikot Superline 400 Dual Electric Geyser 100 L | 18 | 344.34 | 6,198.19 |
| Kwikot Superline 600 Dual Electric Geyser 150 L | 19 | 345.46 | 6,563.82 |
| Kwikot Superline 400 Dual Electric Geyser 200 L | 18 | 542.58 | 9,766.51 |
| Kwikot Superline 400 Dual Electric Geyser 250 L | 2 | 1,098.66 | 2,197.33 |
| 2kW Spiral Element (KwiKot) | 18 | 17.86 | 321.55 |
| 3kW Spiral Element (KwiKot) | 19 | 18.48 | 351.12 |
| 4kW Spiral Element (KwiKot) | 20 | 19.10 | 381.92 |
| Acm60 0.60kw centrifugal booster pump | 1 | 190.79 | 190.79 |
| ITS 20 Tube ETC Collector | 8 | 699.94 | 5,599.55 |
| 11kW Commercial Heat Pump | 1 | 1,567.72 | 1,567.72 |
| SR609C Intelligent Geyser Temperature Controller 3000W | 58 | 83.72 | 4,855.76 |
| EBARA 2CDX 70/20T 1.5KW booster pump | 2 | 610.18 | 1,220.35 |
| 110℃ Air Release Valve | 58 | 13.94 | 808.75 |
| Labour | - | 39,200.00 | 39,200.00 |
| | | Total initial investment costs of the Proposed system: | **93,335.37** |

**Cumulative energy and cost comparison**

The cumulative energy consumption and costs of the baseline and optimally controlled systems were obtained and compared for the summer and winter seasons. Two approaches were conducted and analysed in this section. The first approach was through the simulation results obtained from MATLAB. In this approach, the cumulative energy costs were calculated in correspondence with the switching profiles during the operation of the systems. For the optimal system, the cumulative costs of the heat pump unit and the multifarious ESTWH systems have been combined as the resultant cumulative costs.

For the second approach, the average daily cumulative energy and costs were calculated by considering the incorporation of the energy management practice of the ToU pricing structure and the optimal control to the primary objective function. To determine the annual cumulative energy and costs, the Eskom high and low demand season structure may be applied to determine the number of days for the low demand season and the high demand season per annum. Finally, the daily and annual energy and cost savings were subsequently calculated and presented.

- Daily cumulative costs through simulation

A. Summer season daily cumulative cost comparison

The baseline for the summer season has accumulated costs gradually throughout the day, with the highest costs incurred during the peak periods. Figure 4.73 shows that the baseline system incurred the highest power consumption for the multifarious ESTWH systems due to the continual accumulation of power consumption throughout the day.

For the optimal case, the power consumption of the heat pump and the multifarious ESTWH systems was incurred only during the early morning and evening off-peak periods, which resulted in significantly lower costs compared to the baseline system. A rough estimation shows the cumulative costs for the summer season at the end of the 24-hour period were 261.57 USD for the baseline system and 133.57 USD for the optimal system, respectively.

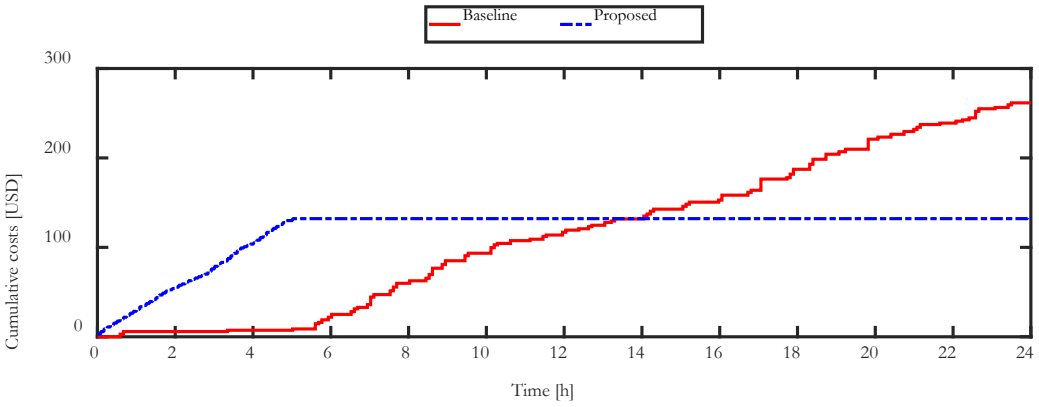


Figure 4.73. Daily cumulative energy costs for summer season.

B. Winter daily cumulative cost comparison

The baseline system accumulated higher costs as compared to the proposed system. This is due to the continuous operation of the system and the power consumption (Figure 4.74) that was incurred during the operation. The cumulative costs of the optimally operated system were accumulated only during the morning and evening off-peak ToU tariff price signals. The low energy consumption cost rates during these periods resulted in very low costs compared to the baseline system. The daily cumulative costs of the baseline system and the optimally controlled system for winter season are approximately 625.34 USD and 145.09 USD, respectively.

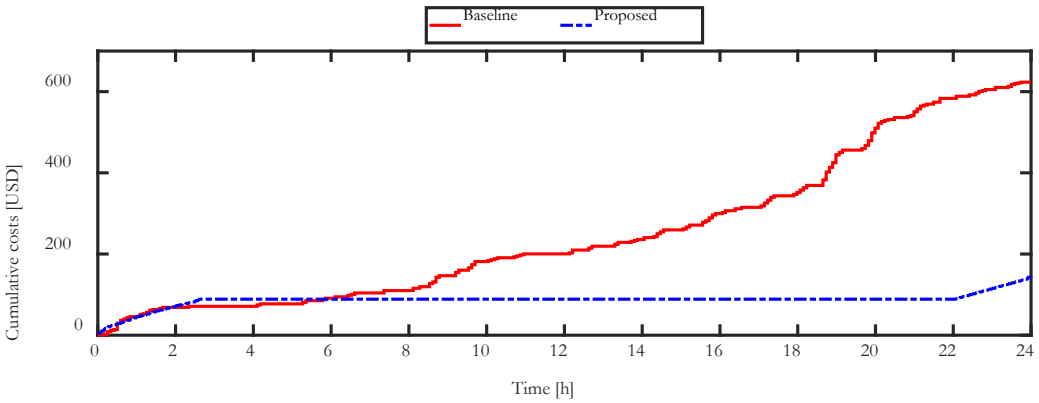


Figure 4.74. Daily cumulative energy costs for winter season.

- Calculated energy costs

The daily average cumulative energy and costs ($C_{d-EC}$) may be calculated by adapting the aggregate objective function in Eq. (4.3) into Eq. (4.11). The days of the year may be divided according to the Eskom high and low demand season's structure. The seasons are defined as 273 days of low demand (summer season) and 92 days of high demand (winter season) per annum, respectively [128]:

$$C_{d-EC} = \left[ t_s \left( \sum_{k=1}^{N} P_{EL(1),k} S_{EL(2),k} \times p_k + \sum_{k=1}^{N} P_{EL(1),k} S_{EL(2),k} \times p_k + \cdots + \sum_{k=1}^{N} P_{EL(N),k} S_{EL(N),k} \times p_k \right) + t_s \times p_{k,MAX} \sum_{k=1}^{N} \left( P_{EL(1),k} S_{EL(2),k} + P_{EL(1),k} S_{EL(2),k} + \cdots + P_{EL(N),k} S_{EL(N),k} \right) + t_s \sum_{k=1}^{N} \left( COP \times P_{hp,k} S_{hp,k} \right) \times p_k + t_s \times p_{k,MAX} \sum_{k=1}^{N} \left( COP \times P_{hp,k} S_{hp,k} \right) \right] \times C_{ToU,k} \quad (4.11)$$

Where $t_s$ is the sample interval; $P_{hp.k}$ is the rated power of the heat pump (kW); $P_{EL.k}$ is the power of the electric resistive element (kW); $S_{hp_k}$ the switching status of the heat pump; $S_{e_k}$ the switching status of the electric resistive element; and $C_{TOU_k}$ is the time-based cost of electricity at each $k^{th}$ interval (USD/kWh).

The annual cumulative energy and costs may, therefore, be summed up using the values from the summer and winter seasons. The total annual cumulative energy and costs ($C_{annual-EC}$) are determined by the product of the number of days and the energy costs accumulated in each respective season as shown in Eq. (4.12) [128].

$$C_{annual-EC} = C_{dl-EC} \times 273 + C_{dh-EC} \times 92 \quad (4.12)$$

Where $C_{dl-EC}$ is the daily cumulative energy and cost for the summer (low demand) season (USD); $C_{dh-EC}$ is the daily cumulative energy and cost for the winter (high demand) season (USD).

Table 4.4 presents the average daily cumulative energy consumption and costs of the baseline system and the optimally controlled proposed system, indicating the average daily energy and cost savings for a typical summer and a typical winter day, respectively. The average daily cost savings obtained are approximated to 16.44 USD and 65.40 USD for a typical summer and winter day, respectively.

For the annual cumulative energy and costs, the calculated results are presented in Table 4.5, showing the seasonal cumulative energy and costs, which are then added to determine the cumulative energy and costs over the first year of the project. The results show significant energy and costs savings from the optimally controlled proposed system, particularly for the winter season, as compared to the baseline system. This consequently yields a higher average for the annual savings.

Table 4.4. Daily energy and cost consumptions and savings.

| Season | Baseline operation | | Optimal control (Proposed) | | Daily Savings | |
|---|---|---|---|---|---|---|
| | Energy (kWh) | Cost (USD) | Energy (kWh) | Cost (USD) | Energy (kWh) | Cost (USD) |
| Summer | 69.42 | 32.05 | 42.70 | 15.61 | 26.72 | 16.44 |
| Winter | 122.81 | 83.96 | 39.02 | 18.55 | 83.79 | 65.40 |

Incorporating Time-of-Use (TOU) tariff structure and the optimal control made a significant impact due to the loads shifting to the notably low-cost pricing as compared to the baseline. Additionally, retrofitting the renewable energy system has contributed to the shaving off large amounts of energy, particularly during the day, which resulted in the significant energy and cost savings, and consequently, the owners gained significant costs savings.

The seasonal energy and costs savings for the baseline and optimally controlled systems may be approximated to 7,293.65 kWh and 4,488.34 USD for the summer season, and 7,708.28 kWh and 6,017.10 USD for the winter season, respectively. This means that the optimally controlled system may save approximately 38.50% and 68.20% of the energy, and 51.30% and 77.90% of the costs used by the baseline systems during the summer and winter seasons, respectively. The results at the end of the first year of the project indicate the total possible energy savings of 15,001.93 kWh and cost savings of 10,505.44 USD, which approximates to 49.60% and 63.80%, respectively. Given that South Africa's energy generation is highly $CO_2$-intensive, with an average $CO_2$ emission of approximately

942g/kWh of energy produced [131], this saving therefore means that a reduction of 15.93 metric tons of $CO_2$ emissions may be achieved.

Table 4.5. The seasonal energy and cost consumption and savings over the first year of the project.

| Season | Baseline operation | | Optimal control (Proposed) | | Annual Savings | | Annual Savings (%) | |
|---|---|---|---|---|---|---|---|---|
| | Energy (kWh) | Cost (USD) | Energy (kWh) | Cost (USD) | Energy (kWh) | Cost (USD) | Energy | Cost |
| Summer | 18,950.75 | 8,750.06 | 11,657.10 | 4,261.72 | 7,293.65 | 4,488.34 | 38.50 | 51.30 |
| Winter | 11,298.37 | 7,724.14 | 3,590.09 | 1,707.04 | 7,708.28 | 6,017.10 | 68.20 | 77.90 |
| **Total** | 30,249.12 | 16,474.20 | 15,247.19 | 5,968.76 | 15,001.93 | 10,505.44 | 49.60 | 63.80 |

- The annual cumulative energy costs

For the annual accumulative energy costs after the first year, the total annual cost of energy, shown in Table 4.5, is added to the initial implementation costs, which equals to the total cumulative cost for the first year after implementation. For the second year of the project, a 10% increase in the price of electricity is considered to calculate the annual energy costs, and is this figure is subsequently added to the previous year's cumulative costs. The process is then systematically applied year after year for the duration of the project.

The cumulative energy costs at the end of the project period, therefore, accumulated to 74,817.81 USD for the baseline system and 94,755.08 USD for the proposed system.

**Cumulative replacement cost**

The replacement costs ($C_{rep}$) may be determined by calculating the costs of each component that may require replacement during the period of the project, with respect to the number of replacements needed. The replacement costs for each component may be calculated using Eq. (4.13), where the average of the inflation rate (Figure 4.75 [132]) for a 20-year period (2003 to 2023) is considered. The total replacement costs are then summed up at the end of the project lifespan [ 53]:

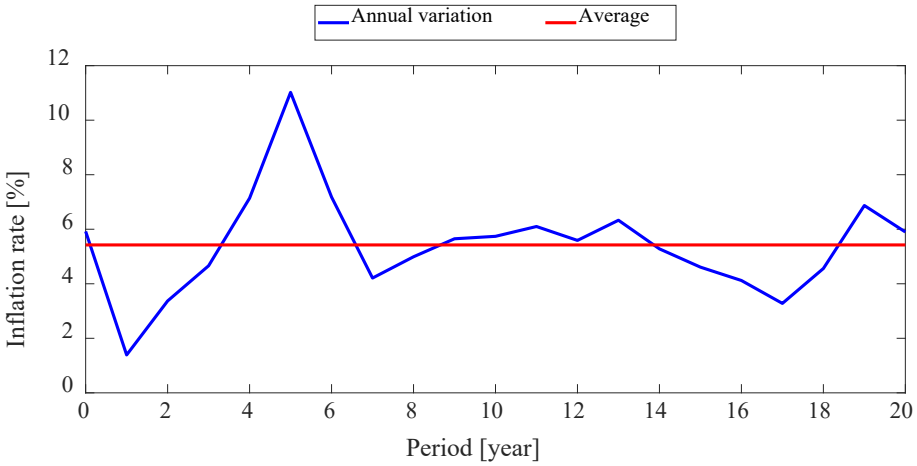


Figure 4.75. Inflation rate of South Africa (from 2003 to 2023) [132].

$$C_{rep} = t_s \sum_{k-1}^{N_{rep}} C_{cap} \times k(1 + n \times r) \quad (4.13)$$

Where $C_{cap}$ is the initial investment cost for each component; $N_{rep}$ is the number of component replacements of the project lifespan; $n$ is the specific component's lifespan (in years); $r$ is the average inflation rate over the predefined historic timeframe; and $k$ represents each year in the project lifespan.

Tables 4.6 and 4.7 present lists of the components for the baseline and the proposed systems, indicating the lifespan of each component, the number of replacements required, where required, and the possible costs associated with those replacements. It can be seen that most of the components require replacements, and only a few may be replaced more than once.

The cumulative replacement costs at the end of the project period are approximated to 74,817.81 USD for the baseline system and 94,755.08 USD for the proposed systems, respectively.

### Operation and maintenance costs

The total operation and maintenance cost ($C_{OM}$) during the project lifespan may be acquired using Eq. (4.14) The initial operation and maintenance cost at the end of the first year may be taken as 1% of the initial implementation cost ($C_{ini-imp}$) of the entire system [128]:

Table 4.6. Total replacement cost for the baseline system.

| **Components** | **Quantity** | **Lifespan (n) [years]** | **Replacements ($N_{rep}$)** | **Costs ($C_{rep}$) [USD]** |
|---|---|---|---|---|
| Baseline system study lifetime: n = 20 years | | | | |
| AL-2000L Hot Water Storage Tank | 2 | 15 | 1 | 25,594.13 |
| Kwikot Superline 400 Dual Electric Geyser 100 L | 18 | 15 | 1 | 11,241.31 |
| Kwikot Superline 400 Dual Electric Geyser 150 L | 19 | 15 | 1 | 11,904.42 |
| Kwikot Superline 400 Dual Electric Geyser 200 L | 18 | 15 | 1 | 17,712.96 |
| Kwikot Superline 400 Dual Electric Geyser 250 L | 2 | 15 | 1 | 3,985.17 |
| 2kW Spiral Element (KwiKot) | 18 | 15 | 1 | 583.18 |
| 3kW Spiral Element (KwiKot) | 19 | 15 | 1 | 636.81 |
| 4kW Spiral Element (KwiKot) | 20 | 15 | 1 | 692.67 |
| Acm60 0.60kw centrifugal booster pump | 3 | 8 | 2 | 2,467.17 |
| **$C_{rep}$ BTC (USD)** | | | | **74,817.81** |

$$C_{OM} = t_s \sum_{k-1}^{N_{rep}} C_{OM-initial} \times k(1 + n \times r) \quad (4.14)$$

Where: $C_{OM-initial}$ is the initial operation and maintenance costs; and $N$ is the number of years in the project lifetime.

The calculated cumulative operation and maintenance costs at the end of the project period are approximated to 13,996.05 USD and 32,283.01 USD for the baseline and optimal (proposed) system, respectively.

Table 4.7. Total replacement cost for the proposed system.

| Components | Quantity | Lifespan (n) [years] | Replacements ($N_{rep}$) | Costs ($C_{rep}$) [USD] |
|---|---|---|---|---|
| Hybrid system lifetime: n = 20 years | | | | |
| AL-2000L Hot Water Storage Tank | 2 | 15 | 1 | 25,594.13 |
| Kwikot Superline 400 Dual Electric Geyser 100 L | 18 | 15 | 1 | 11,241.31 |
| Kwikot Superline 400 Dual Electric Geyser 150 L | 19 | 15 | 1 | 11,904.42 |
| Kwikot Superline 400 Dual Electric Geyser 200 L | 18 | 15 | 1 | 17,712.96 |
| Kwikot Superline 400 Dual Electric Geyser 250 L | 2 | 15 | 1 | 3,985.17 |
| 2kW Spiral Element (KwiKot) | 18 | 15 | 1 | 583.18 |
| 3kW Spiral Element (KwiKot) | 19 | 15 | 1 | 636.81 |
| 4kW Spiral Element (KwiKot) | 20 | 15 | 1 | 692.67 |
| Acm60 0.60kw centrifugal booster pump | 1 | 8 | 2 | 822.39 |
| ITS 20 Tube ETC solar collectors | 8 | 25 | 0 | 0.00 |
| ITS 20 Vacuum Tubes ETC solar collectors | 8 | 15 | 1 | 4,671.94 |
| 22kW Commercial Heat Pump | 1 | 15 | 1 | 2,843.28 |
| SR609C Intelligent Geyser Temperature Controller 3000W | 58 | 15 | 1 | 8,806.61 |
| EBARA 2CDX 70/20T 1.5KW booster pump | 2 | 8 | 2 | 5,260.21 |
| 110℃ Air Release Valve lifetime | 1 | 20 | 0 | 0.00 |
| **$C_{rep}$ TC (USD)** | | | | **94,755.08** |

### Salvage costs

The salvage costs ($C_{salvage}$) were marked at 20% of the initial implementation costs ($C_{ini-imp}$) of the system, as shown in Eq. (4.15). This accounts for replacements and upgrades to higher efficiency systems in the future [128]:

$$C_{salvage} = 0.2 \times C_{ini-imp} \tag{4.15}$$

The calculated salvage costs for the baseline system and the proposed system are approximated to 8,092.96 USD and 18,667.07 USD, respectively.

### Total life cycle costs

The total life cycle costs (LCC) may be obtained by adding the initial implementation cost ($C_{ini-imp}$) with the costs described in Eqs. (4.12) through (4.14) and subtracting Eq. (4.15). This calculation results in the following, as shown in Eq. (4.16) [128]:

$$LCC = C_{ini-imp} + C_{annual-EC} + C_{rep} + C_{OM} - C_{salvage} \tag{4.16}$$

- Life cycle costs of the baseline and proposed systems

The summary of the 20-year calculated cumulative costs for the baseline system and the proposed system are presented in Table 4.8. The results show that the baseline system had low initial implementation costs, replacement costs, and the operation and maintenance costs. This may be due to the fewer components used to implement the baseline system, yielding to fewer components requiring replacement, operation and maintenance, as compared to the proposed system. However, the cumulative energy and costs of consumption is very high because the baseline system operates even during the costly periods of the TOU pricing structure and consequently obtaining the highest total life-cycle costs of the two systems.

The total life cycle costs over the 20-year period are approximated to 1,064,745.62 USD for the baseline system and 543,567.18 USD for the proposed system. The total life-cycle cost savings when using the proposed optimally controlled system are therefore

estimated to be 521,178.43 USD, which is about 48.95% of the costs of the baseline system saved.

Table 4.8. Life cycle costs comparison for over 20 years.

| **Cumulative Costs (USD)** | **Baseline** | **Proposed** | **Total savings** |
|---|---|---|---|
| $C_{INITIAL}$ (USD) | 40,464.82 | 93,335.37 | |
| $C_{rep}$ (USD) | 74,125.14 | 94,755.08 | |
| $C_{OM}$ (USD) | 13,996.05 | 32,283.01 | |
| $C_{EC}$ (USD) | 943,559.91 | 341,860.80 | |
| $C_{salvage}$ (USD) | 8,092.96 | 18,667.07 | |
| **Total LCC (USD)** | 1,064,745.62 | 543,567.18 | 521,178.43 |
| **LCC (%)** | | | 48.95 |

- Break-even point (BEP)

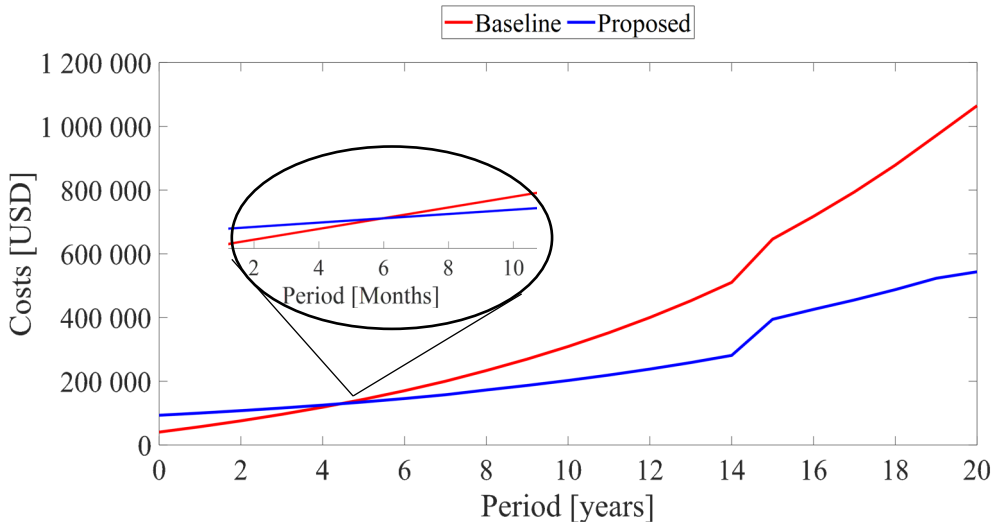


Figure 4.76. Break-even point.

The break-even point is the point where the life cycle costs of the two systems coincide at any given point during the 20-year project lifetime. This point is determined from the

graph illustrating the annual cumulative life cycle costs of a 20-year project lifespan, as shown in Figure 4.76, where it depicts the curves lines of the of the cumulative life cycle costs for the baseline and the optimally controlled systems.

The baseline system started with lower initial costs compared to the optimally controlled system., but immediately after the break-even point, its costs begin to accumulate more rapidly than the optimally controlled system. This rapid accumulation may be attributed to the high energy costs incurred during the operation of the baseline system, which lacks energy management and optimal control. The break-even point of this project is estimated to occur after 4 years and 6 months of the 20-year period at a cost of 129,385.76 USD.

## 4.5 SUMMARY

In this chapter, the mathematical models of the baseline system and the proposed hybrid-source WHR-TWS integrated with the SAHP system operated with the optimal control algorithm under the ToU pricing were developed, simulated and compared. While the baseline system utilises the WHR to pre-warm the water inside the TWS tank, the SAHP system retrofitted to the TWS tank supplements thermal heat through the STCs and heat pump unit, which work simultaneously to preheat the water inside the TWS tanks. The baseline system was operated without optimal control, leading to continuous operation throughout the day. Conversely, the proposed optimally controlled system is programmed to shift the loads from the peak periods, where the cost of operation is very high, to the low cost (off-peak) periods.

The simulation results for the operation of the systems presented switching function profiles and their corresponding hot temperatures of the multifarious ESTWH systems for both systems. For the proposed system, the heat pump unit's switching function was introduced, and the new-pre-heated water temperature profiles were also presented. The findings indicated that proposed system could optimally shift the loads to the off-peak regions and significantly reduce the operation of the electric resistive elements. Consequently, the hot water temperatures inside the multifarious ESTWH systems were maintained within the range of 50 ℃ to 60 ℃, which is safe considering the health of the

patients. Additionally, the simulated power consumption profiles of the baseline and optimally controlled systems were analysed and compared, indicating that the optimally controlled proposed system operated at reduced electric power consumption as compared to the baseline system, while maintaining the required heating loads, while simultaneously maintaining the required heating loads and delivering water at a safe temperature to the end-users.

For the economic analysis, the initial costs of the baseline case were lower as compared to the optimally controlled proposed case, but the baseline costs accumulated to be very high at the end of the project lifespan. This is due to the high cumulative costs incurred from continuous energy consumption throughout the day, even during the peak periods when the energy costs are very high. Conversely, the optimally controlled proposed system accumulated lower costs at the end of the project lifespan due to the retrofitted SAHP system, the optimal control operation, and load shifting of the energy demand to the off-peak TOU pricing signals.

The analysis indicated accumulated energy costs of 261.57 USD and 133.57 USD for the summer case and 625.34 USD and 145.09 USD for the winter case for the baseline system and optimally controlled proposed system, respectively, from the simulated results for a period of 24 hours. From the economic analysis calculations, the cumulative energy costs obtained for the baseline system and proposed optimally controlled system are 32.05 USD and 15.61 USD for the summer case and 83.96 USD and 18.55 USD for the winter case, respectively.

For the energy and cost savings analysis, the potential annual energy savings were estimated to be 15,001.93 kWh, which approximates to 49.60% per annum. This energy saving is equivalent is equivalent to a reduction of 15.93 metric tons of $CO_2$ emissions per year. At the beginning of the project, the initial implementation costs for the baseline and the proposed systems were approximated to 40,464,82 USD and 93,335.37 USD, respectively. Over the estimated 20-year project duration, based on the calculated results, the baseline system and the proposed optimally controlled system accumulated the following costs and salvage values: the cumulative energy costs were 943,559.91 USD and 341,860.80 USD, respectively. The cumulative replacement costs were 74,817.81 USD and 94,755.08 USD, respectively. The cumulative operation and maintenance costs were 13,996.05 USD

and 32,283.01 USD, respectively, and the salvage costs were 8,092.96 USD and 18,667.07 USD, respectively.

Finally, at the end of the project span, comparing the baseline system with the proposed optimally controlled system, the total life-cycle costs are approximated to 1,064,745.62 USD and 543,567.18 USD, respectively. These estimates equate to the cost savings of 521,178.43 USD, represents approximately 48.95% of the baseline system's costs saved.

These results demonstrate that the proposed hybrid-source WHR-TWS system, integrated with the SAHP system operated using the optimal control algorithm under the ToU pricing, guarantees the best energy management for high-capacity buildings with load shifting and optimal operational control. Furthermore, the economic analysis reveals significant economic and energy-saving potential, demonstrating a viable solution for reducing costs. The proposed system is therefore the best choice for high-capacity healthcare buildings and can also be extended to other types of high-capacity buildings that have a high demand for hot water production and utilize central TWS tanks.

The proposed system, which integrates renewable energy sources, waste heat recovery, and optimal energy management, offers significant savings and a potential reduction in $CO_2$ emissions, making it a sustainable alternative to conventional water heating methods. This success paves the way for further studies on its broader implementation and optimization.

# CHAPTER 5: PERFORMANCE EVALUATION OF THE PROPOSED SYSTEM USING ANN MODELLING

## 5.1 INTRODUCTION

In this chapter, a model validation of the proposed multifarious water heating systems, incorporating the hybrid-source WHR-TWS tanks integrated with the SAHP system, is conducted using the ANN modelling. The performance evaluation focuses on the thermal output temperatures of the TWS tanks and the multifarious ESTWH systems.

The TWS tanks and ESTWH systems were modelled separately. The 57 ESTWH systems had different sizes (100 L, 150 L, 200 L and 250 L), possessed different internal parameters. Consequently, these systems were grouped into four different models and trained separately. All trained models were conducted for both the summer and winter cases. System parameters were selected, and corresponding inputs and outputs were chosen for each system. The TWS tanks utilized five input variables and one output variable. The ESTWH systems utilized the same types of input and output variables, consisting of four input variables and one output variable for each ESTWH system.

This Chapter is structured into four sections: Section 5.2 describes the selection of variables and data processing. Section 5.3 presents the structure and the description of the ANN methodology. Section 5.4 presents the simulation results of the evaluation. Section 5.5 contains the summary of the chapter.

## 5.2 VARIABLE SELECTION AND DATA PROCESSING FOR THE ANN MODEL

In this section, the process of data selection for the model training of the TWS tanks and the ESTWH systems is described. This section outlines the data selection process, determines the input and output variables and presents the method of processing the raw data and importing it into MATLAB for simulation.

**Parameter selection and datasets**

The parameters for the ANN model training were determined from the energy balance equations used to model the thermal performance of the TWS tanks and ESTWH systems, as shown in Eqs. (3.13) and (3.26), respectively. The TWS tank and the ESTWH systems were predicted separately by creating two distinct prediction models, as illustrated in Figures 3.9 and 3.10.

The variable datasets from these equations represent the main parameters that contribute significantly to the final temperatures of the TWS tanks and ESTWH systems. The datasets used for the model training are presented in Section 3.2, which includes the solar thermal energy, the ambient air conditions, and the pre-warmed temperature for the baseline and proposed systems (demonstrated as profiles in Figures 3.5 - 3.8). Also included are the rated parameters of the systems and the simulation parameters presented in Tables 3.1 and 3.2. Other datasets utilized are the simulated preheated and hot water temperatures of the TWS tanks and ESTWH systems, along with the switching profiles and power consumptions of the heat pump unit and the electric resistive elements, presented in section 4.3.

**Determination and correlation of the inputs and outputs (targets)**

The input and output variables were chosen based on the parameters that causes the thermal energy gains and losses in the energy balance, specifically, those that provide power and thermal energy, causing energy gain to the system, and those that cause thermal energy losses by releasing thermal energy.

In the TWS tank, as shown in Eq. (3.13) and demonstrated in Figure 3.9, the energy gain is produced by the product of the heat pump power input and the COP ($P_{hp} \times COP$), and the product of the collector tube efficiency and the total incidence radiation ($\eta \times I_{\beta}(t)A_{abs}$) of the solar thermal energy over the surface area of the solar collector. The pre-warmed water temperature ($T_{mfc}(t)$) also contributes to the energy gain by warming the initially cold makeup water. The thermal heat loss coefficient of the surface area of the TWS tank ($U_L A_{TWS}$) and the ambient temperature ($T_{amb}(t)$) are the heat loss parameters that determines the heat lost to the surroundings through the walls of the TWS tank. These parameters have been selected as input variables of the TWS tank, as they affect the variation

in the pre-heated water temperature ($T_{TWS}(t)$) inside the TWS tank, which is TWS tank's output.

For the ESTWH systems, shown in Eq. (3.26) and illustrated in Figure 3.10, the energy gain is produced by the power input ($P_{EL}$) of the electric resistive element and the temperature of the pre-heated water temperature ($T_{TWS}(t)$) from the TWS tank when supplied to each ESTWH system. Also, for each ESTWH system, the thermal heat loss coefficient of the surface area of each ESTWH system ($U_L A_S$) and the ambient temperature ($T_{amb}(t)$) cause heat losses to the tank's surroundings. These parameters, therefore, the input variables of each ESTWH system, as they affect the variation in the hot water temperature ($T_S(t)$) inside the tank, which is the output variable for the ESTWH system.

**Data processing and importing data into MATLAB.**

For data processing, the datasets were taken at 5-minute time intervals over a 24-hour period, yielding a total of 288 points per parameter, as presented in Table 3.3 for the TWS tank and each ESTHW system. The datasets were aligned by grouping the input variables first and then the output variables in an excel file (.xslx). Four cases of datasets were arranged in separate sheets in the excel document, grouped for the summer and winter cases of the TWS tank and the ESTWH systems.

For the ESTWH systems, due to the systems having different sizes as shown in Table 3.1, the datasets were grouped by size and then by parameter type. This approach was necessary to ensure that parameters sharing the same physical limits and engineering ranges were grouped together and processed separately, preventing datasets being processed differently despite representing the same physical quantity.

The first stage of processing all datasets involved cleaning the data through the MATLAB software's "clean data" tool. The datasets were imported directly from the excel file into the software for each case and processed separately for each parameter type. The cleaning process consisted of three steps: first, identifying and correcting missing values in each parameter series; second, identifying and correcting outlier values that fell outside the expected distribution of the parameters; and lastly, smoothing the data to reduce high frequency fluctuations and measurement noise.

After separately cleaning all the data for each case, the second step was to export all the data back to the Excel file, followed by a consistency check.

The final step was data normalisation. The approached used to normalise the parameters involved using the engineering rated or maximum values of the parameters. This method was employed to make the parameters dimensionless while remaining consistent with their physical system limits. The general formula applied for the normalization was:

$$X_{norm} = \frac{X_{actual}}{X_{rated}} \quad \text{or} \quad X_{norm} = \frac{X_{actual}}{X_{max}} \tag{5.1}$$

Where: $X_{norm}$ is the normalized value of the parameter, $X_{actual}$ is the actual value of the parameter, and $X_{rated}$ / $X_{max}$ is the rated or maximum value of the parameter in a particular dataset.

This approach was chosen to avoid the issue of datasets containing zero denominator when using statistical scaling and to ensure that all values were consistently expressed between 0 and 1 under normal operating conditions. The average ranges of the actual values of the input and output variables is presented in Table 5.1.

Table 5.1. Summary of average ranges for input and output variables

| **Variables** | **Unit** | **Average range** | |
|---|---|---|---|
| $P_{hp} \times COP$ | kW | 0 –39,474 | |
| $P_{EL}$ | kW | 0 – 7,200 (100L); 10,800 (150L); 14,400 (200L & 250L) | |
| $U_L A_{TWS}$ | W/°C | 0 – 7.4188 | |
| $U_L A_S$ | W/°C | 0 – 1.476 (100L); 1.861 (150L); 1.757 (200L); 1.564 (250L) | |
| $T_S(t)$ | °C | 50 – 60 | |
| | | ***Summer case*** | ***Winter case*** |
| $\eta \times I_\beta(t) A_{abs}$ | W | 1.0187 – 57,343.7 | 0.0798 – 24,018.6 |
| $T_{mfc}(t)$ | °C | 29 – 47.2 | 35.4 – 46.5 |
| $T_{TWS}(t)$ | °C | 53,44 – 65 | 53.08 – 65 |
| $T_{amb}(t)$ | °C | 18.85 – 36.47 | 0.367 – 17.35 |

## 5.3 STRUCTURE AND DESCRIPTION OF ANN MODEL INPUT-OUTPUT FITTING, REGRESSION AND CURVE-FITTING (NFTOOL)

Following the data selection and processing, this section, the ANN models of the proposed system were trained, validated and tested for the summer and winter cases using the Levenberg-Marquardt backpropagation (LM-BP) function. Each variable had 288 data points, representing a 5-minute interval over a 24-hour period. For training, the ANN model utilized a data split proportion of 70% for training, 15% for validation, and 15%, for testing.

This section presents the ANN model formulation and details the ANN modelling and training of the proposed system.

### ANN model formulation

The Multilayer Perceptron (MLP) is comprised mainly of three layers: an input layer, one or more hidden layers, and an output layer. Within each layer, there are several neurons, with every neuron connected to the neurons of the subsequent layer by a different weight. Initially, these weights have no meaning, but they contain meaningful information after training [134]. Each neuron receives input data from other neurons, passes it through the hidden layers, and finally to the output layer. The output of each neuron is the result of a weighted set of inputs. The sum of weighted inputs formed by neurons is given as [135]:

$$X = \sum_{i=1}^{n} (w_i a_i - b) \tag{5.2}$$

where, $n$ is the number of input data ($i = 1,2,3, \ldots n$) and $w_i$ are the interconnecting weights of the input data itself $a_i$, respectively. $b$ is the bias for the neuron.

The knowledge is stored in the form of set of connection weights and biases. A transfer function F processes the sum of the weighted inputs and the bias, and the resulting output is given by [135]:

$$Y = F(X) = F\left[\sum_{i=1}^{n} (w_i x_i - b)\right] \tag{5.3}$$

The number of hidden neurons directly determines the model complexity of ANN. However, increasing the number of hidden layer neurons increases the chances of over-fitting the training data, reduces the ANN's generalization capability, and minimizes the training error [103]. Additionally, increasing the number of hidden layers has been proven to not necessarily improve the network's precision in estimation [117].

An appropriate learning algorithm is applied to adjust corresponding weights and bias values for the developed ANN model. In the present study, the LM-BP function was selected due to its fast training capability [117], its ability to minimize errors [98] and its effectiveness in maximizing the prediction accuracy of the model [136].

The performance of developed ANN is validated by the correlation coefficient (R) and the mean square error (MSE) as defined in Eqs. (5.4) and (5.5), respectively [117]:

$$R = \frac{\sum_{i=1}^{N}(X_{est,i} - \overline{X}_{est})(X_{ANN,i} - \overline{X}_{ANN})}{\sqrt{\sum_{i=1}^{N}(X_{est,i} - \overline{X}_{est})^2 \sum_{i=1}^{N}(X_{ANN,i} - \overline{X}_{ANN})^2}} \tag{5.4}$$

$$MSE = \frac{1}{N}\sum_{i=1}^{N}(X_{est,i} - X_{ANN,i})^2 \tag{5.5}$$

Where: $X_{est,i}$ is the estimated values for the i-th sample, $X_{ANN}$ is the actual target value using ANN for the i-th sample; and $\overline{X}$ denotes the average values of the estimated data and actual target values.

### ANN model training and testing

Before training the model, the datasets were first run in the MATLAB software to import the data to the workspace, where they were grouped as input and output variables. Subsequently, the neural network tool was started. The input and output variables were then imported to the two-layer feedforward network utilizing sigmoid hidden neurons and linear output neurons.

The TWS tank have five input variables and 1 output variable, and the ESTWH system model has four input variables and one output variable, as presented by their structures/architectures in Figures 5.1 and 5.2, respectively.

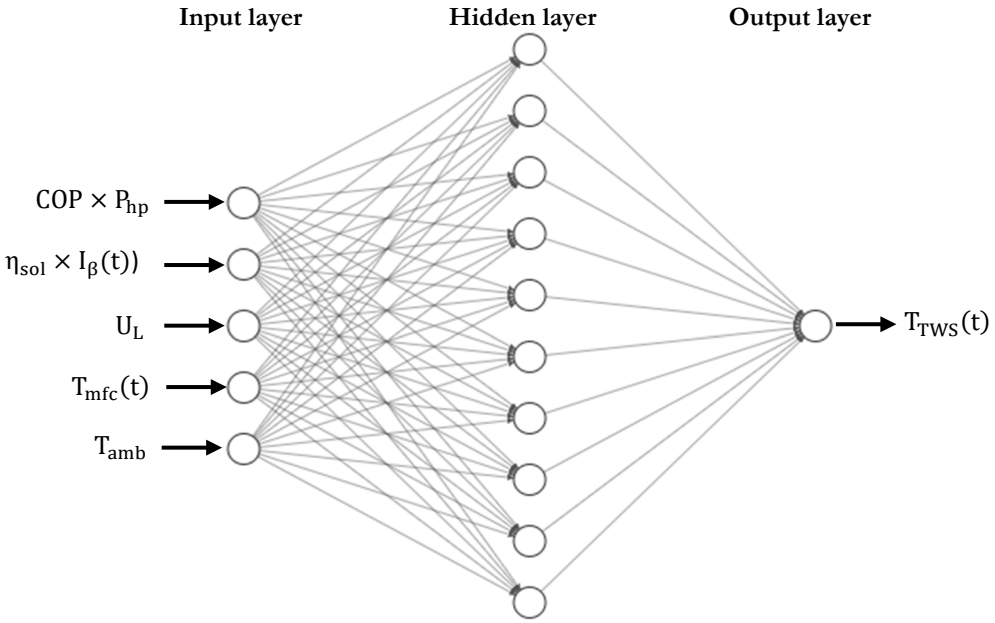


Figure 5.1. Schematic structure of an ANN Architecture for the TWS tank.

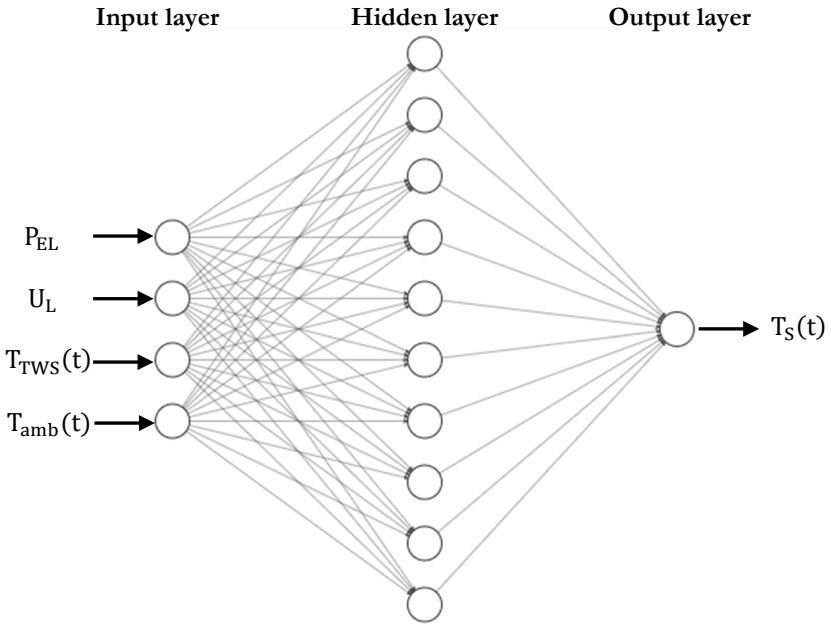


Figure 5.2. Schematic structure of an ANN Architecture for the ESTWH systems.

For training, the ANN model was carried out using the proportions of 70 % for the training set, 15 % for the validation set, and 15 % for the testing set. The structures/architectures of the ANN models each consist of three layers: an input layer, a hidden layer, and an output layer. Specifically, the ANN architecture for the TWS system, as

shown in Figure 5.1, consists of four neurons for the input layer, ten neurons for the hidden layer, and one neuron for the output layer. The ANN architecture model for the ESTWH system, shown in Figure 5.2, has five neurons in the input layer, ten neurons in the hidden layer and one neuron in the output layer.

## 5.4 RESULTS AND DISCUSSION OF THE ANN MODELS

This section discusses the results obtained for the summer and winter cases, respectively. The findings of this study consist of the ANN model predictions of the TWS tank and ESTWH systems for the cases of a typical summer day in the month of January 2023 and a typical winter day in the month of July 2023. The ESTWH systems were trained as per the size parameters of the 100L, 150L, 200L, and 250L, and the models were trained for the summer and winter case for each size parameter.

The models were evaluated across three standard phases: training, validation, and testing. From the simulated results, the analysis of the training state variables plots is presented, showing the gradient error, the value of μ, and the validation check error pattens. This is followed by the training results of the regression performance plots, showing the correlations and coefficient of correlation (R) of each phase, as well as for the case of the three phases combined (ALL). Then, the performance validation figures, indicating the MSE curves, are also analysed. Lastly, the error distribution histogram plots showing the error distributions of the three phases, each with 20 Bins, are presented.

### Training state variables

- TWS tank

Figures 5.3 and 5.4 present the gradient error, value of μ, and the validation check error of the TWS tank for the summer and winter cases, respectively. For the summer case (Figure 5.3), the model was trained at epoch 14, achieving a gradient error of 2.2847e-05, a μ value of 1e-07, and successfully completing 6 validation checks. For the winter case (Figure 5.4), the model trained at epoch 16, achieving a gradient error of 8.8894e-06, a μ value of 1e-06, and successfully completing 6 validation checks.

- ESTWH systems

The training results for the 100 L, 150 L, 200 L and 250 L size parameters are presented in Figures 5.6 - 5.9 for the summer case and Figures 5.10 - 5.12 for the winter case, respectively.

For the 100 L size parameter, the gradient error, μ and the validation check error, for the summer case (Figure 5.5), were achieved at epoch 14 with values of 5.441e-05, 1e-09, and 6, respectively. For the winter case (Figure 5.9), the training state was reached at epoch 13 at values of 2.5126e-07, 1e-07 and 6, respectively.

For the 150 L size parameter, the values of the gradient error, μ and the validation check error were 9.4729e-06, 1e-08 and 6 at epoch 12 for the summer case (Figure 5.6), and 4.2063e-06, 1e-08, and 6 at epoch 27 for the winter case (Figure 5.10), respectively.

For the 200 L size parameter, the model was trained at epoch 18 with values of 6.288e-07, 1e-08, and 6 for the summer case (Figure 5.7). For the winter case (Figure 5.11), the state variables were 1.095e-05, 1e-08, and 6 at epoch 15, for the gradient error, μ and the validation check error, respectively.

For the 250 L size parameter, the gradient error, μ and the validation check error values were 9.2253e-08, 1e-08, and 0 at epoch 21 for the summer case (Figure 5.8) and 9.5572e-08, 1e-08, and 0 at epoch 13 for the winter case (Figure 5.12), respectively.

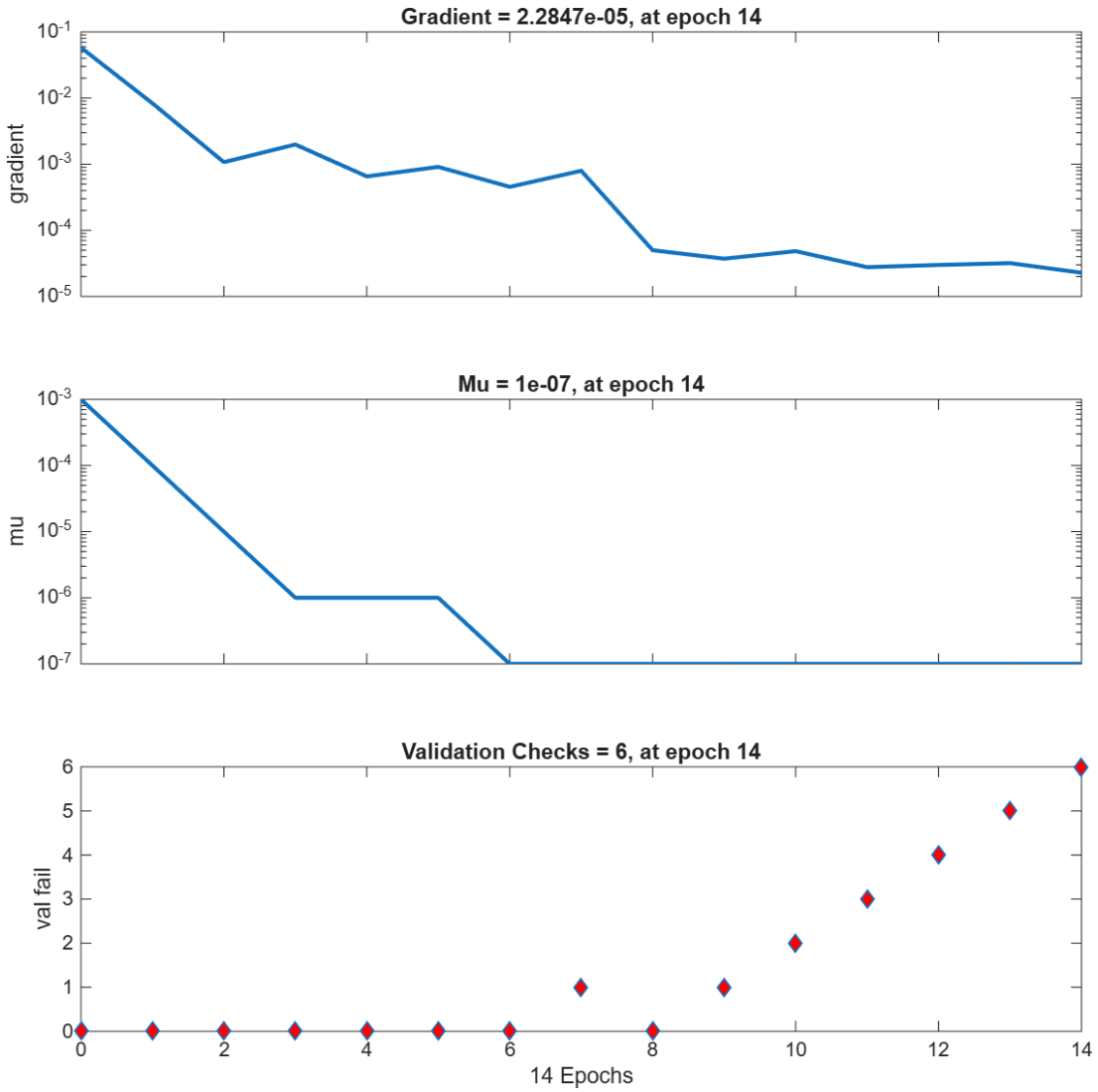


Figure 5.3. Training state variables plots of the TWS tank for the summer case.

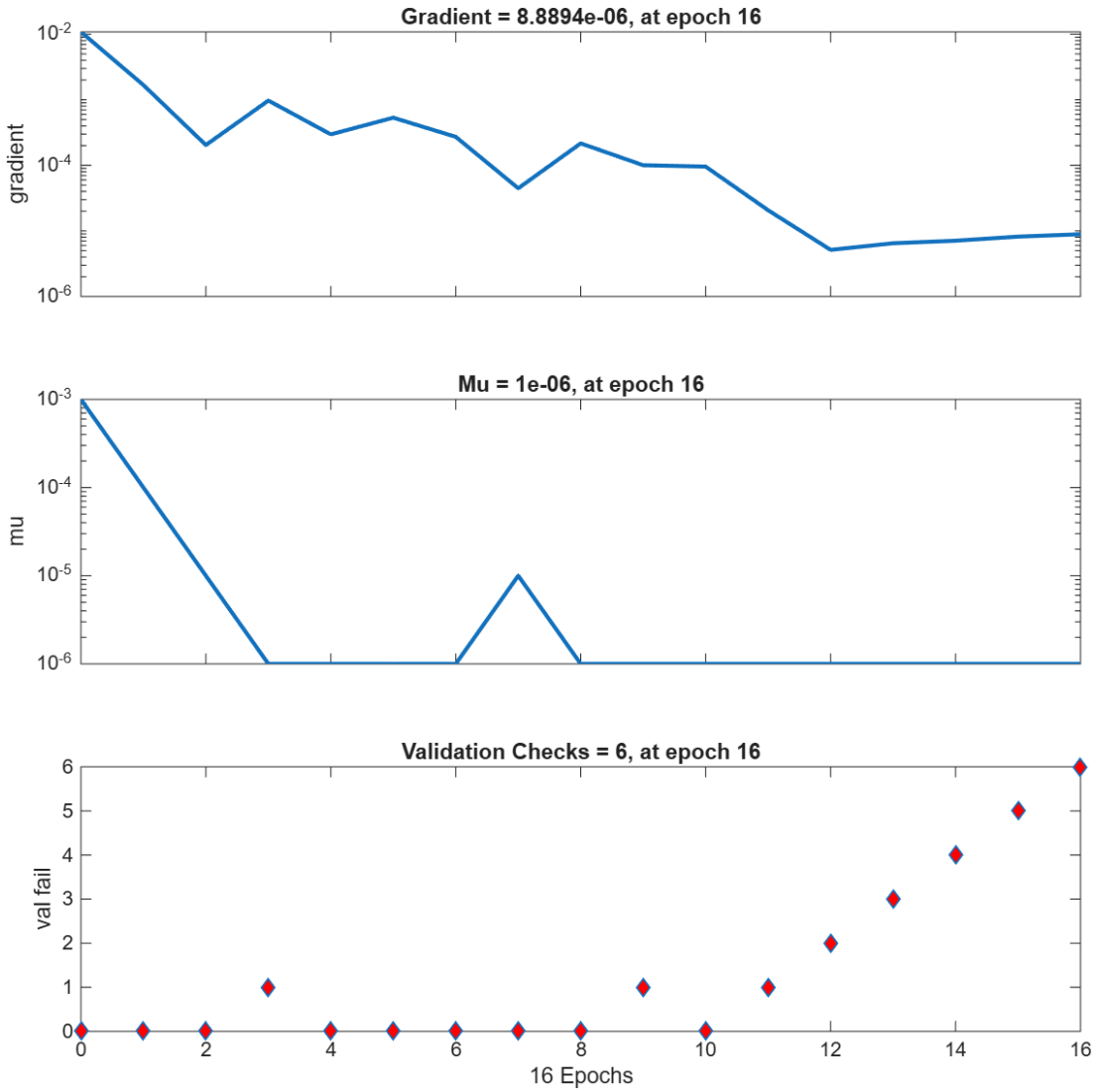


Figure 5.4. Training state variables plots of the TWS tank for the winter case.

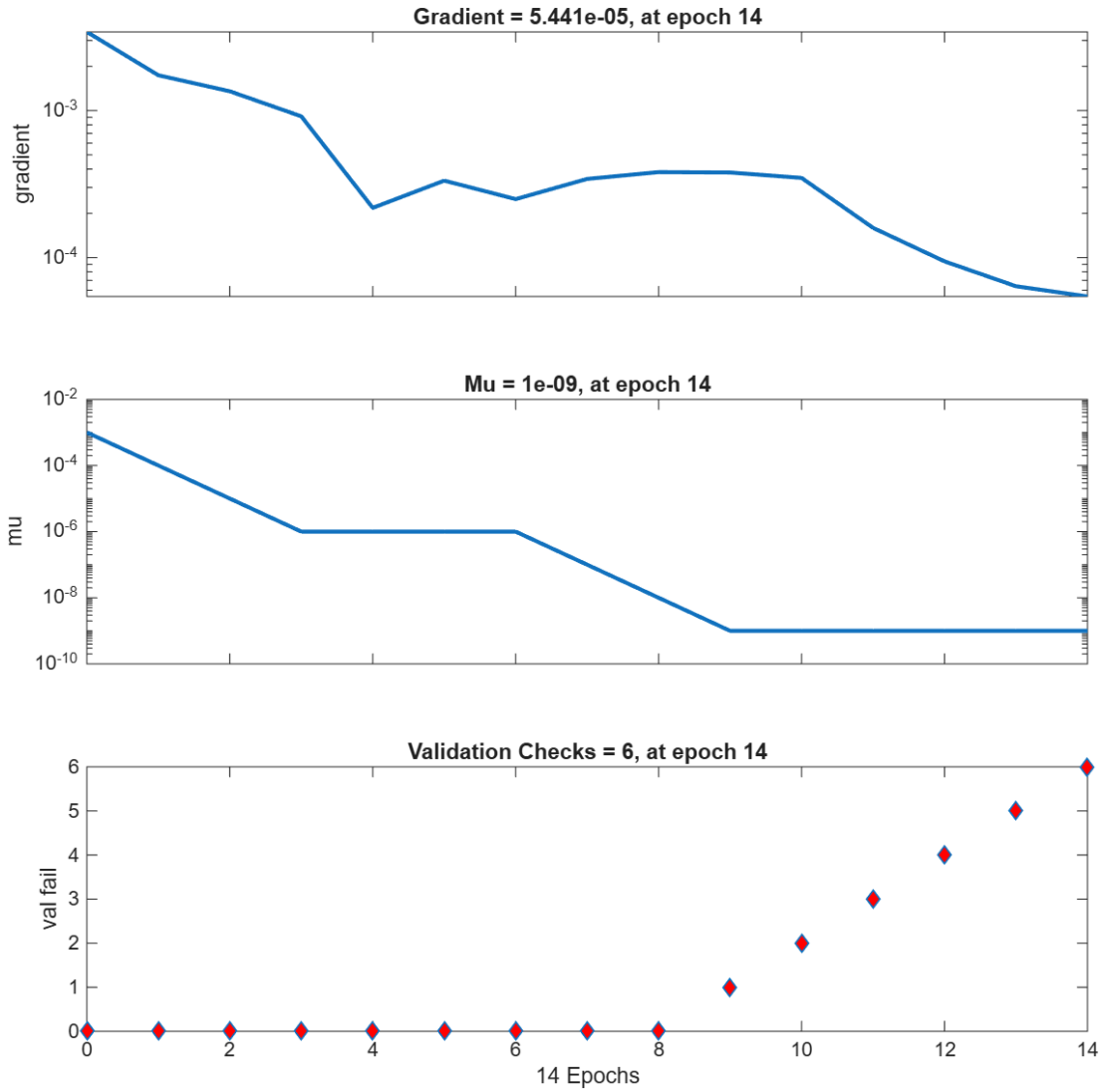


Figure 5.5. Training state variables plots of the 100L ESTWH systems for the summer case.

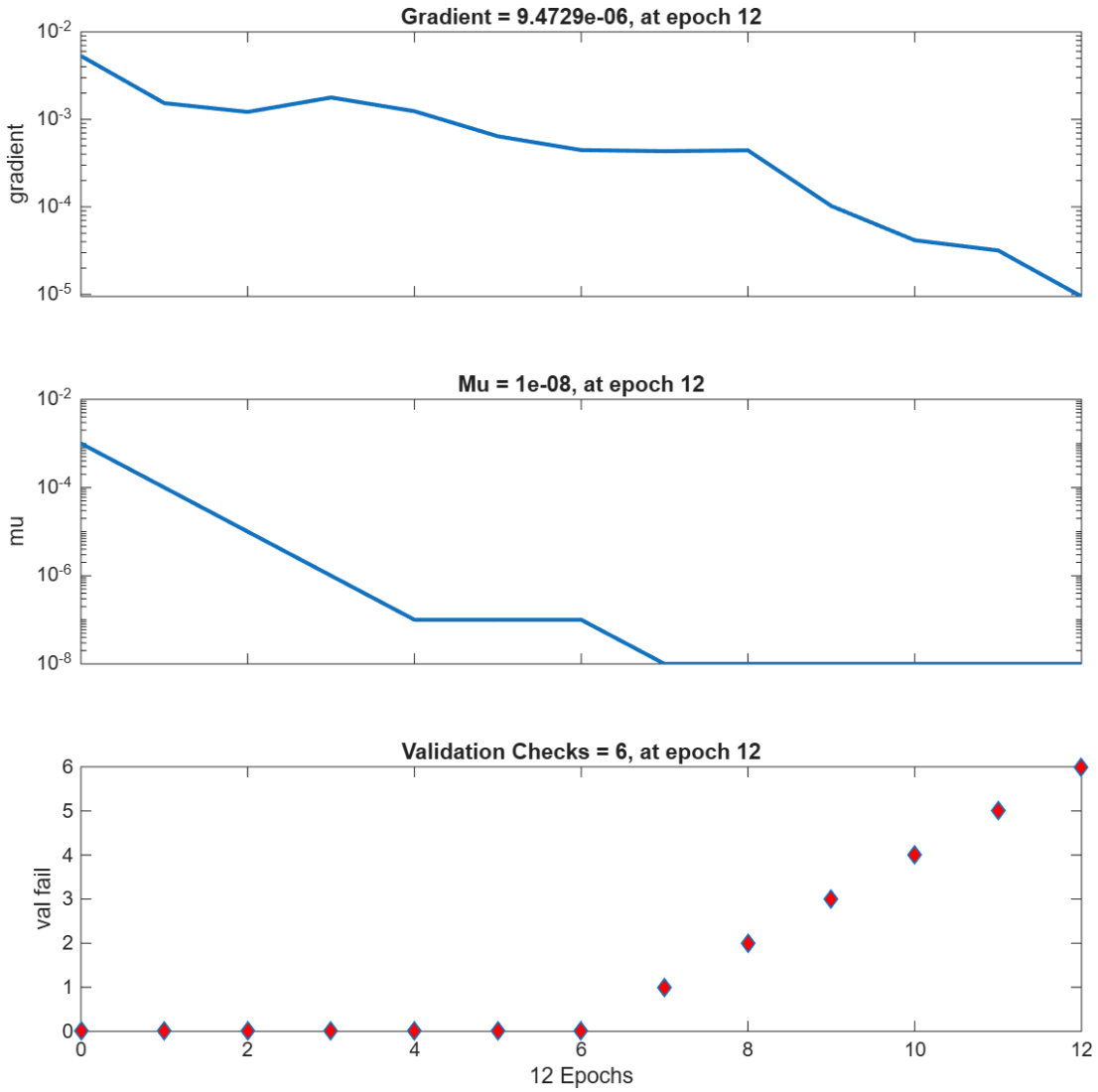


Figure 5.6. Training state variables plots of the 150L ESTWH systems for the summer case.

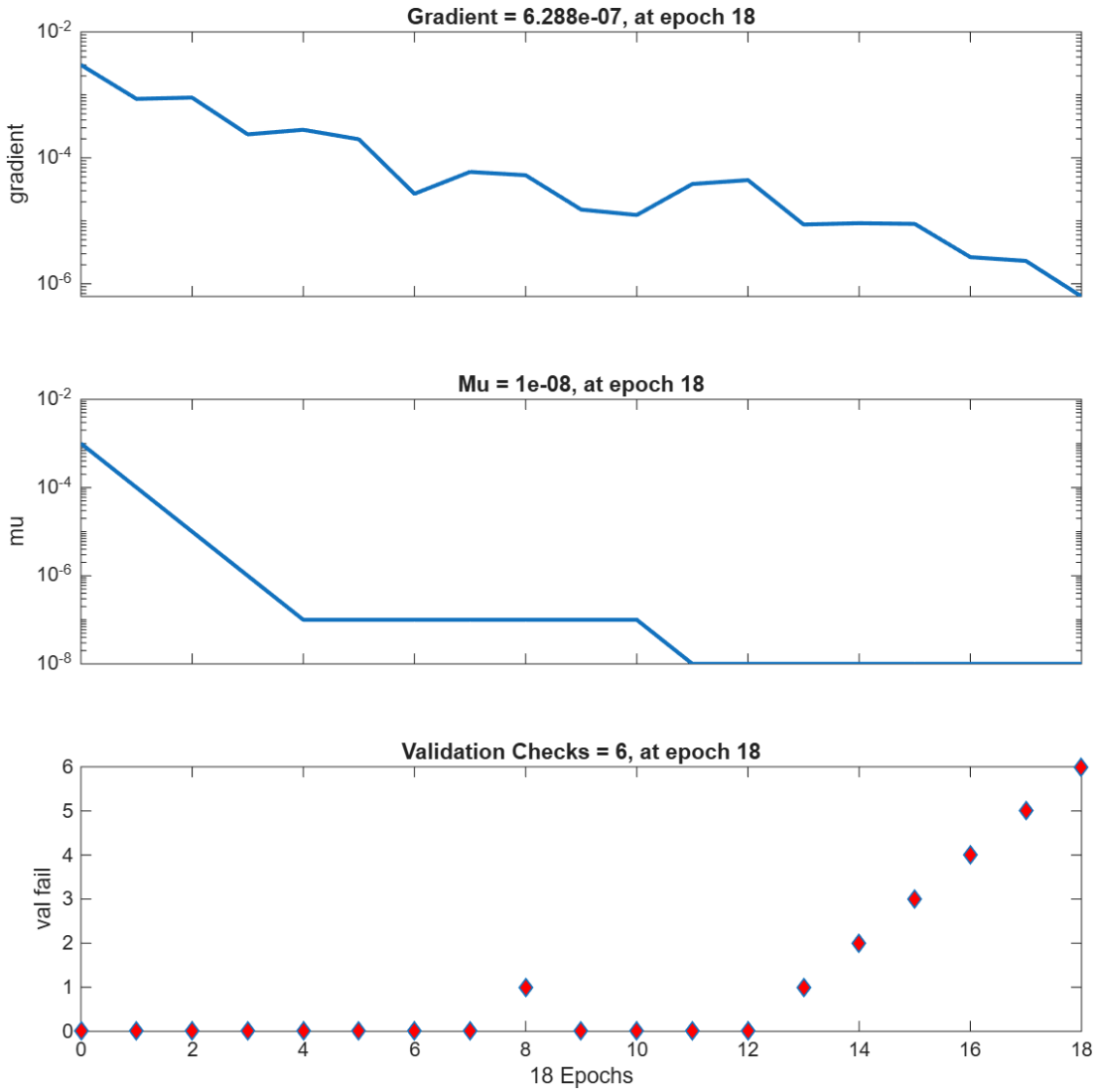


Figure 5.7. Training state variables plots of the 200L ESTWH systems for the summer case.

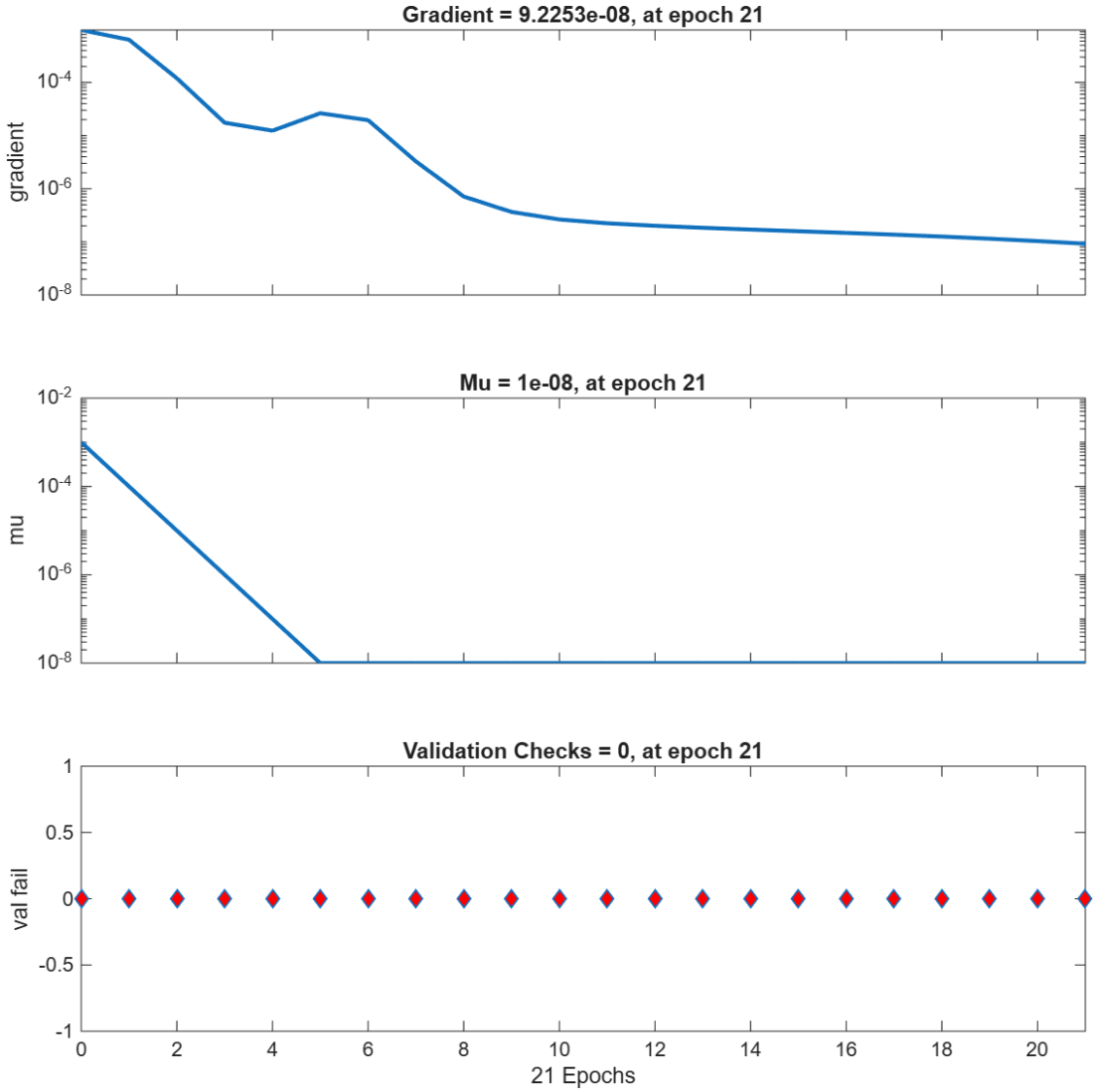


Figure 5.8. Training state variables plots of the 250L ESTWH systems for the summer case.

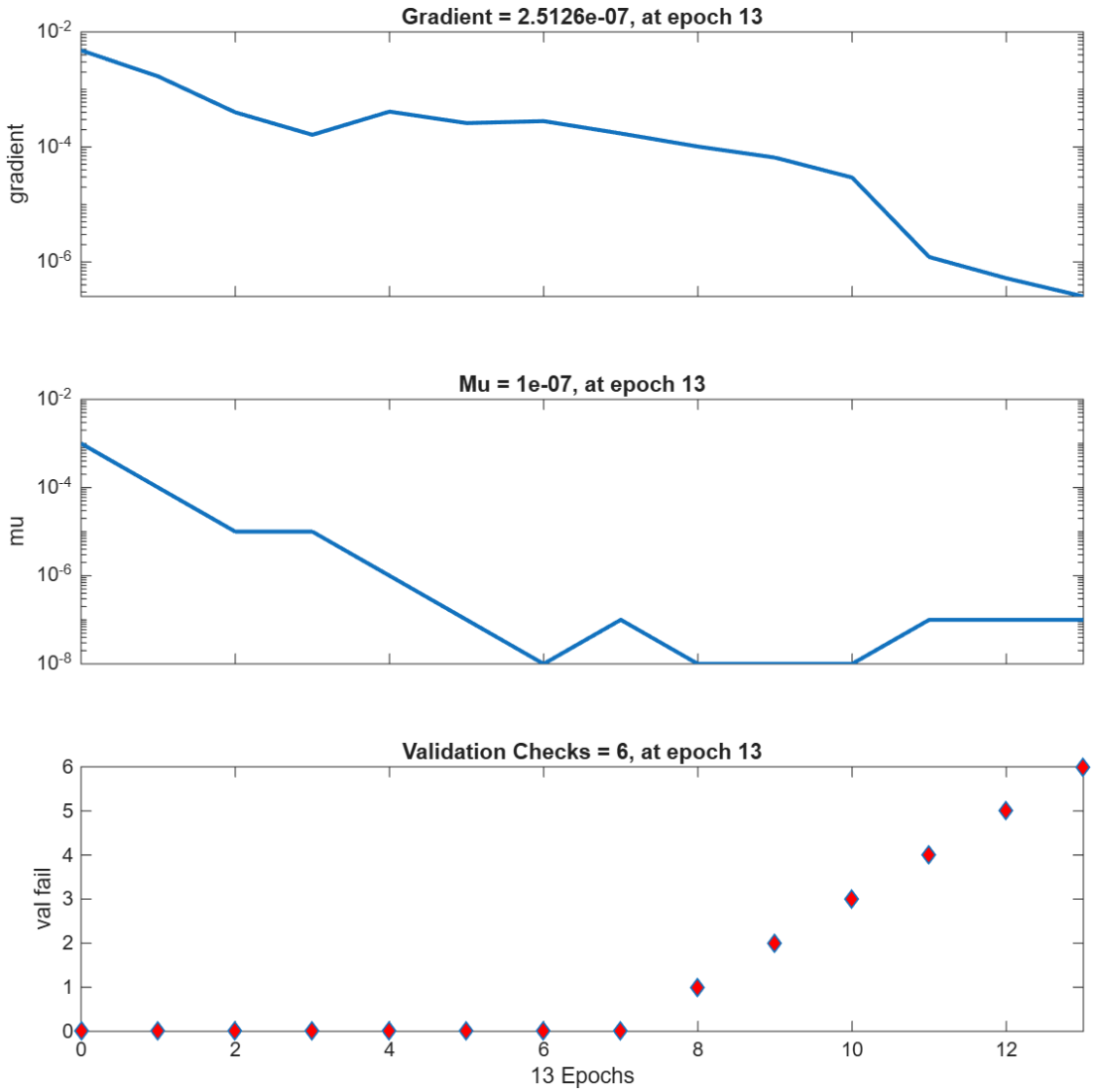


Figure 5.9. Training state variables plots of the 100L ESTWH systems for the winter case.

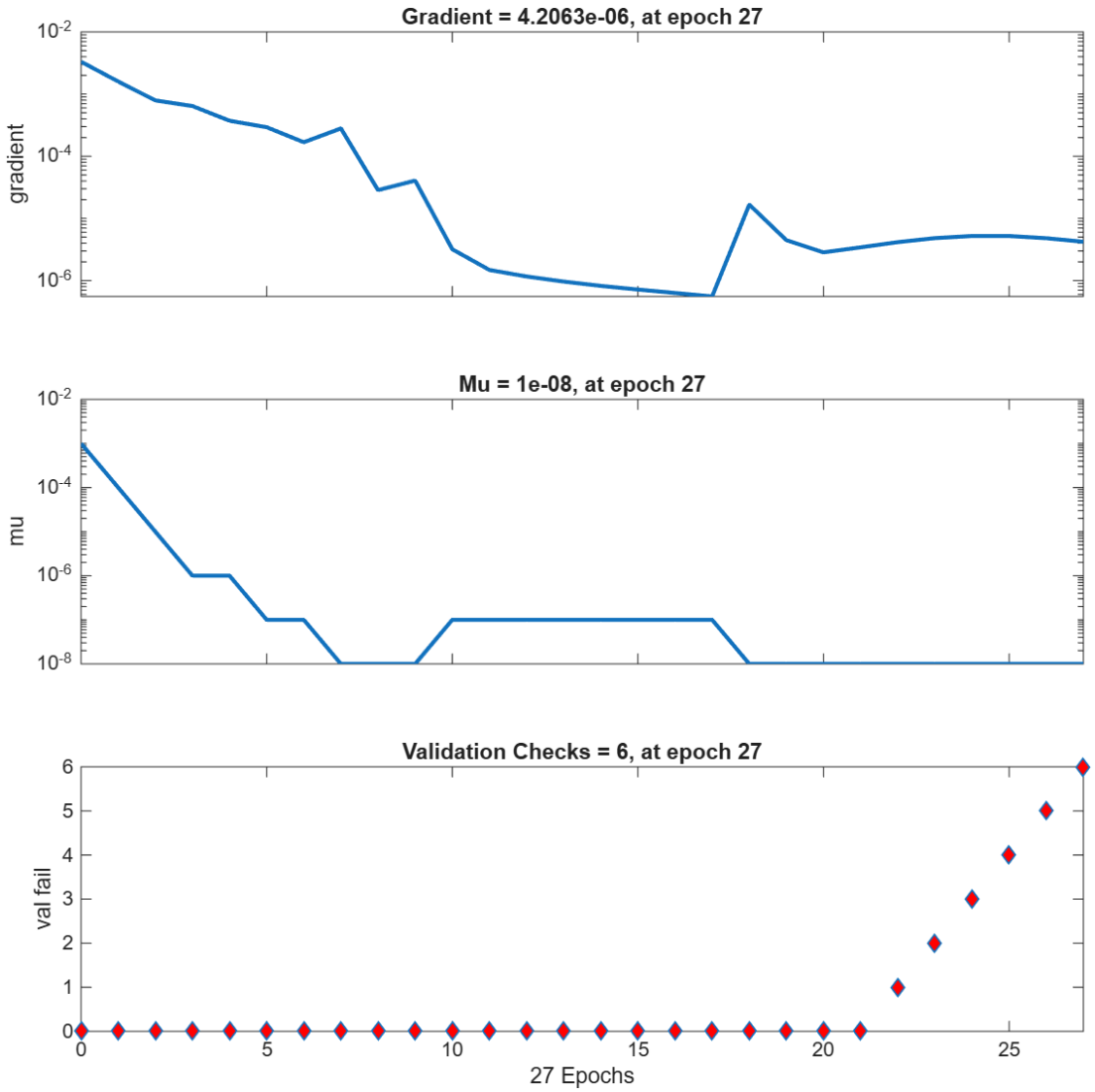


Figure 5.10. Training state variables plots of the 150L ESTWH systems for the winter case.

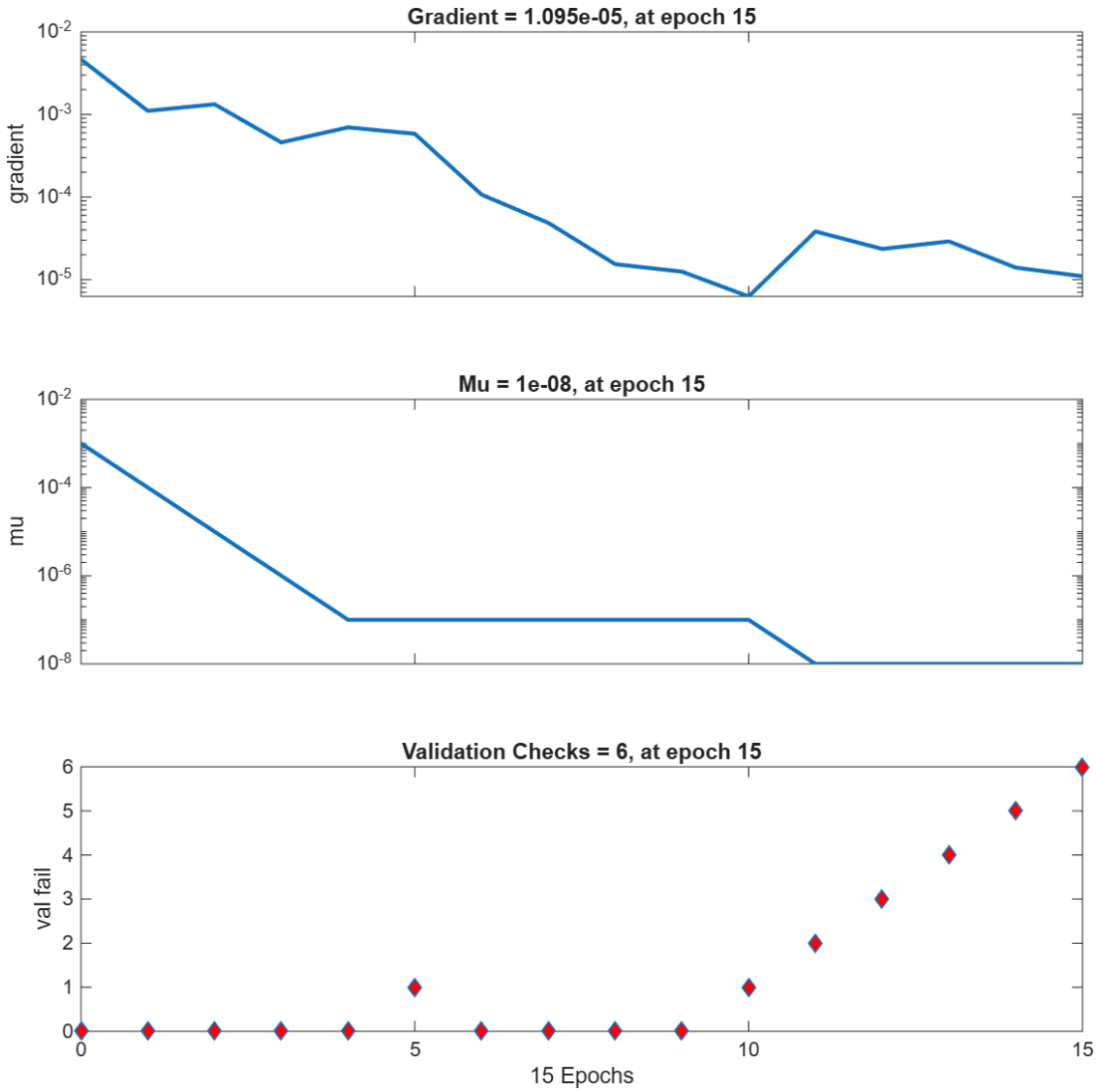


Figure 5.11. Training state variables plots of the 200L ESTWH systems for the winter case.

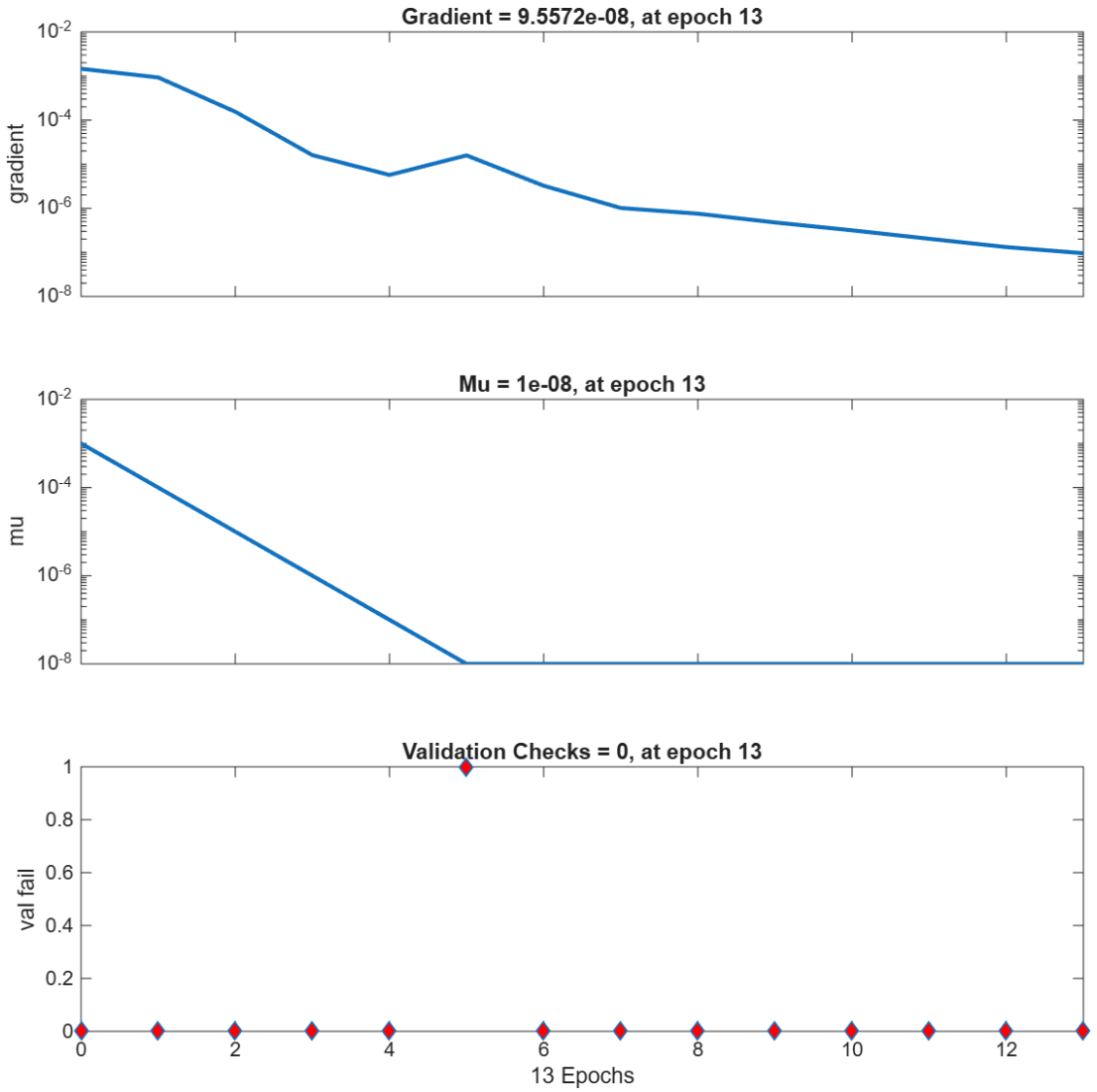


Figure 5.12. Training state variables plots of the 250L ESTWH systems for the winter case.

**Regression Performance: Correlation Coefficient (R)**

- TWS tank

The regression plots showing the Correlation Coefficient (R-values) for training, validation, test, and overall (ALL) phases for the TWS tank are presented in Figures 5.13 and 5.14 for the summer and winter cases, respectively. The R-values for the summer case (Figure 5.13) are 0.99414 (training), 0.99518 (validation), 0.98063 (test), and 0.99219 (ALL). The R-values for the winter case (Figure 5.14) are 0.96184 (training), 0.95444 (validation), 0.95494 (test) and 0.95971 (ALL). The summer case obtained higher R-values compared to the winter case. Furthermore, the regression plots for the summer case shows the dashed lines aligned closely along the ideal predictions, which indicates more accurate predictions.

- ESTWH systems

For the ESTWH systems, the regression plots showing the R-values for training, validation and test, for the size parameters of 100 L, 150 L, 200 L and 250 L, are presented in Figures 5.15 through 5.18 for the summer case and Figures 5.19 through 5.22 for the winter case, respectively.

The R-values of the 100 L size parameter are 0.99099 (training), 0.98313 (validation), 0.98563 (test) and 0.98895 (ALL) for the summer case (Figure 5.15), and 0.99859 (training), 0.98745 (validation), 0.99252 (test) and 0.99593 (ALL) for the winter case (Figure 5.19). The R-values of the 150 L size parameter are 0.99466 (training), 0.98531(validation), 0.9733 (test) and 0.98997 (ALL) for the summer case (Figure 5.16), and 0.99959 (training), 0.99742 (validation), 0.99311 (test), and 0.99838 (ALL) for the winter case (Figure 5.20). For 200 L size parameter, the R-values for training, validation, test and ALL are 0.99959, 0.99854, 0.992 and 0.99822 for the summer case (Figure 5.17) and 0.99918, 0.98106, 0.99109 and 0.99505 for the winter case (Figure 5.21), respectively. For the 250 L size parameter, the R-values for training, validation, test and ALL are 0.99988, 0.99984, 0.99988 and 99987 for the summer case (Figure 5.18) and 0.99986, 0.99984, 99981 and 99984 for the winter case (Figure 5.22), respectively.

From the results presented, it can be observed that the R-values for the 100 L and 150 L size parameters are higher for the winter case compared to the summer case. Conversely, for the 200 L and 250 L size parameters, the higher R-values were obtained in the summer case as compared to the winter case.

Although exceptionally high R-values were obtained, cross-validation was conducted to verify the robustness of the model and to minimize the risk of overfitting. The dataset was divided into 70% training, 15% validation, and 15% testing subsets, and comparable performance levels were observed across all sets. This consistency confirms that the model generalizes well and that the results are realistic and reliable.

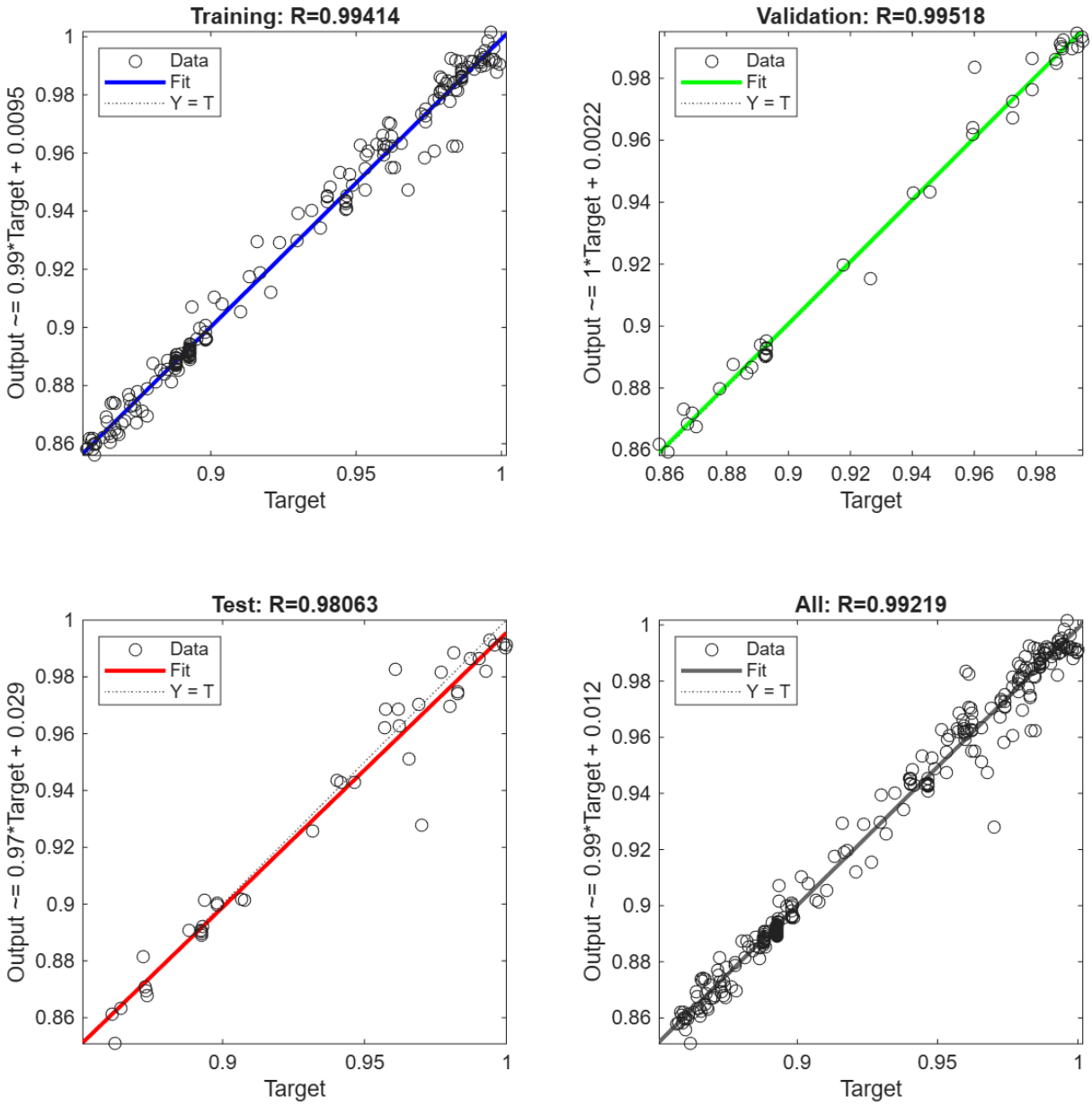


Figure 5.13. Regression plots of the TWS tank for the summer case.

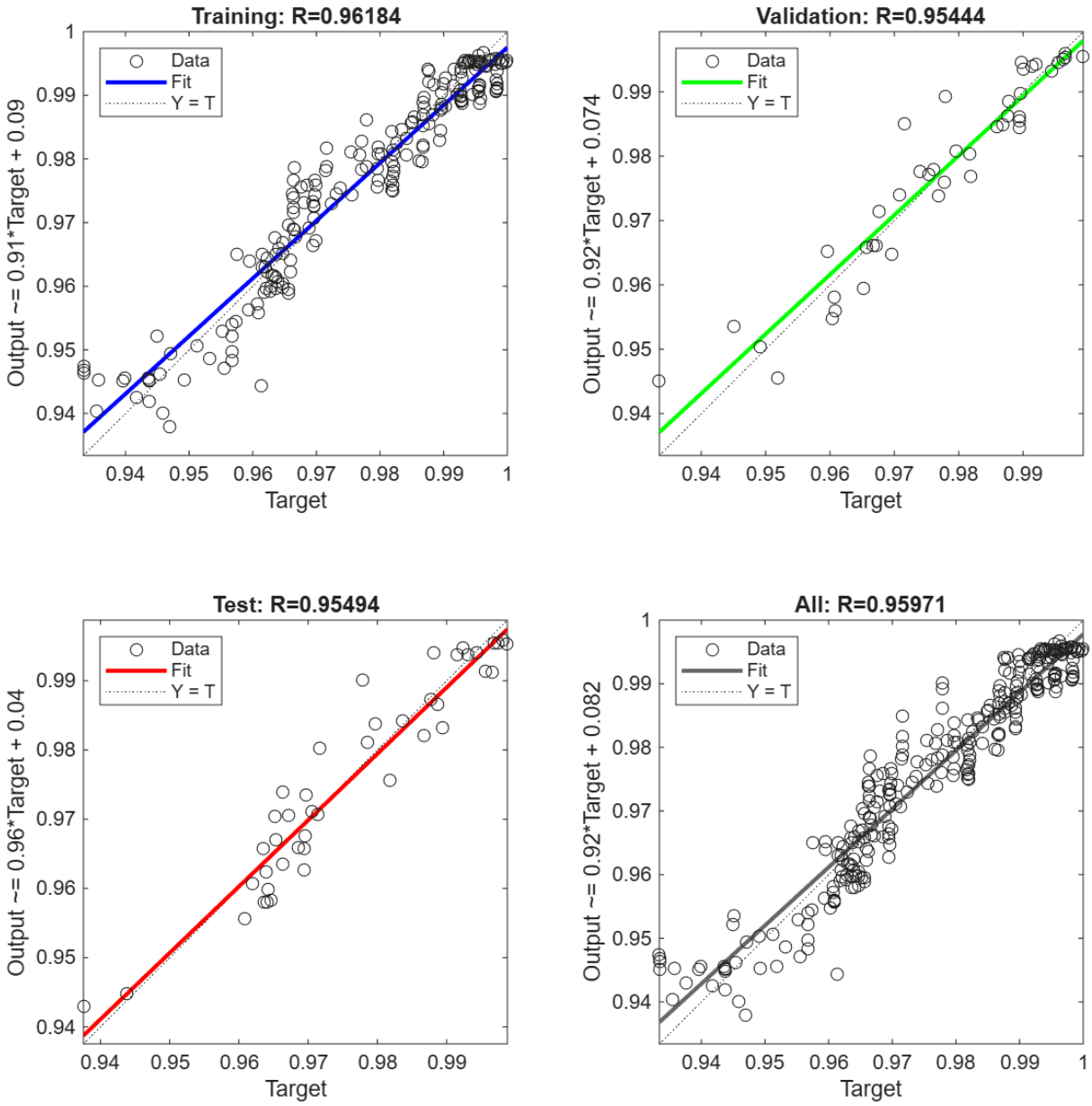


Figure 5.14. Regression plots of the TWS tank for the winter case.

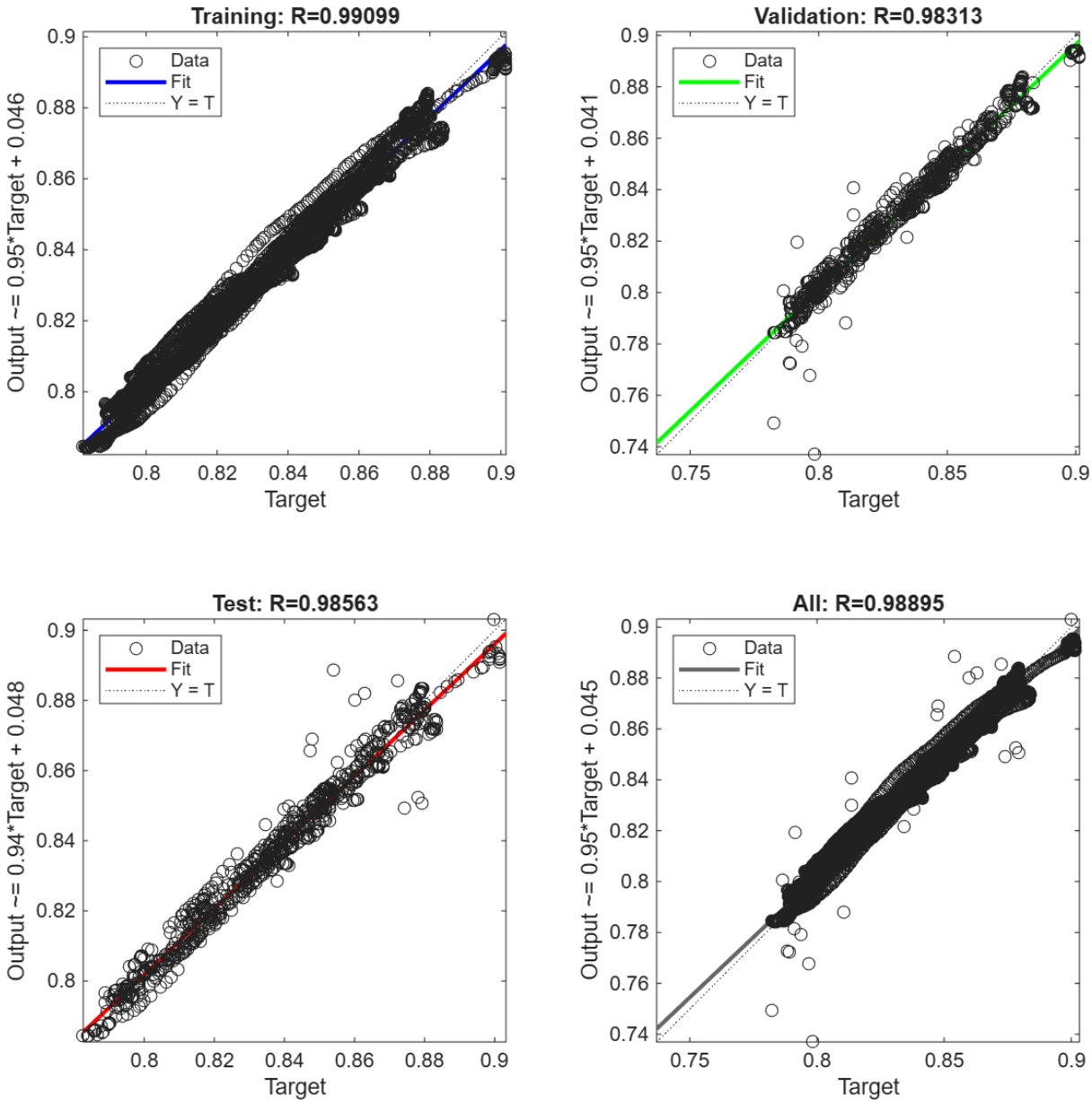


Figure 5.15. Regression plots of 100 L ESTWH systems for the summer case.

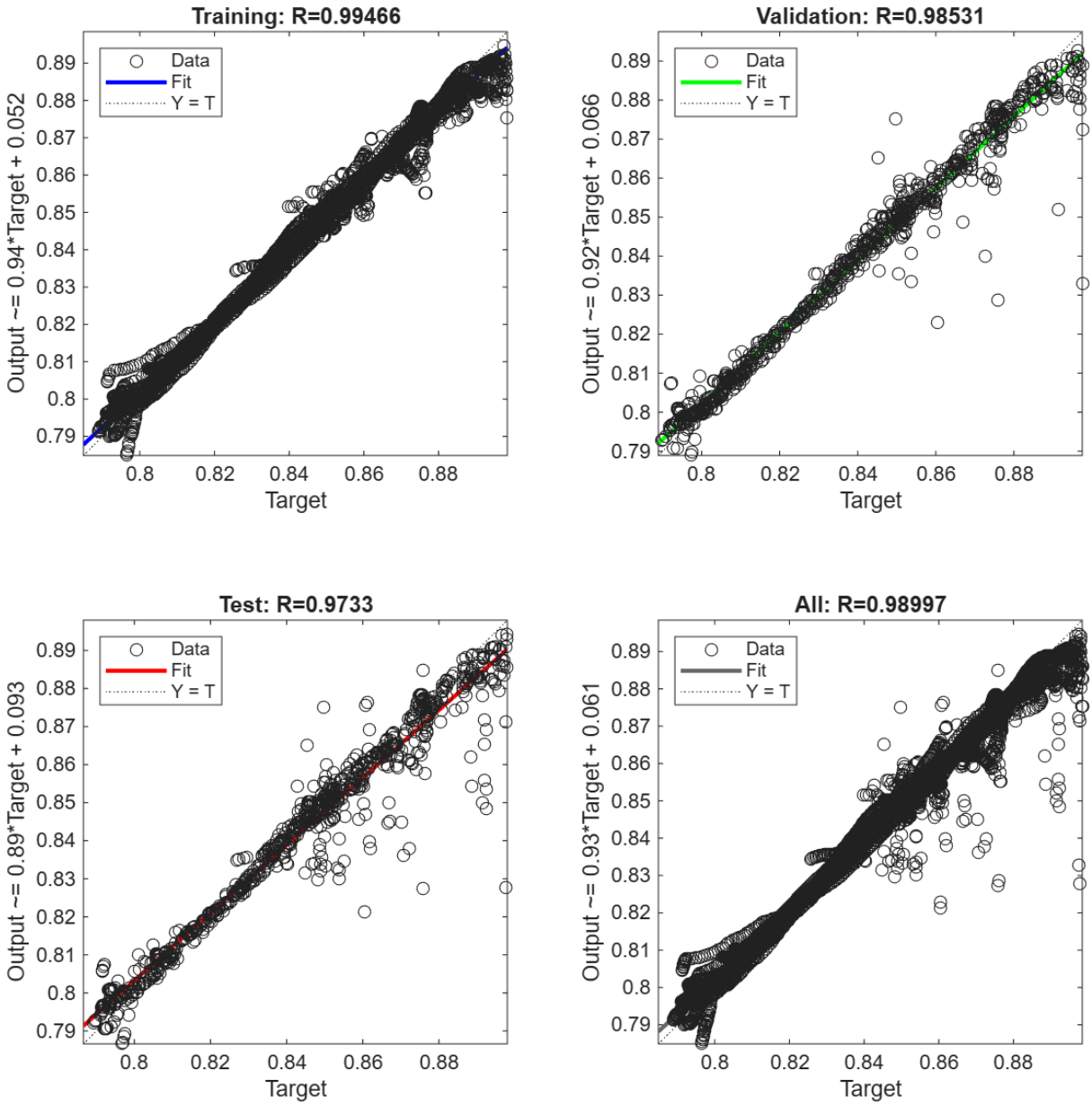


Figure 5.16. Regression plots of 150 L ESTWH systems for the summer case.

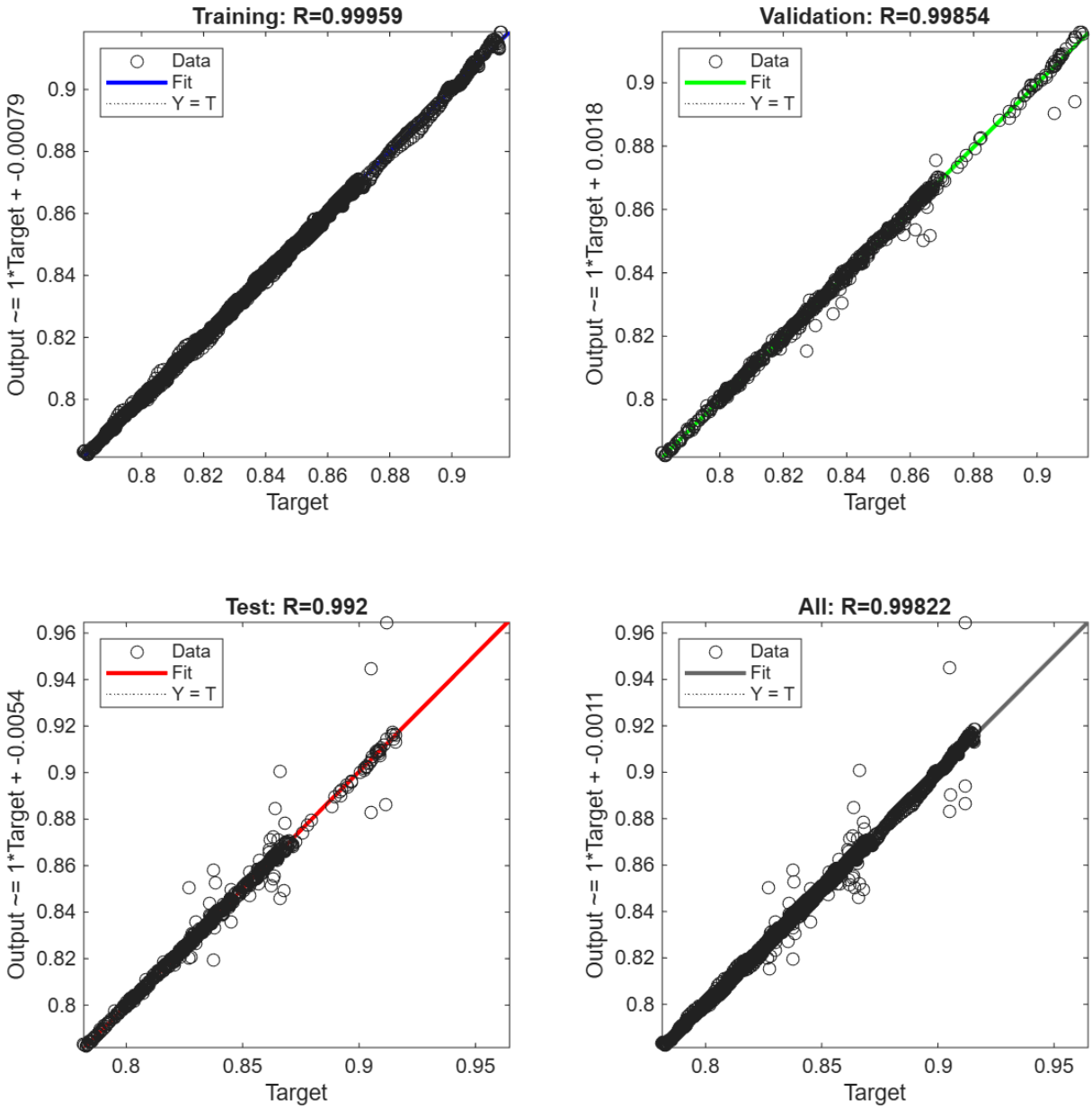


Figure 5.17. Regression plots of 200 L ESTWH systems for the summer case.

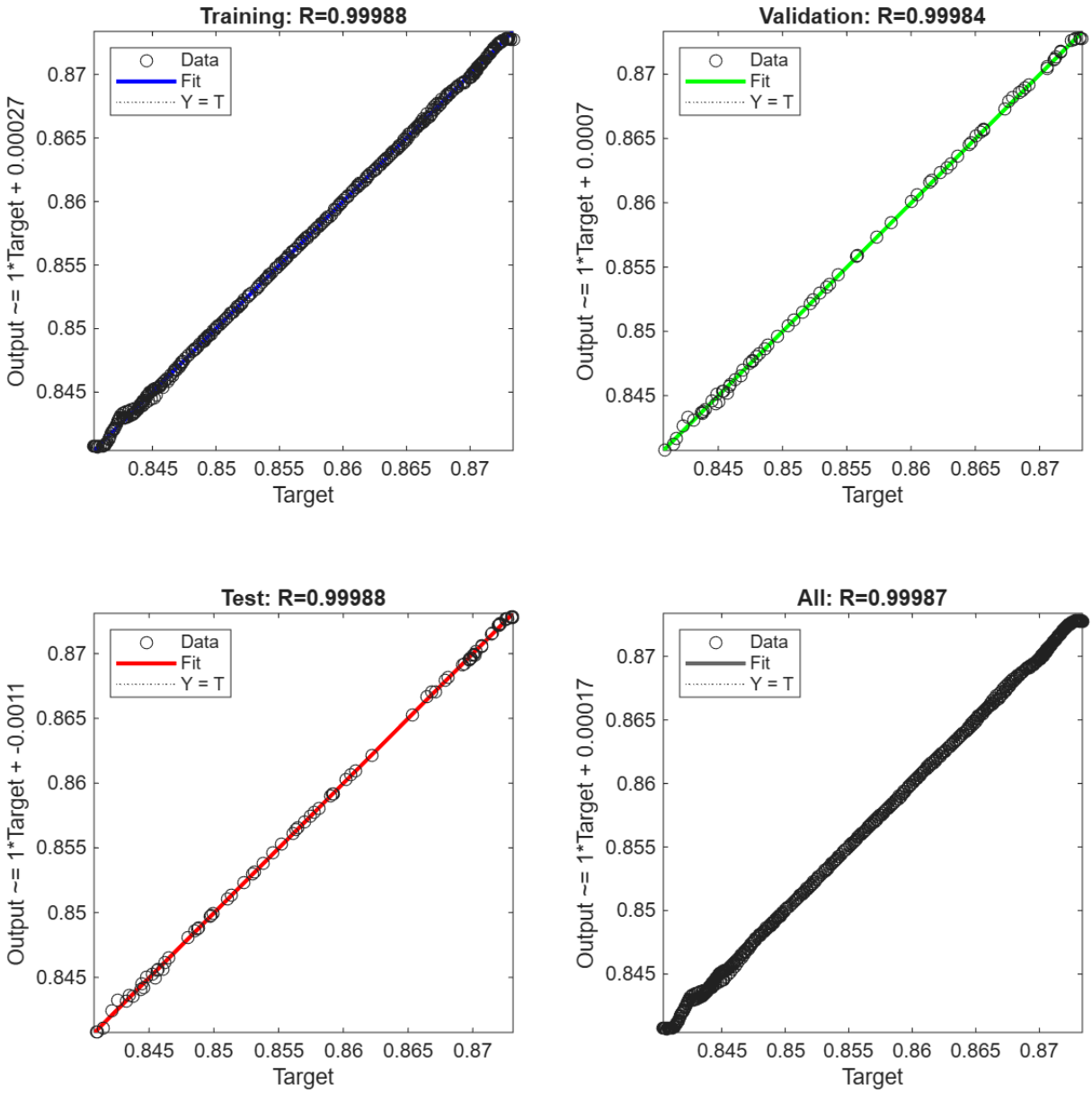


Figure 5.18. Regression plots of 250 L ESTWH systems for the summer case.

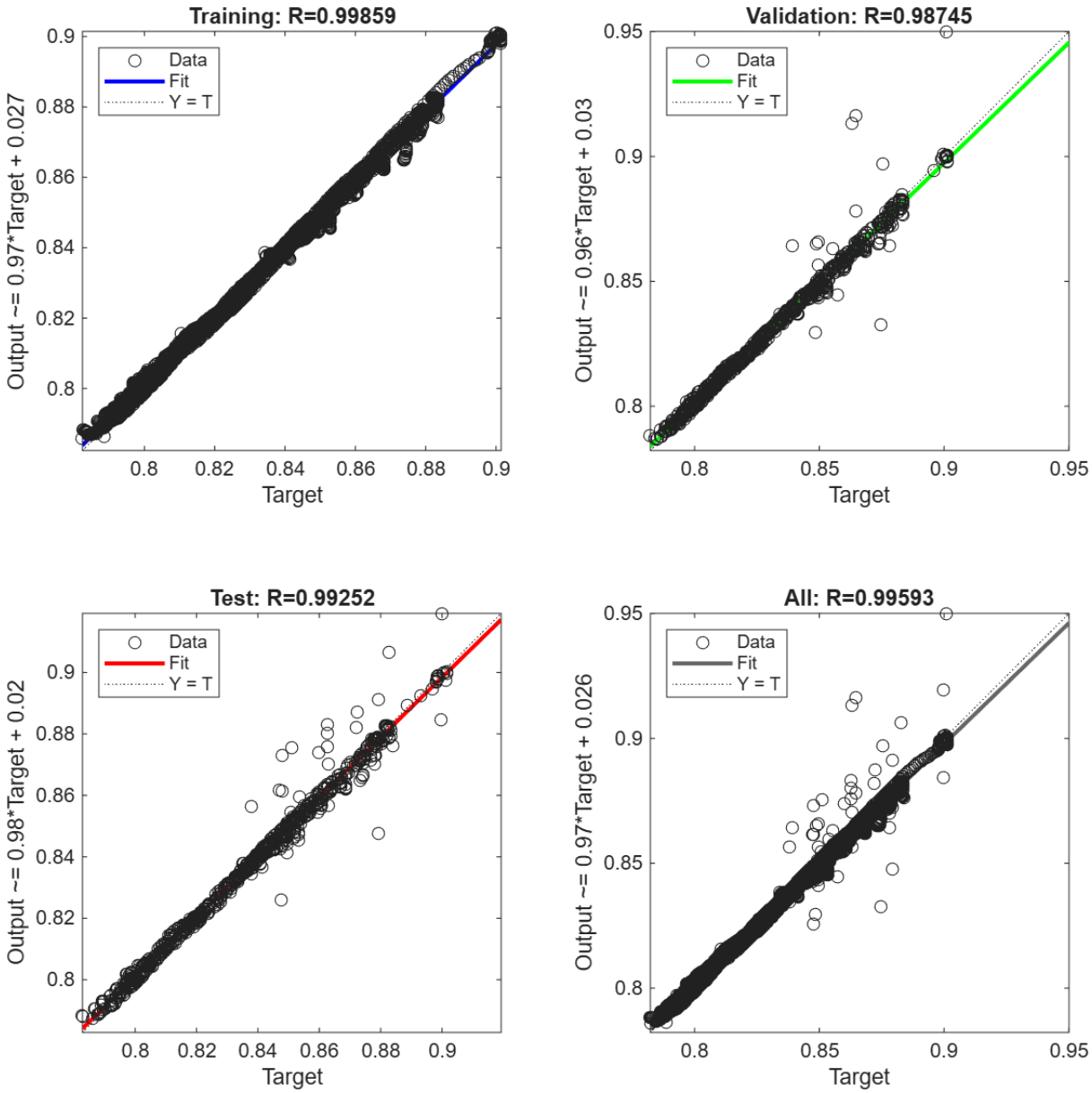


Figure 5.19. Regression plots of 100 L ESTWH systems for the winter case.

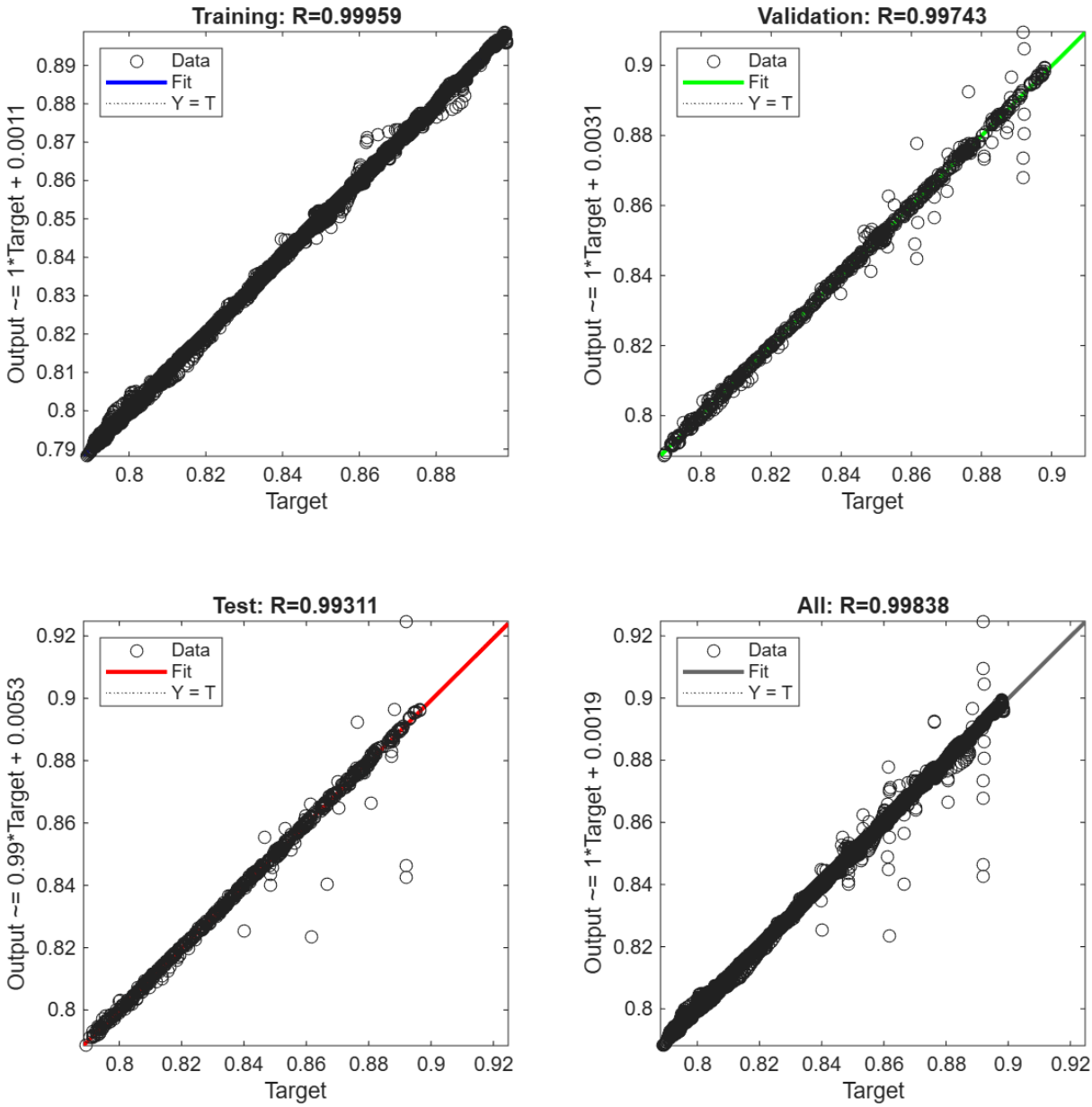


Figure 5.20. Regression plots of 150 L ESTWH systems for the winter case.

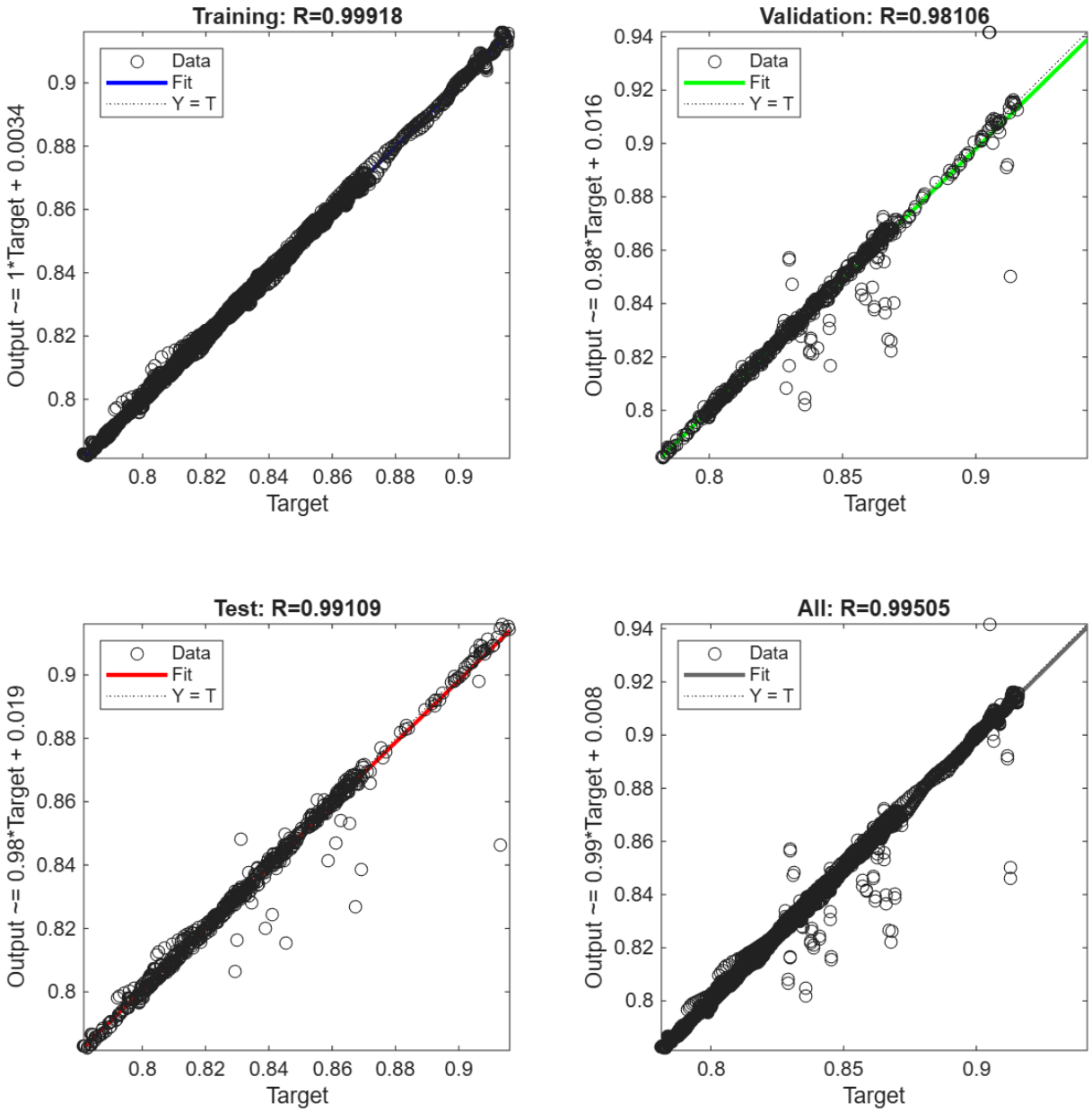


Figure 5.21. Regression plots of 200 L ESTWH systems for the winter case.

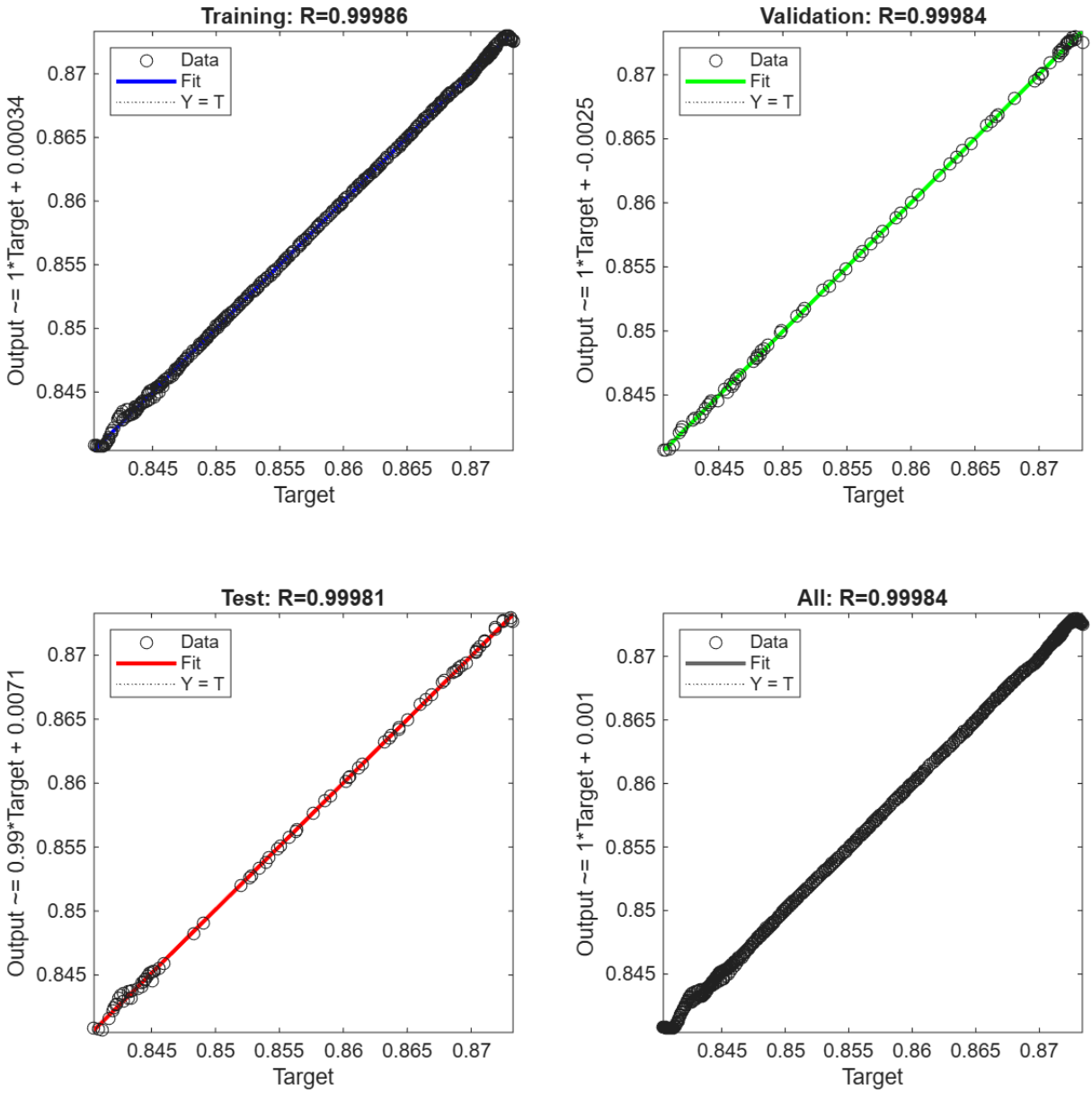


Figure 5.22. Regression plots of 250 L ESTWH systems for the winter case.

**Validation of performance**

- TWS tank

The performance plots for the TWS tank for the summer and winter cases are presented in Figures 5.23 and 5.24, respectively. The validation performance for the summer case (Figure 5.23) underwent 14 epochs, demonstrating the error results and coefficients of the training. The results indicated the MSE values for the training phase, cross-validation phase, and the testing phase were 2.56e-05, 2.38e-05 and 8.99e-05, respectively, achieved at the 8$^{th}$ epoch. For the winter case (Figure 5.24), the model trained for 16 epochs and the

best error results and coefficients were obtained at the 10th epoch, with 2.22e-05 (training MSE), 2.14e-05 (cross-validation MSE) and 1.97e-05 (testing MSE).

These findings indicate that if the model is trained beyond the 8th epoch for summer case and the 10th epoch for the winter case, the process could be denoted as overtraining. Overall, comparing the two cases, it can be deduced that the training was more effective for the winter case as the model achieved a lower MSE error and sustained good performance longer duration, thereby suggesting more accurate predictions.

- ESTWH systems

The performance plots for the 100L, 150 L, 200 L and 250 L size parameters of the ESTWH systems are presented in Figures 5.25 through 5.28 for the summer case and 5.29 through 5.32 for the winter case, respectively.

For 100 L size parameter, in the summer case (Figure 5.25), the model was trained for 14 epochs and obtained the best results at the 8th epoch, with the Mean Square Error (MSE) values for the training, cross-validation, and testing phases being at 1.48e-05, 2.77e-05 and 2.23e-05, respectively. For the winter case (Figure 5.29), the model trained for 13 epochs and obtained the MSE values of 2.86e-06, 2.02e-05, and 1.15e-05 at the 7th epoch for the training, cross-validation, and the testing phases, respectively.

For 150 L size parameter, the model underwent 12 epochs, and the best results were obtained at the 6th epoch for the summer case (Figure 5.26), indicating the MSE values of 1.21e-05 (training), 2.97e-05 (cross-validation), and 5.39e-05 (testing). Conversely, the winter case (Figure 5.30) trained for 27 epochs, and the best performance was at the 21st epoch, indicating the values of 7.41e-07, 4.58e-06 and 1.13e-05 for the training, cross-validation, and the testing phases MSE, respectively.

For the 200 L size parameter, the model trained for 18 epochs for the summer case (Figure 5.27) and obtained best results at epoch 12, indicating 6.74e-07 (training MSE), 2.47e-6 (cross-validation MSE) and 1.41e-05 (testing MSE). For the winter case (Figure 5.31), the model trained for 15 epochs and achieved the best results at the 9th epoch, with MSE values of 1.33e-06, 3.31e-05 and 1.54e-05, respectively.

For the 250 L size parameter, the model underwent 21 epochs and obtained the best results of 2.91e-08 (training MSE), 4.08e-08 (cross-validation MSE), and 3.08e-08 (testing

MSE), for the summer case (Figure 5.28). For the winter case (Figure 5.32), after 13 epochs, the model obtained the best results at the 13th epoch, with MSE values of 3.26e-08, 4.54e-08 and 6.00e-08, respectively

From the results obtained, any training beyond the epochs where the best performance was indicated for each size parameter is regarded as overtraining the models. When comparing the MSE values between the two cases for each season, the 100 L and 150 L size parameters achieved lower MSE errors, indicating more effective training for the winter case. Conversely, for the 200 L and 250 L size parameters, the lower MSE errors were achieved in the summer case.

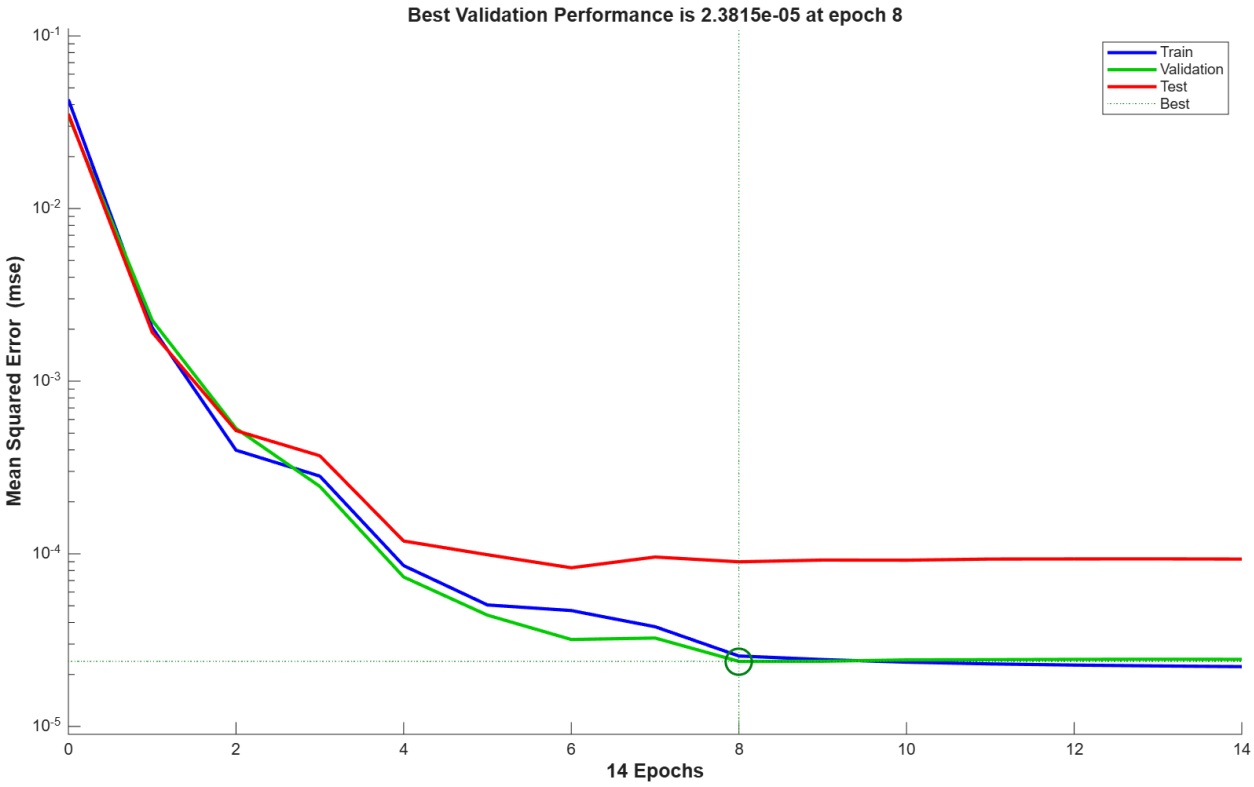


Figure 5.23. MSE performance plot of the TWS tank for summer case.

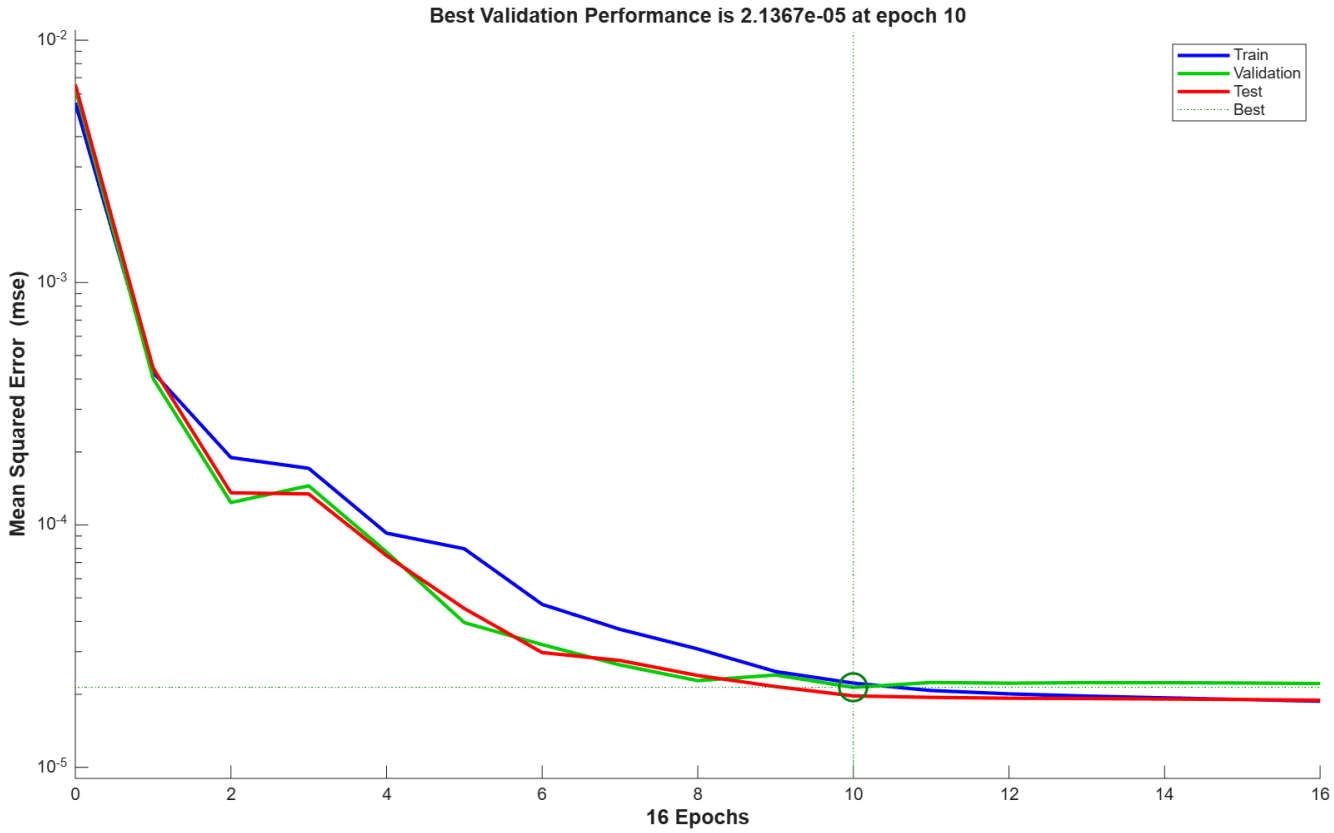


Figure 5.24. MSE performance plot of the TWS tank for winter case.

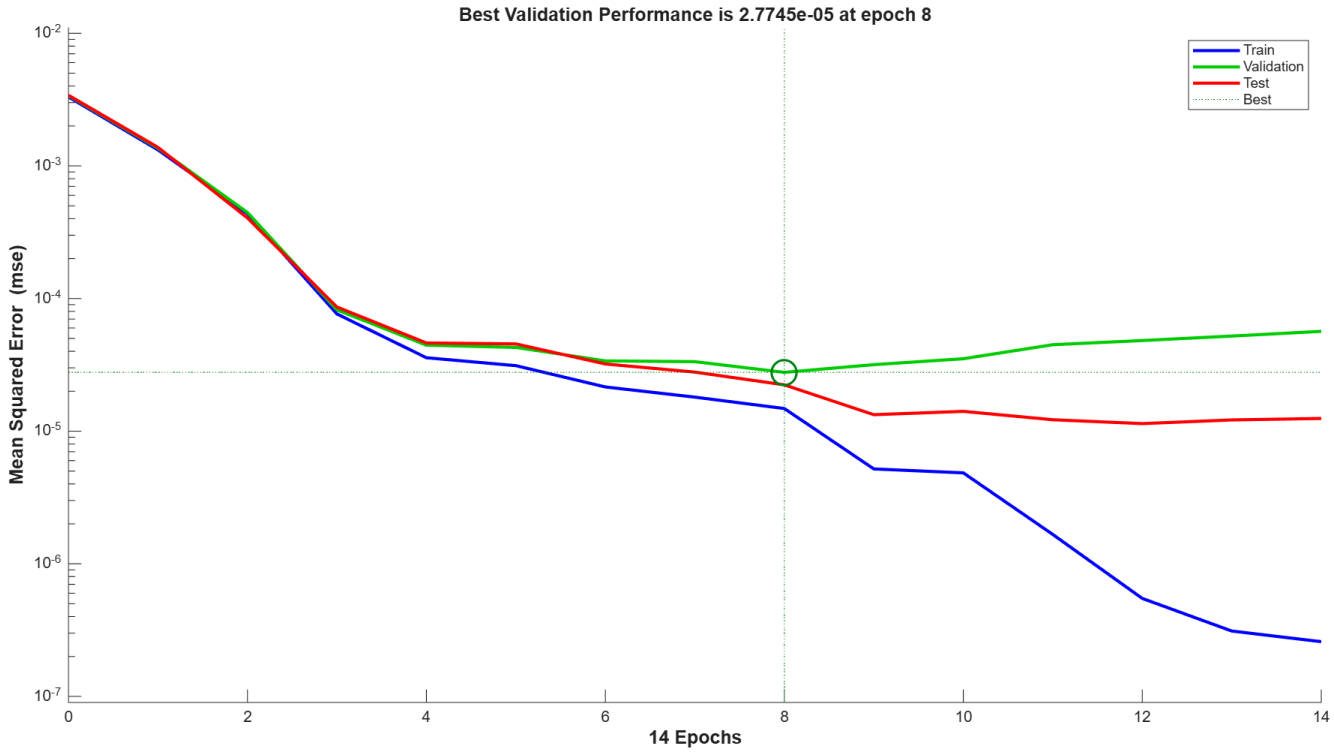


Figure 5.25. MSE performance plot of the 100 L ESTWH systems for summer case.

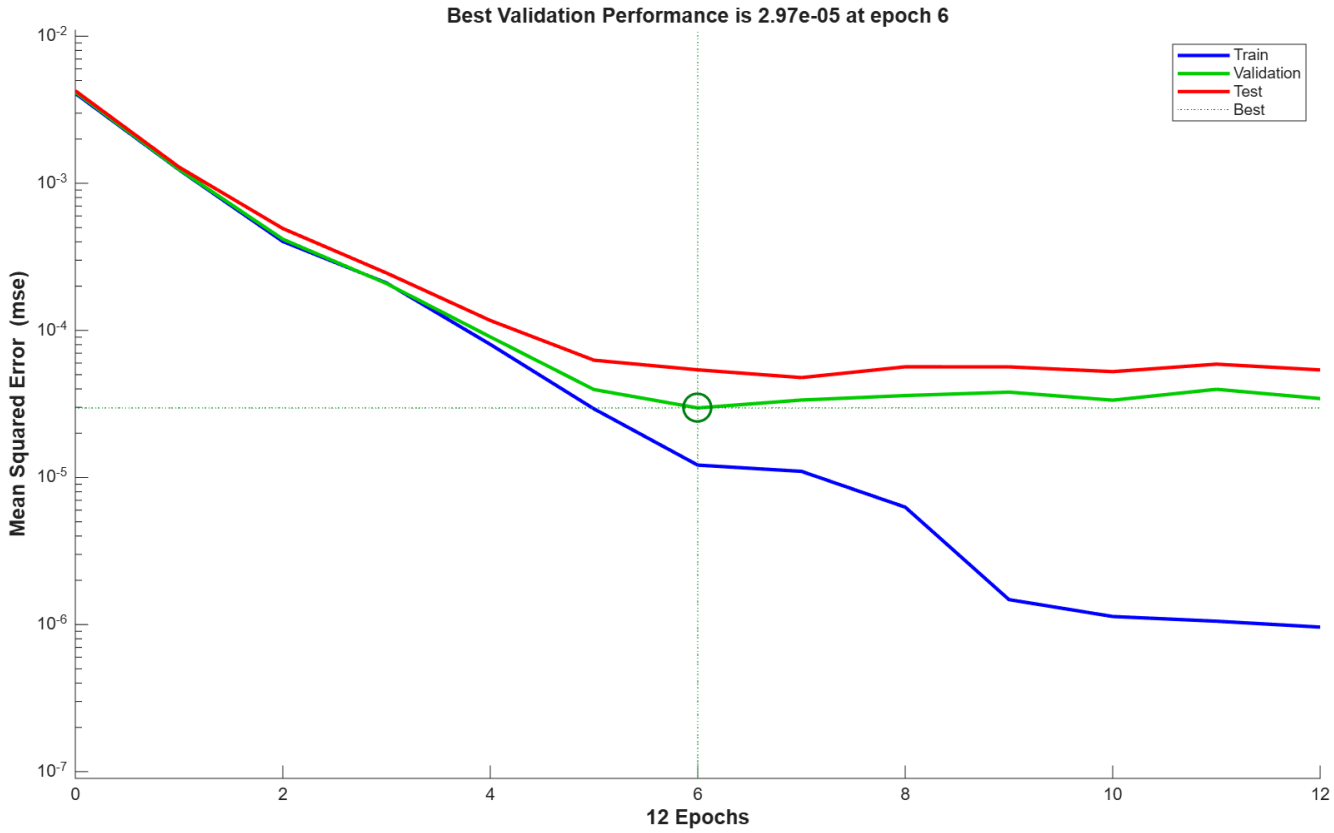


Figure 5.26. MSE performance plot of the 150 L ESTWH systems for summer case.

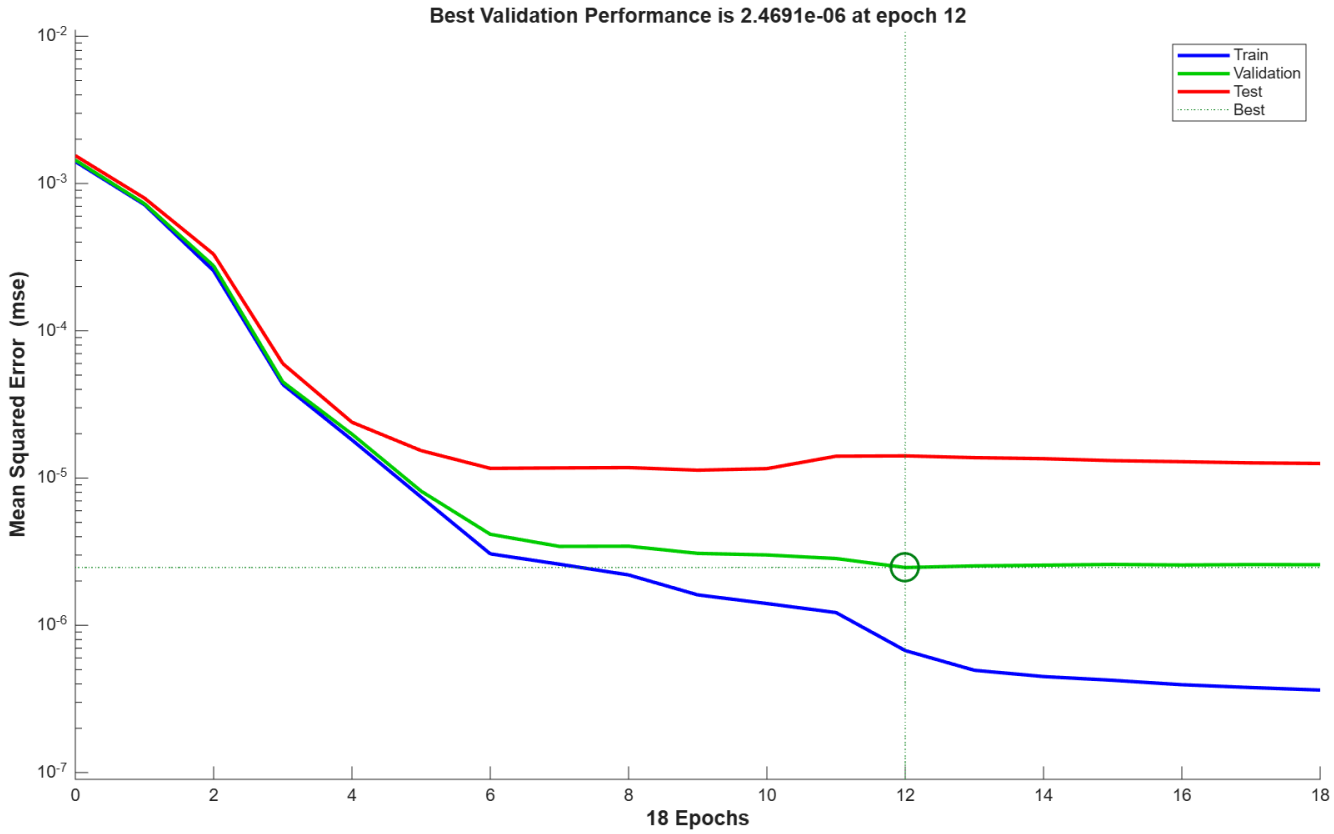


Figure 5.27. MSE performance plot of the 200 L ESTWH systems for summer case.

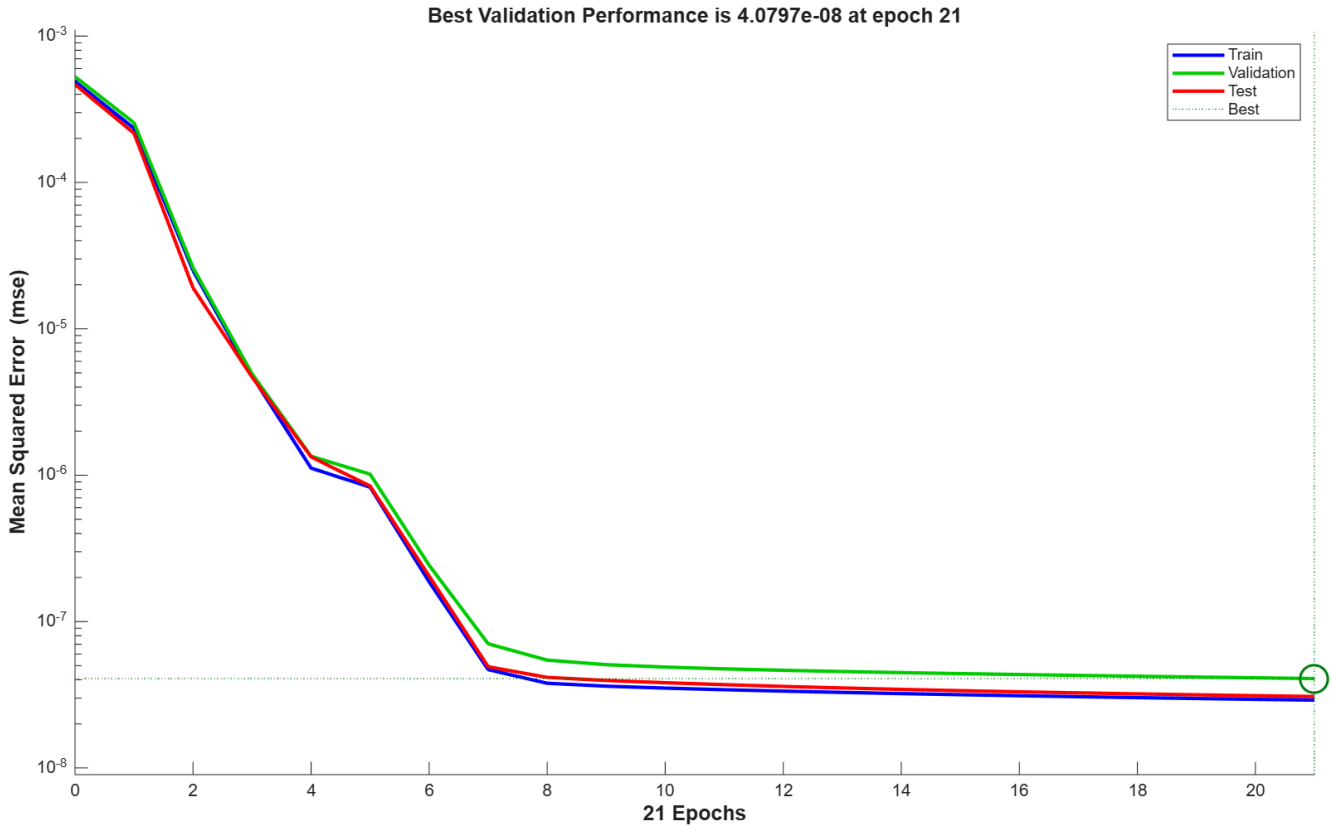


Figure 5.28. MSE performance plot of the 250 L ESTWH systems for summer case.

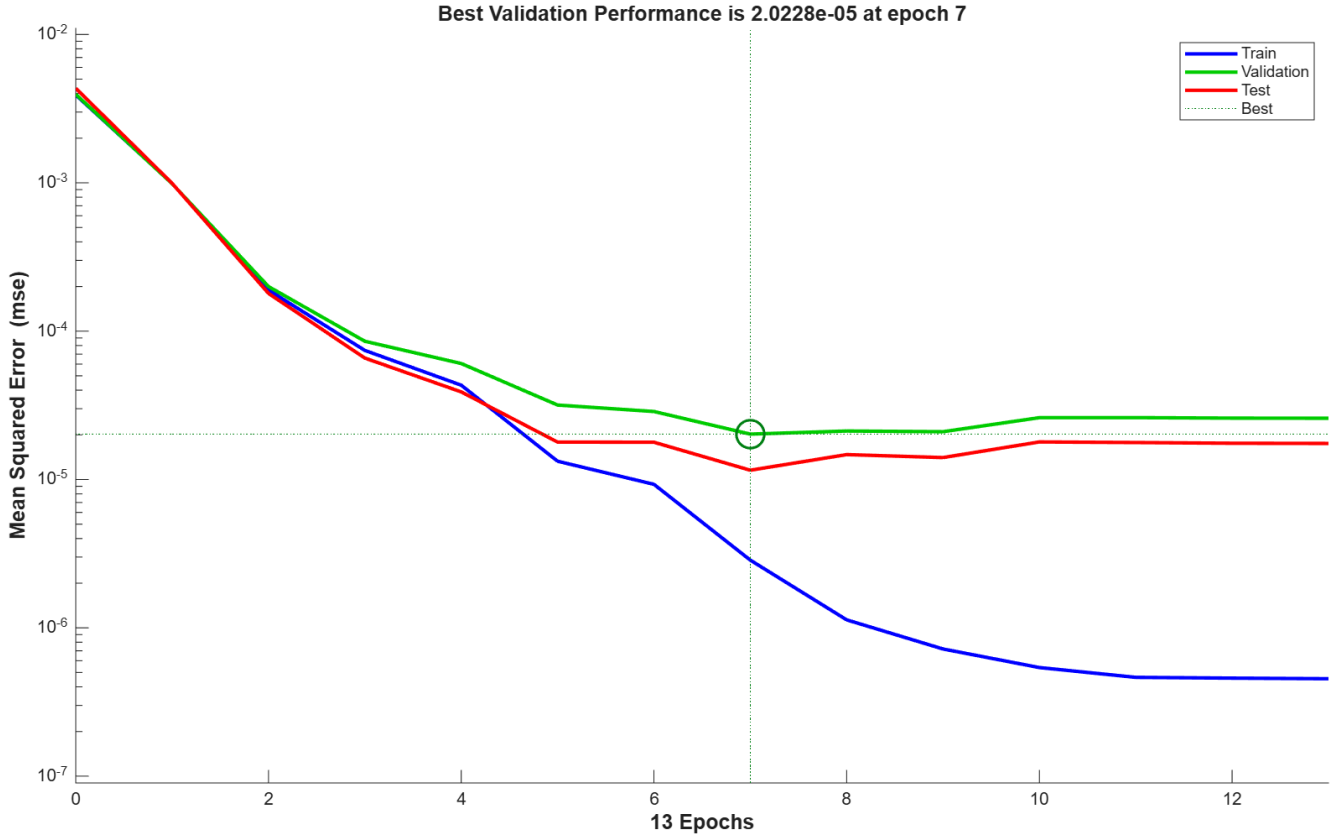


Figure 5.29. MSE performance plot of the 100 L ESTWH systems for winter case.

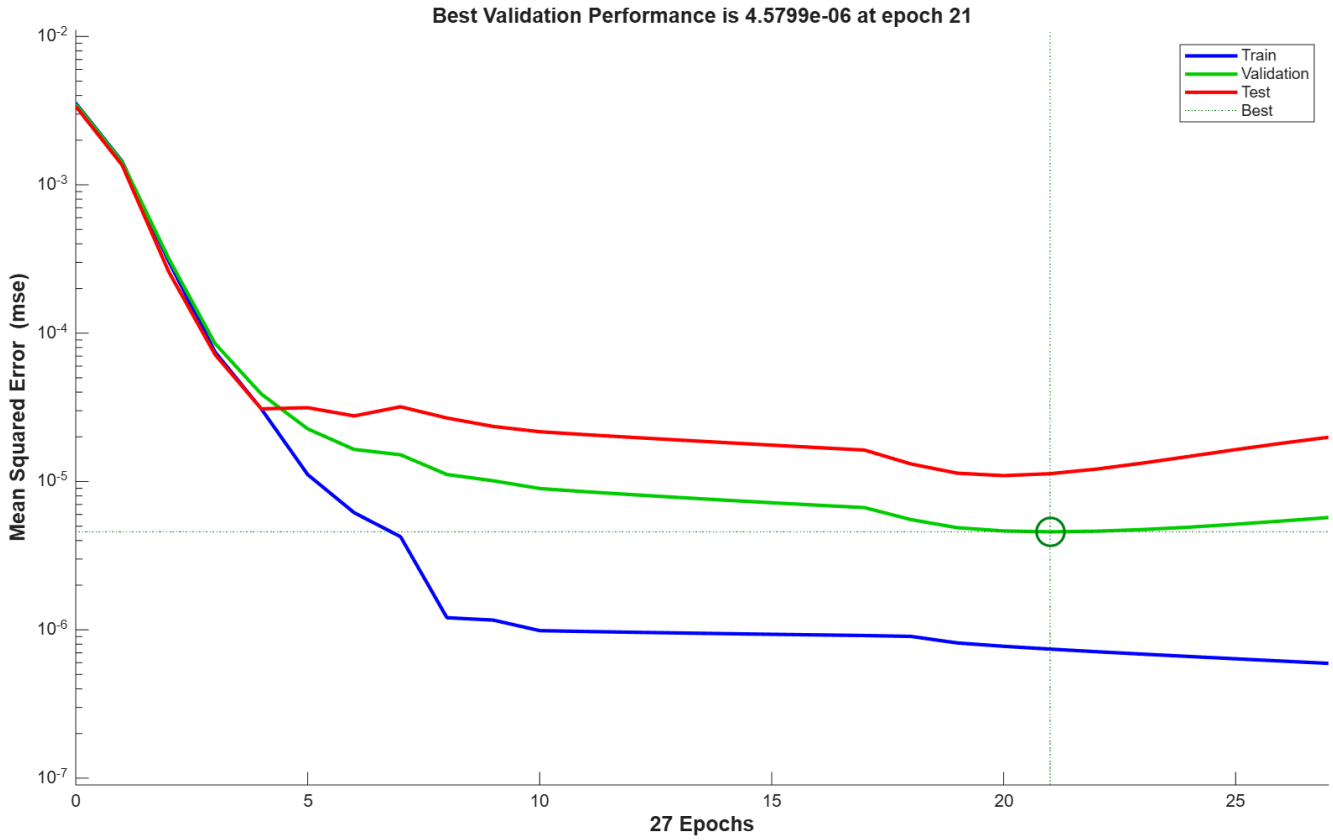


Figure 5.30. MSE performance plot of the 150 L ESTWH systems for winter case.

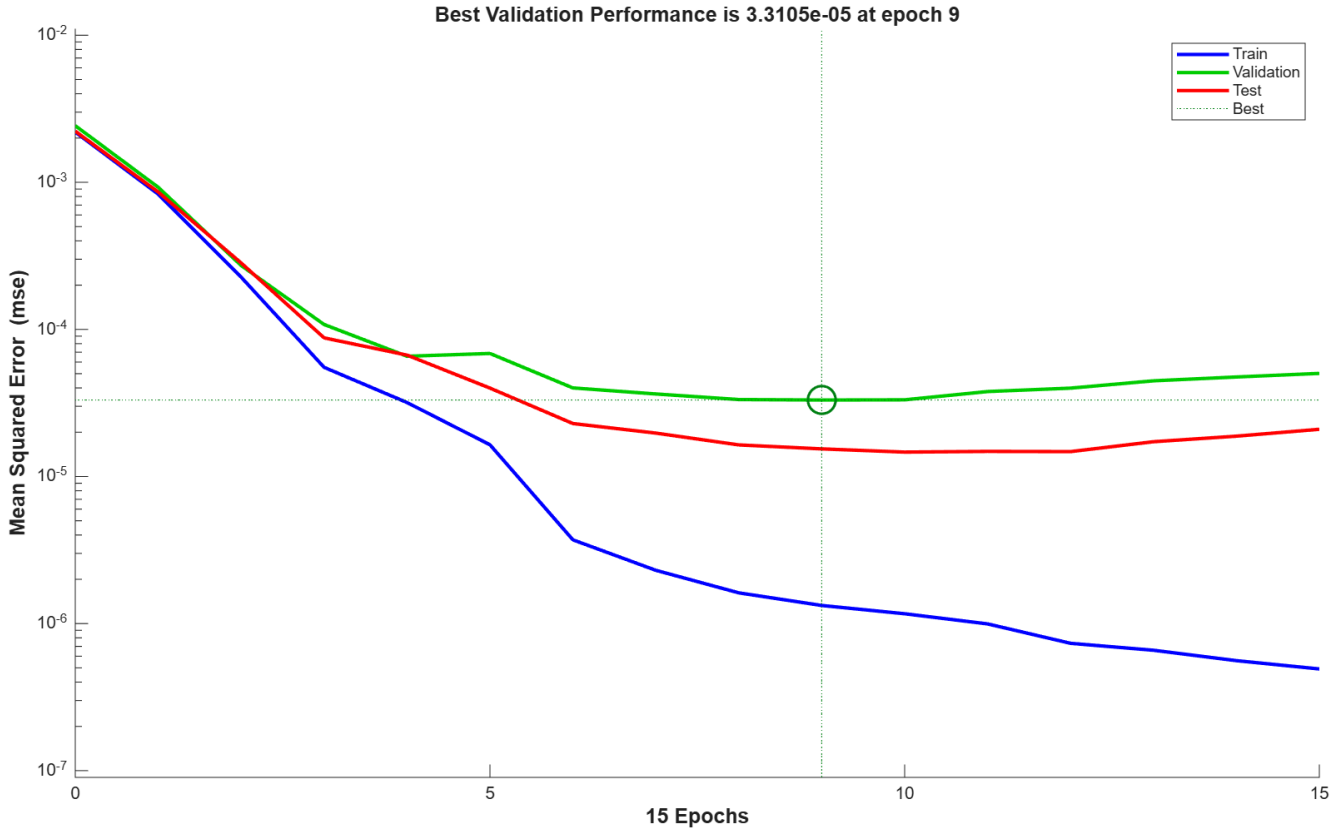


Figure 5.31. MSE performance plot of the 200 L ESTWH systems for winter case.

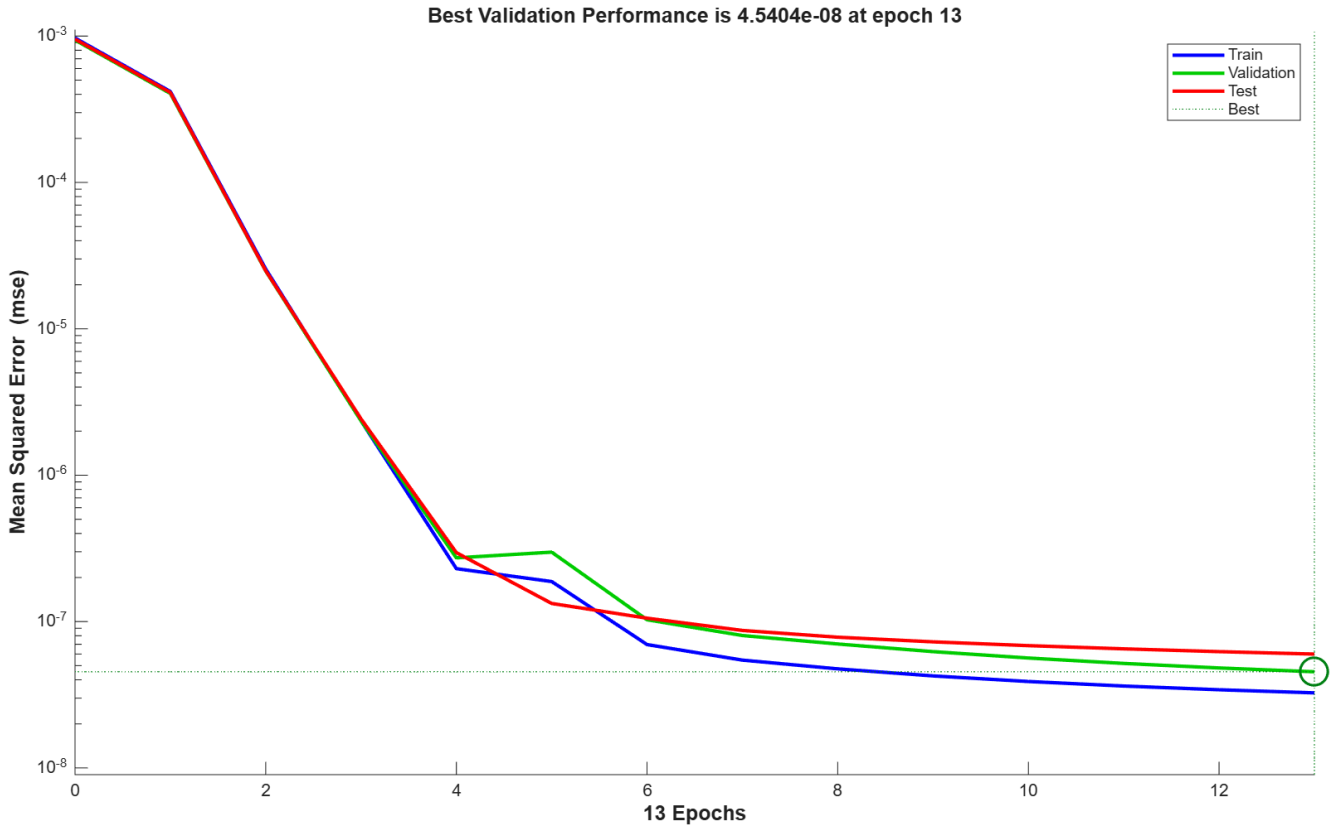


Figure 5.32. MSE performance plot of the 250 L ESTWH systems for winter case.

**Error distribution**

- TWS tank

In Figures 5.33 and 5.34, the error histogram plots show the distribution of prediction errors for the summer and winter cases, respectively.

The summer case (Figure 5.33) shows the majority of the bars for the training, validation and test sets are sharply concentrated around the zero-error region. The central bin spans approximately -0.00205 to 0.001236. Roughly 70 to 80% of the data points fall around the zero-error region. The maximum errors are generally within ±0.04, with specific peaks observed in the bin ranging from -0.02178 to 0.03741. For the winter case (Figure 5.34), the majority of the bars for the training, validation and test sets are highly concentrated around the zero-error region, specifically within the bin spanning approximately-0.00079 to 0.000765. Approximately 70 to 80% of the data points fall around the zero-error region. The maximum errors are within ±0.015, with specific peaks observed in the bin ranging from -0.0132 to 0.01473.

- ESTWH systems

The error histogram plots showing the distribution of prediction errors for the 100 L, 150 L, 200 L, and 250L size parameters of the ESTWH systems are presented in Figures 5.35 - 5.38 for the summer case and in Figures 5.39 through 5.42 for the winter cases.

For the 100 L size parameter, the summer case (Figure 5.35) shows the majority of the bars for the training, validation and test sets are sharply concentrated around the zero-error region, with the central bin spanning approximately -0.0039 to 0.000863. Roughly 70 to 80% of the data points fall within the zero-error region. The maximum errors are generally within ±0.06, specifically in the bin ranging -0.03227 to 0.06279. For the winter case (Figure 5.39), the majority of the bars are highly concentrated around the zero-error region, within the bin spanning approximately -0.00255 to 0.002121. Approximately 70 to 80% of the data points fall around the zero-error region. The maximum errors are contained within ±0.04, with peaks in the bin ranging from -0.04926 to 0.03949.

For the 150 L size parameter, the summer case (Figure 5.36) shows the majority of the bars for the training, validation and test are sharply concentrated around the zero-error region and the bin spanning approximately -0.0039 to 0.000863. Approximately 70 - 80% of the data points fall around the zero-error region. The maximum errors are within ±0.06, specifically noted in the bin ranging -0.02295 to 0.06279. For the winter case (Figure 5.40), the majority of the bars for the training, validation and test concentrated highly around the zero-error region, within the bin spanning approximately -0.00193 to 0.002179. A very high percentage of the data points, likely above 90% fall within the central bin. The maximum errors are within ±0.04, with peaks in the bin ranging from -0.03067, 0.04735.

For the 200 L size parameter, the summer case (Figure 5.37) shows the majority of the bars for the training, validation and test concentrated sharply around the zero-error region, with the central bin spanning approximately -0.00016 to 0.00375. A very high percentage of the data points, likely above 90%, fall within the central bin. The maximum errors are within ±0.05, with peaks in the bin ranging from -0.05093 to 0.01937. For the winter case (Figure 5.41), the majority of the bars are highly concentrated around the zero-error region, within the bin spanning approximately -0.00302 to 0.002156. A very high percentage of the data points, likely above 90% fall around the zero error. The maximum errors are within ±0.06, with peaks in the bin ranging from -0.03406 to 0.06424.

For the 250 L size parameter, the summer case (Figure 5.38) shows the majority of the bars for the training, validation and test concentrated sharply around the zero-error region, with the central bin spanning approximately -5.3e-05 to 1.62e-05. A very high percentage, possibly above 90%, of the data points fall around the zero-error region. The maximum errors are within ±0.0007, with peaks in the bin ranging from -0.00067, 0.000634. For the winter case (Figure 5.42), the majority of the bars for the training, validation and test concentrated highly around the zero-error region, within the bin spanning approximately -3.2e-05 to 5.4e-05. A very high percentage, likely above 90% of the data points fall around the zero-error region. The maximum errors are within ±0.0008, with peaks in the bin ranging from -0.0008 to 0.000824.

From the above findings, it can be deduced that the 200 L and 250 L size parameters show a strong concentration of data points (over 90%) around the zero-error region for both the summer and winter cases, which indicate high accuracy. The 100 L size parameter shows good concentration ranging between 70 to 80% around the zero, but with a wider spread of errors. The 150 L size parameter shows strong concentration over 90% of data plots around the zero-error region for the winter, but only good concentration (70 to 80%) for the summer case. Additionally, the maximum error ranges from significantly very small values (such as in the 250 L size parameter) to larger values from the 100 L, 150 L and 200 L size parameters.

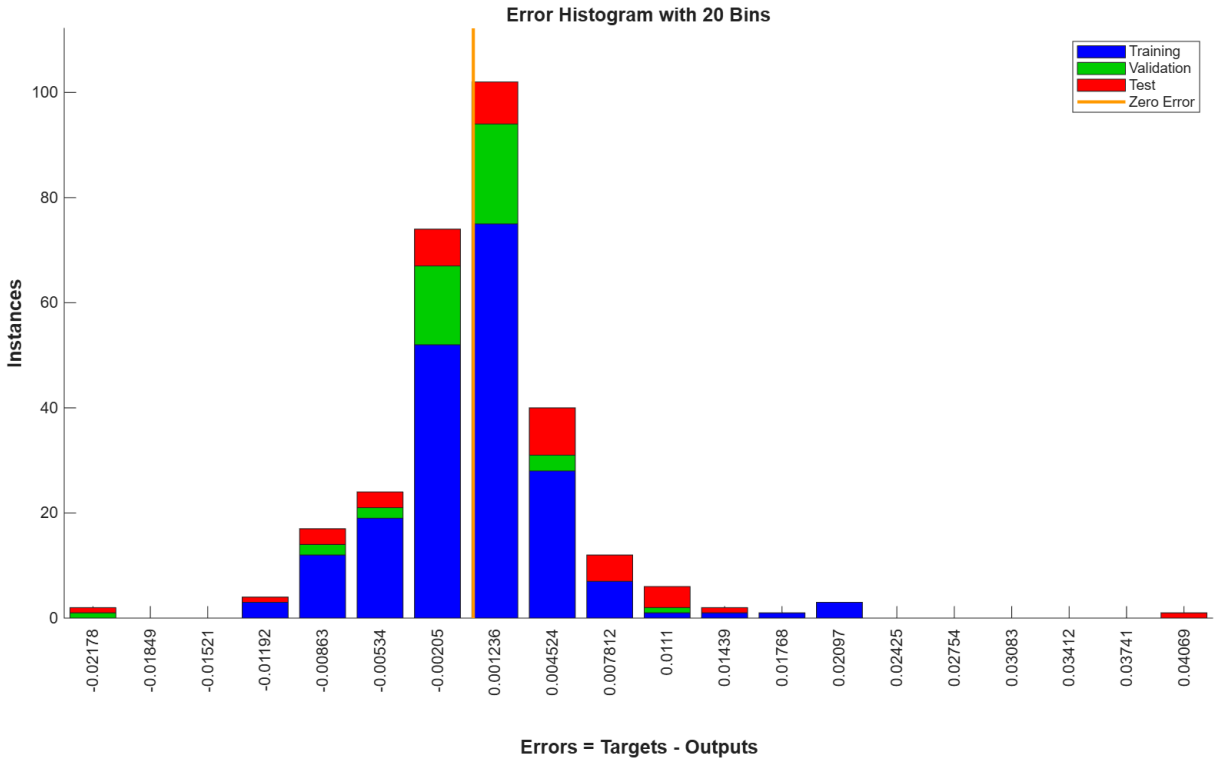


Figure 5.33. Error distribution plot of the TWS tank for the summer case.

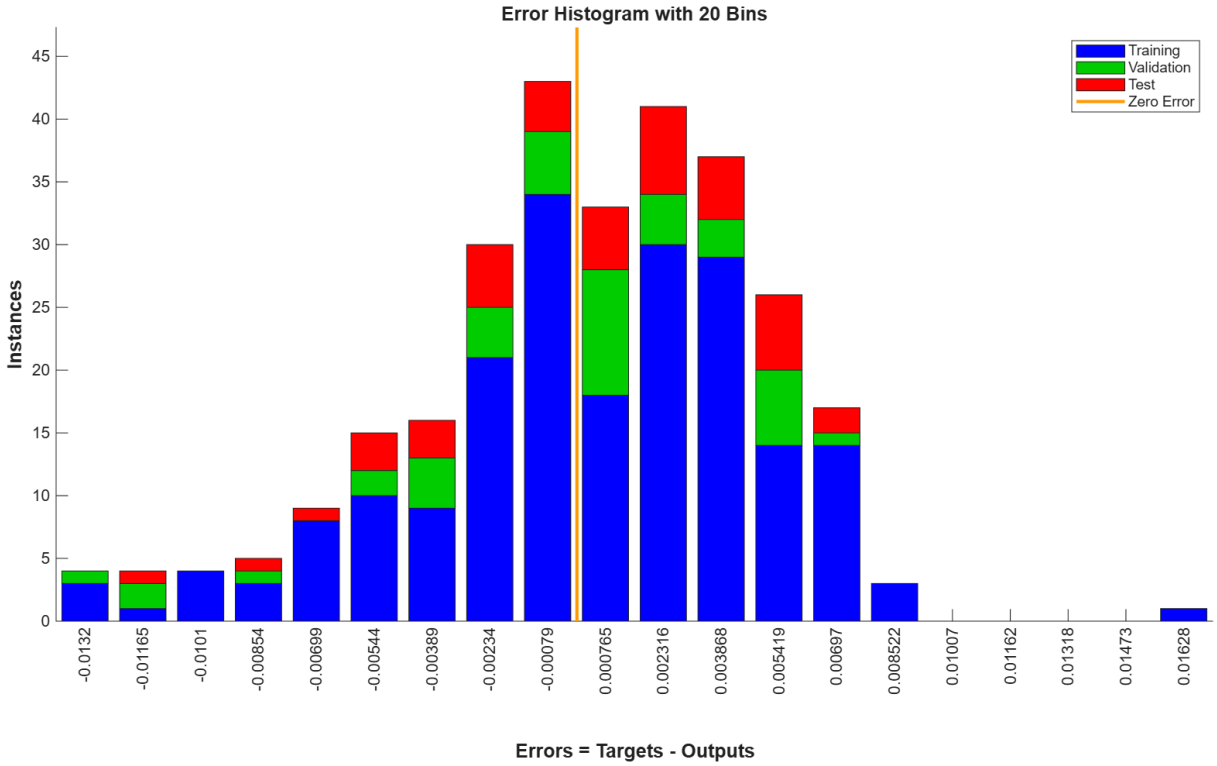


Figure 5.34. Error distribution plot of the TWS tank for the winter case.

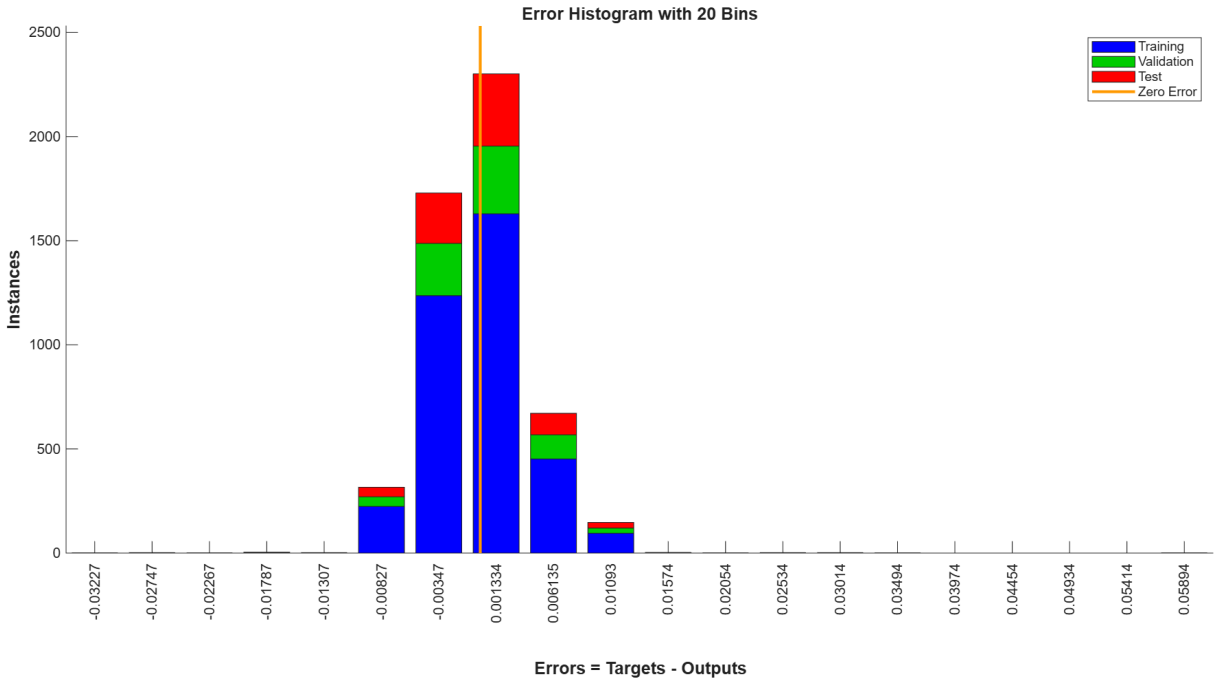


Figure 5.35. Error distribution plot of the 100 L ESTWH systems for the summer case.

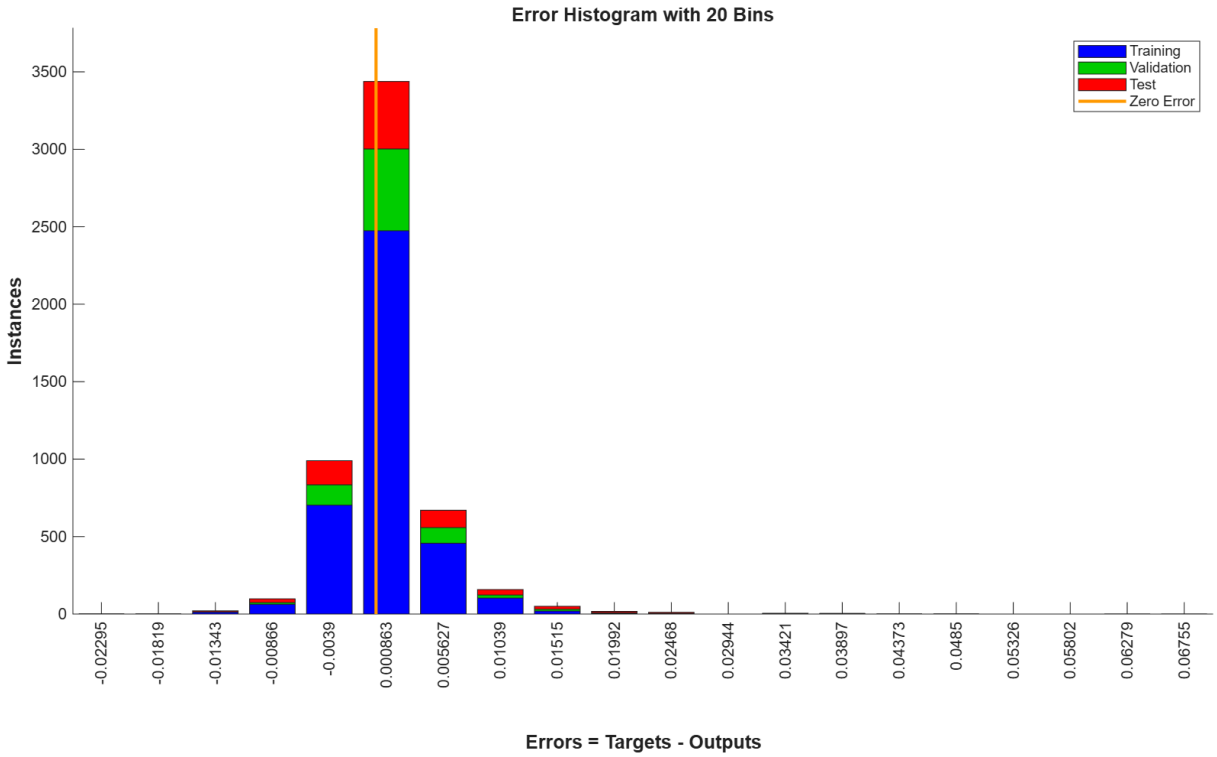


Figure 5.36. Error distribution plot of the 150 L ESTWH systems for the summer case.

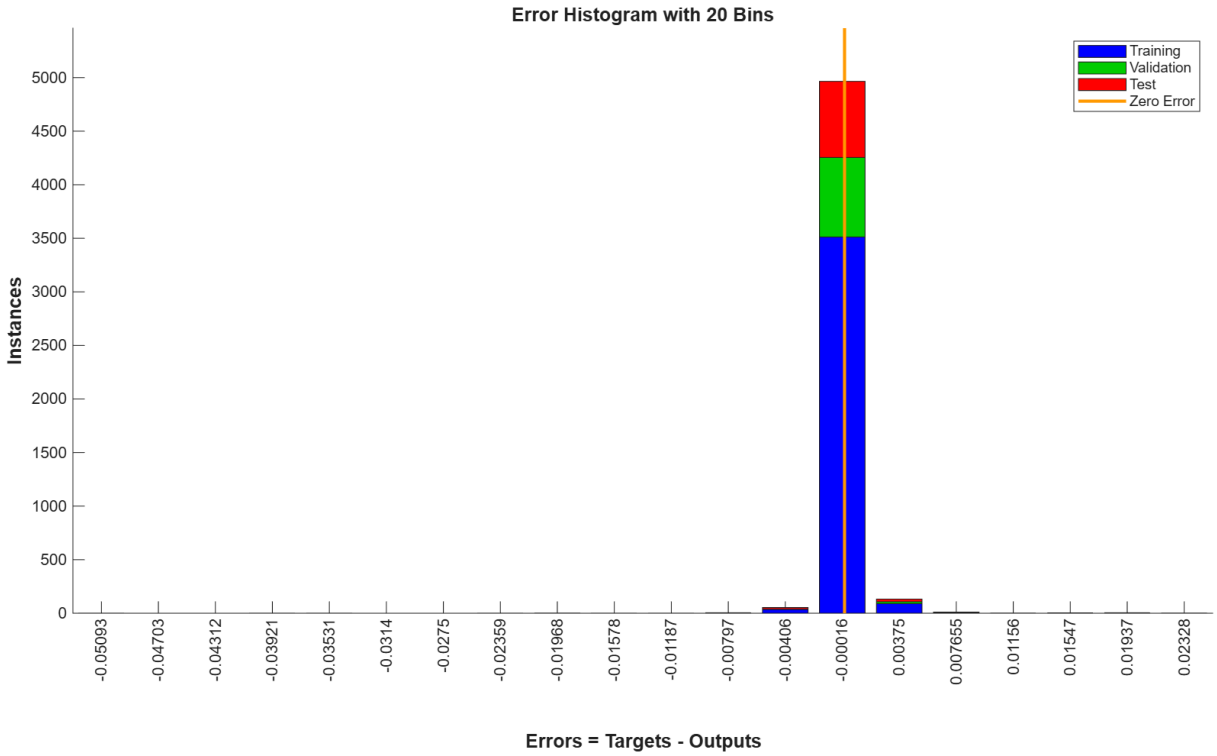


Figure 5.37. Error distribution plot of the 200 L ESTWH systems for the summer case.

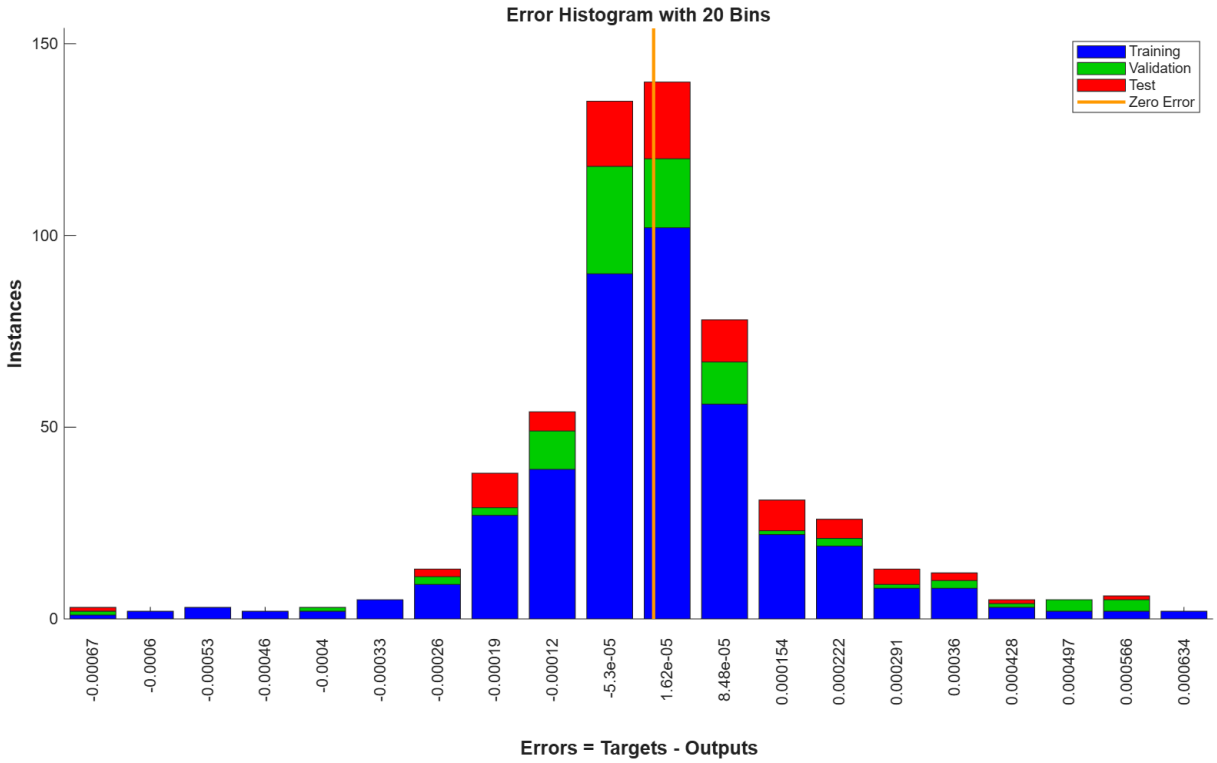


Figure 5.38. Error distribution plot of the 250 L ESTWH systems for the summer case.

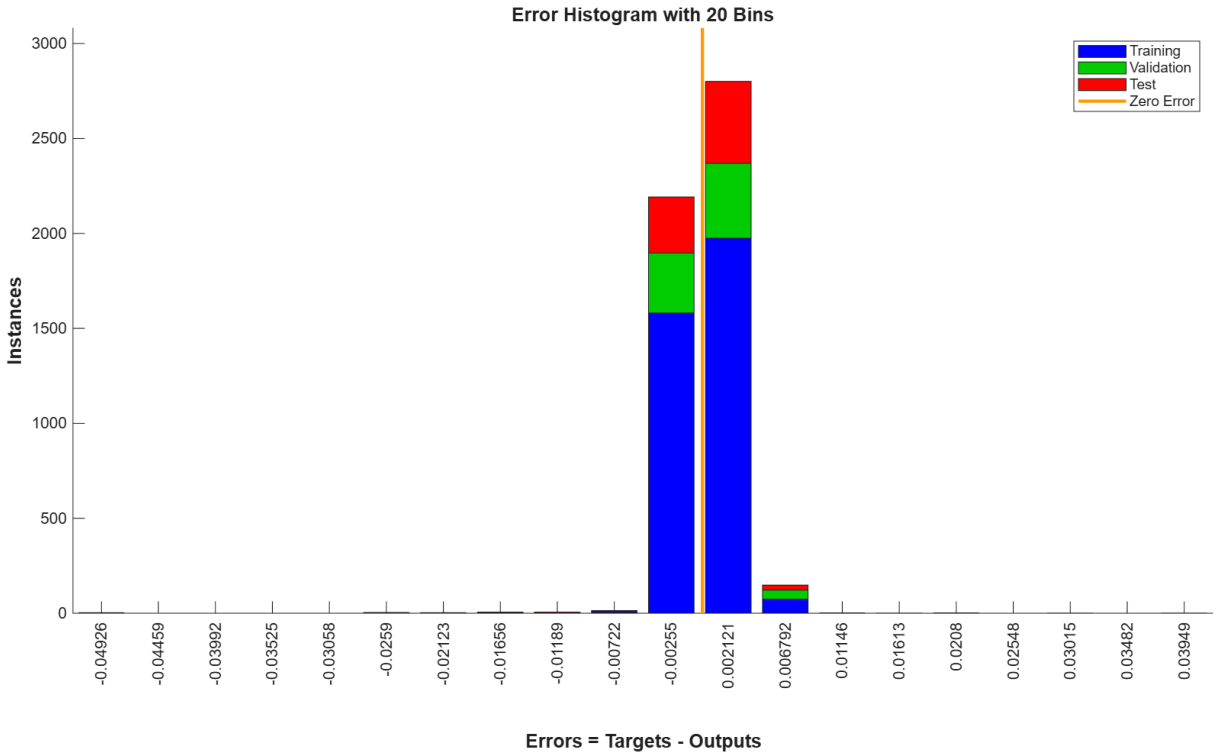


Figure 5.39. Error distribution plot of the 100 L ESTWH systems for the winter case.

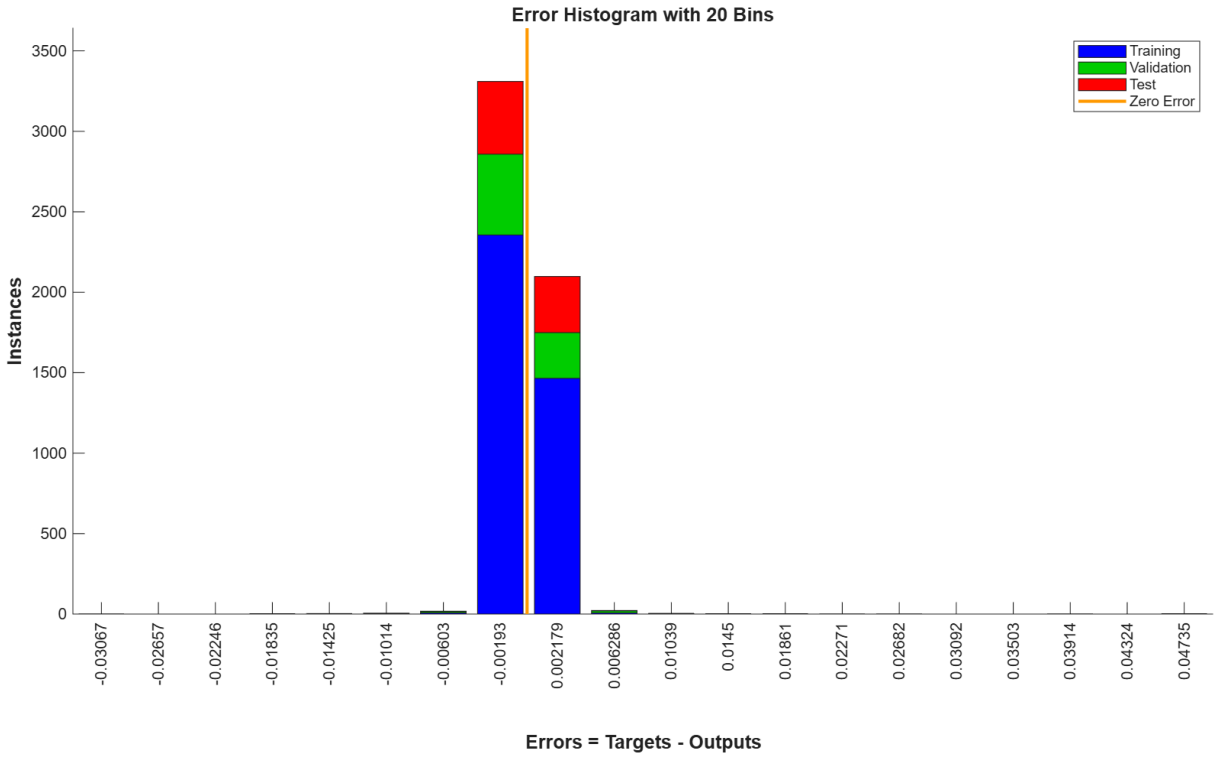


Figure 5.40. Error distribution plot of the 150 L ESTWH systems for the winter case.

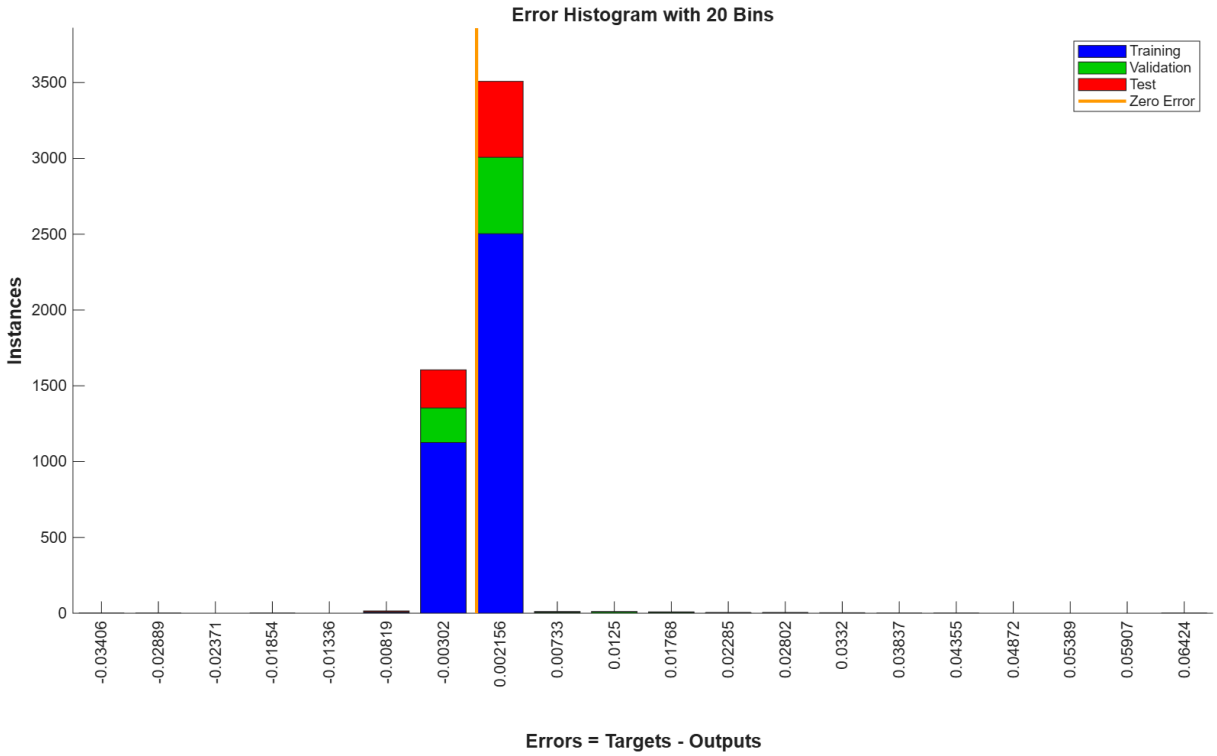


Figure 5.41. Error distribution plot of the 200 L ESTWH systems for the winter case.

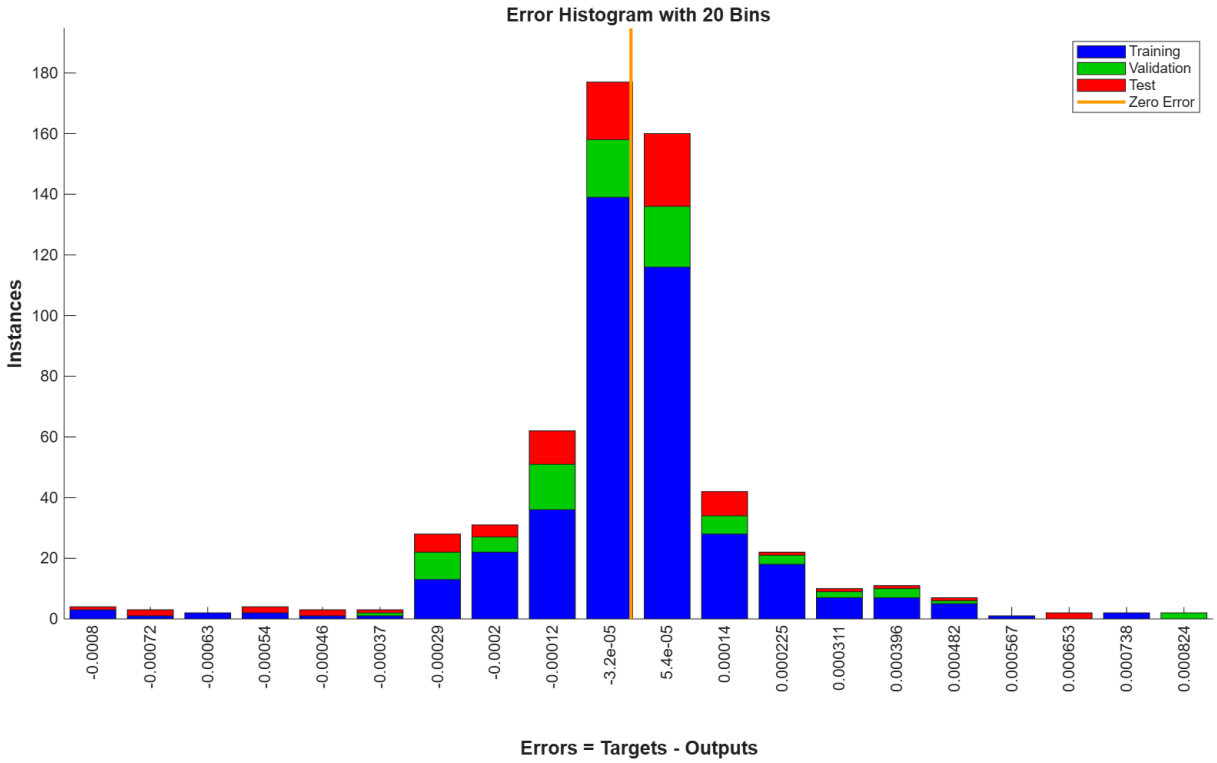


Figure 5.42. Error distribution plot of the 250 L ESTWH systems for the winter case.

## 5.5 SUMMARY

In this Chapter, the thermal performance of the proposed multifarious water heating systems with the hybrid-source WHR-TWS tanks integrated with the SAHP system was evaluated using the ANN training model. The TWS tanks and ESTWH systems were modelled separately. The 57 ESTWH systems had different sizes (100 L, 150 L, 200 L, and 250 L) and different parameters, were grouped into four distinct models and trained separately for the summer and winter cases. The TWS tanks used five input variables and one output variable, and the ESTWH systems used four input variables and one output variable for each ESTWH model. The ANN models were developed and generated to train, validate and test the systems under the summer and winter conditions using the Multilayer Perceptron Levenberg Marquardt (LM) backpropagation function.

The models were evaluated across the training, validation and testing phases. From the simulated results, the training state variables, regression performance plots, MSE performance validation and the error distributions for each model were presented and analysed. From the results obtained, all the models showed high prediction accuracy with correlations (R-values) above 0.95 for training, validation, test phases. The TWS tank obtained higher R-values for the summer case (0.99414 training, 0.99518 validation, and 0.98063 test, with 0.99219 overall. For the ESTWH systems, the 100 L and 150 L size parameters obtained higher R-values for the winter case and 200 L and 250 L size parameter models for the summer case. The 250 L size parameter obtained the highest overall R-values, reaching 0.99988, 0.99984 and 0.99988 for the summer training, validation and test results, respectively and 0.99986, 0.99984, and 99981 for the corresponding winter results.

For performance validation, the TWS tanks obtained the lowest MSE errors for the winter case, training for 16 epochs and indicating training phase MSE, cross-validation phase MSE and the testing phase MSE errors of 2.22e-05, 2.14e-05, and 1.97e-05, respectively, achieved at the 10th epoch. For the ESTWH systems, comparing the MSE errors between summer and winter cases for each season, showed that the 100 L and 150 L size parameters achieved lower MSE errors, indicating more effective training for the winter case, whereas the 200 L and 250 L size parameters performed better in the summer case. When comparing between the size parameters, the 250 L size parameters obtained the lowest errors for both cases, training for 21 epochs, obtaining 2.91e-08, 4.08e-08 and 3.08e-08 at the 21st epoch

for the summer training, cross-validation, and testing phase MSE results, respectively. For the winter case, it trained for 13 epochs, obtaining 3.26e-08, 4.54e-08 and 6.00e-08 at the 13th epoch.

For error distribution, the TWS tanks indicate good concentration ranging between 70 and 80% around the zero for both summer and winter cases, indicating lowest maximum error range of ±0.015 for the winter case. For the ESTWH systems, the 200L and 250L size parameters show strong concentration of data points (over 90%) around the zero-error region for both the summer and winter cases, with the lowest maximum error range obtained in the summer case for both size parameters, within ±0.05 and ±0.0007, respectively. For the 100 L size parameter, good concentration ranges between 70 and 80% around the zero, and the maximum error range obtained in the winter case within ±0.04. The 150 L size parameter shows strong concentration (over 90%) of data plots around the zero-error region for the winter case, but only and good concentration, ranging between 70 and 80% around zero for the summer case, where the lowest maximum error range is obtained in the winter case within ±0.04.

# CHAPTER 6: CONCLUSIONS AND SUGGESTIONS

## 6.1 INTRODUCTION

In this study, a hybrid-source WHR-TWS integrated with SAHP system for high-capacity hot water production was proposed. The system consists of the TWS tanks utilising thermal waste heat recovered from the multifunctional chiller systems to preheat the water from the main water supply. The TWS tanks are also main source of makeup water supplied to the multifarious water heating systems, which consist of 57 ESTWH systems already existing at the Mediclinic healthcare building, located in Bloemfontein in South Africa, and used as a case study. The integration of the SAHP system, consisting of STC and a HP unit, retrofitted to the TWS tanks supplementing simultaneous heating, was proposed to increase the preheated water temperature before being transferred to the multifarious water heating loads.

Additionally, the proposed system was operated under energy management and optimal control operation to showcase the real-world behaviour and effectiveness of the controller for large-capacity buildings, such as healthcare facilities. The purpose of the method is to assist in the load shifting of the energy demand from the peak periods to the off-peak periods, which will consequently reduce peak load demand while maintaining the load requirement, improve system energy efficiency, decrease energy consumption in buildings and may, therefore, decrease the costs of operation, as well as indirectly, the $CO_2$ emissions. Furthermore, this study presents the application of ANN modelling for validation of thermal performance of complex water heating systems. By training the ANN model on the simulated data, the study aimed to determine accurate predictions of the system's thermal temperatures under various operating conditions at significantly reduced modelling and simulation time, offering a practical, rapid, and reliable tool for system analysis of thermal heating applications.

The ANN model was developed and generated to train, validate and test the system under the summer and winter conditions using the Levenberg-Marquardt backpropagation function, at the proportions of 70% training, 15% validation and 15% testing of the ANN model, each variable with 288 data points. The models for the TWS tanks and ESTWH

systems were developed for summer and winter cases, with the input variables selected based on the parameters that have effect on the variation of the thermal heating of the TWS tank and ESTWH systems. The TWS tanks have five input variables and one output variable, which is the pre-heated water temperature inside the TWS tank. For the ESTWH systems, the 57 ESTWH systems had different sizes (100 L, 150 L, 200 L and 250 L), which had different parameters. The systems were grouped into four different models and trained separately. The ESTWH systems, as per the size parameters, have four input variables and one output variable, which is the hot water temperature inside each ESTWH system.

## 6.2 SUMMARY OF MAINI FINDINGS

For the economic analysis, the initial costs of the baseline case were lower as compared to the optimally controlled proposed case, which have however accumulated to be very high at the end of the project lifespan. This is due to the high cumulative costs incurred because of the continuous energy consumption throughout the day, even during the peak periods, where the energy costs are very high. Conversely, the optimally controlled proposed system accumulated lower costs at the end of the project lifespan due to the retrofitted renewable energy source water heating system, the optimal control, and shifting the water heating loads according to the TOU pricing signals.

From the 24-hour simulation results, the analysis indicated the accumulated energy costs of 261.57 USD and 133.57 USD for the summer case and 625.34 USD and 145.09 USD for the winter case, for the baseline system and optimally controlled proposed system, respectively. From the economic analysis calculations, the cumulative energy costs obtained for the baseline system and proposed optimally controlled system are 32.05 USD and 15.61 USD for a typical summer day and 83.96 USD and 18.55 USD for a typical winter day, respectively.

For the energy and cost savings analysis, the potential annual energy savings was estimated as results 15,001.93 kWh, which approximates to 49.60% per annum. This amount of energy may equate to 15.93 metric tons of $CO_2$ per year. At the beginning of the project, the costs of implementation of the baseline and the proposed systems are approximated to 40,464,82 USD and 93,335.37 USD, respectively. Over the estimated project duration of 20 years, based on the calculated results, the baseline system and the proposed optimally

controlled system may achieve 943,559.91 USD and 341,860.80 USD of the cumulative energy costs, 74,817.81 USD and 94,755.08 USD of the cumulative replacement costs, 13,996.05 USD and 32,283.01 USD of the cumulative operation and maintenance costs, and 8,092.96 USD and 18,667.07 USD of the salvage costs, respectively.

Finally, at the end of the project span, comparing the proposed optimally controlled system with the baseline system, the total life-cycle costs may therefore be approximated to 1,064,745.62 USD and 543,567.18 USD, respectively. These estimates equate to the cost savings of 521,178.43 USD, which is about 48.95% of the costs of the baseline system saved. These results show significant economic and energy-saving potential, demonstrating a viable solution for reducing the energy consumption and operational costs in healthcare facilities.

The main results highlighted that all the models showed high prediction accuracy with correlations (R-values) above 0.95 for training, validation, test phases, with TWS tank obtaining higher R-values for the summer case of 0.99414, 0.99518, and 0.98063 and 0.99219 for training, validation and test, respectively. For the ESTWHS, the 100L and 150L size parameters obtaining higher R-values for the summer case and 200L and 250L size parameter models for the winter case. The 250 L size parameter obtained the highest R-values of 0.99988, 0.99984 and 0.99988 for the summer case and 0.99986, 0.99984 and 99981 for the winter case, respectively, for training, validation, test results.

For performance validation of the models, TWS tanks obtained the lowest MSE errors for the winter case, training for 16 epochs and indicating training phase MSE, cross-validation phase MSE and the testing phase MSE errors of 2.22e-05, 2.14e-05 and 1.97e-05, respectively, at 10th epoch. For the ESTWH systems, comparing the MSE errors between summer and winter cases for each season, 100 L and 150 L size parameters achieved lower MSE errors, indicating more effective training for the winter case, whereas for the 200 L and 250 L size parameters achieved lower errors for the summer case. When comparing between the size parameters, the 250 L size parameters obtained the lowest errors for both cases, training for 21 epochs, obtaining 2.91e-08, 4.08e-08 and 3.08e-08 at 21$^{st}$ epoch for the summer case and training for 13 epochs, obtaining 3.26e-08, 4.54e-08 and 6.00e-08 at 13$^{th}$ epoch of training phase MSE, cross-validation phase MSE and the testing phase MSE results, respectively.

For error distribution, the TWS tanks indicate a good concentration ranging between 70 and 80% around the zero for both summer and winter cases, indicating lowest maximum error range of ±0.015 for the winter case. For the ESTWH systems, the 200 L and 250 L size parameters show strong concentration of data points (over 90%) around the zero-error region, for both the summer and winter cases, with the lowest maximum error range obtained in the summer case for both size parameters, within ±0.05 and ±0.0007, respectively. For the 100 L size parameter, good concentration ranges between 70 and 80% around the zero, and the maximum error range obtained in the winter case within ±0.04. The 150 L size parameter shows strong concentration (over 90%) of data plots around the zero-error region for the summer case and a good concentration ranging between 70 and 80% around zero, where the lowest maximum error range is obtained in the winter case within ±0.04.

These results confirm the robustness and adaptability of the developed ANN model to diverse operating conditions, making it a valuable tool for thermal system performance prediction of complex thermal systems such as the evaluated advanced hybrid water heating systems.

## 6.3 KEY ORIGINAL CONTRIBUTIONS

Overall, this study contributes a practical, rapid, and reliable AI-based modelling approach for thermal heating systems, offering opportunities for improved energy efficiency, system responsiveness, and informed decision-making in building energy management contexts. Additionally, the proposed integration method of WHR, TWS, and renewable energy sources, incorporated with energy management and optimal control, offers significant cost and energy savings, and potentially reduces $CO_2$ emissions. This makes the system a sustainable alternative to conventional water heating methods, as well as paving the way for further studies on its broader implementation and optimization.

## 6.4 SUGGESTIONS FOR FURTHER RESEARCH

This thesis is part of the ongoing studies of the optimal energy management and optimal control of the water heating systems in commercial buildings, especially in high-

capacity buildings. With the healthcare building used as a case study, under the weather conditions of Bloemfontein, further studies may be conducted on the following aspects:

- The proposed method may further be customized for various commercial buildings, from small clinics to large hospitals, hotels, etc., depending on their energy needs and available infrastructure.
- Further research on the components of the various solar and/or pump types may be explored in different climate conditions or geographical locations of South Africa, or Africa, with different input variables.
- This system should, additionally, be developed and tested with other forms of solar collectors, as well as different system configurations.
- For machine learning, future research may explore the integration of optimisation algorithms (e.g. GA, PSO) into the ANN model of this particular or similar system, as well as incorporating hybrid AI models (e.g. ANFIS or ANN-LSTM). Also, assessing the environmental and economic impacts of ANN-integrated control strategies is recommended to quantify potential energy cost savings and carbon emission reductions for the particular or similar system.

## 6.5 FINAL CONCLUSION

In conclusion, the study has been successfully completed, achieving its objectives of developing and validating an energy management and optimal control framework for complex water heating systems. The modelling, simulation, and ANN-based predictive analyses demonstrate the system's effectiveness in improving energy efficiency, optimising operational costs, and providing reliable performance insights, confirming the overall success and practical relevance of the research.

Additionally, with the benefit of the abovementioned recommendations, the study not only addresses the identified research gaps but also provides a structured framework for future investigations and practical implementation. The integration of WHR, TES, SAHP systems, and ANN-based predictive control demonstrates a scalable and adaptable approach, offering guidance for optimising similar complex water heating systems in other commercial and industrial contexts.

# REFERENCES

[1] A. Atienza-Márquez, F. Domínguez Muñoz, F. Fernández Hernández, and J. M. Cejudo López, "Domestic hot water production system in a hospital: Energy audit and evaluation of measures to boost the solar contribution," *Energy*, vol. 261, no. August, 2022, doi: 10.1016/j.energy.2022.125275.

[2] C. A. Balaras, E. Dascalaki, and A. Gaglia, "HVAC and indoor thermal conditions in hospital operating rooms," *Energy Build.*, vol. 39, no. 4, pp. 454–470, 2007, doi: 10.1016/j.enbuild.2006.09.004.

[3] M. J. Ritchie, J. A. A. Engelbrecht, and M. J. Booysen, "A probabilistic hot water usage model and simulator for use in residential energy management," *Energy Build.*, vol. 235, p. 110727, 2021, doi: 10.1016/j.enbuild.2021.110727.

[4] P. A. Hohne, K. Kusakana, and B. P. Numbi, "Model validation and economic dispatch of a dual axis pv tracking system connected to energy storage with grid connection: A case of a healthcare institution in South Africa," *J. Energy Storage*, vol. 32, no. October, p. 101986, 2020, doi: 10.1016/j.est.2020.101986.

[5] J. Ma, J. Qin, T. Salsbury, and P. Xu, "Demand reduction in building energy systems based on economic model predictive control," *Chem. Eng. Sci.*, vol. 67, no. 1, pp. 92–100, 2012, doi: 10.1016/j.ces.2011.07.052.

[6] M. Đukić and M. Zidar, "Sustainability of Investment Projects with Energy Efficiency and Non-Energy Efficiency Costs: Case Examples of Public Buildings," *Sustainability*, vol. 13, no. 11, p. 5837, May 2021, doi: 10.3390/su13115837.

[7] W. A. Fadzlin, M. Hasanuzzaman, N. A. Rahim, N. Amin, and Z. Said, "Global Challenges of Current Building-Integrated Solar Water Heating Technologies and Its Prospects: A Comprehensive Review," *Energies*, vol. 15, no. 14, p. 5125, Jul. 2022, doi: 10.3390/en15145125.

[8] T. Kim, B. Il Choi, Y. S. Han, and K. H. Do, "A comparative investigation of solar-assisted heat pumps with solar thermal collectors for a hot water supply system," *Energy Convers. Manag.*, vol. 172, no. April, pp. 472–484, 2018, doi: 10.1016/j.enconman.2018.07.035.

[9] T. P. Gaonwe, K. Kusakana, and P. A. Hohne, "Walk-through Energy Audit and Savings opportunities: Case of Water Heaters at CUT Residential Buildings," in *2019 Open Innovations Conference, OI 2019*, 2019, pp. 434–439. doi: 10.1109/OI.2019.8908172.

[10] M. M. Modise, K. Kusakana, and S. Tangwe, "Techno-Economic Analysis of Hybrid Solar-Assisted Air Source Heat Pump Systems in University Residences," in *2025 33rd Southern African Universities Power Engineering Conference (SAUPEC), Pretoria, South Africa*, 2025, pp. 1–6. doi: 10.1109/SAUPEC65723.2025.10944321.

[11] P. Gabrielli, A. Poluzzi, G. J. Kramer, C. Spiers, M. Mazzotti, and M. Gazzani, "Seasonal energy storage for zero-emissions multi-energy systems via underground hydrogen storage," *Renew. Sustain. Energy Rev.*, vol. 121, p. 109629, Apr. 2020, doi: 10.1016/j.rser.2019.109629.

[12] W. T. Ho and F. W. Yu, "Determinants of low energy performance in a multi-chiller system serving an educational premise," *Int. J. Refrig.*, vol. 114, pp. 47–53, 2020, doi: 10.1016/j.ijrefrig.2020.02.019.

[13] B. Vairamohan, M. Samotyj, S. Bishop, B. Pasley, E. Harmon, and J. Watts, "New Technologies for Reducing and Recovering Wasted Heat Energy in Industry," in *2013 ACEEE Summer Study on Energy Efficiency in Industry*, 2013, pp. 1–13.

[14] I. N. Suamir, I. B. P. Sukadana, and M. E. Arsana, "Minimizing temperature instability of heat recovery hot water system utilizing optimized thermal energy storage," *J. Phys. Conf. Ser.*, vol. 953, no. 1, 2018, doi: 10.1088/1742-6596/953/1/012113.

[15] R. M. Schierloh, S. N. Bragagnolo, J. R. Vega, and J. C. Vaschetti, "Real-Time predictive management of a multi-unit HVAC system based on heuristic optimization. A health center case study," *Energy Build.*, vol. 295, no. March, p. 113315, 2023, doi: 10.1016/j.enbuild.2023.113315.

[16] M. Mir, E. Gholamalizadeh, B. Askarian, M. S. Khoshoei, and P. Jaryani, "Cooling demand uncertainty modeling in solar photovoltaic based multi-chiller systems," *Int. J. Refrig.*, vol. 103, pp. 106–114, 2019, doi: 10.1016/j.ijrefrig.2019.03.040.

[17] T. P. Gaonwe, P. A. Hohne, and K. Kusakana, "Optimal energy management of a

solar-assisted heat pump water heating system with a storage system," *J. Energy Storage*, vol. 56, Dec. 2022, doi: 10.1016/j.est.2022.105885.

[18] L. Aththanayake, N. Hosseinzadeh, and A. Gargoom, "Dynamic Equivalent of a Power Network by Deep Artificial Neural Networks Under Varying Power System Operating Conditions," in *2022 IEEE PES 14th Asia-Pacific Power and Energy Engineering Conference (APPEEC)*, Nov. 2022, pp. 1–7. doi: 10.1109/APPEEC53445.2022.10072231.

[19] R. Guidotti, A. Monreale, S. Ruggieri, F. Turini, F. Giannotti, and D. Pedreschi, "A Survey of Methods for Explaining Black Box Models," *ACM Comput. Surv.*, vol. 51, no. 5, pp. 1–42, Sep. 2019, doi: 10.1145/3236009.

[20] R. Kicsiny, "Black-box model for solar storage tanks based on multiple linear regression," *Renew. Energy*, vol. 125, pp. 857–865, Sep. 2018, doi: 10.1016/j.renene.2018.02.037.

[21] E. Mathioulakis, G. Panaras, and V. Belessiotis, "Artificial neural networks for the performance prediction of heat pump hot water heaters," *Int. J. Sustain. Energy*, vol. 37, no. 2, pp. 173–192, 2018, doi: 10.1080/14786451.2016.1218495.

[22] J. Hu *et al.*, "Thermal load prediction and operation optimization of office building with a zone-level artificial neural network and rule-based control," *Appl. Energy*, vol. 300, no. March, p. 117429, 2021, doi: 10.1016/j.apenergy.2021.117429.

[23] Y. Wang, Z. Yuan, C. Xie, and J. Wang, "Artificial neural network-based spatial gradient models for large-eddy simulation of turbulence," *AIP Adv.*, vol. 11, no. 5, May 2021, doi: 10.1063/5.0053590.

[24] G. Dhiman, A. Y. Tiumentsev, and Y. V. Tiumentsev, "Neural Network and Hybrid Methods in Aircraft Modeling, Identification, and Control Problems," *Aerospace*, vol. 12, no. 1, p. 30, Jan. 2025, doi: 10.3390/aerospace12010030.

[25] E. M. Golafshani, A. Behnood, and M. Arashpour, "Predicting the compressive strength of normal and High-Performance Concretes using ANN and ANFIS hybridized with Grey Wolf Optimizer," *Constr. Build. Mater.*, vol. 232, p. 117266, Jan. 2020, doi: 10.1016/j.conbuildmat.2019.117266.

[26] M. U. Kumar, "Increasing Performance of Thermal Processes In Healthcare Units Under HVAC Systems For Energy Saving: A Critical Review," *Int. J. Adv. Res. Sci. Commer. Manag. Technol.*, vol. 1, no. 1, pp. 12–15, 2021.

[27] S. N. Bragagnolo, R. M. Schierloh, J. R. Vega, and J. C. Vaschetti, "Demand response strategy applied to planning the operation of an air conditioning system. Application to a medical center," *J. Build. Eng.*, vol. 57, no. March, p. 104927, 2022, doi: 10.1016/j.jobe.2022.104927.

[28] Y. Sun, S. Wang, F. Xiao, and D. Gao, "Peak load shifting control using different cold thermal energy storage facilities in commercial buildings: A review," *Energy Convers. Manag.*, vol. 71, pp. 101–114, 2013, doi: 10.1016/j.enconman.2013.03.026.

[29] J. E. Braun, "Load control using building thermal mass," *J. Sol. Energy Eng. Trans. ASME*, vol. 125, no. 3, pp. 292–301, 2003, doi: 10.1115/1.1592184.

[30] H. Jouhara, N. Khordehgah, S. Almahmoud, B. Delpech, A. Chauhan, and S. A. Tassou, "Waste heat recovery technologies and applications," *Therm. Sci. Eng. Prog.*, vol. 6, no. January, pp. 268–289, 2018, doi: 10.1016/j.tsep.2018.04.017.

[31] A. Vannoni, A. Sorce, A. Traverso, and A. Fausto Massardo, "Techno-economic optimization of high-temperature heat pumps for waste heat recovery," *Energy Convers. Manag.*, vol. 290, p. 117194, Aug. 2023, doi: 10.1016/j.enconman.2023.117194.

[32] S. S. Lam *et al.*, "Microwave vacuum pyrolysis of waste plastic and used cooking oil for simultaneous waste reduction and sustainable energy conversion: Recovery of cleaner liquid fuel and techno-economic analysis," *Renew. Sustain. Energy Rev.*, vol. 115, p. 109359, Nov. 2019, doi: 10.1016/j.rser.2019.109359.

[33] D. Brough and H. Jouhara, "The aluminium industry: A review on state-of-the-art technologies, environmental impacts and possibilities for waste heat recovery," *Int. J. Thermofluids*, vol. 1–2, 2020, doi: 10.1016/j.ijft.2019.100007.

[34] C. Ononogbo *et al.*, "Opportunities of waste heat recovery from various sources: Review of technologies and implementation," *Heliyon*, vol. 9, no. 2, p. e13590, Feb. 2023, doi: 10.1016/j.heliyon.2023.e13590.

[35] P. Christodoulides, R. Agathokleous, L. Aresti, S. A. Kalogirou, S. A. Tassou, and G.

A. Florides, "Waste Heat Recovery Technologies Revisited with Emphasis on New Solutions, including Heat Pipes, and Case Studies," *Energies*, vol. 15, no. 1, 2022, doi: 10.3390/en15010384.

[36] D. Di Battista, F. Fatigati, R. Carapellucci, and R. Cipollone, "An improvement to waste heat recovery in internal combustion engines via combined technologies," *Energy Convers. Manag.*, vol. 232, p. 113880, Mar. 2021, doi: 10.1016/j.enconman.2021.113880.

[37] Z. Cheng, Z. Guo, Z. Tan, J. Yang, and Q. Wang, "Waste heat recovery from high-temperature solid granular materials: Energy challenges and opportunities," *Renew. Sustain. Energy Rev.*, vol. 116, p. 109428, Dec. 2019, doi: 10.1016/j.rser.2019.109428.

[38] S. O. Oyedepo and B. A. Fakeye, "Waste Heat Recovery Technologies: Pathway to Sustainable Energy Development," *J. Therm. Eng.*, vol. 7, no. 1, pp. 324–348, Jan. 2021, doi: 10.18186/thermal.850796.

[39] H. O. Njoku, O. V. Ekechukwu, and S. O. Onyegegbu, "Analysis of stratified thermal storage systems: An overview," *Heat Mass Transf. und Stoffuebertragung*, vol. 50, no. 7, pp. 1017–1030, 2014, doi: 10.1007/s00231-014-1302-8.

[40] S. Barbi *et al.*, "Phase Change Material Evolution in Thermal Energy Storage Systems for the Building Sector, with a Focus on Ground-Coupled Heat Pumps," *Polymers (Basel).*, vol. 14, no. 3, 2022, doi: 10.3390/polym14030620.

[41] R. Hirmiz, H. M. Teamah, M. F. Lightstone, and J. S. Cotton, "Performance of heat pump integrated phase change material thermal storage for electric load shifting in building demand side management," *Energy Build.*, vol. 190, no. May, pp. 103–118, 2019, doi: 10.1016/j.enbuild.2019.02.026.

[42] A. Arteconi, N. J. Hewitt, and F. Polonara, "State of the art of thermal storage for demand-side management," *Appl. Energy*, vol. 93, pp. 371–389, 2012, doi: 10.1016/j.apenergy.2011.12.045.

[43] H. Molavi and M. M. Ardehali, "Utility demand response operation considering day-of-use tariff and optimal operation of thermal energy storage system for an industrial building based on particle swarm optimization algorithm," *Energy Build.*, vol. 127, pp.

920–929, 2016, doi: 10.1016/j.enbuild.2016.06.056.

[44] H. Xu, W. Y. Lin, F. Dal Magro, T. Li, X. Py, and A. Romagnoli, "Towards higher energy efficiency in future waste-to-energy plants with novel latent heat storage-based thermal buffer system," *Renew. Sustain. Energy Rev.*, vol. 112, pp. 324–337, Sep. 2019, doi: 10.1016/j.rser.2019.05.009.

[45] H. Jarimi, D. Aydin, Z. Yanan, G. Ozankaya, X. Chen, and S. Riffat, "Review on the recent progress of thermochemical materials and processes for solar thermal energy storage and industrial waste heat recovery," *Int. J. Low-Carbon Technol.*, vol. 14, no. 1, pp. 44–69, Mar. 2019, doi: 10.1093/ijlct/cty052.

[46] O. Dumont and V. Lemort, "Mapping of performance of pumped thermal energy storage (Carnot battery) using waste heat recovery," *Energy*, vol. 211, p. 118963, Nov. 2020, doi: 10.1016/j.energy.2020.118963.

[47] I. Ortega-Fernández and J. Rodríguez-Aseguinolaza, "Thermal energy storage for waste heat recovery in the steelworks: The case study of the REslag project," *Appl. Energy*, vol. 237, pp. 708–719, Mar. 2019, doi: 10.1016/j.apenergy.2019.01.007.

[48] H. Li, J. Hou, T. Hong, Y. Ding, and N. Nord, "Energy, economic, and environmental analysis of integration of thermal energy storage into district heating systems using waste heat from data centres," *Energy*, vol. 219, p. 119582, Mar. 2021, doi: 10.1016/j.energy.2020.119582.

[49] O. M. Popoola and C. Burnier, "Solar water heater contribution to energy savings in higher," *J. Energy South. Africa*, vol. 25, no. 1, pp. 51–58, 2014.

[50] A. Jamar, Z. A. A. Majid, W. H. Azmi, M. Norhafana, and A. A. Razak, "A review of water heating system for solar energy applications," *Int. Commun. Heat Mass Transf.*, vol. 76, pp. 178–187, 2016, doi: 10.1016/j.icheatmasstransfer.2016.05.028.

[51] A. Elkhatat and S. A. Al-muhtaseb, "Combined " Renewable Energy – Thermal Energy Storage," *Energies*, vol. 16, no. May, p. 4471, 2023.

[52] T. P. Gaonwe, K. Kusakana, and P. A. Hohne, "A review of solar and air-source renewable water heating systems, under the energy management scheme," *Energy Reports*, vol. 8, pp. 1–10, Nov. 2022, doi: 10.1016/j.egyr.2022.10.065.

[53] M. Praveen and G. V. S. Rao, "Ensuring the reduction in peak load demands based on load shifting DSM strategy for smart grid applications," *Procedia Comput. Sci.*, vol. 167, pp. 2599–2605, 2020, doi: 10.1016/j.procs.2020.03.319.

[54] S. Yilmaz, A. Rinaldi, and M. K. Patel, "DSM interactions: What is the impact of appliance energy efficiency measures on the demand response (peak load management)?," *Energy Policy*, vol. 139, p. 111323, Apr. 2020, doi: 10.1016/j.enpol.2020.111323.

[55] G. Sánchez-Barroso, J. González-Domínguez, and J. GarcíA-Sanz-Calcedo, "Potential savings in dhw facilities through the use of solar thermal energy in the hospitals of extremadura Spain," *Int. J. Environ. Res. Public Health*, vol. 17, no. 8, 2020, doi: 10.3390/ijerph17082658.

[56] S. Vahidifar, M. N. Sharif, and M. Ghaffari, "Heat Recovery System from Air-Cooled Chillers in Iranian Hospitals," *Int. J. Civ. Archit. Eng.*, vol. 15, no. 1, pp. 6–9, 2021.

[57] E. Dudkiewicz, A. Ludwińska, and K. Rajski, "Implementation of greywater heat recovery system in hospitals," in *E3S Web of Conferences*, 2019, vol. 116, pp. 1–9. doi: 10.1051/e3sconf/201911600018.

[58] N. Putra, T. Anggoro, and A. Winarta, "Experimental study of heat pipe heat exchanger in hospital HVAC system for energy conservation," *Int. J. Adv. Sci. Eng. Inf. Technol.*, vol. 7, no. 3, pp. 871–877, 2017, doi: 10.18517/ijaseit.7.3.2135.

[59] U. Sohail, C. Kwiatek, A. S. Fung, and D. Joksimovic, "Techno-Economic Feasibility of Wastewater Heat Recovery for A Large Hospital in Toronto, Canada," *Proceedings*, vol. 23, pp. 1–7, 2019, doi: 10.3390/proceedings2019023001.

[60] H. Ahn, D. Rim, and J. D. Freihaut, "Performance assessment of hybrid chiller systems for combined cooling, heating and power production," *Appl. Energy*, vol. 225, no. May, pp. 501–512, 2018, doi: 10.1016/j.apenergy.2018.05.045.

[61] J. W. Bujak, "Production of waste energy and heat in hospital facilities," *Energy*, vol. 91, pp. 350–362, 2015, doi: 10.1016/j.energy.2015.08.053.

[62] N. Alam *et al.*, "Performance Analysis of a HVAC System with a Heat Recovery Wheel for a Hospital Building," *J. Eng. Phys. Thermophys.*, vol. 97, no. 5, pp. 1135–1142, 2024,

doi: 10.1007/s10891-024-02985-0.

[63] M. Ghoreishinejad, M. Deymi-dashtebayaz, and M. Norani, "Proposal and multi-objective optimization of a CCHP system based on heat recovery from oxygen generator in hospitals : A case study," *J. Clean. Prod.*, vol. 421, no. August, p. 138549, 2023, doi: 10.1016/j.jclepro.2023.138549.

[64] C. Gulseven and M. Zeki Yilmazoglu, "Heating water and tap water production with an air-to-water heat pump by using the waste heat of an oil-free air compressor," *E3S Web Conf.*, vol. 111, no. 201 9, 2019, doi: 10.1051/e3sconf/201911106034.

[65] J. Kalina and W. Pohl, "Integration of Hospital's Thermal Loads with Municipal District Heating System," 2015. doi: http://dx.doi.org/10.2139/ssrn.4561774.

[66] A. Bekele, D. Alemu, and M. Mishra, "Large-scale solar water heating systems analysis in Ethiopia: A case study," *Int. J. Sustain. Energy*, vol. 32, no. 4, pp. 207–228, 2013, doi: 10.1080/14786451.2011.605951.

[67] P. Ooshaksaraei, B. Ali, S. Mat, K. Ibrahim, A. Zaharim, and K. Sopian, "Large Scale Solar Hot Water Heating Systems for Green Hospital," *Recent Adv. Appl. Math.*, pp. 504–509, 2010, doi: 10.1038/181979a0.

[68] N. Matera, D. Mazzeo, and P. M. Congedo, "Energy-sustainable hospitals: Integration of a novel compound parabolic concentrator system with two storage tanks for domestic hot water production at high and low temperatures," *Appl. Therm. Eng.*, vol. 221, no. August 2022, p. 119773, 2023, doi: 10.1016/j.applthermaleng.2022.119773.

[69] C. Y. Chiang, R. Yang, K. H. Yang, and S. K. Lee, "Performance analysis of an integrated heat pump with air-conditioning system for the existing hospital building application," *Sustain.*, vol. 9, no. 4, 2017, doi: 10.3390/su9040530.

[70] J. Vega and C. Cuevas, "Parallel vs series configurations in combined solar and heat pump systems: A control system analysis," *Appl. Therm. Eng.*, vol. 166, p. 114650, Feb. 2020, doi: 10.1016/j.applthermaleng.2019.114650.

[71] Y. Wang, Y. Xu, Y. Qiu, and S. Ning, *Thermodynamics, economy and environment analyses and optimization of series, parallel, dual-loop Kalina cycles for double-source heat recovery in cement industry*, vol. 20, no. 2 February. 2025. doi: 10.1371/journal.pone.0315972.

[72] Y. Li, Y. Cui, Z. Song, X. Zhao, J. Li, and C. Shen, "Eco-economic performance and application potential of a novel dual-source heat pump heating system," *Energy*, vol. 283, pp. 1–25, 2023, doi: 10.1016/j.energy.2023.128478.

[73] M. G. Yu, X. Ma, B. Huang, K. Devaprasad, F. Brown, and D. Wu, "Enhancing Building Energy Efficiency through Advanced Sizing and Dispatch Methods for Energy Storage," in *2024 ASHRAE Winter Conference*, 2024, vol. 130, pp. 512–519. doi: 10.63044/w24yu0061.

[74] D. Romanchenko, E. Nyholm, M. Odenberger, and F. Johnsson, "Impacts of demand response from buildings and centralized thermal energy storage on district heating systems," *Sustain. Cities Soc.*, vol. 64, no. July 2020, p. 102510, 2021, doi: 10.1016/j.scs.2020.102510.

[75] J. M. Corberán, A. Cazorla-Marín, J. Marchante-Avellaneda, and C. Montagud, "Dual source heat pump, a high efficiency and cost-effective alternative for heating, cooling and DHW production," *Int. J. Low-Carbon Technol.*, vol. 13, no. 2, pp. 161–176, Jun. 2018, doi: 10.1093/ijlct/cty008.

[76] M. Todorović, O. Ećim, and I. Zlatanovic, "Building integrated PV water heating and air conditioning in the special hospital of the SPA Rusanda," in *2nd PALENC Conference and 28th AIVC Conference on Building Low Energy Cooling and Advanced Ventilation Technologies in the 21st Century*, 2007, vol. 2, no. September, pp. 1042–1048.

[77] R. Zhang *et al.*, "Dual-objective optimization of large-scale solar heating systems integrated with water-to-water heat pumps for improved techno-economic performance," *Energy Build.*, vol. 296, no. 13, p. 113281, 2023, doi: 10.1016/j.enbuild.2023.113281.

[78] Y. Ju, J. Jokisalo, and R. Kosonen, "Analyzing different peak shaving control strategies of a short-term thermal energy storage in a district heated office building," *Heal. Build. Eur. 2023 Beyond Discip. Boundaries*, vol. 1, pp. 47–53, 2023.

[79] S. S. Mostafavi Tehrani, M. Saffar-Avval, S. Behboodi Kalhori, Z. Mansoori, and M. Sharif, "Hourly energy analysis and feasibility study of employing a thermocline TES system for an integrated CHP and DH network," *Energy Convers. Manag.*, vol. 68, pp. 281–292, 2013, doi: 10.1016/j.enconman.2013.01.020.

[80] H. Li, J. Hou, Y. Ding, and N. Nord, "Techno-economic analysis of implementing thermal storage for peak load shaving in a campus district heating system with waste heat from the data centre," in *E3S Web of Conferences*, 2021, vol. 246. doi: 10.1051/e3sconf/202124609003.

[81] B. Lamrani, S. El Marbet, T. ur Rehman, and T. Kousksou, "Comprehensive analysis of waste heat recovery and thermal energy storage integration in air conditioning systems," *Energy Convers. Manag. X*, vol. 24, no. August, p. 100708, 2024, doi: 10.1016/j.ecmx.2024.100708.

[82] S. Sultan *et al.*, "Techno-Economic Assessment of Residential Heat Pump Integrated with Thermal Energy Storage," *Energies*, vol. 16, no. 10, 2023, doi: 10.3390/en16104087.

[83] E. Ryan, B. G. McDaniel, and D. (Beka) Kosanovic, "Application of Thermal Energy Storage with Electrified Heating and Cooling in a Cold Climate," *Appl. Energy*, vol. December, no. 328, p. 120147, 2022, doi: https://doi.org/10.1016/j.apenergy.2022.120147.

[84] L. Shi, X. Liu, M. Qu, G. Liu, and Z. Li, "Potential of Utilizing Thermal Energy Storage Integrated Ground Source Heat Pump System to Reshape Electricity Demand in the United States," *J. Eng. Sustain. Build. Cities*, vol. 2, no. 3, 2021, doi: 10.1115/1.4051992.

[85] G. Wang and J. Blondeau, "Multi-Objective Optimal Integration of Solar Heating and Heat Storage into Existing Fossil Fuel-Based Heat and Power Production Systems," *Energies*, vol. 15, no. 5, 2022, doi: 10.3390/en15051942.

[86] S. Mellouli, T. Alqahtani, and S. Algarni, "Parametric Analysis of a Solar Water Heater Integrated with PCM for Load Shifting," *Energies*, vol. 15, no. 22, pp. 1–16, 2022, doi: 10.3390/en15228741.

[87] B. Yildiz *et al.*, "Analysis of electricity consumption and thermal storage of domestic electric water heating systems to utilize excess PV generation," *Energy*, vol. 235, p. 121325, 2021, doi: 10.1016/j.energy.2021.121325.

[88] Y. Li, G. Rosengarten, and A. Mojiri, "Performance sensitivity of hot and cold thermal

storage with onsite photovoltaics and heat pumps," *Sol. Energy*, vol. 263, 2023, doi: 10.1016/j.solener.2023.111946.

[89] M. Madhiarasan and M. Louzazni, "Analysis of Artificial Neural Network: Architecture, Types, and Forecasting Applications," *J. Electr. Comput. Eng.*, vol. 2022, pp. 1–23, Apr. 2022, doi: 10.1155/2022/5416722.

[90] Y. Wu and J. Feng, "Development and Application of Artificial Neural Network," *Wirel. Pers. Commun.*, vol. 102, no. 2, pp. 1645–1656, Sep. 2018, doi: 10.1007/s11277-017-5224-x.

[91] A. Behnood and E. M. Golafshani, "Predicting the compressive strength of silica fume concrete using hybrid artificial neural network with multi-objective grey wolves," *J. Clean. Prod.*, vol. 202, pp. 54–64, Nov. 2018, doi: 10.1016/j.jclepro.2018.08.065.

[92] D. J. Armaghani and P. G. Asteris, "A comparative study of ANN and ANFIS models for the prediction of cement-based mortar materials compressive strength," *Neural Comput. Appl.*, vol. 33, no. 9, pp. 4501–4532, May 2021, doi: 10.1007/s00521-020-05244-4.

[93] P. W. Tien, S. Wei, J. Darkwa, C. Wood, and J. K. Calautit, "Machine Learning and Deep Learning Methods for Enhancing Building Energy Efficiency and Indoor Environmental Quality – A Review," *Energy AI*, vol. 10, no. May, 2022, doi: 10.1016/j.egyai.2022.100198.

[94] O. Y. Odufuwa, L. K. Tartibu, K. Kusakana, P. A. Hohne, and B. P. Numbi, "Application of artificial neural networks in predicting the performance of ice thermal energy storage systems," *J. Energy Storage*, vol. 95, no. June, p. 112547, 2024, doi: 10.1016/j.est.2024.112547.

[95] Q. Yin, C. Han, A. Li, X. Liu, and Y. Liu, "A Review of Research on Building Energy Consumption Prediction Models Based on Artificial Neural Networks," *Sustainability*, vol. 16, pp. 1–30, 2024.

[96] A. G. Olabi *et al.*, "Application of artificial intelligence for prediction, optimization, and control of thermal energy storage systems," *Therm. Sci. Eng. Prog.*, vol. 39, no. February, pp. 1–21, 2023, doi: 10.1016/j.tsep.2023.101730.

[97] P. Michailidis, I. Michailidis, S. Gkelios, and E. Kosmatopoulos, "Artificial Neural Network Applications for Energy Management in Buildings: Current Trends and Future Directions," *Energies*, vol. 17, no. 3, pp. 1–47, 2024, doi: 10.3390/en17030570.

[98] J. E. Conduah, K. Kusakana, O. Y. Odufuwa, P. A. Hohne, and T. Ma, "Forecasting energy consumption and enhancing sustainability in microbreweries: Integrating ANN-based models with thermal storage solutions," *J. Energy Storage*, vol. 112, no. October 2024, 2025, doi: 10.1016/j.est.2025.115508.

[99] A. H. Elsheikh, S. W. Sharshir, M. A. Elaziz, and A. E. Kabeel, "Modeling of solar energy systems using artificial neural network: A comprehensive review," *Sol. Energy*, vol. 180, no. January, pp. 622–639, 2019, doi: 10.1016/j.solener.2019.01.037.

[100] S. Lu, Q. Li, L. Bai, and R. Wang, "Performance predictions of ground source heat pump system based on random forest and back propagation neural network models," *Energy Convers. Manag.*, vol. 197, no. July, p. 111864, 2019, doi: 10.1016/j.enconman.2019.111864.

[101] B. Jahani and B. Mohammadi, "A comparison between the application of empirical and ANN methods for estimation of daily global solar radiation in Iran," *Theor. Appl. Climatol.*, vol. 137, no. 1–2, pp. 1257–1269, Jul. 2019, doi: 10.1007/s00704-018-2666-3.

[102] L.-G. Maltais and L. Gosselin, "Predicting Domestic Hot Water Demand Using Machine Learning for Predictive Control Purposes," in *MDPI*, 2019, vol. 23, no. 6, pp. 1–7. doi: 10.3390/proceedings2019023006.

[103] A. Afram, F. Janabi-Sharifi, A. S. Fung, and K. Raahemifar, "Artificial neural network (ANN) based model predictive control (MPC) and optimization of HVAC systems: A state of the art review and case study of a residential HVAC system," *Energy Build.*, vol. 141, pp. 96–113, 2017, doi: 10.1016/j.enbuild.2017.02.012.

[104] S. Tangwe and K. Kanzumba, "The employment of artificial neural network to predict the performance of an air to water heat pump," *Int. J. Smart Grid Clean Energy*, no. December 2021, pp. 29–40, 2022, doi: 10.12720/sgce.11.1.29-40.

[105] Z. Liu, H. Li, K. Liu, H. Yu, and K. Cheng, "Design of high-performance water-in-

glass evacuated tube solar water heaters by a high-throughput screening based on machine learning : A combined modeling and experimental study," *Sol. Energy*, vol. 142, pp. 61–67, 2017, doi: 10.1016/j.solener.2016.12.015.

[106] A. A. Alnaqi, H. Moayedi, A. Shahsavar, and T. K. Nguyen, "Prediction of energetic performance of a building integrated photovoltaic/thermal system thorough artificial neural network and hybrid particle swarm optimization models," *Energy Convers. Manag.*, vol. 183, no. October 2018, pp. 137–148, 2019, doi: 10.1016/j.enconman.2019.01.005.

[107] A. H. A. Al-Waeli, K. Sopian, J. H. Yousif, H. A. Kazem, J. Boland, and M. T. Chaichan, "Artificial neural network modeling and analysis of photovoltaic/thermal system based on the experimental study," *Energy Convers. Manag.*, vol. 186, no. March, pp. 368–379, 2019, doi: 10.1016/j.enconman.2019.02.066.

[108] H. K. Ghritlahre and R. K. Prasad, "Exergetic performance prediction of solar air heater using MLP , GRNN and RBF models of arti fi cial neural network technique," *J. Environ. Manage.*, vol. 223, no. March, pp. 566–575, 2018, doi: 10.1016/j.jenvman.2018.06.033.

[109] N. Gunasekar, M. Mohanraj, and V. Velmurugan, "Artificial neural network modeling of a photovoltaic-thermal evaporator of solar assisted heat pumps," *Energy*, vol. 93, pp. 908–922, 2015.

[110] R. Jovanović, A. A. Sretenović, and B. D. Živković, "Ensemble of various neural networks for prediction of heating energy consumption," *Energy Build.*, vol. 94, pp. 189–199, 2015, doi: 10.1016/j.enbuild.2015.02.052.

[111] S. K. Park, H. J. Moon, K. C. Min, C. Hwang, and S. Kim, "Application of a multiple linear regression and an artificial neural network model for the heating performance analysis and hourly prediction of a large-scale ground source heat pump system," *Energy Build.*, vol. 165, pp. 206–215, 2018.

[112] H. Kalani, M. Sardarabadi, and M. Passandideh-Fard, "Using artificial neural network models and particle swarm optimization for manner prediction of a photovoltaic thermal nanofluid based collector," *Appl. Therm. Eng.*, vol. 113, pp. 1170–1177, 2017, doi: 10.1016/j.applthermaleng.2016.11.105.

[113] A. El Jery, A. K. Khudhair, S. Q. Abbas, A. M. Abed, and K. M. Khedher, "Numerical simulation and artificial neural network prediction of hydrodynamic and heat transfer in a geothermal heat exchanger to obtain the optimal diameter of tubes with the lowest entropy using water and Al2O3/water nanofluid," *Geothermics*, vol. 107, no. September 2022, p. 102605, 2023, doi: 10.1016/j.geothermics.2022.102605.

[114] C. Yılmaz, I. Koyuncu, and Ö. Kaşka, "An Artificial Neural Network Modeling of Solar Assisted Heat Pump System for Buildings," in *16th International Conference on Clean Energy (ICCE-2018)*, 2018, no. December 2019, pp. 1–10.

[115] M. J. Deka *et al.*, "An approach towards building robust neural networks models using multilayer perceptron through experimentation on different photovoltaic thermal systems," *Energy Conversion and Management*, vol. 292, no. July. Elsevier Ltd, pp. 1173–1195, 2023. doi: 10.1016/j.enconman.2023.117395.

[116] A. Heidari and D. Khovalyg, "Short-term energy use prediction of solar-assisted water heating system: Application case of combined attention-based LSTM and time-series decomposition," *Sol. Energy*, vol. 207, no. July, pp. 626–639, 2020, doi: 10.1016/j.solener.2020.07.008.

[117] S. Motahar and H. Bagheri-Esfeh, "Artificial neural network based assessment of grid-connected photovoltaic thermal systems in heating dominated regions of Iran," *Sustain. Energy Technol. Assessments*, vol. 39, no. January, pp. 1–15, 2020, doi: 10.1016/j.seta.2020.100694.

[118] M. V. Kulkarni, D. S. Deshmukh, and S. P. Shekhawat, "An innovative design approach of hot water storage tank for solar water heating system using artificial neural network," *Mater. Today Proc.*, vol. 46, pp. 5400–5405, 2020, doi: 10.1016/j.matpr.2020.09.058.

[119] Z. Wang, X. Liu, H. Shen, Y. Wang, and H. Li, "Energy performance prediction of vapor-injection air source heat pumps in residential buildings using a neural network model," *Energy Build.*, vol. 228, 2020, doi: 10.1016/j.enbuild.2020.110499.

[120] Z. Pang, F. Niu, and Z. O'Neill, "Solar radiation prediction using recurrent neural network and artificial neural network: A case study with comparisons," *Renew. Energy*, vol. 156, pp. 279–289, 2020, doi: 10.1016/j.renene.2020.04.042.

[121] S. Borhani, A. Kasaeian, P. Pourmoghadam, and M. Omid, "Regional performance evaluation of solar combined cooling heating and power systems for household demands," *Appl. Therm. Eng.*, vol. 230, no. April, 2023, doi: 10.1016/j.applthermaleng.2023.120666.

[122] H. U. Cho *et al.*, "Comparative analysis of the optimized ANN, SVM, and tree ensemble models using Bayesian optimization for predicting GSHP COP," *J. Build. Eng.*, vol. 44, no. September, pp. 1–11, 2021, doi: 10.1016/j.jobe.2021.103411.

[123] M. Ma, O. Pektezel, V. Ballerini, P. Valdiserri, and E. Rossi di Schio, "Performance Predictions of Solar-Assisted Heat Pumps: Methodological Approach and Comparison Between Various Artificial Intelligence Methods," *Energies*, vol. 17, no. 22, 2024, doi: 10.3390/en17225607.

[124] S. A. Kalogirou, E. Mathioulakis, and V. Belessiotis, "Artificial neural networks for the performance prediction of large solar systems," *Renew. Energy*, vol. 63, pp. 90–97, 2014, doi: 10.1016/j.renene.2013.08.049.

[125] A. O. Eldokaishi, M. Y. Abdelsalam, M. M. Kamal, and H. A. Abotaleb, "Modeling of water-PCM solar thermal storage system for domestic hot water application using Artificial neural networks," *Appl. Therm. Eng.*, vol. 204, no. September 2021, p. 118009, 2022, doi: 10.1016/j.applthermaleng.2021.118009.

[126] W. Yaïci and E. Entchev, "Performance prediction of a solar thermal energy system using artificial neural networks," *Appl. Therm. Eng.*, vol. 73, no. 1, pp. 1348–1359, 2014, doi: 10.1016/j.applthermaleng.2014.07.040.

[127] E. M. Wanjiru, S. M. Sichilalu, and X. Xia, "Model predictive control of heat pump water heater-instantaneous shower powered with integrated renewable-grid energy systems," *Appl. Energy*, vol. 204, pp. 1333–1346, 2017, doi: 10.1016/j.apenergy.2017.05.033.

[128] P. A. Hohne, K. Kusakana, and B. P. Numbi, "Optimal energy management and economic analysis of a grid-connected hybrid solar water heating system: A case of Bloemfontein, South Africa," *Sustain. Energy Technol. Assessments*, vol. 31, pp. 273–291, 2019, doi: 10.1016/j.seta.2018.12.027.

[129] Eskom, "Tariffs & Charges booklet 2024/2025," vol. 2025, no. March, pp. 1–60, 2024, [Online]. Available: www.eskom.co.za/tariffs

[130] P. A. Hohne, K. Kusakana, and B. P. Numbi, "Energy cost minimization of a multifarious water heating system with energy recovery: A case of a healthcare institution," *J. Energy Storage*, vol. 51, no. March, p. 104451, 2022, doi: 10.1016/j.est.2022.104451.

[131] F. and the E. South African Department of Forestry, "South Africa's 2023 Grid Emission Factors Report," 2025.

[132] Statista, "South Africa: Inflation rate from 1987 to 2029." https://www.statista.com/statistics/370515/inflation-rate-in-south-africa/ (accessed Dec. 18, 2024).

[133] T. P. Gaonwe, "Optimal Energy Management of Solar-Assisted Heat Pump Water Heating Sytems: A Case of Student Residences at the Central University of Technology , Free State," Central University of Technology, 2022.

[134] A. Qazi, H. Fayaz, A. Wadi, R. G. Raj, N. A. Rahim, and W. A. Khan, "The artificial neural network for solar radiation prediction and designing solar systems: A systematic literature review," *J. Clean. Prod.*, vol. 104, pp. 1–12, 2015, doi: 10.1016/j.jclepro.2015.04.041.

[135] H. K. Ghritlahre and R. K. Prasad, "Application of ANN technique to predict the performance of solar collector systems - A review," *Renew. Sustain. Energy Rev.*, vol. 84, no. December 2017, pp. 75–88, 2018, doi: 10.1016/j.rser.2018.01.001.

[136] S. R. Mohandes, X. Zhang, and A. Mahdiyar, "A comprehensive review on the application of artificial neural networks in building energy analysis," *Neurocomputing*, vol. 340, pp. 55–75, 2019, doi: 10.1016/j.neucom.2019.02.040.